DEVELOPMENT OF SELF-INTERROGATION NEUTRON RESONANCE DENSITOMETRY (SINRD) TO MEASURE THE FISSILE CONTENT IN NUCLEAR FUEL

A Dissertation

by

ADRIENNE MARIE LAFLEUR

Submitted to the Office of Graduate Studies of
Texas A&M University
in partial fulfillment of the requirements for the degree of

DOCTOR OF PHILOSOPHY

August 2011

Major Subject: Nuclear Engineering

Development of Self-Interrogation Neutron Resonance Densitometry (SINRD) to Measure the Fissile Content in Nuclear Fuel

DEVELOPMENT OF SELF-INTERROGATION NEUTRON RESONANCE DENSITOMETRY (SINRD) TO MEASURE THE FISSILE CONTENT IN NUCLEAR FUEL

A Dissertation

by

ADRIENNE MARIE LAFLEUR

Submitted to the Office of Graduate Studies of
Texas A&M University
in partial fulfillment of the requirements for the degree of

DOCTOR OF PHILOSOPHY

Approved by:

Chair of Committee,	William S. Charlton
Committee Members,	Marvin L. Adams
	Pavel V. Tsvetkov
	Wolfgang Bangerth
Head of Department,	Raymond J. Juzaitis

August 2011

Major Subject: Nuclear Engineering

ABSTRACT

Development of Self-Interrogation Neutron Resonance Densitometry (SINRD) to Measure the Fissile Content in Nuclear Fuel. (August 2011)

Adrienne Marie LaFleur, B.S., Texas A&M University

Chair of Advisory Committee: Dr. William S. Charlton

The development of non-destructive assay (NDA) capabilities to directly measure the fissile content in spent fuel is needed to improve the timely detection of the diversion of significant quantities of fissile material. Currently, the International Atomic Energy Agency (IAEA) does not have effective NDA methods to verify spent fuel and recover continuity of knowledge in the event of a containment and surveillance systems failure. This issue has become increasingly critical with the worldwide expansion of nuclear power, adoption of enhanced safeguards criteria for spent fuel verification, and recent efforts by the IAEA to incorporate an integrated safeguards regime.

In order to address these issues, the use of Self-Interrogation Neutron Resonance Densitometry (SINRD) has been developed to improve existing nuclear safeguards and material accountability measurements. The following characteristics of SINRD were analyzed: (1) ability to measure the fissile content in Light Water Reactors (LWR) fuel assemblies and (2) sensitivity and penetrability of SINRD to the removal of fuel pins from an assembly. The Monte Carlo Neutral Particle eXtended (MCNPX) transport code was used to simulate SINRD for different geometries. Experimental measurements were also performed with SINRD and were compared to MCNPX simulations of the experiment to verify the accuracy of the MCNPX model of SINRD. Based on the results from these simulations and measurements, we have concluded that SINRD provides a number of improvements over current IAEA verification methods. These improvements include:

1) SINRD provides absolute measurements of burnup independent of the operator's declaration.

2) SINRD is sensitive to pin removal over the entire burnup range and can verify the diversion of 6% of fuel pins within 3σ from LWR spent LEU and MOX fuel.
3) SINRD is insensitive to the boron concentration and initial fuel enrichment and can therefore be used at multiple spent fuel storage facilities.
4) The calibration of SINRD at one reactor facility carries over to reactor sites in different countries because it uses the ratio of fission chambers (FCs) that are not facility dependent.
5) SINRD can distinguish fresh and 1-cycle spent MOX fuel from 3- and 4-cycles spent LEU fuel without using reactor burnup codes.

ACKNOWLEDGEMENTS

I would like to thank my advisor, Dr. William Charlton, for the many years of guidance, support, and advice he has provided throughout the course of this research. I would also like to thank my committee members, Dr. Marvin Adams, Dr. Pavel Tsvetkov, and Dr. Wolfgang Bangerth, for their time and support. Their comments and suggestions have been greatly appreciated.

Many staff members at Los Alamos National Laboratory aided in development of this verification technique. I must thank Dr. Howard Menlove for his oversight, support and guidance throughout this research. His help in developing a complete understanding of the underlying physics of this technique and its application to international safeguards was invaluable. I would like to thank Dr. Martyn Swinhoe for all of his help in developing MCNPX models of this technique and improving my understanding of the simulation results. I would also like to thank Dr. Sang Yoon Lee, Carlos Rael, and Isaac Martinez for all of their time and help in performing experimental measurements with this technique. Thanks are also due to Dr. Stephen Tobin and Dr. Johnna Marlow for their time and support throughout this research.

I would also like to thank my friends and family for their continued support. A special thanks to my mom, Karen Keller, who has always supported and encouraged me.

Last, I would like to acknowledge the Department of Energy National Nuclear Security Administration's Office of Global Security Engagement and Cooperation (NA-242) and the Office of Nuclear Safeguards and Security (NA-241) for their support in the development of the SINRD method. This work was funded in part under the NA-24 Next Generation Safeguards Initiative (NGSI) program.

NOMENCLATURE

α	False Alarm Probability
β	Nondetection Probability
BU	Burnup
BWR	Boiling Water Reactor
C/S	Containment and Surveillance
DU	Depleted Uranium Fuel
FA	Fuel Assembly
FC	Fission Chambers
IAEA	International Atomic Energy Agency
IE	Initial Enrichment
LEU	Low Enriched Uranium Fuel (UO_2)
LWR	Light Water Reactors
MOX	Mixed Oxide Fuel (PuO_2-UO_2)
NDA	Nondestructive Assay
Pu	Plutonium
PWR	Pressurized Water Reactor
SINRD	Self-Interrogation Neutron Resonance Densitometry
SNM	Special Nuclear Material
SQ	Significant Quantity

TABLE OF CONTENTS

Page

LIST OF FIGURES

FIGURE Page

FIGURE Page

FIGURE Page

FIGURE Page

FIGURE Page

FIGURE Page

FIGURE Page

LIST OF TABLES

TABLE Page

1. INTRODUCTION

1.1. Motivations

The development of non-destructive assay (NDA) capabilities to directly measure the fissile content in spent fuel is needed to improve the timely detection of the diversion of significant quantities of fissile material. This NDA capability is important to the implementation of integrated safeguards for spent fuel verification by the International Atomic Energy Agency (IAEA) and would improve deterrence of possible diversions by increasing the risk of early detection [1]. Furthermore, this assay capability would also improve material accountability information at reprocessing plants prior to fuel dissolution and thus increase operational efficiency and reduce material unaccounted for (MUF) [2].

Thus, the development of accurate verification methods for spent fuel materials in both wet and dry storage areas continues to be of significant importance to both the IAEA and the United States. Currently, the IAEA does not have effective NDA methods to verify spent fuel and recover continuity of knowledge in the event of a containment and surveillance systems failure. This issue has become increasingly critical with the worldwide expansion of nuclear power, adoption of enhanced safeguards criteria for spent fuel verification, and recent efforts by the IAEA to incorporate an integrated safeguards regime [3].

To further address this issue, the U.S. Department of Energy National Nuclear Security Administration established the Next Generation Safeguards Initiative (NGSI) to revitalize U.S. safeguards technology and human capital base [4]. In 2009, NGSI funded a five year research effort to develop and assess 14 potential NDA techniques for quantifying plutonium in commercial spent fuel. The first two years of this research effort is primarily focused on Monte Carlo modeling and the following three years will include fabrication of hardware and measuring spent fuel assemblies (FAs). The main

---

This dissertation follows the style of Nuclear Instruments and Methods in Physics Research Section A.

objectives of this modeling effort include: (1) quantify the expected capability of each technique as an independent instrument and (2) determine how to cost effectively integrate a few NDA techniques to accurately measure the elemental mass of plutonium and detect fuel pin diversions [5,6,7,8].

1.2. Objectives

The primary objective of this research is to develop and assess the use of Self-Interrogation Neutron Resonance Densitometry (SINRD) for nuclear safeguards and material accountability measurements. The following characteristics of SINRD will be analyzed: (1) ability to measure the fissile content in Light Water Reactors (LWR) fuel assemblies and (2) sensitivity and penetrability of SINRD to the removal of fuel pins from an assembly. Recent interest in this approach was stimulated by an IAEA request related to spent fuel verification. The main application of SINRD is for use at a spent fuel storage facility for measurements in water, although SINRD could also be used for measurements in different mediums, such as air or sodium and at reprocessing facilities that have spent fuel pools.

In order to develop this technique for verification of LWR fuel assemblies, the Monte Carlo Neutral Particle eXtended (MCNPX) transport code [9] was used to simulate SINRD for the following geometries:

- ^{235}U and ^{239}Pu metals plates (0.25 to 3.5 mm thick) [10,11]
- Mixed Oxide (MOX) fuel pins containing pellets with different Pu loadings [12,13]
- LWR fresh and spent Low Enriched Uranium (LEU) and MOX assemblies [14,15]

For the MCNPX simulations of LWR fuel assemblies, the design specifications for a Westinghouse Pressurized Water Reactor (PWR) 17x17 FA and General Electric (GE-11) Boiling Water Reactor (BWR) 9x9 FA were used. The purpose of the MCNPX simulations of SINRD was to: (1) validate the use of MCNPX as a computational tool for simulating SINRD signals, (2) obtain a better understanding of the underlying physics of this measurement technique, and (3) optimize the SINRD detector configuration and signal analysis for LWR LEU and MOX fuel assemblies.

Experimental measurements were also performed in air with SINRD using the reference PWR 15x15 fresh LEU fuel assembly at Los Alamos National Laboratory (LANL) [16,17]. These measurements were compared to MCNPX simulations of the experiment to verify the accuracy of the MCNPX model of SINRD. The results of this research will determine whether SINRD is a viable technique for measuring the fissile content in LWR spent fuel assemblies. In addition, these results will also quantify the sensitivity and penetrability of this technique to partial defects* [18] and whether or not SINRD could be used to detect the diversion of fuel for proliferation purposes. An overview of the MCNPX simulations and experimental measurements performed and their corresponding significance to the overall project is shown in Fig. 1.1.

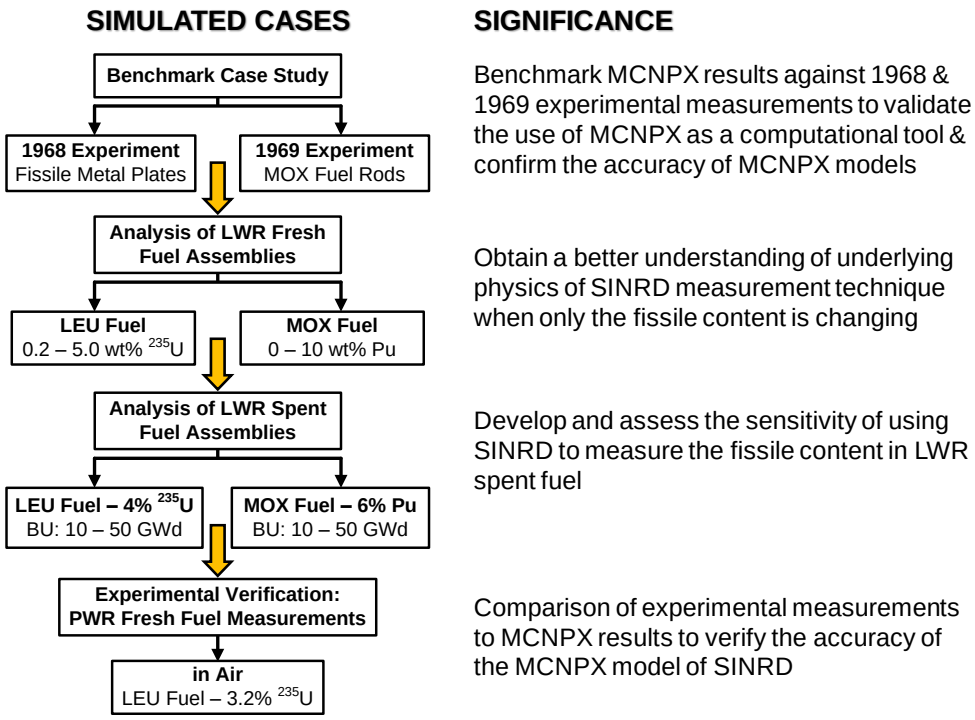

Fig. 1.1. Overview of simulated cases and the corresponding significance to the overall project.

* *Partial defects* is defined as the removal of 50% or more of the irradiated fuel pins from an assembly. The spent fuel pins removed can be replaced with nothing (except water) or replaced with non-irradiated dummy pins, such as iron or depleted uranium (DU) pins.

1.3. Theory and Background Information

The use of SINRD to measure the fissile content in LWR spent fuel is a promising technique for the improvement of nuclear safeguards and material accountability measurements. The development and implementation of SINRD for verification of LWR spent fuel requires a thorough understanding of the properties of LWR spent fuel within the context of NDA verification measurements and the IAEA detection requirements for spent fuel verification. It is also important to understand the underlying physics of the SINRD measurement technique.

1.3.1. Properties of LWR Spent Fuel

The two most common types of nuclear power reactors in operation throughout the world are PWRs and BWRs. These reactors are referred to as LWRs because light water is used for both the coolant and moderator. LEU is the main type of fuel used in LWRs. This fuel is in the form of uranium dioxide (UO_2) ceramic pellets approximately 1-cm in diameter and 2-cm in length [19]. MOX fuel, a mixture of uranium and plutonium oxides in the form PuO_2-UO_2, is also used in LWRs as an advanced fuel form. This fuel is fabricated from recovered plutonium from spent LEU fuel via reprocessing [20]. The fuel pellets are stacked in Zircaloy metal tubing (referred to as cladding) and sealed to form a fuel pin which is then bundled together to form a fuel assembly [21]. There are numerous types of PWR and BWR fuel assembly designs used throughout the world. This research is focused on the properties of LEU and MOX spent fuel generated from a PWR 17x17 fuel assembly and BWR 9x9 fuel assembly which are two of the most common types of assemblies used. A top-down view of a PWR 17x17 fuel assembly and BWR 9x9 fuel assembly is shown in Fig. 1.2(a) and (b), respectively.

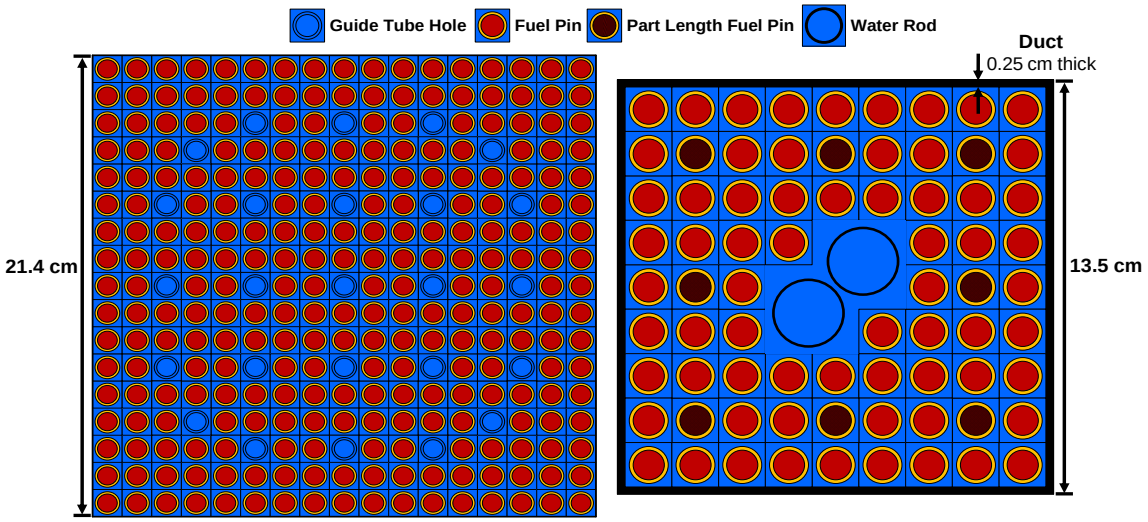

Fig. 1.2. Top-down view of (a) PWR 17x17 fuel assembly and (b) BWR 9x9 fuel assembly.

The typical cycle of a LWR fuel assembly from fresh fuel to final disposition of spent fuel is illustrated in Fig. 1.3 [22,23]. The boxes outlined in red represent the primary places where spent fuel verification measurements with SINRD are applicable. The cycle begins with a fresh fuel assembly which can be stored in air or in the spent fuel pool. After being loaded into the reactor, the fuel assemblies will remain in the core for approximately three to five years depending on the fuel type (LEU or MOX) and refueling schedule of the reactor. While in the reactor, uranium in the fuel assembly will undergo reactions (Fig. 1.4) resulting in the depletion of ^{235}U (LEU) or ^{239}Pu (MOX) and production of transuranic nuclides and fission products. Once the fuel assembly has reached its maximum design burnup, it is discharged from the reactor and transferred to a spent fuel pool located at the reactor site. The highly radioactive spent fuel assemblies may remain in the spent fuel pool for several years to allow the majority of short-lived fission products to decay away. The spent fuel assemblies are then loaded into heavily shielded transport casks and shipped to either an interim storage facility for permanent geological disposal or to a reprocessing plant [21]. Table 1.1 provides the total neutron and gamma-ray production rates in BWR and PWR spent LEU and MOX fuel (30-GWd/MTU, 5-yrs cooled) calculated using OrigenARP [24].

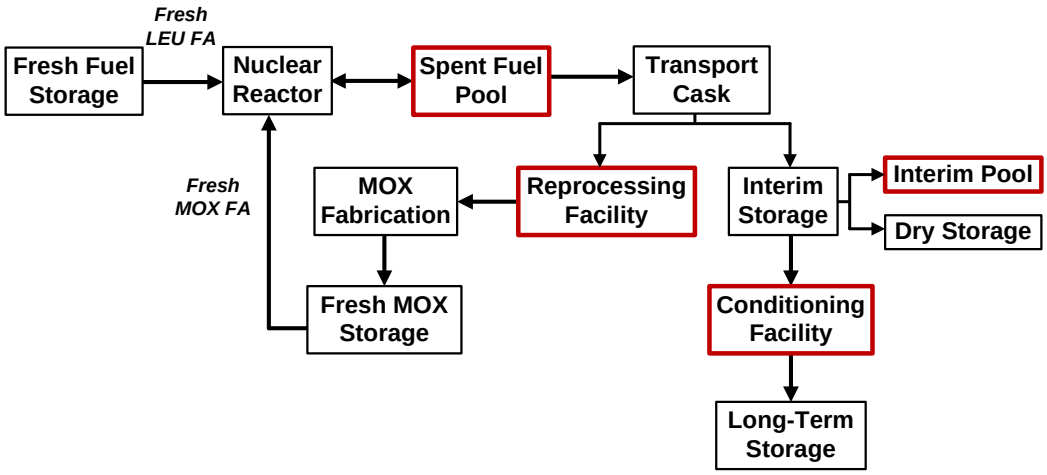

Fig. 1.3. Typical cycle of a LWR fuel assembly from fresh fuel to final disposition of spent fuel.

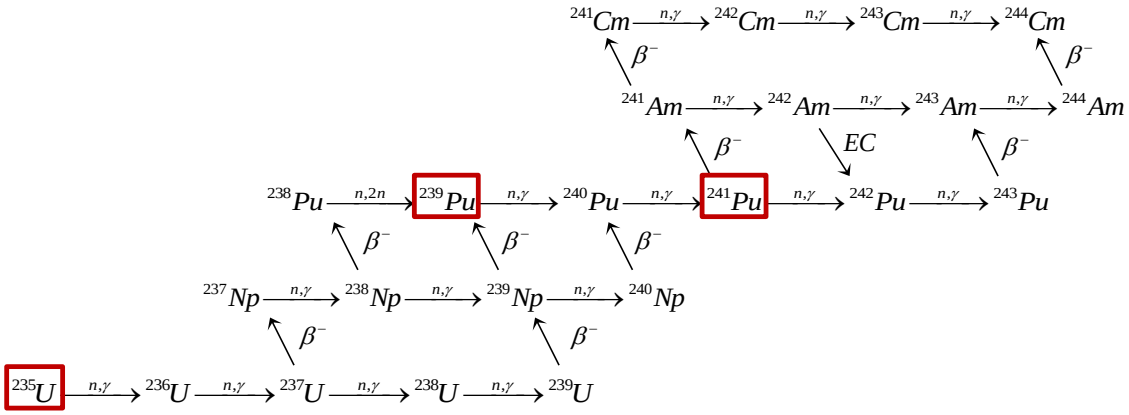

Fig. 1.4. Primary neutron capture and radioactive decay reactions leading to the production of transuranic nuclides in spent fuel [19]. Primary fissile isotopes are outlined in red.

Table 1.1. Total neutron and gamma-ray production rates for 30-GWd spent fuel (5-yrs cooled).

Source Term	*BWR 9x9 Assembly*		*PWR 17x17 Assembly*	
	3% ^{235}U LEU	6% Pu MOX	4% ^{235}U LEU	6% Pu MOX
(α,*n*) Neutrons [n/s]	3.11E+06	5.56E+07	3.49E+06	6.11E+07
SF* Neutrons [n/s]	1.25E+08	4.13E+09	1.10E+08	4.92E+09
Total Neutron [n/s]	1.28E+08	4.19E+09	1.13E+08	4.98E+09
Total Gamma [γ/s]	8.21E+15	8.31E+15	8.70E+15	9.06E+15

** SF ≡ Spontaneous Fission*

The location of the spent FA determines whether or not verification measurements are possible. Containment and Surveillance (C/S) and item accounting, are used to maintain continuity of knowledge of the fuel assemblies when transported in and out of a facility. Once a spent FA has been transferred and sealed in a shielded fuel cask or canister, NDA measurements become very difficult, if even possible at all [23]. Therefore, only NDA verification measurements at a spent fuel pool are considered. It should be noted that spent fuel pools can be located at the reactor site, interim storage facility, and reprocessing facility.

A typical spent fuel storage pool is 6-m wide, 12-m long, and 13-m deep. The walls and floor of the pool are made of reinforced concrete with a stainless steel liner [25]. The spent fuel assemblies are stored vertically in racks. The spacing of the spent fuel assemblies in the racks and whether or not boron is added to the pool water depends on the throughput of the facility and the country's licensing requirements. The capacity of a BWR storage pool typically ranges from 800 to 1000 fuel assemblies and from 250 to 350 assemblies for a PWR storage pool [25]. Initial enrichment, burnup and cooling time are the three main parameters used to characterize and verify spent fuel. These parameters are declared by the facility operator and must be verified by the inspection agency with NDA measurements. The level of verification required is based on the type and throughput of the facility and will determine the types of NDA measurements needed. For safeguards measurements at a spent fuel pool, it is important to note that facility operators generally want to minimize the movement of spent fuel assemblies and to not allow the detector to touch the assembly because of the risk of damaging the fuel assembly and contaminating the water in the spent fuel pool [22].

1.3.2. IAEA Requirements for Verification of LWR Spent Fuel

The technical objective of international safeguards as stated under Article 28 of INFCIRC/153 is "the *timely detection* of diversion of *significant quantities* of nuclear material from peaceful nuclear activities to the manufacture of nuclear weapons or other nuclear explosive devices or for purposes unknown and deterrence of such diversion by risk of early detection [26]." A *significant quantity* (SQ) is the approximate amount of

nuclear material needed to manufacture a nuclear explosive device. The *timely detection* of diversion refers to a set of timeliness goals that are based on the time required to convert diverted material into the components of a nuclear explosive device and the type of material in question [27].

In order to achieve this objective, the IAEA has established detection goals with a specified probability of detection to be used at different types of nuclear facilities. For verification of LWR spent fuel, the following special nuclear material (SNM) SQs and timeliness detection goals set by the IAEA are applicable:

- A diversion of *8 kg of plutonium* (all isotopes) is to be detected within:
  - 1-month for *fresh* fuel
  - 3-months for *spent* (irradiated) fuel
- A diversion of *75 kg of* ^{235}U contained in LEU (less than 20% ^{235}U), natural, or depleted uranium is to be detected within 12-months [27].

Current practice for IAEA inspections at LWRs includes unattended C/S monitoring of storage pools and onsite inspections during scheduled shutdown periods for refueling. During an onsite inspection, IAEA inspectors verify the spent fuel inventory declared by the facility operator via item accounting and measuring a sample of the assemblies to ensure the validity of the operator's accountancy system. Inspectors must also review the operating records and surveillance information for consistency [28]. The following equations are used to estimate the number of samples, *n*, that need to be measured to achieve the desired detection probability, *P*, of a diversion of 1 SQ of SNM:

$$n = N \cdot \left(1 - \beta^{1/D}\right) \tag{1.1}$$

$$\beta = 1 - P \tag{1.2}$$

where β is the nondetection probability, N is the total number items from which the sample is taken, and D is the number of diverted items to be detected [27]. It is important to note that the maximum time allowed per year for routine inspections of reactors is 50 *man-days* per facility where a man-day of inspection is an 8-hr day during which a single

inspector has access to a facility at any time [26]. Thus, in practice, an inspector selects a level of verification based on the constraint of time available [25].

To put these detection goals in the context of LWR spent fuel, the number of BWR and PWR spent fuel assemblies that would need to be diverted to acquire 1 SQ of Pu and ^{235}U are summarized in Table 1.2. In addition, the corresponding fraction of the total number of fuel assemblies, *n*/*N*, that would need to be sampled to detect the diversions with 5% nondetection probability are also given in Table 1.2. TransLAT [29] was used to calculate the concentration of Pu and ^{235}U in spent LEU and MOX fuel for burnup of 30-GWd/MTU and 5-yrs cooled.

Table 1.2. Number of BWR and PWR spent LEU and MOX fuel assemblies that must be diverted to obtain 1-SQ of Pu (8-kg) and ^{235}U (75-kg).

Material Safeguards		***BWR 9x9 Assembly***		***PWR 17x17 Assembly***	
		3% ^{235}U LEU	**6% Pu MOX**	**4% ^{235}U LEU**	**6% Pu MOX**
Pu	Pu Mass per FA [kg]	1.24	7.44	3.96	22.3
	# FAs to acquire 1 SQ	6.46	1.08	2.02	0.36
	Fraction of FAs to Sample [n/N]	37%	94%	77%	100%
^{235}U	^{235}U Mass per FA [kg]	1.21	0.19	7.21	0.56
	# FAs to acquire 1 SQ	62.1	393	10.4	135
	Fraction of FAs to Sample [n/N]	4.7%	0.8%	25%	2.2%

Comparing the results for safeguarding Pu, we see that twice as many PWR spent LEU fuel assemblies must sampled in order to detect the diversion of 1 SQ of Pu compared to BWR spent LEU fuel assemblies. This is because a BWR 9x9 FA is smaller than a PWR 17x17 FA and thus contains about half as much total Pu in a single assembly. For MOX spent fuel, essentially all of the fuel assemblies must be sampled regardless of the type of assembly. However, it should be noted that one PWR spent MOX assembly contains ~2.8 SQs of Pu whereas one BWR spent MOX assembly only contains ~0.9 SQ of Pu. It is also important to recognize that even though PWR spent LEU and MOX fuel assemblies contain twice as much Pu compared to BWR spent fuel

assemblies, a typical spent fuel pool can store over twice as many BWR spent fuel assemblies compared to PWR spent fuel assemblies. Based on the IAEA detection goals and the results shown in Table 1.2, it is clear that verifying the Pu content in LWR spent fuel is of primary importance to international safeguards with the residual ^{235}U content being less significant.

1.3.3. Self-Interrogation Neutron Resonance Densitometry (SINRD)

The neutron resonance cross-section structure is unique for each of the fissionable isotopes such as ^{235}U, ^{239}Pu, and ^{241}Pu, and the resonance structure can provide a signature for the measurement of these materials of importance for safeguards and non-proliferation. The sensitivity of SINRD is based on using the same fissile materials in the sample and fission chamber because the effect of resonance absorption in the transmitted flux is amplified by the corresponding (*n,f*) reaction peaks in the fission chamber. For instance, a ^{235}U fission chamber has a high sensitivity to the neutron resonance absorption in ^{235}U present in the sample, and similarly for other fissile isotopes. SINRD uses spontaneous fission neutrons from ^{244}Cm to self-interrogate the spent fuel pins. The concentration of ^{235}U and ^{239}Pu in the spent fuel is then determined by measuring the distinctive resonance absorption lines from ^{235}U and ^{239}Pu using both ^{235}U and ^{239}Pu fission chambers (FCs) placed adjacent to the side of the fuel assembly. Thus, the self-interrogation signature is a result of having the same fissile material in the fission chamber and the sample [10,14].

In Fig. 1.5, the ^{239}Pu fission cross-section is compared to the resonance absorption lines in the neutron flux after transmission through a 0.11-mm Gd filter and ^{239}Pu metal samples 0.25-mm and 2.5-mm thick. It is important to note that as the sample thickness increases, the resonance absorption from ^{239}Pu in the sample also increases which decreases the transmitted flux reaching the FCs. Thus, the self-interrogation signature is inversely proportional to the amount of resonance absorption in the sample [10]. The results shown for the transmitted flux through ^{239}Pu metal samples of different thicknesses were obtained from MCNPX simulations and the ^{239}Pu fission cross-section was obtained from the JANIS ENDF-VII cross-section database [30].

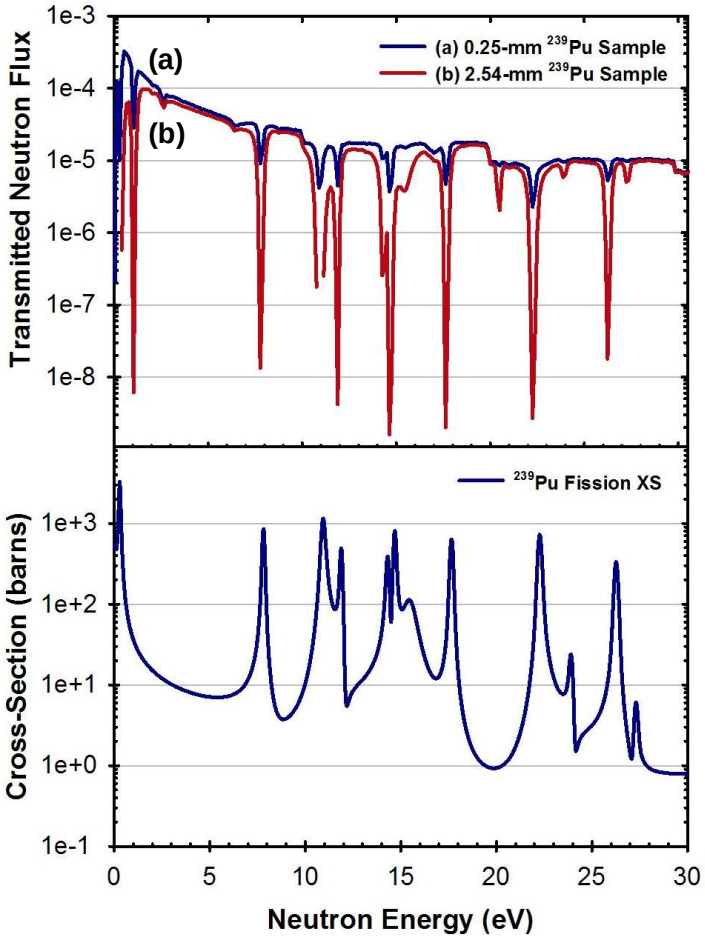

Fig. 1.5. Comparison of absorption lines in neutron flux after transmission through Gd filter and (a) 0.25-mm and (b) 2.5-mm ^{239}Pu metal sample (upper plot) to ^{239}Pu fission cross-section (bottom plot).

2. PRESENT STATUS OF SPENT FUEL VERIFICATION METHODS

2.1. Overview of IAEA Spent Fuel Verification Methods

Improvement of current spent fuel verification methods is needed to ensure the timely detection of the diversion of significant quantities of fissile material and recover continuity of knowledge in the event of a C/S system failure. A variety of NDA methods are available for verification of spent fuel assemblies. Neutron methods are generally preferred for detecting the diversion of fuel pins because of their higher penetrability compared to gamma-ray methods which only see the outer pins of the fuel assembly. Gamma-ray methods are typically used to verify the operator's declaration of burnup and cooling time. In this section, an overview of current IAEA verification methods is provided within the context of the desired safeguards detection capabilities. These capabilities include the following possible diversion scenarios that may be used by the adversary to obtain plutonium [3,31]:

- removal of a LEU spent fuel assembly and replacement with an irradiated dummy
- removal of part of a spent fuel assembly (with or without pin substitution)
- diversion of a fresh MOX assembly and replacement with either a dummy fuel assembly or an irradiated LEU assembly

All of these scenarios may be accompanied by falsification of one or more values in the operator's declaration of initial enrichment, burnup, and cooling time.

2.1.1. Digital Cerenkov Viewing Device (DCVD)

The DCVD measures the Cerenkov glow emanating from a spent fuel assembly and can be used to verify that the fuel has been irradiated. The Cerenkov light emitted is a result of gamma-rays from the decay of fission and activation products interacting in the assembly and water and producing electrons [19]. The DCVD, shown in Fig. 2.1(a), is mounted on a bridge above the fuel assembly [32]. This minimizes contamination issues and provides a rapid nonintrusive measurement method for spent fuel verification.

The DCVD produces high resolution digital images of the measured Cerenkov light to improve the detection of unirradiated pin substitutions. Fig. 2.1(b) shows a digital Cerenkov image produced from a PWR spent fuel assembly [33]. It is important to note that the ability of the DCVD to detect dummy fuel pins assumes that the substituted pins are not radioactive and will not contribute to the measured Cerenkov glow. Recent field tests have shown that the DCVD is capable of verifying a spent fuel assembly with a burnup of 10-GWd/MTU and 40-yrs cooling time [34].

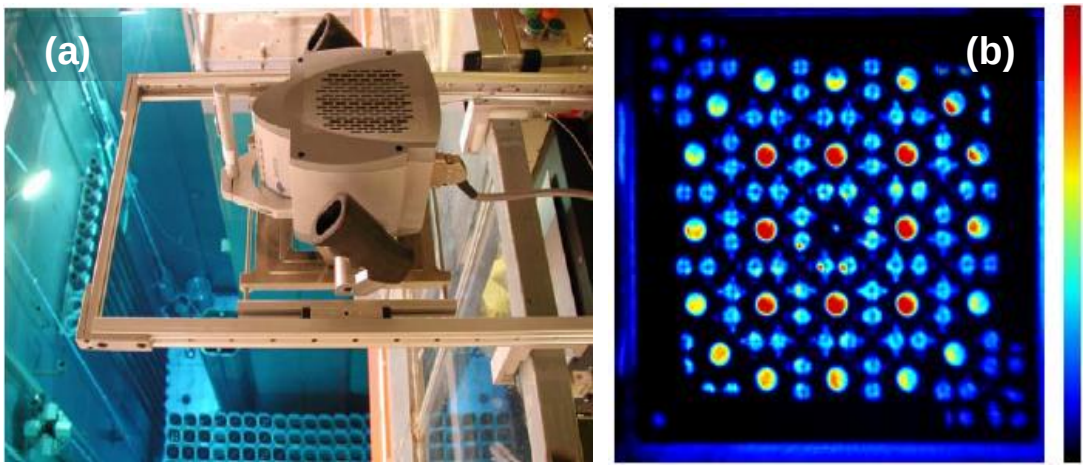

Fig. 2.1. (a) DCVD mounted on fueling machine, (b) Digital Cerenkov image of PWR assembly.

2.1.2. FORK Detector (FDET)

The FDET measures gross neutrons and gamma-rays emitted from a spent fuel assembly. This device consists of two detector arms that extend from a common base and are spaced apart so that each arm is positioned on opposite sides of a submerged spent fuel assembly. Each arm of the FDET contains an ionization chamber for gross gamma-ray measurements, a bare ^{235}U FC for measuring thermal neutrons, and a Cd shielded ^{235}U FC for measuring epi-cadmium (>0.5-eV) neutrons [35]. An isometric view of the FDET and a picture of the FDET measuring a PWR assembly in a spent fuel pool are shown in Fig. 2.2(a) and (b), respectively.

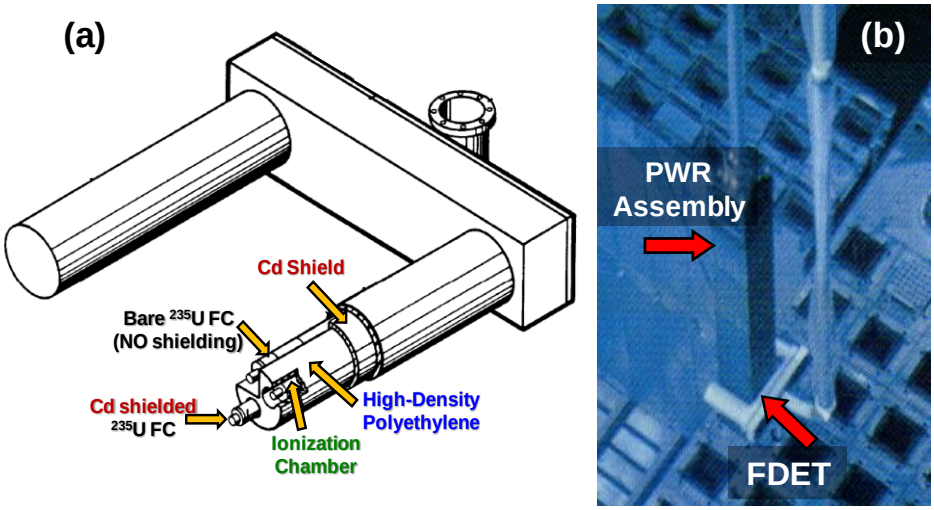

Fig. 2.2. (a) Isometric view of FDET, (b) picture of FDET measuring a PWR assembly [35].

FDET measurements can be used to verify irradiation cycle history and consistency of the operator's declaration of burnup and cooling time. For partial defect verification of spent fuel assemblies, the FDET requires use of declared data by the reactor operator. If the reactor operator's declaration is available and the burnup is correctly declared, the sensitivity of the FDET to partial defects is limited to 20% pin removal (90% confidence level) for a BWR 8x8 fuel assembly at burnup of 18-GWd/MTU or higher. It is important to note that there are specific cases (e.g. low burnup, long cooling time) that cannot be detected by the FDET even with 50% of the fuel pins removed [36].

2.1.3. Safeguards MOX Python (SMOPY)

Similar to the FDET, the SMOPY device uses both neutron and gamma-ray measurements to characterize spent fuel assemblies. This device consists of one fission chamber and one CdZnTe probe. A schematic of the SMOPY device and a picture of this device underwater taking measurements is shown in Fig. 2.3(a) and (b), respectively [37]. Compared to the FDET, an embedded depletion code that can perform online depletion calculations to aid in interpretation of the measurements and room temperature gamma spectroscopy capabilities using the CdZnTe probe have been added to the SMOPY device. The embedded depletion code is an important addition because it

enables 1-cycle spent MOX fuel assemblies to be distinguished from 3-cycle spent LEU fuel assemblies. MCNP simulations have estimated the detection of limit of SMOPY to be 25% partial defects [37]. Despite these improvements, the SMOPY device, like the FDET, cannot detect some diversion scenarios of pin removals and substitutions [3].

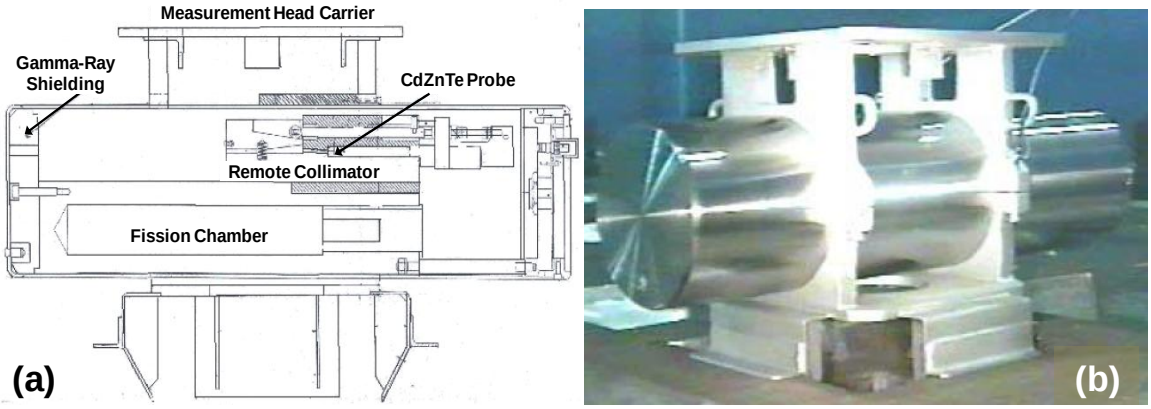

Fig. 2.3. (a) Schematic of SMOPY, (b) picture of SMOPY underwater taking measurements [37].

2.2. Summary of Spent Fuel Verification Methods

An overview of current IAEA verification methods for LWR spent fuel has been provided within the context of the desired safeguards detection capabilities. The performance of these verification methods for possible diversion scenarios is summarized in Table 2.1 [3]. The DCVD is commonly used by the IAEA to verify that a fuel assembly has been irradiated but can only detect two of the five possible diversion scenarios. Thus, additional measurement methods are needed to verify LWR spent fuel. While the FDET and SMOPY can be used to verify the majority of possible diversion scenarios, it is important to note that both of these methods still cannot detect long cooled assemblies with certain configurations of substituted pins. Furthermore, both of the FDET and SMOPY rely on information provided by the operator's declaration the existence of calibration curves for different fuel assembly types [3].

Table 2.1. Performance of IAEA verification methods for possible diversion scenarios [3].

Possible Diversion Scenarios	IAEA Verification Methods		
	DCVD	FDET	SMOPY
Replace entire LEU Fuel Assembly with Irradiated Dummy	NO	YES	YES
Replace entire LEU Fuel Assembly with Unirradiated Dummy	YES	YES	YES
50% Pin Removal from Spent Fuel Assembly with Pin Substitutions	NO	YES[(1)]	YES[(1)]
50% Pin Removal from Spent Fuel Assembly with No Pin Substitutions	YES	YES[(1)]	YES[(1)]
3σ Detection Limit [% Pins Removed]	N/A	40%[(2)]	25%[(3)]
Diversion of Fresh MOX Assembly with Irradiated Spent LEU Assembly	NO	NO	YES[(4)]

(1) *Cannot detect long cooled assemblies with certain configurations of substituted pins. Verification measurement of cooling time is needed.*

(2) *Depends on IAEA records and operator's declaration of discharge date and initial enrichment and on the existence of calibration curve for different fuel assembly types* [36].

(3) *Based on numerical simulations for cases studied in IAEA report IAEA-SM-367/14/03* [37].

(4) *Requires the use of online burnup codes.*

Based on these results, key gaps in current spent fuel verification methods include: the ability to verify LWR spent fuel assemblies independent of the operator's declaration and the existence of a measurement method that can be used for all types of fuel assemblies regardless of initial fuel enrichment, burnup, or cooling time. Thus, the improvement of these methods continues to be of significant importance to both the IAEA and U.S. and is one of the primary motivations behind the development of SINRD.

3. BENCHMARK CASE STUDY OF 1968 AND 1969 EXPERIMENTS

3.1. Self-Indication Neutron Resonance Absorption Densitometry (SINRAD)

The SINRD measurement technique was originally developed in 1968 by Howard Menlove at LANL using the name, Self-Indication Neutron Resonance Absorption Densitometry [10]. This was abbreviated as SINRAD. In 1968, a set of experiments were conducted with SINRAD using a reactor beam as the interrogating neutron source to determine the fissile concentration in ^{235}U and ^{239}Pu metals plates of different thicknesses [10]. In 1969, another set of experiments were conducted with SINRAD to determine the plutonium enrichment of pellets in MOX fuel rods [11,12]. These experiments provided the basic concept of SINRAD.

The primary objective of this research is to develop the same basic physics signature as SINRAD but applied to LWR spent fuel assemblies. However, in spent fuel, there is an adequate neutron source from the spontaneous fission of ^{244}Cm in the spent fuel to be self-interrogating and no reactor beam is necessary. Thus, the original name was modified to the current name, Self-Interrogation Neutron Resonance Densitometry, for spent fuel applications to reflect the different neutron sources. This has been abbreviated as SINRD to attempt to avoid confusion between the two techniques.

3.2. Fissile Metal Plates – 1968 Experiment

The purpose of the 1968 experiment was to investigate the use SINRAD to measure the thickness of ^{235}U and ^{239}Pu metal plates. The data from this experiment and the details of the experimental setup were acquired from literature and from the original experimenter [10]. These measurements were then simulated using MCNPX and the experimental and computational results were compared. The results from this study were used to obtain a better understanding of how self-shielding affects the SINRAD measurements and at what thickness of ^{235}U and ^{239}Pu metal this effect becomes

significant. These results were also used to better understand the physics of SINRAD and to determine the ability of MCNPX to model this technique.

3.2.1. 1968 Experimental Setup and Procedure

The neutron source used in the 1968 experiment was a collimated neutron beam from the LASL Water Boiler Reactor. The neutron beam first passed through a thin foil of Gd or Cd to remove thermal neutrons, then through the fissile sample (^{235}U or ^{239}Pu), and finally through three parallel-plate fission chambers containing deposits of ^{239}Pu, ^{235}U, and ^{10}B. The fissile samples consisted of 5.0 cm diameter metallic disks of 94 wt% ^{239}Pu or 93 wt% ^{235}U with thicknesses ranging from 0.25 to 3.5 mm [10]. In order to simulate the neutron source from the LASL Reactor, MCNPX was used to calculate the energy-dependent neutron flux spectrum of a typical LWR by modeling a fresh UO_2 fuel pin (3 wt% ^{235}U) surrounded by water with reflecting boundaries. We tallied the neutron flux in the water as a function of energy. The initial flux spectrum and a diagram of the 1968 experimental setup simulated in MCNPX are shown in Fig. 3.1 [13].

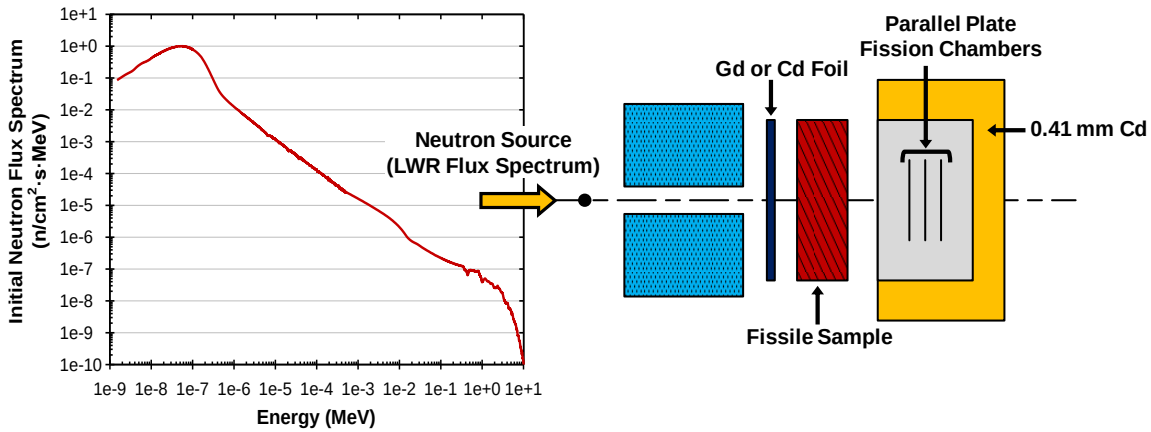

Fig. 3.1. Initial neutron flux spectrum and 1968 experimental setup simulated in MCNPX.

A schematic of the three parallel-plate ionization detectors used in the 1968 experiment is shown in Fig. 3.2. These detectors were operated as gas flow proportional

counters during sample irradiation using a gas mixture of 90% Ar and 10% CH_4. In order to reduce the neutron background, the sides and back of the detector pod were covered with 0.41-mm of Cd. The count rate for each detector was recorded both with and without the fissile sample present for normalization purposes [10]. Since the attenuation of the neutron flux between the parallel-plate fission foils was small, the geometry of these foils was not explicitly modeled in the MCNPX simulation. Instead, a thin rectangular box filled with a void was modeled and the ^{239}Pu and ^{235}U fission rates and ^{10}B (n,α) rate were calculated using f4 tallies based on the neutron flux in the box.

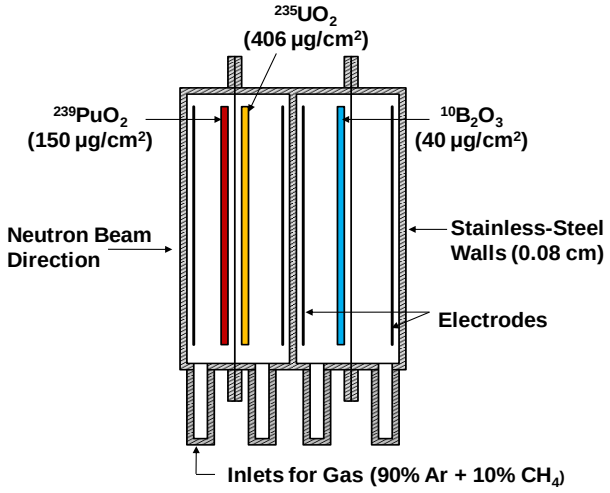

Fig. 3.2. Parallel-plate ionization chambers used for self-indication measurements in 1968 experiment.

3.2.2. Benchmark Results for Fissile Metal Plates

The normalized response of ^{235}U and ^{239}Pu fission chambers versus fissile sample thickness is shown in Fig. 3.3 using a 0.11-mm Gd filter. The fissile sample thicknesses shown in the following results were corrected to account for the 5.8 wt% ^{240}Pu in the ^{239}Pu samples and the 7.0 wt% ^{238}U in the ^{235}U samples. Therefore, the values shown on the x-axis in Fig. 3.3 represent the thickness of ^{239}Pu and ^{235}U in the samples not the total sample thickness. It is important to note that the dashed lines correspond to the 1968 measured results and the solid lines correspond to the MCNPX results. In addition, all

results have been normalized relative to the result for the zero sample thickness. The normalized detector fission rate is a measure of the transmission of epithermal neutrons through the sample weighted by the fission cross-section of the detector. These results decrease as a function of fissile sample thickness because the resonance absorption by ^{239}Pu or ^{235}U in the sample increases as the sample thickness increases. As a result, the transmitted flux reaching the detectors decreases as the sample thickness increases.

The self-indication effect is inversely proportional to the amount of resonance absorption in the sample. This effect is greater for ^{239}Pu because the ^{239}Pu fission resonance at 0.3-eV is an order of magnitude larger than the ^{235}U fission resonance at this energy. Thus, significantly more neutrons are absorbed by ^{239}Pu in this energy region. It is also important to note that there is good agreement between the 1968 measurements and MCNPX results. The percent difference between the MCNPX and experimental results for the normalized detector fission rate ranged from 3% to 12% for the ^{235}U detector and from 1% to 15% for the ^{239}Pu detector.

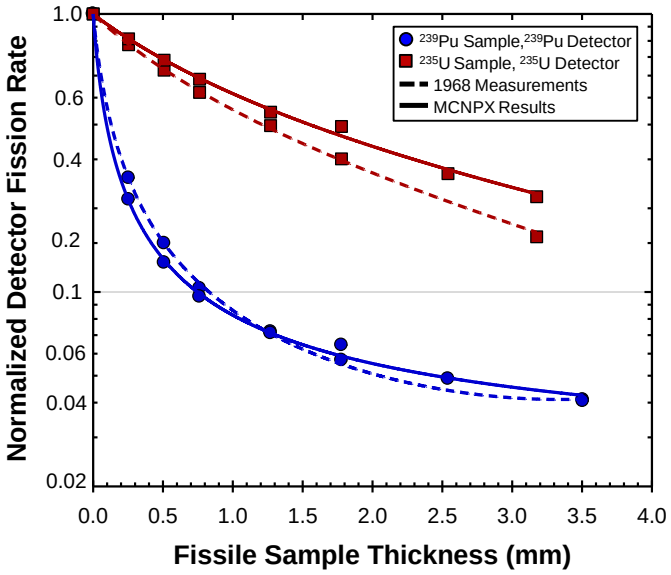

Fig. 3.3. Normalized detector fission rates versus fissile sample thickness using a 0.11-mm Gd filter.

The ratios of ^{235}U and ^{239}Pu detector responses to the ^{10}B detector response as a function of ^{239}Pu sample thickness are shown in Fig. 3.4. A 0.08-mm Gd filter was used to obtain these results. Similar to the previous results, the ^{239}Pu sample thickness was corrected to account for the 5.8 wt% ^{240}Pu in the samples. Using the ratio of detector fission rates to the ^{10}B(n,α) rate greatly reduces the sensitivity of the measured response to extraneous material present in the fissile sample. This occurs because the presence of extraneous material reduces both the ^{10}B detector and fission chamber response rates by approximately the same amount. The shapes of the curves for the ^{239}Pu and ^{235}U detectors in Fig. 3.4 indicate that ^{239}Pu is the fissile sample in the neutron beam. This is based on the fact that the results for the ^{239}Pu detector decrease with increasing ^{239}Pu sample thickness whereas the results for the ^{235}U detector increase with increasing ^{239}Pu sample thickness. Thus, the results obtained using the ^{239}Pu detector clearly show the self-indication effect.

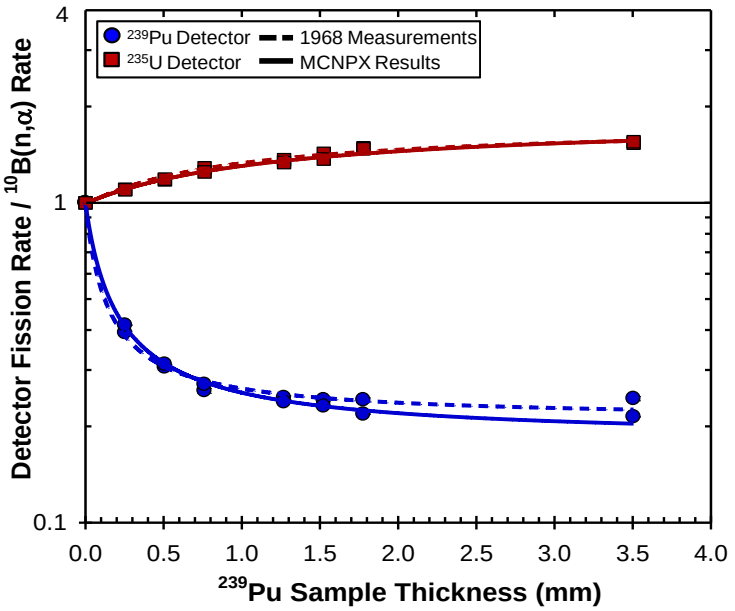

Fig. 3.4. Ratio of ^{239}Pu and ^{235}U detector fission rates to the ^{10}B detector (n,α) rate versus ^{239}Pu sample thickness using 0.08-mm Gd filter.

Referring to Fig. 3.4, it is also important to note that for ^{239}Pu sample thicknesses greater than ~1.5-mm the ratio of the ^{239}Pu fission rate to ^{10}B(n,α) rate levels off due to self-shielding effects occurring from saturation of the large ^{239}Pu resonance at 0.3-eV. For thicker samples, a Cd filter can be used to eliminate neutrons from the 0.3-eV region and to extend the sensitivity to the higher energy resonance region. In addition, we see very good agreement between the 1968 measurements and MCNPX results which validates the use of MCNPX to model SINRAD [10,13]. The percent difference between the MCNPX and experimental results for the normalized detector fission rate to ^{10}B(n,α) rate ratio ranged from 0.3% to 4% for the ^{235}U detector and from 2% to 12% for the ^{239}Pu detector. It should be noted that the percent difference in the ^{239}Pu detector ratio was less than 5% for all ^{239}Pu sample thicknesses except for 1.8-mm and 3.5-mm.

3.3. MOX Fuel Rods – 1969 Experiment

In 1969, General Electric and a consortium of research institutes, built the South East Fast Oxide Reactor (SEFOR) in Arkansas. This was a fast breeder reactor with liquid sodium coolant. During the initial fuel fabrication, some of the MOX fuel rods were mistakenly loaded with pellets containing the incorrect plutonium fraction. These rods, after receiving a low level of irradiation in SEFOR, were transferred to LASL for NDA of the plutonium loading in the pellets. Reactivity measurements of the fuel rods indicated that the Pu content in some rods was 5% to 40% less than specified by the manufacturer. To help resolve this problem, the 1969 experiment was conducted. In this experiment, SINRAD was used to measure the pellet-to-pellet Pu distribution in MOX fuel rods [11].

3.3.1. 1969 Experimental Setup and Procedure

In Fig. 3.5, a diagram of the 1969 experimental setup simulated in MCNPX is shown. Similar to the 1968 experiment, the neutron beam from the LASL Water Boiler Reactor was also used for the 1969 measurements. This beam was collimated through a 1.6-cm hole and filtered by 0.025-mm-thick Gd filter before passing through the MOX fuel rod and into the ^{239}Pu fission chamber. A mechanical scanner was used to advance

the MOX fuel rod across the neutron beam path in 0.76-cm increments. The MOX fuel rods consisted of cylindrical pellets approximately 2.3-cm in diameter and 1.6-cm high with a Pu enrichment ranging from 12 to 27 wt% Pu [12].

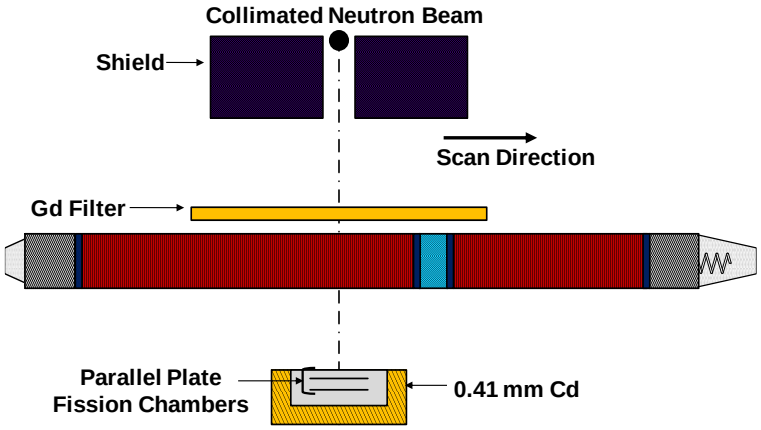

Fig. 3.5. Simulated experimental setup of 1969 experiment.

A schematic of the SEFOR fuel rod and the corresponding profile of the transmitted neutron flux measured using a 0.025-mm Gd filter and BF_3 neutron detector is shown in Fig. 3.6. This measurement was simulated in MCNPX by modeling each segment of the fuel element individually and tallying the transmitted neutron flux. The transmitted neutron flux is lowest at both ends of the fuel rod due to the dense nickel reflectors and is highest near the center of the rod due to the air gap that separates the fuel segments. The ^{238}U insulator pellets are clearly distinguishable from the MOX fuel pellets and can be used to eliminate the possibility of a rod containing only ^{238}U pellets [11,13].

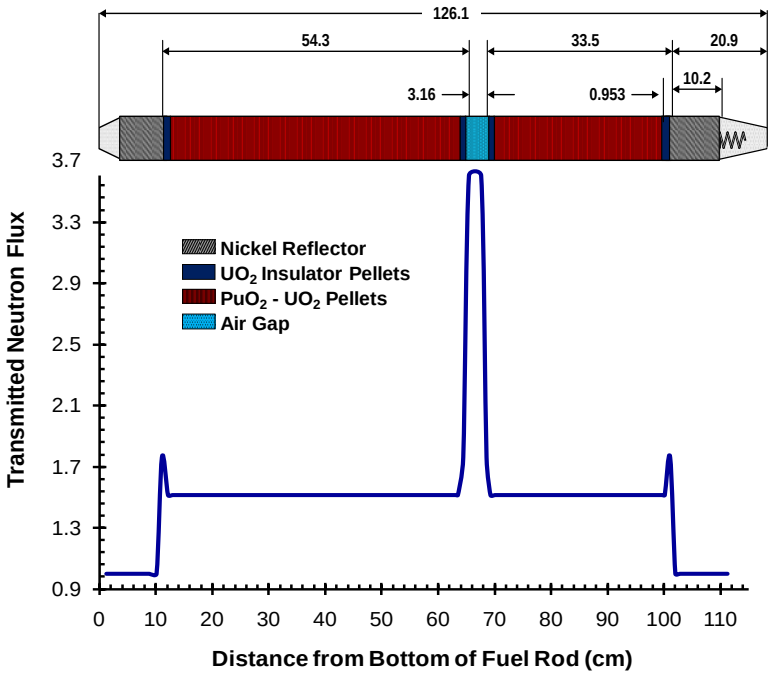

Fig. 3.6. Schematic of SEFOR fuel element and profile of neutron transmission data.

3.3.2. Benchmark Results for 1969 Experiment

The nondestructive assay results for six different SEFOR MOX fuel rods are given in Table 3.1. Rods 473 and A13 were given as standards with known Pu enrichments of 27.3% and 20.4%, respectively. The delayed-neutron yield technique was used to measure the amount of fissile material (^{239}Pu + ^{241}Pu), as well as, the total amount of fuel (U + Pu) in the other four rods that had previously been irradiated in the reactivity measurements. Gross neutron counting of (α,n) reactions in the MOX fuel was used to determine the total Pu content of the fuel rods. It is important to note that the amount of Pu in the four irradiated rods is significantly less than the amount of Pu in the two standard rods. The results given for the six different fuel rods were used to calculate the initial composition of the MOX pellets used in the MCNPX model of the 1969 experiment [11].

Table 3.1. Nondestructive assay results for SEFOR fuel rods.

Rod Number	*Delayed-Neutron Yield*			*Gross Neutron*
	U + Pu [g]	$Pu_{fissile}$ [g][c]	Pu / (U + Pu)	Pu [g]
473[a]	2930	549	20.4%	599
A13[a]	2949	738	27.3%	805
873[b]	2956 ± 30	339 ± 9	12.5%	416
878[b]	2926 ± 29	484 ± 12	18.1%	529
919[b]	2862 ± 29	458 ± 11	17.5%	501
920[b]	2900 ± 29	445 ± 11	16.8%	496

[a] *Specifications for the standard rods (A13 & 473)*
[b] *Rods previously irradiated in reactor reactivity measurements*
[c] $Pu_{fissile} = {}^{239}Pu + {}^{241}Pu$

The axial Pu distribution measured in SEFOR fuel rod 878 obtained from the SINRAD neutron scan is shown in Fig. 3.7. This measurement was simulated in MCNPX for selected data points and the results are shown in red in Fig. 3.7. The excellent agreement between the 1969 measurements and the MCNPX results for the selected data points confirms that MCNPX is accurately modeling the physics of SINRAD. In the 1969 experiment, the total ^{239}Pu content was obtained by integrating the area under the axial Pu scan using the following equation:

$$C_{Total}^{Pu239} = \sum_{n=1}^{N} \frac{1}{C_n^{Pu239}} \tag{3.1}$$

where C_{Total}^{Pu239} is the total inverse ^{239}Pu fission rate for a fuel rod, C_n^{Pu239} is the inverse ^{239}Pu fission rate at axial position n on the fuel rod, and N is the total number of axial measurements made along the fuel rod. Standard fuel rods A13 and 473 were used to establish the calibration curve. The total inverse ^{239}Pu fission rate versus total fissile plutonium mass is shown in Fig. 3.8 for five different MOX fuel rods. These values were normalized to MCNPX results for inverse ^{239}Pu fission rate to obtain the calibration curves shown in Fig. 3.8. It is important to note that the SINRAD measurements for the SEFOR fuel pins was accurate enough to identify the Pu enrichment of the misplaced

pellets, and show that the production pellets of 12 wt% Pu had been accidentally loaded into the MOX rod with 20 wt% Pu pellets [12,13].

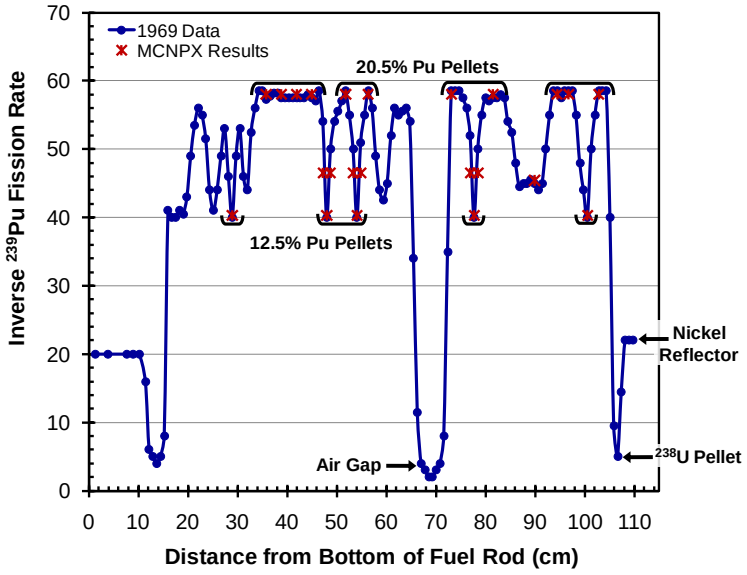

Fig. 3.7. Axial Pu distribution in SEFOR Rod 878 obtained from "self-indication" neutron scan.

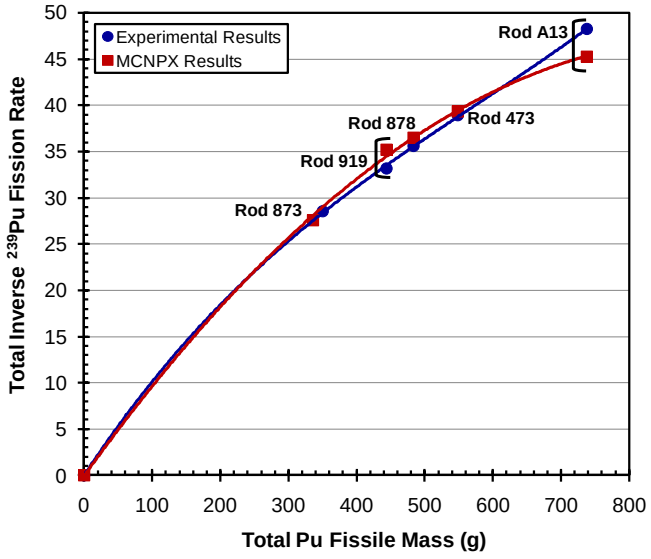

Fig. 3.8. Total inverse ^{239}Pu fission rate for each fuel rod as function of total fissile plutonium mass.

3.4. Summary of Benchmark Case Study Results

MCNPX simulations of SINRAD were performed to determine the thickness of ^{235}U and ^{239}Pu metals plates (1968 experiment) and the plutonium enrichment of pellets in MOX fuel rods (1969 experiment). For the 1968 experiment, the percent difference between the MCNPX and experimental results for ^{239}Pu metal plates ranged from 0.3% to 4% for the ^{235}U(n,f) / ^{10}B(n,α) ratio and from 2% to 12% for the ^{239}Pu(n,f) / ^{10}B(n,α) ratio. For the 1969 experiment, the percent difference between the MCNPX and experimental results for the total inverse ^{239}Pu fission rate ranged from 0.7% to 5% for five different Pu loadings in the MOX fuel rods. The good agreement between the MCNPX results and the 1968 and 1969 experimental measurements confirms the accuracy of the MCNPX models used. Benchmarking simulated results against experimental data is of significant importance to validate the use of MCNPX as a computational tool to simulate SINRAD and assess the accuracy of the MCNPX models used. Furthermore, this enables these models of SINRAD to be applied to more complex geometries, such as LWR fuel assemblies.

3.5. Application of 1968 Experiment to LWR Spent Fuel Assemblies

In the 1968 experiment, the thickness of ^{239}Pu and ^{235}U metal plates was measured using ^{239}Pu and ^{235}U FCs to obtain a better understanding of self-shielding effects on the SINRD measurements [10]. This can be related to LWR spent fuel by calculating the effective ^{239}Pu heavy metal (HM) thickness of the assembly using the following equation:

$$t^{Pu239} = \frac{M^{Pu239}}{\rho_{Pu} \cdot A_{FA}} \tag{3.2}$$

where t^{Pu239} is the effective ^{239}Pu HM thickness of the fuel assembly [cm ^{239}Pu HM], M^{Pu239} is the mass of ^{239}Pu in the fuel assembly [g ^{239}Pu HM], ρ_{Pu} is the density of plutonium metal (where ρ_{Pu} = 19.8 g/cm^3), and A_{FA} is the effective area (width x height) of fuel assembly (where A_{FA} = 8247 cm^2 for PWR 17x17 fuel assembly and A_{FA} = 4799

cm^2 for BWR 9x9 fuel assembly). The above equation can also be easily modified to calculate the effective ^{235}U HM thickness of the assembly.

The 1968 results for the normalized detector fission rate as a function of (a) ^{239}Pu and (b) ^{235}U metal sample thickness is shown in Fig. 3.9. The dashed lines represent the effective ^{239}Pu and ^{235}U HM thickness of PWR 17x17 spent LEU and MOX fuel assemblies with burnup of 40-GWd/MTU and cooling time of 5-yrs. An initial enrichment (IE) of 4% ^{235}U and 6% Pu was used for spent LEU and MOX fuel, respectively. For LEU spent fuel, the effective ^{239}Pu and ^{235}U HM thickness is 0.16 mm and 0.3 mm, respectively. For MOX spent fuel, the effective ^{239}Pu HM thickness is 0.43 mm. The effective ^{235}U and ^{239}Pu HM thickness of fresh LEU and MOX fuel assemblies is 1.26 mm and 1.0 mm, respectively. Referring to Fig. 3.9(a), it is important to note that for ^{239}Pu samples greater than 1.5-mm thick, the self-interrogation signature for both ^{235}U and ^{239}Pu FCs has saturated due to self-shielding effects. Based on these results, we can clearly see that the effective ^{239}Pu HM thickness of PWR spent LEU and MOX fuel assemblies is well below the thickness at which self-shielding effects occur.

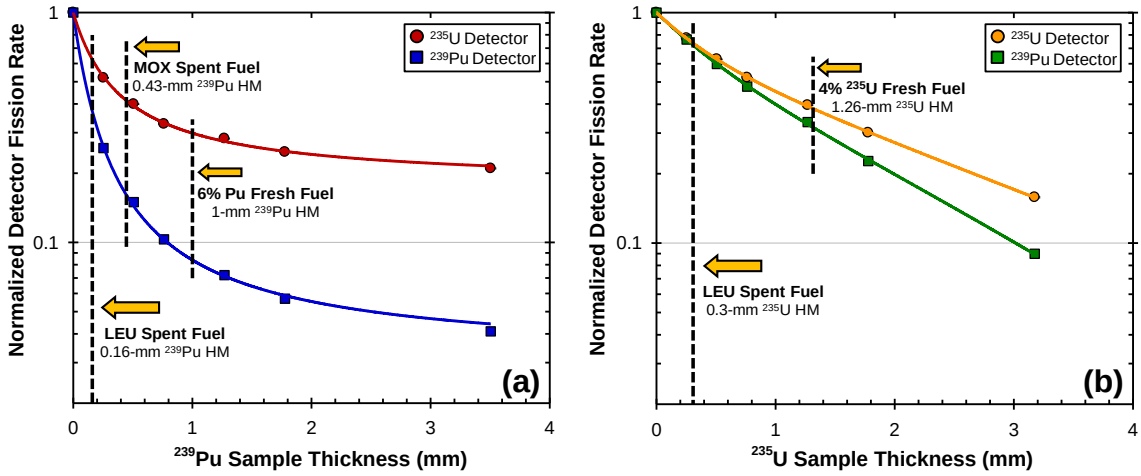

Fig. 3.9. Normalized detector fission rate as a function of (a) ^{239}Pu and (b) ^{235}U metal sample thickness using 0.11 mm Gd filter.

4. DESCRIPTION OF SINRD MEASUREMENT SYSTEM

4.1. SINRD Instrument Concept

Using the basic physics concept for SINRD described in section 3, we have designed a detector system for measuring LWR fuel assemblies. Since the fuel assemblies considered in this research have square lattices, the SINRD detector unit was designed to be rectangular where the width of the SINRD unit is equal to the width of the assembly. The SINRD detector unit consists of four FCs:

- Bare FC: expected to measure thermal neutrons leaking from the FA
- Boron Carbide (B_4C) FC: expected to measure fast neutrons leaking from the FA
- Gd covered FC: expected to measure neutrons above 0.13-eV leaking from the FA
- Cd covered FC: expected to measure neutrons above 1.25-eV leaking from the FA

It should be noted that throughout the rest of this dissertation, we refer to the B_4C FC as FFM (or Fast Flux Monitor). The SINRD FCs are directly related to the physical characteristics of the fuel assembly. We can derive these relationships using a 3-group neutron lifecycle shown in Fig. 4.1 and some simple definitions, specifically:

$$P_{FL} = 1 - P_{FNL} \tag{4.1}$$

$$P_{EL} = 1 - P_{ENL} \tag{4.2}$$

$$P_{TL} = 1 - P_{TNL} \tag{4.3}$$

$$\varepsilon_{abs}^{FFM} \equiv \textit{absolute detector efficiency for the FFM} \tag{4.4}$$

$$\varepsilon_{abs}^{Bare} \equiv \textit{absolute detector efficiency for the Bare FC} \tag{4.5}$$

$$\varepsilon_{abs}^{Gd} \equiv \textit{absolute detector efficiency for the Gd covered FC} \tag{4.6}$$

$$\varepsilon_{abs}^{Cd} \equiv \textit{absolute detector efficiency for the Cd covered FC} \tag{4.7}$$

where P_{FL}, P_{EL}, and P_{TL} are the fast, epithermal and thermal leakage probabilities, respectively.

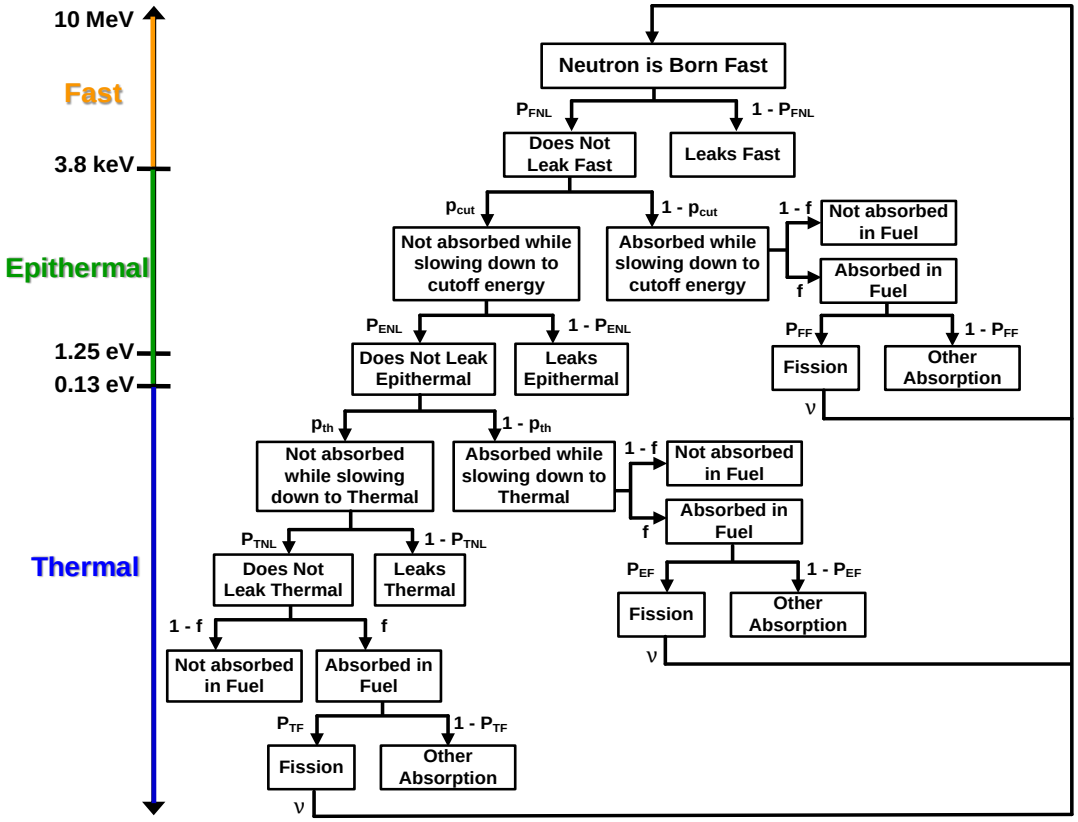

Fig. 4.1. 3-group neutron lifecycle.

The 3-group neutron lifecycle begins with a neutron born fast. The probability that the neutron does not leak from the assembly while fast is the fast nonleakage probability, P_{FNL}. If the neutron did not leak while fast, then p_{cut} is the probability that the neutron will not get absorbed in a resonance while slowing down from 3.8-keV to the epithermal cutoff energy (either 0.13-eV for Gd or 1.25-eV for Cd). The epithermal nonleakage probability, P_{ENL}, is the probability that the neutron does not leak from the assembly while epithermal given it was not absorbed while slowing down. If the neutron did not leak while epithermal, then p_{th} is the probability that the neutron will not get absorbed in a resonance while slowing down from the epithermal cutoff to thermal energies. The probability that the neutron does not leak from the assembly while thermal is the thermal nonleakage probability, P_{TNL}. If the neutron is absorbed while slowing down from fast to

thermal energies, the fuel utilization factor, *f*, represents the fraction of neutrons that are absorbed in the fuel out of the total number of neutrons absorbed in the FA [38]. P_{FF}, P_{EF}, and P_{TF} represent the probabilities of fast, epithermal, and thermal fission, respectively, given that the neutron was absorbed in the fuel.

The Bare FC is used to measure the gross neutron leakage from the fuel assembly. For a given geometry and material composition, this FC would serve as a measure of the neutron source strength in the FA. It is also a measure of the neutron multiplication† [38], the resonance escape probability from the B_4C cutoff energy (3.8-keV) to thermal energies, and the thermal leakage probability of the assembly. Thus, the expected count rate in the Bare FC can be expressed by the following equation:

$$C_{Bare} = S \cdot M \cdot P_{FNL} \cdot p_{th} \cdot p_{cut} \cdot P_{ENL} \cdot \left(1 - P_{TNL}\right) \cdot \varepsilon_{abs}^{Bare} \tag{4.8}$$

where C_{Bare} is the expected count rate in the Bare FC [cps], S is the neutron source strength [n/s], and M is the neutron multiplication.

The FFM measures the fast neutron leakage from the fuel assembly. This FC is a function of the neutron source strength, neutron multiplication and the fast leakage probability of the fuel assembly. The expected count rate in the FFM is given by:

$$C_{FFM} = S \cdot M \cdot \left(1 - P_{FNL}\right) \varepsilon_{abs}^{FFM} \tag{4.9}$$

where C_{FFM} is the count rate in the FFM [cps].

The Gd and Cd covered FCs are intended to measure the resonance absorption from ^{235}U and ^{239}Pu in LWR spent fuel. Both Gd and Cd have large absorption cross-sections in the resonance energy region. The thickness of each of these absorber filters was chosen based on the desired absorption cutoff energy relative to the ^{235}U and ^{239}Pu fission cross-sections. We chose to use 0.025-mm thick Gd with cutoff energy of 0.13-eV and 3-mm thick Cd with cutoff energy of 1.25-eV. The transmitted flux through Gd, Cd, and B_4C relative to ^{235}U and ^{239}Pu fission cross-sections is shown in Fig. 4.2. Based on the location of the Gd and Cd absorption cut-off energies, we see that the thick Cd

† Neutron multiplication, *M*, is defined as the ratio of the total number of neutrons produced from induced fission and spontaneous fission to the total number of neutrons produced from spontaneous fission.

filter (3.0 mm) absorbs the majority of neutrons in the low energy region of the ^{235}U and ^{239}Pu fission resonances whereas the thin Gd filter (0.025 mm) transmits the majority of these lower energy neutrons. The expected count rates in the Gd and Cd covered FCs given below are a function of the neutron source strength, multiplication, epithermal leakage probability, and the resonance escape probability from the B_4C cutoff energy to the Gd and Cd cutoff energies of the assembly:

$$C_{Gd} = S \cdot M \cdot P_{FNL} \cdot p_{cut}^{Gd} \cdot \left(1 - P_{ENL}^{Gd}\right) \varepsilon_{abs}^{Gd} + S \cdot M \cdot \left(1 - P_{FNL}\right) \varepsilon_{abs}^{fast} \tag{4.10}$$

$$C_{Cd} = S \cdot M \cdot P_{FNL} \cdot p_{cut}^{Cd} \cdot \left(1 - P_{ENL}^{Cd}\right) \varepsilon_{abs}^{Cd} + S \cdot M \cdot \left(1 - P_{FNL}\right) \varepsilon_{abs}^{fast} \tag{4.11}$$

where C_{Gd} and C_{Cd} are the expected count rates in the Gd and Cd FCs [cps], respectively.

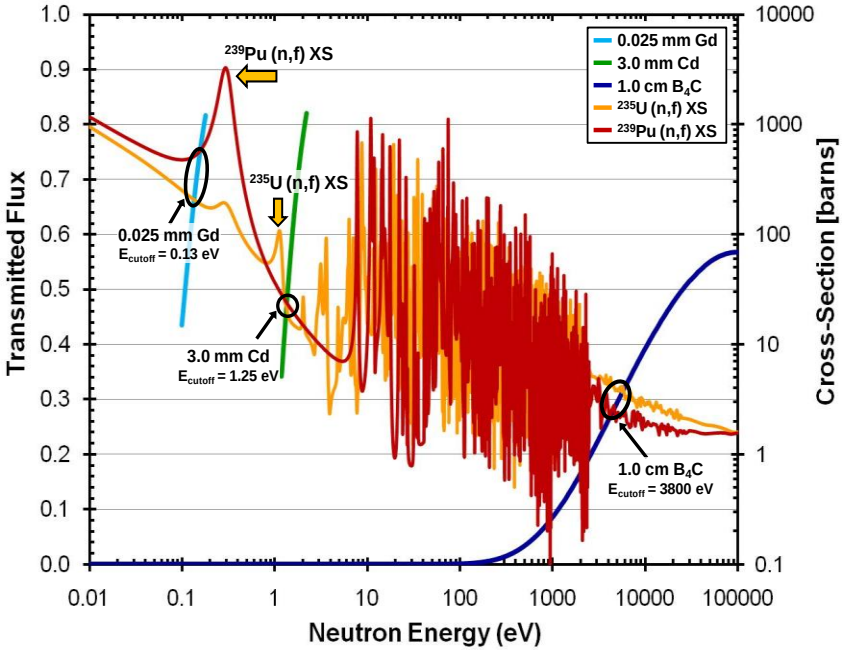

Fig. 4.2. Cut-off energies of SINRD absorber filters relative to ^{235}U and ^{239}Pu fission cross-sections**.**

SINRD uses ratios of different fission chambers to reduce the sensitivity of the measurements to extraneous material present in fuel (e.g. fission products). This also

reduces the number of unknowns we are trying measure because the neutron source strength and detector-fuel assembly coupling cancels in the ratio. Using the relationships given above for each FC, we can derive the equations for different SINRD ratios. For instance, the FFM / Bare FC ratio is given by:

$$\frac{C_{FFM}}{C_{Bare}} = \frac{S \cdot M \cdot \left(1 - P_{FNL}\right) \varepsilon_{abs}^{FFM}}{S \cdot M \cdot P_{FNL} \cdot p_{th} \cdot p_{cut} \cdot P_{ENL} \cdot \left(1 - P_{TNL}\right) \cdot \varepsilon_{abs}^{Bare}} \tag{4.12}$$

The neutron source strength and multiplication cancel in the ratio. Substituting Eq.(4.1), (4.2), and (4.3) for P_{FL}, P_{EL}, and P_{TL}, respectively, we obtain:

$$\frac{C_{FFM}}{C_{Bare}} = \frac{P_{FL}}{\left(1 - P_{FL}\right)} \frac{1}{p_{th} \cdot p_{cut} \cdot \left(1 - P_{EL}\right)} \frac{1}{P_{TL}} \frac{\varepsilon_{abs}^{FFM}}{\varepsilon_{abs}^{Bare}} \tag{4.13}$$

It should be noted that $p = p_{th} \cdot p_{cut} \cdot (1 - P_{EL})$ for the 2-group form of a neutron lifecycle. Therefore, we can express the FFM / Bare FC ratio as:

$$\frac{C_{FFM}}{C_{Bare}} = \frac{P_{FL}}{\left(1 - P_{FL}\right)} \frac{1}{p \cdot P_{TL}} \frac{\varepsilon_{abs}^{FFM}}{\varepsilon_{abs}^{Bare}} \tag{4.14}$$

This ratio is proportional to $P_{FL} / (1 - P_{FL})$ and inversely proportional to $p \cdot P_{TL}$. The fast leakage probability, P_{FL}, is primarily a function of the geometry of the system and thus, the term $P_{FL} / (1 - P_{FL})$ is essentially a constant. The ratio of detector efficiencies is also a constant. The thermal leakage probability, P_{TL}, and the resonance escape probability, p, are a function of the system geometry and the composition of the fuel pins. In regards to the fuel composition, these terms are most sensitive to the amount of thermal absorbers (e.g. ^{235}U, ^{239}Pu, and ^{149}Sm) present in the fuel. These terms are also sensitive to the concentration of boron in the water. Thus, the FFM / Bare FC ratio is sensitive to reactivity changes in the fuel assembly due to changes in the concentrations of thermal absorbers.

Next, we will derive the relationship for the FFM / (Gd – Cd) FC ratio. Using Eq.(4.9), (4.10), and (4.11), this SINRD ratio is given by:

$$\frac{C_{FFM}}{C_{Gd}-C_{Cd}}=\frac{S\cdot M\cdot\left(1-P_{FNL}\right)\varepsilon_{abs}^{FFM}}{S\cdot M\cdot P_{FNL}\cdot p_{cut}^{Gd}\cdot\left(1-P_{ENL}^{Gd}\right)\varepsilon_{abs}^{Gd}-S\cdot M\cdot P_{FNL}\cdot p_{cut}^{Cd}\cdot\left(1-P_{ENL}^{Cd}\right)\varepsilon_{abs}^{Cd}} \quad (4.15)$$

Similar to the FFM / Bare ^{235}U FC ratio, the neutron source strength and multiplication cancel in the ratio. Substituting Eq.(4.1) and (4.2) for P_{FL} and P_{EL}, respectively, and factoring out P_{FNL} in the denominator, we obtain:

$$\frac{C_{FFM}}{C_{Gd}-C_{Cd}}=\frac{P_{FL}\varepsilon_{abs}^{FFM}}{P_{FNL}\cdot\left(p_{cut}^{Gd}\cdot P_{EL}^{Gd}\varepsilon_{abs}^{Gd}-p_{cut}^{Cd}\cdot P_{EL}^{Cd}\varepsilon_{abs}^{Cd}\right)} \quad (4.16)$$

Assuming that $\varepsilon^{Gd} = \varepsilon^{Cd} = \varepsilon^{epi}$ and substituting in the relationship $P_{FNL} = 1 - P_{FL}$, we obtain the following equation for the FFM / (Gd – Cd) ^{235}U FC ratio:

$$\frac{C_{FFM}}{C_{Gd}-C_{Cd}}=\frac{P_{FL}}{\left(1-P_{FL}\right)}\frac{1}{\left(p_{cut}^{Gd}\cdot P_{EL}^{Gd}-p_{cut}^{Cd}\cdot P_{EL}^{Cd}\right)}\frac{\varepsilon_{abs}^{FFM}}{\varepsilon_{abs}^{epi}} \quad (4.17)$$

This ratio is inversely proportional to ($p_{cut}^{Gd}\cdot P_{EL}^{Gd} - p_{cut}^{Cd}\cdot P_{EL}^{Cd}$) and proportional to P_{FL} / (1 – P_{FL}). The Gd and Cd resonance escape probabilities, p_{cut}, and the epithermal leakage probabilities, P_{EL}, are a function of the system geometry and the composition of the fuel pins. These terms are sensitive to resonance absorbers (e.g. ^{235}U, ^{238}U, and ^{239}Pu) present in the fuel. We expect the Gd and Cd epithermal leakage probabilities to be fairly close since the difference between the Gd and Cd cutoff energies is small. However, the Gd and Cd resonance escape probabilities will be different. To better understand why these terms are different, let us assume that $p_{cut} = p^{U238}\cdot p^{U235}\cdot p^{Pu239}\cdot p^{other}$. For the Gd ^{235}U FC, the values for p^{U235} and p^{Pu239} will be lower compared to the Cd ^{235}U FC due to resonance absorption in ^{239}Pu and ^{235}U fission resonances near 0.3-eV. Since ^{238}U does not have an absorption resonance between 0.13-eV and 1.25-eV, we expect p^{U238} to be the same for both Gd and Cd FCs. Thus, the FFM / (Gd – Cd) ^{235}U FC ratio primarily a measure of 1 / $P_{EL}\cdot$ ($p_{cut}^{Gd} - p_{cut}^{Cd}$) which is sensitive to resonance absorption within the (Gd – Cd) energy window. It is also important to note that this ratio is only sensitive to absorbers that have resonances in this energy window which makes it insensitive to most fission product absorbers.

4.2. SINRD Detector Configuration

The SINRD detector unit, shown in Fig. 4.3, is approximately 10.4-cm high, 9.0-cm long, and 21.4-cm wide for a PWR assembly and 13.5-cm wide for a BWR assembly. In practice, SINRD would be located adjacent to the assembly. To increase counting statistics, the FFM was embedded in polyethylene to thermalize the fast neutrons that penetrated the boron shielding. The polyethylene was covered with 1.0-mm of Cd to reduce the background from thermal neutrons reentering the SINRD unit. We modeled a fissile loading of 1.5-mg/cm^2 in the SINRD FCs using a 2-layer deposit thickness typical of standard commercial FCs. The ^{235}U FCs contained 93 wt% ^{235}U metal (19.1-g/cm^3) and the ^{239}Pu FCs contained 94 wt% ^{239}Pu metal (19.8-g/cm^3).

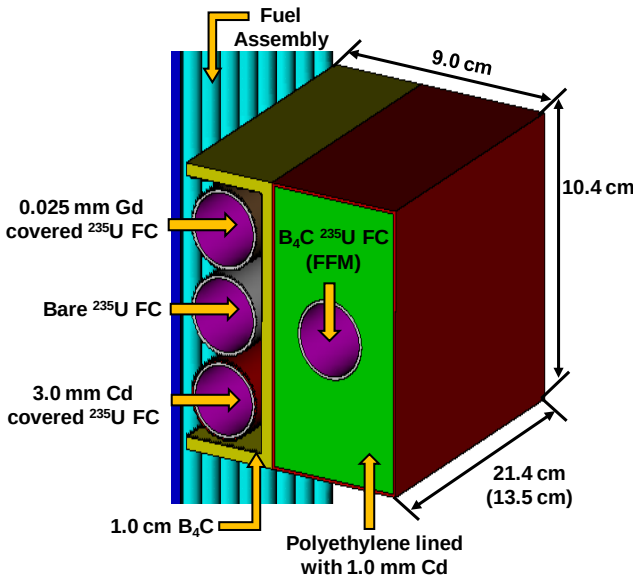

Fig. 4.3. SINRD detector configuration simulated in MCNPX.

The SINRD detector configuration was optimized for PWR and BWR spent fuel based on the concentration of ^{239}Pu relative to ^{240}Pu over the burnup range of 0 to 50-GWd (see Sections 8 and 9). For the spent fuel simulations, we have investigated the use of Gd and Cd ^{239}Pu FCs to determine how using ^{239}Pu in FCs affects the sensitivity of

the SINRD detector ratio to the ^{239}Pu in spent fuel. This is especially important for spent LEU fuel because the ^{239}Pu and ^{235}U fractions are nearly equal at burnups greater than 30-GWd/MTU. It should be noted, however, that ^{239}Pu FCs are not commercially available and would have to be specially manufactured. This could greatly increase the cost of SINRD. Also, due to licensing constraints of nuclear facilities, it may be difficult to get approval to bring ^{239}Pu FCs into a facility. As a result, the IAEA might prefer all ^{235}U FCs for the actual implementation of SINRD. Thus, for the fresh fuel simulations, only ^{235}U FCs were modeled for SINRD. It is important to note that the SINRD method requires a calibration with a reference assembly of similar geometry. However, since this densitometry method uses the ratios of different detectors, most of the systematic errors related to calibration and positioning cancel in the ratios. In addition, SINRD can be calibrated with a fresh fuel assembly because it is not sensitive to neutron absorbing fission products in spent fuel [14].

4.3. Overview of MCNPX Simulations of SINRD

In order to simulate the expected count rates in the SINRD fission chambers in MCNPX, three separate runs were performed using three different input decks. Due to the very thin deposit of fissile material in the fission chambers and the use of different absorber filters, only a small fraction of the particle histories will actually contribute to the fission rate tally in the detector. Thus, the problem was divided into three parts and variance reduction was used in order to ensure adequate statistics were obtained for each fission rate tally in the SINRD detectors. It is important to note that the problem geometry remained fixed for all MCNP runs; the only difference was what detectors were specified in the tallies. For the three separate runs, the fission rate was tallied in the following SINRD detectors: (1) FFM and Bare ^{235}U FCs, (2) Gd covered ^{235}U FC, and (3) Cd covered ^{235}U FC. Appendix A contains example MCNPX input decks used to model SINRD for a PWR 17x17 spent LEU fuel assembly (4% ^{235}U) and a BWR 9x9 spent MOX fuel assembly (6% Pu) in water with burnup of 40-GWd/MTU and cooling time of 5-yrs.

4.2.1. Variance Reduction Techniques

In order to achieve good statistics on the fission rate tallies in the SINRD detectors and minimize the total computational time required, the following variance reduction techniques were used: forced collisions, weight windows, and analog capture. The goal of variance reduction (VR) is to improve the tally precision, uncertainty in the mean, by increasing the history-scoring efficiency of the tally and decreasing the spread of nonzero history scores. The precision of a tally is determined by statistical fluctuations in the tally histories for the portion of phase space sampled [39]. Thus, it is very important to ensure that the variance reduction techniques used in the problem improve the sampling of particles that contribute to the tally.

4.2.1.1. Forced Collisions (FCL:n)

In order to improve the estimate of the fission rate in the SINRD detectors, the forced collision method was used to increase the sampling of collisions in the cells that contain the ^{235}U/^{239}Pu FC deposits. This method splits particles into collided and uncollided components. The collided part is forced to collide within the current cell and the uncollided part exits the cell without collision. The particle weights of the collided and uncollided components are calculated using the following equations:

$$W_C = W_0\left(1 - e^{-\Sigma_t d}\right) \tag{4.18}$$

$$W_U = W_0 e^{-\Sigma_t d} \tag{4.19}$$

where W_C is the collided particle weight, W_U is the uncollided particle weight, W_0 is the current particle weight before the forced collision, Σ_t is the total macroscopic cross-section of the cell material, and d is the distance to the cell surface in the particle's direction [39]. Thus, the forced collisions method increases the fraction of neutrons that contribute to the tally without increasing the number of histories (N) calculated in the problem. This is needed because the ^{235}U deposit thickness in a fission chamber is only ~79-μm which is orders of magnitude smaller than the average neutron mean free path in ^{235}U metal. A schematic of the forced collisions method is shown in Fig. 4.4(a).

4.2.1.2. Weight Windows (WWG, WWP:n, MESH)

The weight windows variance reduction method uses splitting and Russian roulette to improve the sampling of particles [Fig. 4.4(b)]. We have used mesh-based weight windows to generate an importance function for neutrons in space and energy. Three important weights are used to define a weight window: lower weight bound W_L, the survival weight for Russian roulette W_S, and upper weight bound W_U. In important regions, neutrons are split into several neutrons with an appropriate weight adjustment. In unimportant regions, the Russian roulette game is played and the neutron's weight is either increased by the reciprocal of the survival probability or the neutron history is terminated [39]. The entire geometry (spent fuel assembly, SINRD pod, and surrounding water) is covered by a non-uniform rectangular mesh that varies from coarse to fine based on spatial location relative to the SINRD detector unit. The use of weight windows significantly improves the statistics on f4 fission rate tallies by generating an optimum importance function that estimates the importance of neutrons in each space-energy region defined in the mesh. This also reduces computational time required because more time is used to track neutrons that will likely contribute to the tally based on the higher importance of the space-energy region.

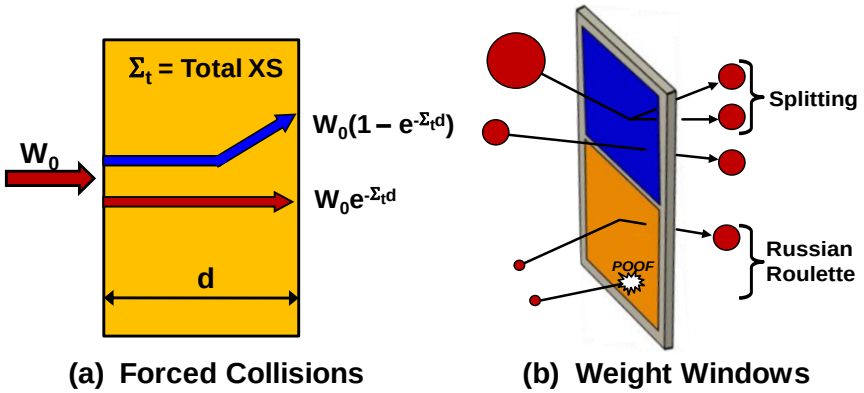

Fig. 4.4. Schematic of (a) forced collisions and (b) weight windows variance reduction methods.

4.2.1.3. Analog Capture (CUT:n)

When using weight windows, it is important to change the default for neutrons from implicit capture to analog capture. In analog absorption, a neutron is killed based the probability σ_a / σ_t where σ_a and σ_t are the microscopic absorption and total cross-sections of the collision nuclide at the incoming neutron energy [39]. The use of analog capture prevents low weight neutrons generated by the weight windows from being overly killed by Russian roulette from the default weight cutoff in regions of phase space where weight windows are not generated ($W = 0$).

Fig. 4.5 shows an example of how these variance reduction techniques would be implemented in an MCNPX input deck (a) and the optimized weight windows generated for the FFM and Bare ^{235}U FCs (b). These results are shown for PWR 17x17 spent LEU fuel (30-GWd/MTU, 5-yrs cooled). The f4 tallies were specified for FFM and Bare ^{235}U FCs. The FCL:n card is highlighted in yellow because the values on this card are the only values that will change if the f4 tallies are changed to Gd or Cd ^{235}U FCs.

```
CUT:n 2j 0 0                $ Turns on Analog Capture
FCL:n 1j 1 2j 1 27j         $ Forces Collisions in Bare & FFM FCs
WWG 44 0                    $ Optimize Weight Windows for TALLY 44
WWP:n 5 3 5 0 -1            $ Default Weight Window Parameters
MESH geom=rec ref 0 0 0 origin -26 -26 -202
     imesh -11 11 26  iints 3  5  3
     jmesh -11 11 12.4 13.8 16.2 17.5 18.8 26  jints 3 5 1 1 1 1 1 1
     kmesh -30 -10 -4.3 -1.5 1.4 4.1 10 30 202 kints 1 1 1 1 1 1 1 1 1
```

(a)

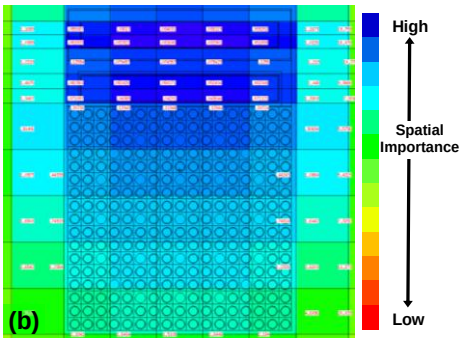

Fig. 4.5. Use of variance reduction techniques to optimize the total fission rate in Bare and FFM ^{235}U FCs for PWR spent LEU fuel with 30-GWd burnup.

4.2.2. Effect of Variance Reduction on SINRD Results

MCNPX uses the following 10 statistical checks to assess the statistical behavior of each tally based on the results for the estimated mean ($\bar{x}$), relative error (R), variance of variance (VOV), figure of merit (FOM), and slope of the largest history scores of $f(x)$:

1) no up or down trend in $\bar{x}$ as a function of histories *N* for last half of problem
2) magnitude of R is < 0.10 for a non-point detector tally
3) R monotonically decreases as a function of *N* for last half of problem
4) $1/\sqrt{N}$ decrease in R as a function of *N* for last half of problem
5) magnitude of VOV is < 0.10 for all types of tallies
6) VOV monotonically decreases as a function of *N* for last half of problem
7) $1/N$ decrease in VOV as a function of *N* for last half of problem
8) FOM is statistically constant as a function of *N* for last half of problem
9) nonmonotonic behavior in FOM as a function of *N* for last half of problem
10) ***slope*** of the top 25 to 201 largest history scores, x, should be >3.0 such that the 2nd moment, $\int_{-\infty}^{\infty} x^2 f(x) dx$ exists if the slope is extrapolated to infinity

It is important to note that passing all of these checks does not guarantee that the confidence intervals formed will always cover the expected results the correct fraction of the time [39].

The effect of variance reduction on the 10 statistical checks for each SINRD FC is compared in Table 4.1 and Table 4.2 for 30-GWd/MTU BWR spent LEU fuel (3% ^{235}U IE) and PWR spent MOX fuel (6% Pu IE), respectively. The time shown in the tables below represents the computational time, in minutes, required to complete the problem. All cases were run on the same cluster using 128 processors and divided into three separate runs as described above.

The FOM is the best measure of the computational efficiency of a MCNPX calculation where FOM = 1 / (Time·R^2). For BWR spent LEU fuel, the use of variance reduction increased the FOM by a factor of 68 for the FFM, a factor of 11 for Bare ^{235}U FC, a factor of 23 for Gd ^{235}U FC, and a factor of 28 for Cd ^{235}U FC. For PWR spent MOX fuel, variance reduction increased the FOM by a factor of 50 for the FFM, a factor of 9 for Bare ^{235}U FC, a factor of 16 for Gd ^{235}U FC, and a factor of 13 for Cd ^{235}U FC. Thus, based on these results, we can conclude that the use of variance reduction has significantly improved the computational efficiency of our MCNPX simulations.

Table 4.1. Comparison of MCNPX statistical checks for BWR spent LEU fuel with and without variance reduction.

SINRD Detector Tally		*Statistical Checks for BWR Spent LEU Fuel*						
		Mean	**R**	**VOV**	**Slope**	**FOM**	**Pass/Fail**	**Time**
Bare ^{235}U	NO VR	6.969E-06	0.0027	0.0014	5.1	11	passed	13284
	VR	6.955E-06	0.0028	0.0016	4.6	120	passed	1056
FFM ^{235}U	NO VR	2.123E-05	0.0028	0.0001	7.4	10	passed	13284
	VR	2.123E-05	0.0012	0.0000	5.6	648	passed	1056
Gd ^{235}U	NO VR	2.232E-06	0.0027	0.0026	3.2	11	passed	13263
	VR	2.247E-06	0.0025	0.0026	3.6	250	missed 1	640
Cd ^{235}U	NO VR	1.271E-06	0.0032	0.0169	3.5	7	missed 2	13264
	VR	1.268E-06	0.0026	0.0130	3.5	204	passed	712

Table 4.2. Comparison of MCNPX statistical checks for PWR spent MOX fuel with and without variance reduction.

SINRD Detector Tally		*Statistical Checks for PWR Spent MOX Fuel*						
		Mean	**R**	**VOV**	**Slope**	**FOM**	**Pass/Fail**	**Time**
Bare ^{235}U	NO VR	5.230E-06	0.0026	0.0039	4.0	7	missed 2	21474
	VR	5.225E-06	0.0025	0.0008	5.4	57	passed	2742
FFM ^{235}U	NO VR	3.298E-05	0.0022	0.0001	10.0	10	passed	21474
	VR	3.291E-05	0.0009	0.0000	10.0	486	passed	2742
Gd ^{235}U	NO VR	2.596E-06	0.0023	0.0040	4.0	9	passed	21484
	VR	2.586E-06	0.0018	0.0012	6.1	149	passed	2037
Cd ^{235}U	NO VR	1.835E-06	0.0023	0.0020	5.0	9	passed	21483
	VR	1.849E-06	0.0020	0.0030	4.3	118	passed	2084

5. ANALYSIS OF PWR 17X17 FRESH FUEL ASSEMBLY

In order to obtain a better understanding of the underlying physics of the SINRD measurement technique, we have simulated PWR 17x17 fresh LEU and MOX fuel assemblies in water where only the concentration of fissile material (either ^{235}U or ^{239}Pu) was changing. For the fresh LEU fuel cases, the initial enrichment was varied from 1.0 to 5.0 wt% ^{235}U to observe how the measured response changes as a function of the ^{235}U content in the fuel. Similarly, for the fresh MOX fuel cases, the Pu loading in the MOX fuel was varied from 2 to 10 wt% Pu to observe how the measured response changes as a function of the ^{239}Pu content in the fuel. The PWR fresh LEU and MOX fuel assemblies were simulated in water with and without 2200-ppm boron to determine how the absorption of low energy neutrons by boron in water affects the detector response. The specifications used to model the PWR 17x17 fuel assembly are given in Table 5.1.

Table 5.1. Specifications for PWR 17x17 fresh fuel assembly.

Assembly Data		
Lattice geometry		17 x 17 (square)
Assembly width		21.4 cm
Fuel pin pitch		1.25 cm
Number of fuel pins		264
Moderator		Light Water
Fuel Pin Data		
Fuel material		UO_2 / MOX
Cladding material		Zircaloy-2
Fissile Content	LEU Fuel	0.2% – 5% ^{235}U
	MOX Fuel	0% – 5.5% ^{239}Pu
Fuel pellet density		10.4 g/cm^3
Fuel pellet diameter		0.82 cm
Outer pin diameter		0.95 cm
Cladding thickness		0.065 cm
Active fuel height		388.1 cm

5.1. PWR LEU and MOX Fresh Fuel Results

The concentration of fissile material in the fresh LEU and MOX fuel pins was determined by tallying the fission rate in ^{235}U FCs located adjacent to the fuel assembly. Spontaneous fission neutrons from ^{238}U in LEU fuel and ^{240}Pu in MOX fuel were used to self-interrogate the fresh fuel pins in the MCNPX simulations of SINRD. It should be noted that in practice an external source, such as ^{252}Cf, would be used to boost the source strength and reduce the count time for measurements of a fresh LEU fuel assembly.

It is also important to note that the designs for PWR fresh MOX fuel assemblies are more complicated than fresh LEU assemblies. For instance, a common design for a PWR fresh MOX assembly consists of high Pu content fuel (~10% Pu) in the outer row, medium Pu content fuel (~6 – 8% Pu) in the second row, and low Pu content fuel (~4 – 6% Pu) in the interior. In the MCNPX simulations of SINRD, variations in the Pu enrichment of the MOX fuel across the assembly were not accounted for. Since SINRD is more sensitive to the outer rows of the assembly compared to the center, we expect the SINRD ratios to be higher for a PWR fresh MOX assembly design described above. However, this needs to be further investigated in future work.

In Fig. 5.1(a) and (c), we show how the large ^{235}U and ^{239}Pu fission resonances can be windowed in energy by using the (Gd – Cd) ^{235}U fission rate based on the location of Gd and Cd absorption cut-off energies relative to the ^{235}U and ^{239}Pu fission cross-sections, respectively. The FFM / Gd ^{235}U FC ratio is compared to the FFM / (Gd – Cd) ^{235}U FC ratio as a function of ^{235}U (LEU fuel) and ^{239}Pu (MOX fuel) fraction in Fig. 5.1 (b) and (d), respectively. It is important to note that we have normalized the results to the ratio with all depleted uranium (DU) fuel pins in assembly (0.2 wt% ^{235}U). Using the (Gd – Cd) ^{235}U fission rate in the SINRD detector ratio, increased the slope of the SINRD signature by 53% for fresh LEU fuel and by 75% for fresh MOX fuel.

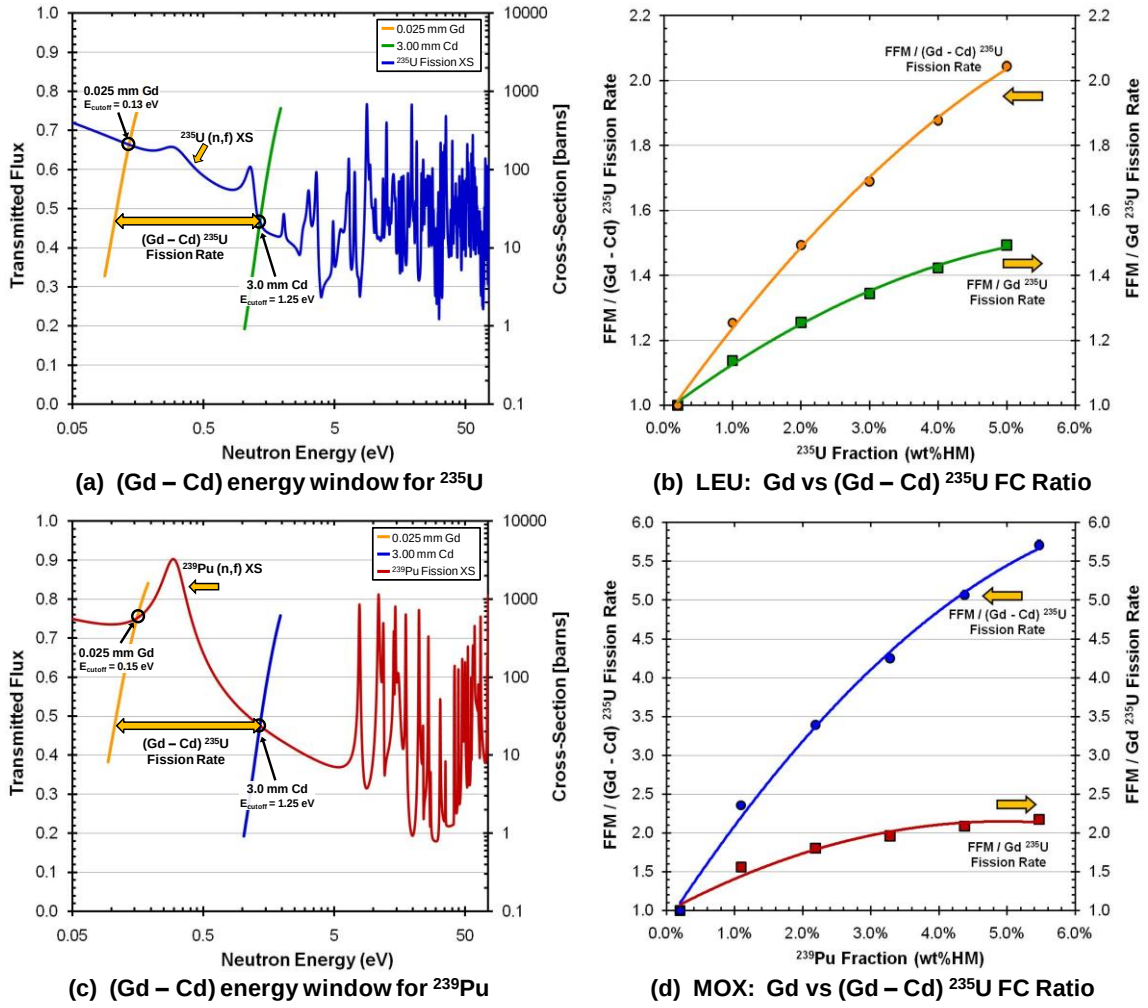

Fig. 5.1. (a) ^{235}U and (c) ^{239}Pu fission cross-sections within (Gd – Cd) cutoff energy window and comparison of FFM / (Gd – Cd) to FFM / Gd ^{235}U FC ratios for fresh (b) LEU and (d) MOX fuel.

The effect of adding 2200-ppm boron to the water on the FFM / (Gd – Cd) ^{235}U FC ratio is shown in Fig. 5.2 for (a) fresh LEU fuel and (b) fresh MOX fuel. To illustrate how boron affects the slope of the curves in Fig. 5.2, these results were not normalized to the case with all DU pins. The addition of boron in water absorbs low energy neutrons reducing the absorption of neutrons in the low lying ^{235}U and ^{239}Pu fission resonances. This hardens the neutron energy spectrum. The slope of the SINRD detector ratio decreased by 18% for LEU fuel and increased by 2.3% for MOX fuel when 2200-ppm boron was added to the water. The higher sensitivity of fresh LEU fuel to the addition of

boron in water compared to MOX fuel may be attributed to the fact that MOX fuel has a harder neutron energy spectrum. Thus, the boron in the water "hardening" the neutron energy spectrum has less of an effect on MOX fuel because the neutron energy spectrum was harder in the first place.

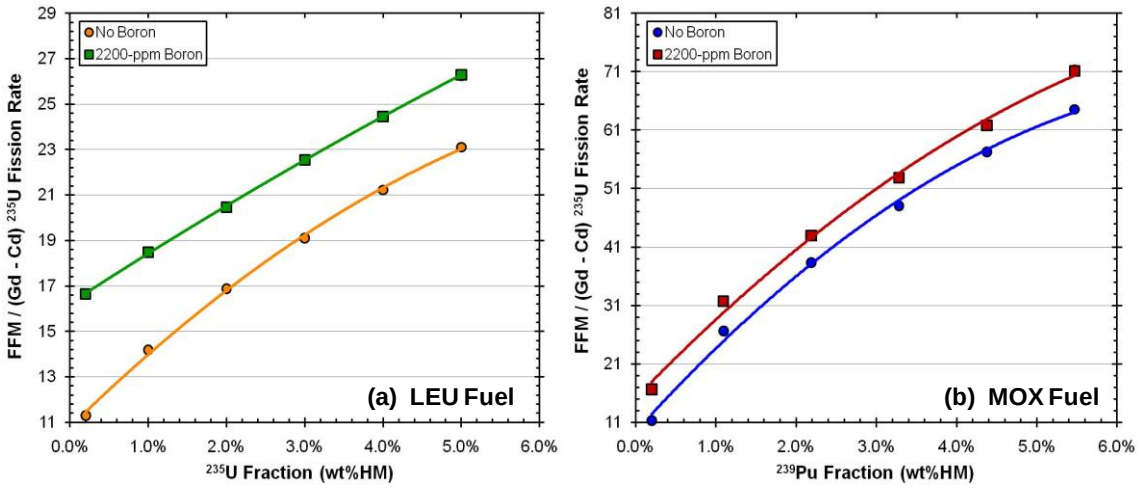

Fig. 5.2. Effect of adding 2200-ppm boron in water on FFM / (Gd – Cd) ^{235}U FC ratio for PWR fresh (a) LEU and (b) MOX fuel.

Comparisons of the ^{235}U and ^{239}Pu fission cross-sections (a) and the FFM / (Gd – Cd) ^{235}U FC ratio for fresh LEU versus MOX fuel (b) is shown in Fig. 5.3. The solid lines represent the results with no boron and the dashed lines represent the results with 2200-ppm boron in the water. These results were normalized to the case with all DU pins. The SINRD signature for fresh MOX fuel is approximately 79% greater than that for fresh LEU fuel. This is primarily due to the fact that the ^{239}Pu fission cross-section is an order of magnitude larger than the ^{235}U fission cross-section within the (Gd – Cd) absorption cutoff energy window.

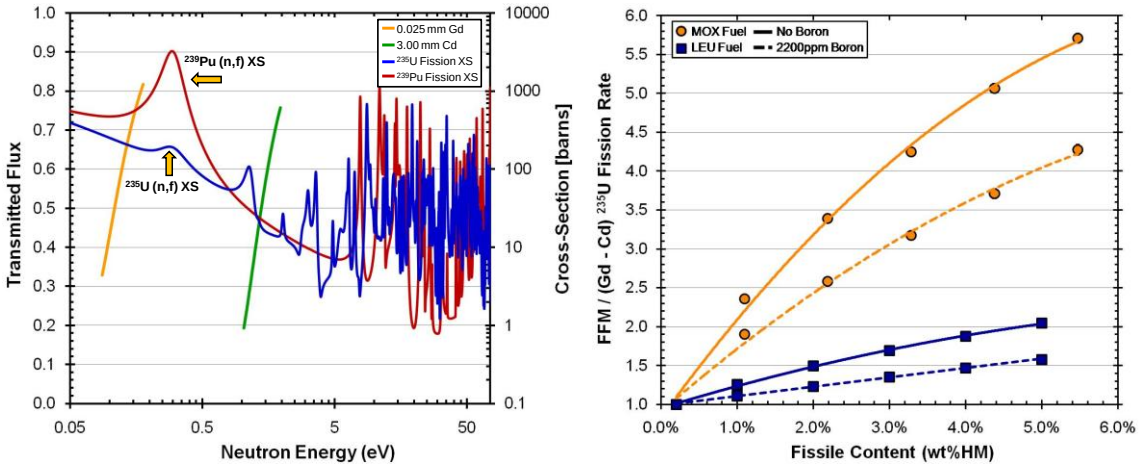

(a) ^{235}U vs ^{239}Pu Fission Cross-Section **(b) LEU vs MOX: (Gd – Cd) ^{235}U FC Ratio**

Fig. 5.3. (a) ^{235}U and ^{239}Pu fission cross-sections at neutron energies ≤ 50-eV, (b) comparison of the FFM / (Gd - Cd) ^{235}U FC ratio for PWR fresh LEU versus MOX fuel.

5.2. Sensitivity of SINRD to Pin Removal in a PWR Fuel Assembly

The sensitivity and penetrability of SINRD was assessed by modeling partial defects in PWR 17x17 fresh LEU and MOX fuel assemblies with initial enrichments of 4% ^{235}U (LEU) and 6% Pu (MOX). We have uniformly removed 16 and 56 fuel pins from three different radial regions of the assembly assuming four-quadrant symmetry and replaced them with DU pins. The fuel pin removal locations of partial defects for Regions 1 – 3 are shown in Fig. 5.4. Region 1 consists of 2 rows on the outer surface of the assembly (excluding the 1st row), Region 2 consists of rows in the mid region, and Region 3 consists of rows in the center of the assembly. The average depth from the outer surface of the PWR assembly is 1.88-cm for Region 1, 3.75-cm for Region 2 and 8.13-cm for Region 3. It is important to note that a reference assembly for calibration is assumed for all diversion cases.

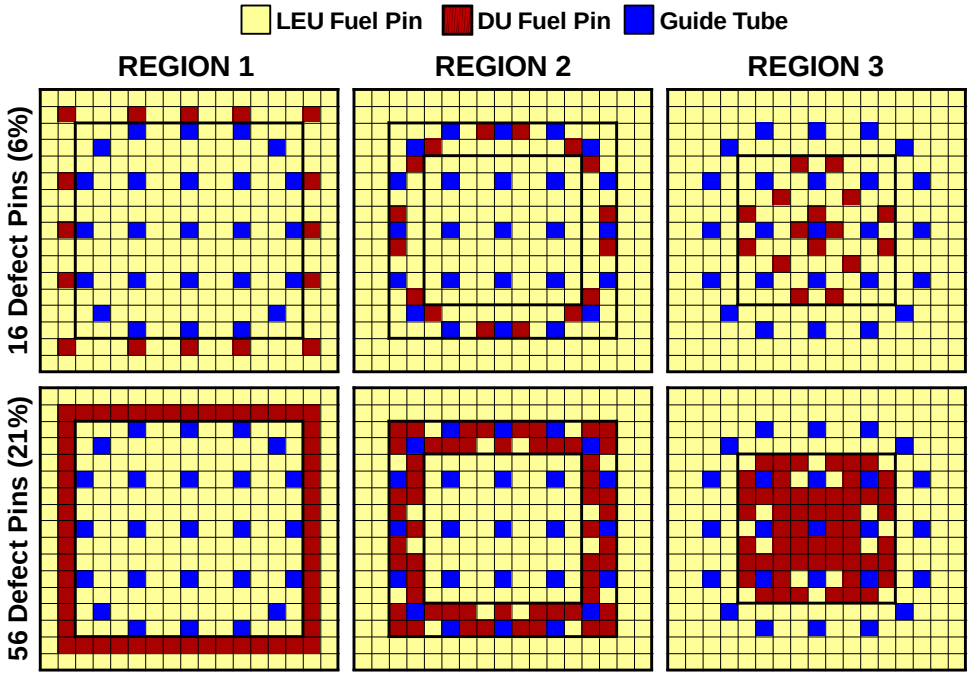

Fig. 5.4. Fuel pin removal locations of defects for Regions 1, 2 and 3 in PWR 17x17 assembly where red pin locations represent fuel pins that were removed, and the blue locations are guide tube holes.

In order to assess the penetrability of SINRD to partial defects, the percent change in different SINRD ratios was calculated for each region to determine if the diverted pins can be detected with a 3σ confidence level. For each region (k = 1, 2, 3), the percent change and its standard deviation in the SINRD ratio was calculated by:

$$P^k = \frac{R_N - R_D^k}{R_N}$$

$$\sigma_P^k = P^k \sqrt{\left(\frac{\sqrt{\left(\sigma_N\right)^2 + \left(\sigma_D^k\right)^2}}{R_N - R_D^k} \right)^2 + \left(\frac{\sigma_N}{R_N} \right)^2} \qquad (4.20)$$

where P^k and σ_P^k are the percent change in the SINRD ratio and its standard deviation, R_N and σ_N are the no diversion ratio and standard deviation, and R_D^k and σ_D^k are the region defect ratio and standard deviation for pin removal from region k.

The sensitivity of different SINRD detector ratios with 6% and 21% of the total number of pins removed from Regions 1, 2, and 3 are given in Table 5.2 and Table 5.3 for PWR fresh LEU and MOX fuel, respectively. The values shown in bold correspond to the maximum positive and negative percent change in ratios that are within *3σ* uncertainty for 6% and 21% pins removed from each region. The cells that are shaded gray correspond to the percent change in the detector ratios that are not within *3σ* uncertainty of an assembly with no diverted pins. It should be noted that the uncertainties in the SINRD ratios are not given because the purpose is to show the ratios that can detect the fuel pin diversions within *3σ*. The sensitivity results shown in Table 5.2 and Table 5.3 are summarized below:

- All SINRD ratios have the highest sensitivity to pin removal in Region 1.
- FFM / Bare ^{235}U FC ratio is the most sensitive SINRD ratio for detecting fuel pin diversions within *3σ* from Regions 1 – 3.
  - This ratio is sensitive to reactivity changes in the fuel assembly due to changes in the concentration of thermal absorbers.
  - The percent change in this ratio is positive for pin removal from Regions 1 (outer) and 2 (middle) and negative for pin removal from Region 3 (center).

Table 5.2. Percent change in SINRD ratios with 6% and 21% fuel pins removed from Regions 1, 2, and 3 for PWR fresh LEU fuel.

% Pin Defects	SINRD Ratios *PWR Fresh LEU*	REGION 1		REGION 2		REGION 3	
		No boron	***2200-ppm***	***No boron***	***2200-ppm***	***No boron***	***2200-ppm***
6% Pin Defects (16 pins)	FFM / (Gd - Cd) ^{235}U	4.66%	**4.62%**	*1.32%*	*1.01%*	*-1.34%*	*-2.42%*
	FFM / Gd ^{235}U	2.37%	2.61%	*0.52%*	*0.23%*	*-1.06%*	-1.71%
	FFM / Bare ^{235}U	**6.99%**	1.04%	**2.49%**	**-3.87%**	-0.91%	**-6.95%**
	Bare ^{235}U / Gd ^{235}U	-4.96%	1.58%	-2.02%	**3.96%**	*-0.14%*	4.90%
	Bare ^{235}U / Cd ^{235}U	**-6.98%**	*0.15%*	**-2.68%**	3.44%	*0.08%*	***5.35%***
21% Pin Defects (56 pins)	FFM / (Gd - Cd) ^{235}U	16.0%	**14.6%**	**4.78%**	*1.50%*	-7.70%	-11.7%
	FFM / Gd ^{235}U	9.31%	8.68%	1.45%	*-0.31%*	-6.24%	-8.08%
	FFM / Bare ^{235}U	**19.0%**	14.4%	3.46%	**-1.17%**	**-12.1%**	**-15.2%**
	Bare ^{235}U / Gd ^{235}U	-11.9%	-6.69%	-2.09%	*0.85%*	5.19%	6.20%
	Bare ^{235}U / Cd ^{235}U	**-19.3%**	**-11.9%**	**-4.96%**	*-0.41%*	**6.19%**	**8.24%**

Table 5.3. Percent change in SINRD ratios with 6% and 21% fuel pins removed from Regions 1, 2, and 3 for PWR fresh MOX fuel.

% Pin Defects	SINRD Ratios *PWR Fresh MOX*	REGION 1		REGION 2		REGION 3	
		No boron	***2200-ppm***	***No boron***	***2200-ppm***	***No boron***	***2200-ppm***
6% Pin Defects (16 pins)	FFM / (Gd - Cd) ^{235}U	**8.79%**	**8.51%**	*1.31%*	*0.94%*	*-0.77%*	*-1.69%*
	FFM / Gd ^{235}U	3.10%	2.94%	*0.23%*	*-0.05%*	*-0.67%*	-1.10%
	FFM / Bare ^{235}U	8.79%	7.25%	**2.15%**	**1.37%**	**-0.73%**	**-1.32%**
	Bare ^{235}U / Gd ^{235}U	-6.24%	-4.65%	-1.96%	-1.44%	*0.06%*	*0.22%*
	Bare ^{235}U / Cd ^{235}U	**-8.72%**	**-6.80%**	**-2.38%**	**-1.77%**	*0.09%*	*0.41%*
21% Pin Defects (56 pins)	FFM / (Gd - Cd) ^{235}U	**26.1%**	**24.6%**	**7.84%**	*3.36%*	-5.93%	-9.20%
	FFM / Gd ^{235}U	10.8%	10.1%	1.50%	*0.03%*	-4.49%	-6.38%
	FFM / Bare ^{235}U	24.9%	21.0%	4.67%	1.96%	**-9.13%**	**-10.9%**
	Bare ^{235}U / Gd ^{235}U	-18.9%	-13.9%	-3.33%	-1.97%	4.26%	4.04%
	Bare ^{235}U / Cd ^{235}U	**-28.7%**	**-21.6%**	**-5.99%**	**-3.14%**	**4.73%**	**4.85%**

It is also important to note the effect of adding boron to water on the sensitivity of the SINRD detector ratios in Regions 2 and 3. Referring to Table 5.2 and Table 5.3, it can be seen that Region 3 has a higher sensitivity than Region 2 when 2200-ppm boron is added to the water. This effect is attributed to the boron in the water "hardening" the neutron energy spectrum. As a result, the number of neutrons absorbed in the low energy resonances for ^{235}U (LEU fuel) and ^{239}Pu (MOX fuel) is reduced which in turn reduces the multiplication of the assembly.

Error propagations (Appendix B) were used to calculate the uncertainties in the percent change in the SINRD ratios for all diversion cases. The count times used for the diversion cases are given in Table 5.4. Since SINRD would require the use of an external ^{252}Cf source to measure a fresh LEU fuel assembly, the times shown for LEU fuel represent the expected count time if a 1.0E+07 n/s ^{252}Cf source was used. The uncertainty in the FFM / Bare ^{235}U FC ratio was between 0.2% – 0.4% for PWR fresh LEU and MOX fuel using the count times given in Table 5.4. Thus, this type of measurement could show the departure from a reference fuel assembly with no defects. For a PWR spent fuel assembly, the ^{244}Cm spontaneous fission rate will provide the same number of neutrons in only a few minutes.

Table 5.4. Count times used to detect fuel pin diversions within *3σ* for PWR fresh fuel.

Fuel Type	Count Time for Diversion Cases	
	No Boron	***2200-ppm Boron***
4% ^{235}U LEU Fuel	0.5 hours	1.5 hours
6% Pu MOX Fuel	1.5 hours	2.5 hours

5.2.1. Graphical Analysis of Partial Defects Results

Next, a graphical analysis of the partial defects results was performed. We chose to use the FFM / Bare ^{235}U FC ratio in this analysis because it was the most sensitive ratio for detecting fuel pin diversions within *3σ* from Regions 1 – 3. The effect of removing fuel pins on the FFM / Bare ^{235}U FC ratio versus diversion case is shown in Fig. 5.5 for (a) LEU and (b) MOX fuel with no boron in the water.

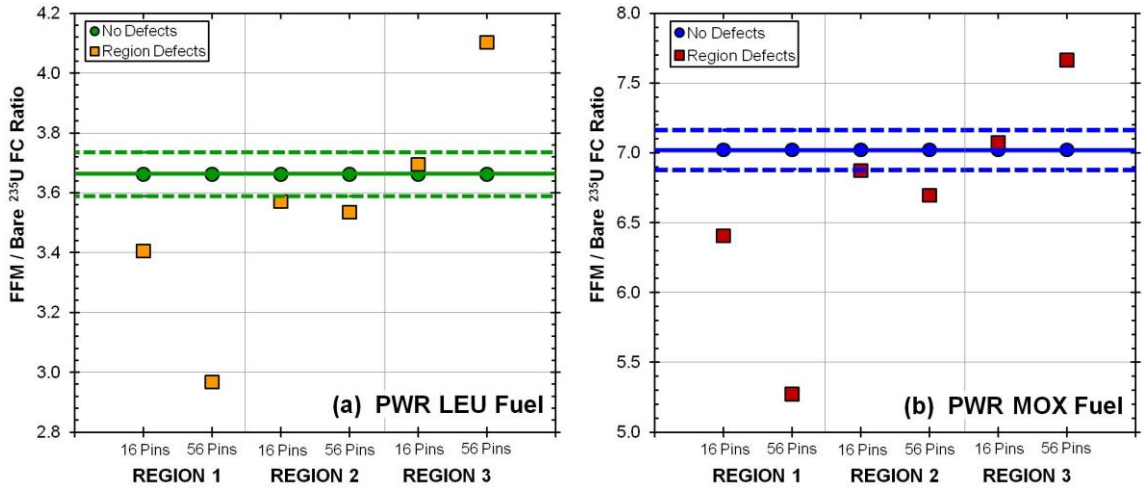

Fig. 5.5. Pin removal results for FFM / Bare ^{235}U FC ratio as a function diversion case for PWR fresh (a) LEU and (b) MOX fuel with no boron in water.

The solid line represents the signal from the case with no diversions; the dashed lines represent ±2% change in the SINRD ratio to account for systematic errors. These results show that the SINRD ratio has the highest sensitivity to fuel pin diversions from

Region 1. The diversion of 16 pins (6%) from Regions 2 and 3 are the only cases that are not clearly within ±2% of the no diversion signal.

5.2.2. Statistical Analysis of Partial Defects Results

A statistical analysis was also performed in order to obtain a better understanding of how the uncertainty in the SINRD ratios affects the ability to detect pin diversions. The purpose of this analysis was to calculate the nondetection probability, β, of different SINRD ratios for each diversion case using a specified false alarm probability, α, and the uncertainties in the SINRD ratios, σ_R. α is the probability that statistical analysis of accountancy verification data would indicate that an amount of nuclear material is missing when, in fact, no diversion has occurred [27]. In this analysis, α was set to 5% and used to calculate the alarm threshold, S. β was then calculated from the threshold. Fig. 5.6 illustrates graphically how S and β can be determined from the FFM / (Gd – Cd) ^{235}U probability distributions, $P(x)$, with 16 pins removed from Regions 2 and 3. PWR fresh MOX fuel (2200-ppm boron) was used to obtain these results.

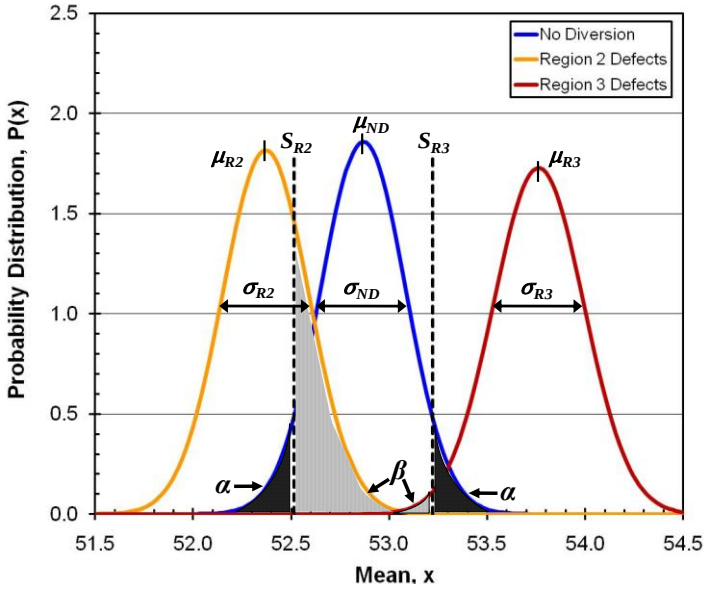

Fig. 5.6. Effect region defects on FFM / (Gd – Cd) ^{235}U probability distributions for PWR fresh MOX fuel with 2200-ppm boron in water.

The uncertainties in the SINRD ratios were assumed to have a normal distribution around the mean. In order to calculate the alarm threshold, *S*, the NORMINV function in MS Excel was used. This function returns the inverse of the normal cumulative distribution for a specified probability (*1-α* or *α*), mean (μ_{ND}), and standard deviation (σ_{ND}). It is important to note that if μ_{ND} is greater than the mean region defect signal (μ_{R1}, μ_{R2}, or μ_{R3}) then the probability of α = 5% is used, otherwise *1-α* = 95% is used. Next, β was calculated using the NORMDIST function in excel that returns the normal distribution for a specified threshold (*S*), mean region defect signal (μ_{R1}, μ_{R2}, or μ_{R3}), and standard deviation (σ_{R1}, σ_{R2}, or σ_{R3}).

In Table 5.5 and Table 5.6, the mean ± 1σ and β are given for different SINRD ratios with 6% fuel pins removed from Regions 1 – 3 for PWR fresh LEU and MOX fuel, respectively. The values for β that are greater than 20% have been shaded gray for LEU and MOX fuel. In general, if β > 20% that is considered a high nondetection probability and that ratio is not considered useful for detecting pin diversions. Based on the results for β, it is clear that the FFM / Bare ^{235}U FC ratio is best ratio for detecting pin diversions.

Table 5.5. Mean ± 1σ and β for SINRD ratios with 6% fuel pins removed from Regions 1, 2, and 3 for PWR fresh LEU fuel.

Medium	SINRD Ratios	No Defects	REGION 1		REGION 2		REGION 3	
		Mean ± 1σ	***Mean ± 1σ***	***β***	***Mean ± 1σ***	***β***	***Mean ± 1σ***	***β***
No Boron	FFM / (Gd - Cd) ^{235}U	21.2 ± 0.140	20.2 ± 0.134	0%	20.9 ± 0.143	*36%*	21.5 ± 0.152	*36%*
	FFM / Gd ^{235}U	9.32 ± 0.023	9.10 ± 0.023	0%	9.27 ± 0.024	*31%*	9.42 ± 0.024	0.6%
	FFM / Bare ^{235}U	3.66 ± 0.006	3.41 ± 0.006	0%	3.57 ± 0.006	0%	3.70 ± 0.006	0%
	Bare ^{235}U / Gd ^{235}U	2.55 ± 0.007	2.67 ± 0.007	0%	2.60 ± 0.007	0%	2.55 ± 0.007	*85%*
	Bare ^{235}U / Cd ^{235}U	4.54 ± 0.015	4.85 ± 0.017	0%	4.66 ± 0.017	0%	4.53 ± 0.016	*91%*
2200-ppm Boron	FFM / (Gd - Cd) ^{235}U	24.5 ± 0.220	23.3 ± 0.206	0%	24.2 ± 0.220	*70%*	25.0 ± 0.235	16%
	FFM / Gd ^{235}U	9.90 ± 0.030	9.64 ± 0.029	0%	9.87 ± 0.030	*80%*	10.1 ± 0.031	0%
	FFM / Bare ^{235}U	4.57 ± 0.010	4.53 ± 0.010	0.1%	4.75 ± 0.011	0%	4.89 ± 0.011	0%
	Bare ^{235}U / Gd ^{235}U	2.16 ± 0.008	2.13 ± 0.007	0.2%	2.08 ± 0.007	0%	2.06 ± 0.007	0%
	Bare ^{235}U / Cd ^{235}U	3.63 ± 0.015	3.63 ± 0.015	*90%*	3.51 ± 0.015	0%	3.44 ± 0.015	0%

Table 5.6. Mean ± 1σ and β for SINRD ratios with 6% fuel pins removed from Regions 1, 2, and 3 for PWR fresh MOX fuel.

Medium	SINRD Ratios	No Defects	REGION 1		REGION 2		REGION 3	
		Mean ± 1σ	*Mean ± 1σ*	*β*	*Mean ± 1σ*	*β*	*Mean ± 1σ*	*β*
No Boron	FFM / (Gd - Cd) ^{235}U	48.0 ± 0.476	43.8 ± 0.405	0%	47.4 ± 0.468	*63%*	48.4 ± 0.487	*80%*
	FFM / Gd ^{235}U	12.9 ± 0.027	12.5 ± 0.026	0%	12.8 ± 0.027	*71%*	12.9 ± 0.027	6.3%
	FFM / Bare ^{235}U	7.02 ± 0.011	6.41 ± 0.010	0%	6.87 ± 0.011	0%	7.07 ± 0.011	0.2%
	Bare ^{235}U / Gd ^{235}U	1.83 ± 0.005	1.94 ± 0.005	0%	1.87 ± 0.005	0%	1.83 ± 0.005	*92%*
	Bare ^{235}U / Cd ^{235}U	2.50 ± 0.007	2.72 ± 0.008	0%	2.56 ± 0.007	0%	2.50 ± 0.007	*90%*
2200-ppm Boron	FFM / (Gd - Cd) ^{235}U	52.9 ± 0.680	48.4 ± 0.600	0%	52.4 ± 0.695	*81%*	53.8 ± 0.731	*62%*
	FFM / Gd ^{235}U	13.1 ± 0.033	12.8 ± 0.033	0%	13.1 ± 0.034	*92%*	13.3 ± 0.035	0.5%
	FFM / Bare ^{235}U	7.94 ± 0.016	7.36 ± 0.015	0%	7.83 ± 0.016	0%	8.04 ± 0.017	0%
	Bare ^{235}U / Gd ^{235}U	1.66 ± 0.005	1.73 ± 0.005	0%	1.68 ± 0.005	0.2%	1.65 ± 0.005	*81%*
	Bare ^{235}U / Cd ^{235}U	2.20 ± 0.007	2.35 ± 0.008	0%	2.24 ± 0.008	0%	2.19 ± 0.008	*66%*

In Fig. 5.7, the effect of 6% region defects on the FFM / Bare ^{235}U probability distribution is shown for PWR fresh (a) LEU and (b) MOX fuel with *no boron* in water. The uncertainty in the FFM / Bare ^{235}U FC ratio is much smaller compared to FFM / (Gd – Cd) ^{235}U FC ratio. Thus, the normal distributions are well separated and β = 0 for Regions 1, 2, and 3.

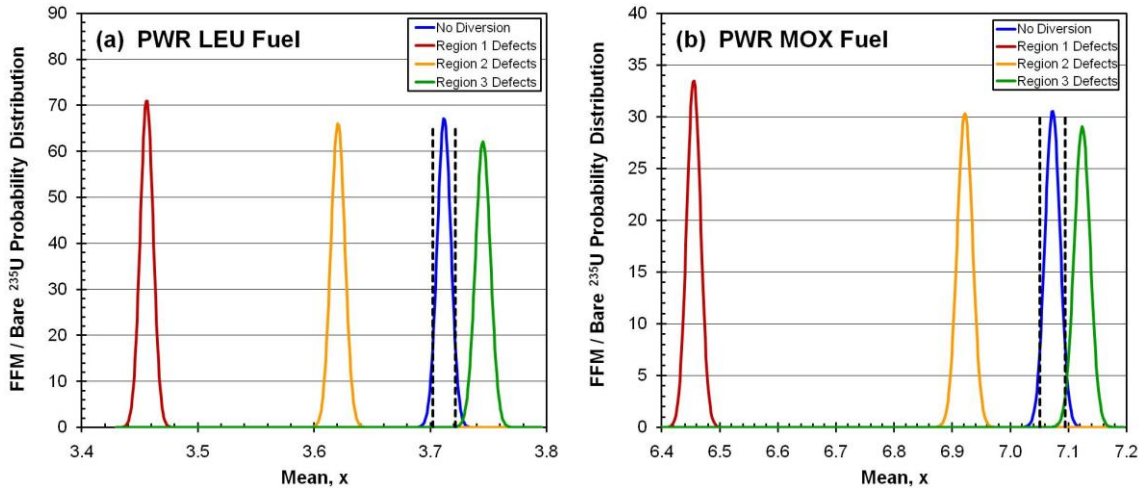

Fig. 5.7. Effect of region defects on the FFM / Bare ^{235}U probability distribution versus mean for PWR fresh (a) LEU and (b) MOX fuel with no boron in water.

In Fig. 5.8, the percent change in (a) FFM / Bare ^{235}U FC ratio and (b) Bare / Cd ^{235}U FC ratio versus the percentage of pins removed is shown for PWR fresh LEU and MOX fuel with no boron in water. Using the diversion results for 6% and 21% partial defects, the average percent change in the SINRD ratio per fuel pin removed was calculated for each region and then multiplied by an increasing number of fuel pins. For both SINRD ratios, the sensitivity to pin removal is highest in Region 1. Based on these results, it should be noted that there exists a combination of fuel pins from Regions 2 and 3 that could result in 0% percent change in FFM / Bare ^{235}U FC ratio; however, the results shown in Fig. 5.8(b) go in the opposite direction as the results shown in (a). Thus, the percent change in the Bare / Cd ^{235}U FC ratio could be used in conjunction with the percent change in FFM / Bare ^{235}U FC ratio such that the removal of pins from Regions 2 and 3 could be detected provided a base measurement of the assembly existed.

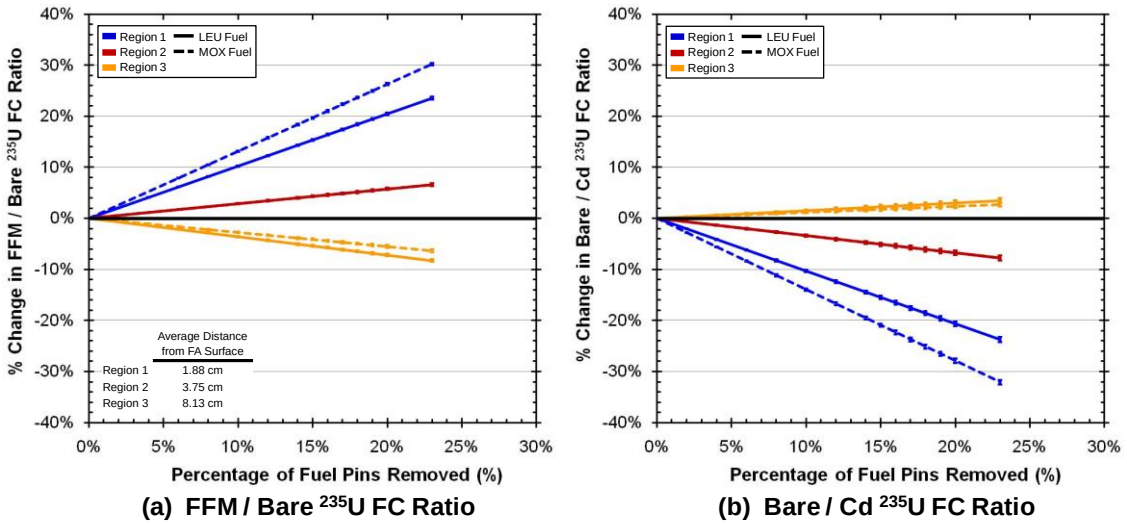

Fig. 5.8. Sensitivity to partial defects: % change in (a) FFM / Bare ^{235}U FC ratio and (b) Bare / Cd ^{235}U FC ratio versus % of fuel pins removed for fresh LEU and MOX fuel with no boron in water.

To obtain a better understanding of the sensitivity of the SINRD ratios to pin removal from the assembly, the percent change in (a) Bare ^{235}U, (b) FFM ^{235}U, (c) Gd ^{235}U, and (d) Cd ^{235}U fission rates versus the percentage of pins removed is shown in

Fig. 5.9 for PWR fresh LEU and MOX fuel with *no boron* in water. In contrast the results shown in Fig. 5.8, all of the SINRD FCs have the highest sensitivity of to pin removal from Region 3 (center). This may be attributed to the fact that the multiplication is highest in the center of the assembly.

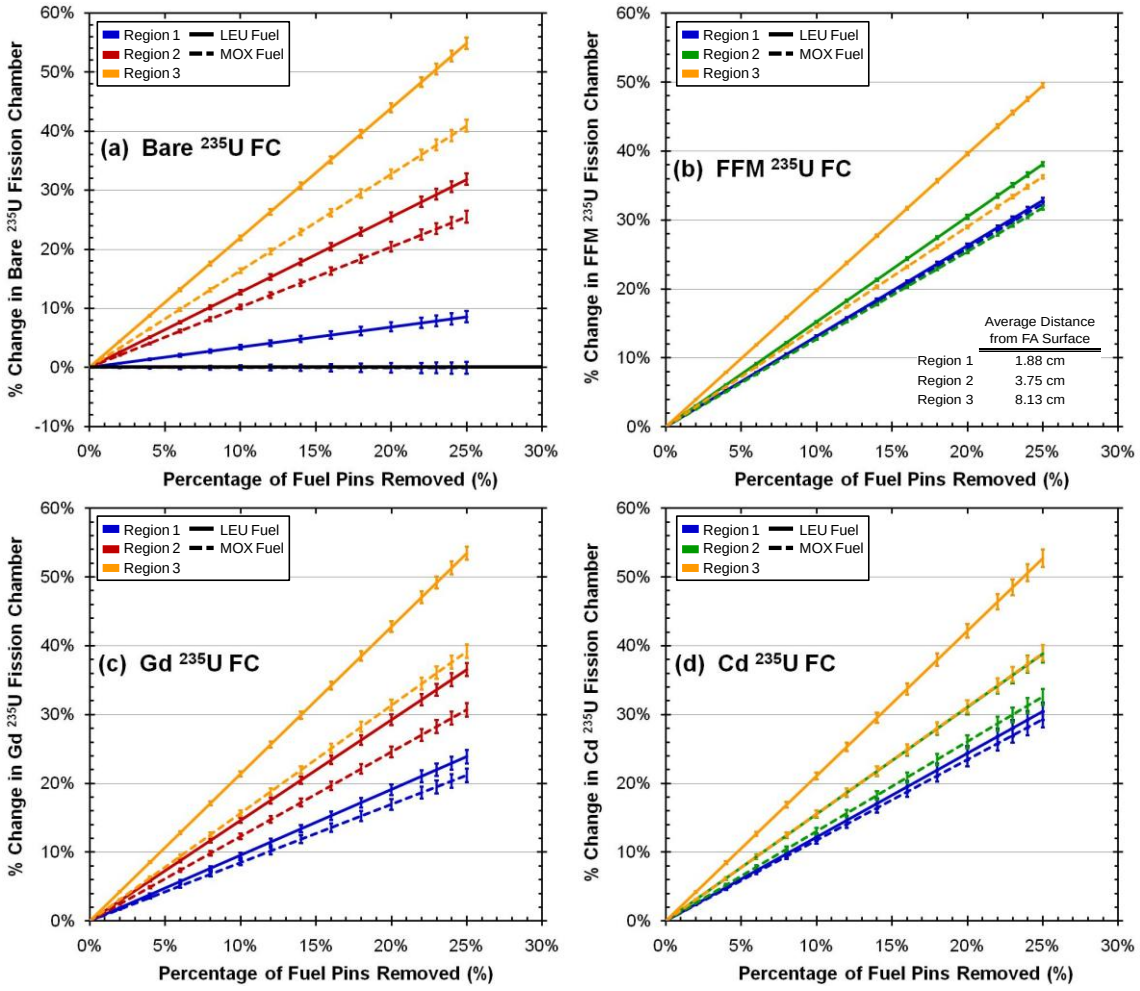

Fig. 5.9. Percent change in (a) Bare ^{235}U, (b) FFM ^{235}U, (c) Gd ^{235}U, and (d) Cd ^{235}U fission rates versus % of fuel pins removed for PWR fresh LEU and MOX fuel with no boron in water.

5.3. Summary of PWR Fresh Fuel Results

We have simulated the change in the FFM / (Gd – Cd) covered ^{235}U FC ratio for PWR 17x17 fresh LEU and MOX fuel assemblies. This ratio is sensitive to the fissile content in both LEU and MOX fuel assemblies and has not saturated for fissile loadings up to 6%. The SINRD signature for PWR fresh MOX fuel is approximately 79% greater than for PWR fresh LEU fuel. This is primarily due to the fact that the ^{239}Pu fission cross-section is an order of magnitude larger than the ^{235}U fission cross-section within the (Gd – Cd) absorption cutoff energy window (0.1 eV – 1.25 eV).

The sensitivity and penetrability of SINRD was assessed by modeling partial defects in PWR 17x17 fresh LEU and MOX fuel assemblies. The percent change in the SINRD ratios was calculated for Regions 1 – 3 to determine if the diverted pins can be detected with a 3σ confidence level. A statistical analysis was also performed to obtain a better understanding of how the uncertainty in the SINRD ratios in affects the ability to detect pin diversions. Based on the results for β, it is clear that the FFM / Bare ^{235}U FC ratio is best ratio for detecting pin diversions. The uncertainty in this ratio was between 0.2% – 0.4% for PWR fresh LEU and MOX fuel. Thus, this type of measurement could show the departure from a reference fuel assembly with no defects.

6. EXPERIMENTAL VERIFICATION OF MCNPX RESULTS: SINRD FRESH FUEL MEASUREMENTS

The SINRD detector was used to measure the ^{235}U content in a PWR fresh fuel assembly in air. We used the LANL PWR 15x15 fresh LEU fuel assembly for these measurements. In addition, the penetrability of the SINRD method was also assessed by uniformly removing LEU fuel pins from three different radial regions of the assembly. These measurements were benchmarked against results from MCNPX simulations to verify the accuracy of the MCNPX model of SINRD, as well as, obtain a better understanding of potential sources of bias in MCNPX. This is essential to validating the results and conclusions obtained from MCNPX simulations of SINRD for LWR spent fuel assemblies.

6.1. Experimental Setup

SINRD fresh fuel measurements were performed in air using a reference PWR 15x15 fresh LEU fuel assembly available at LANL for general calibration purposes. This fuel assembly has a standard PWR 15x15 grid, typical of commercial PWRs, that contains 204 LEU fuel pins enriched to 3.19% ^{235}U and 21 open channels. The measured response from this assembly has been compared to similar fuel assembly measurements at several fuel fabrication facilities and the agreement has been within ±1% [40,41]. The specifications for the LANL PWR assembly are given in Table 6.1.

Prior to beginning the fresh fuel measurements, the gain setting was matched for all four pre-amplifiers and tested with the FCs to ensure all of the detectors were working properly. Next, the SINRD detector unit was assembled. The SINRD unit modeled in MCNPX and an inside-view of the actual SINRD unit to be used in experiment is shown in Fig. 6.1. After assembling the SINRD detector unit, it was placed adjacent to the LANL PWR 15x15 fuel assembly on aluminum stand, ~15-cm high.

Table 6.1. Specifications for LANL PWR 15x15 fresh fuel assembly.

Assembly Data		
Lattice geometry		15 x 15 (square)
Assembly width		21 cm
Fuel pin pitch		1.4 cm
Number of fuel pins		204
Number of open channels		21
Fuel Pin Data		
Fuel material		UO_2
Cladding material		Zircaloy-2
^{235}U Enrichment	LEU Fuel	3.19% ^{235}U
	DU Fuel	0.22% ^{235}U
Fuel pellet density		10.48 g/cm^3
Fuel pellet diameter		0.905 cm
Outer pin diameter		1.08 cm
Cladding thickness		0.095 cm
Active fuel height		103.5 cm

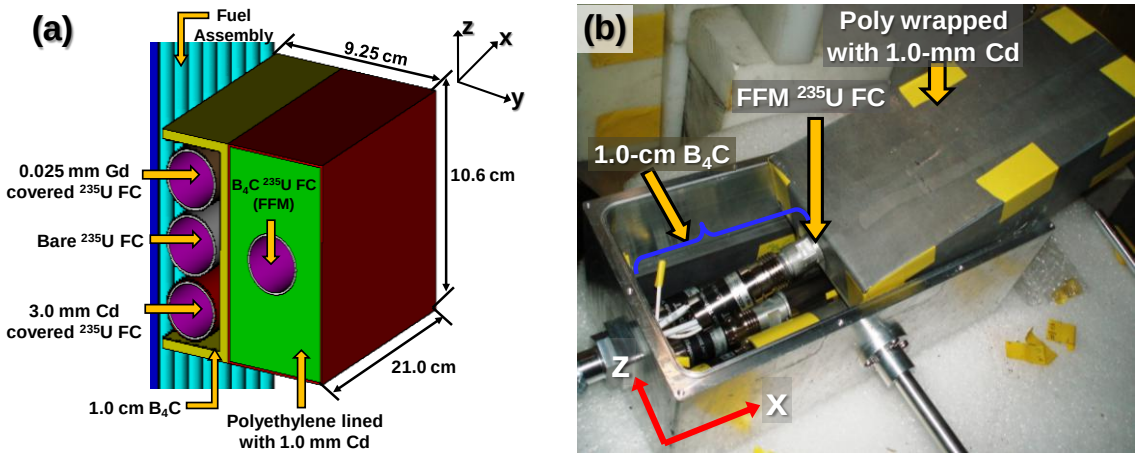

Fig. 6.1. (a) SINRD detector configuration modeled in MCNPX and (b) inside view of the actual SINRD unit used in experimental measurements.

To minimize the probability of introducing systematic errors in our measurements from changes in the geometry while replacing LEU fuel pins with DU pins, the entire experiment was completely contained inside a 55-gallon drum. Pictures of the SINRD

experimental setup are shown in Fig. 6.2. Since this experiment was performed in air, the fuel assembly was surrounded with blocks of high density polyethylene to increase reflection of neutrons back into the assembly (Fig. 6.3). The poly reflector is essential to establishing a neutron slowing-down energy spectrum in the assembly. This moderated neutron spectrum is especially important to achieving good counting statistics in the 3 mm Cd covered ^{235}U FC. In addition, the ^{252}Cf neutron source was placed behind the fuel assembly slightly off-center of a 2" thick block of poly. The location of ^{252}Cf source in the poly block (a) and the SINRD detector unit dimensions (b) are shown in Fig. 6.3.

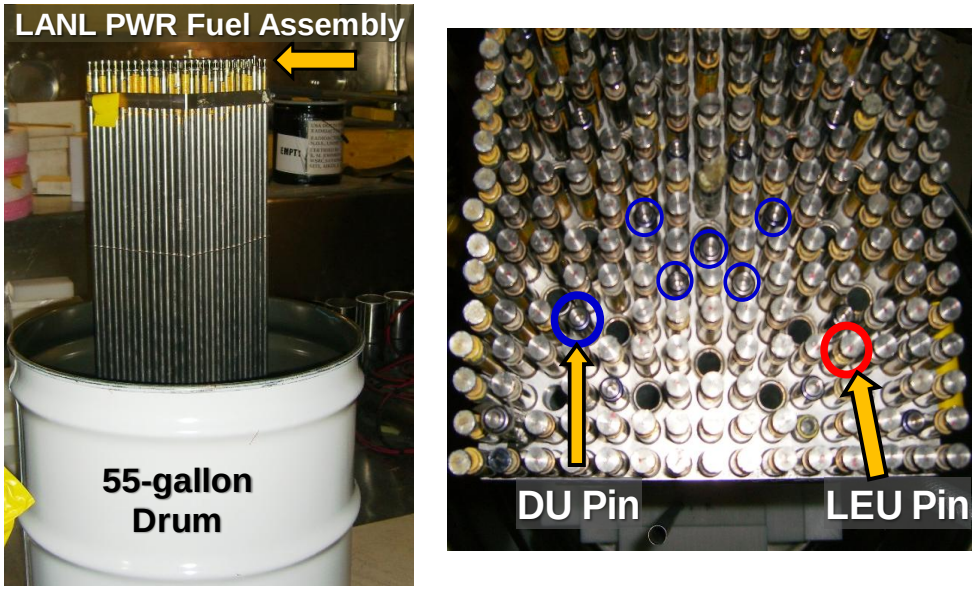

Fig. 6.2. Overview of SINRD experimental setup.

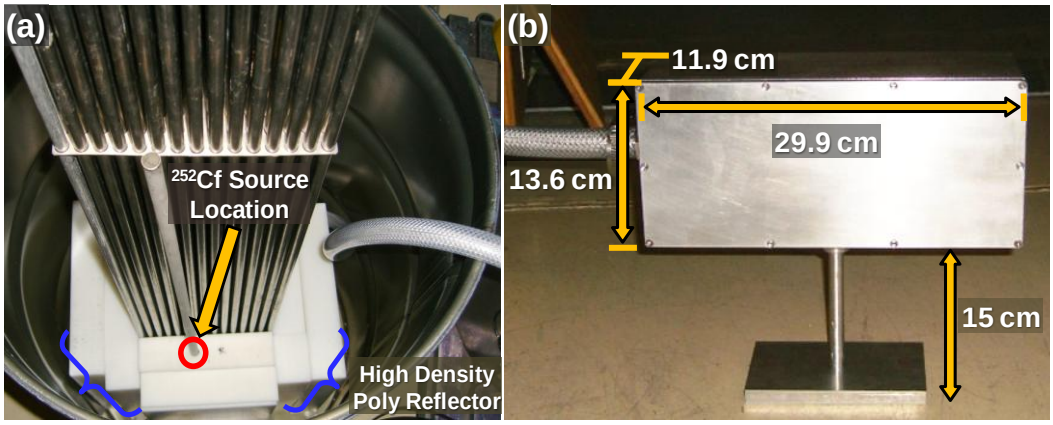

Fig. 6.3. (a) Location of ^{252}Cf neutron source in poly block and (b) SINRD detector pod.

6.2. Procedure

First, the SINRD experiment was setup as described in the previous section and the PWR 15x15 fuel assembly was loaded with 202 LEU fuel pins (3.19% ^{235}U). Then, the SINRD detector cables were connected to two JSR-15 shift registers as shown in Fig. 6.4. The FFM, Gd, and Cd ^{235}U FC signals were connected to one JSR-15 which was connected to the laptop computer. The Bare ^{235}U FC signal was connected to the other JSR-15 and manually operated. Once all of the signal cables were connected, the high voltage was set to 500-V using the INCC software on the laptop. A ^{252}Cf source was placed near the SINRD detector unit to ensure all the FCs were working properly.

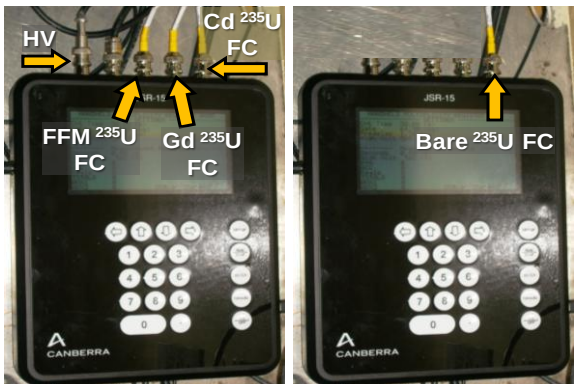

Fig. 6.4. Configuration of SINRD detector electronics.

Next, a background measurement was performed overnight (~10 hours). In INCC, we used 30-seconds per cycle for 1200 cycles (or 30 x 1200). For the FFM, Gd, and Cd covered ^{235}U FCs, the count rates and uncertainties were recorded from INCC. For the Bare ^{235}U FC, the count time and total counts were recorded off of the JSR-15 screen.

In order to determine the optimum count time for the SINRD FCs, a 4-hr test measurement was made with the ^{252}Cf source (1.08E+07 n/s) located in the poly block behind fuel assembly (see Fig. 6.3). The 3-mm Cd covered ^{235}U FC had the lowest count rate of all the SINRD FCs. Therefore, we established the following criteria for the relative uncertainty in the Cd ^{235}U FC ($R_{Cd} = \sigma_{Cd} / C_{Cd}$) to determine the minimum count time required to achieve good counting statistics:

- If $R_{Cd} < 0.3\%$, then count time is too *long* and should be shortened.
- If $R_{Cd} \leq 0.4\%$, then count time is sufficient.
- If $R_{Cd} > 0.4\%$, then the count time is too *short* should be increased.

6.2.1. Measurements of Effective ^{235}U Content

The purpose of the first set of SINRD measurements was to quantify the effective ^{235}U content in the PWR 15x15 fresh LEU fuel assembly in air. To observe how the SINRD signature changes as a function of ^{235}U, we varied the effective enrichment of the fresh fuel assembly from 3.19% to 0.22% ^{235}U by uniformly removing LEU fuel pins and replacing them with DU pins (0.22% ^{235}U). Since SINRD can be applied to any four sides of the assembly, 4-quadrant symmetry was assumed in fuel pin removal.

For the first measurement, the fuel assembly was loaded with all LEU fuel pins (3.19% ^{235}U). The ^{252}Cf source was placed in the poly block behind fuel assembly. A minimum count time of 4-hrs was used for all measurements. After the measurement was completed, the ^{252}Cf source was removed and the count rates and uncertainties were recorded for the FFM, Gd, and Cd covered ^{235}U FCs and the count time and total counts were recorded for Bare ^{235}U FC. This process was repeated for measurements #2 – #10 using the fuel pin configurations shown in Fig. 6.5.

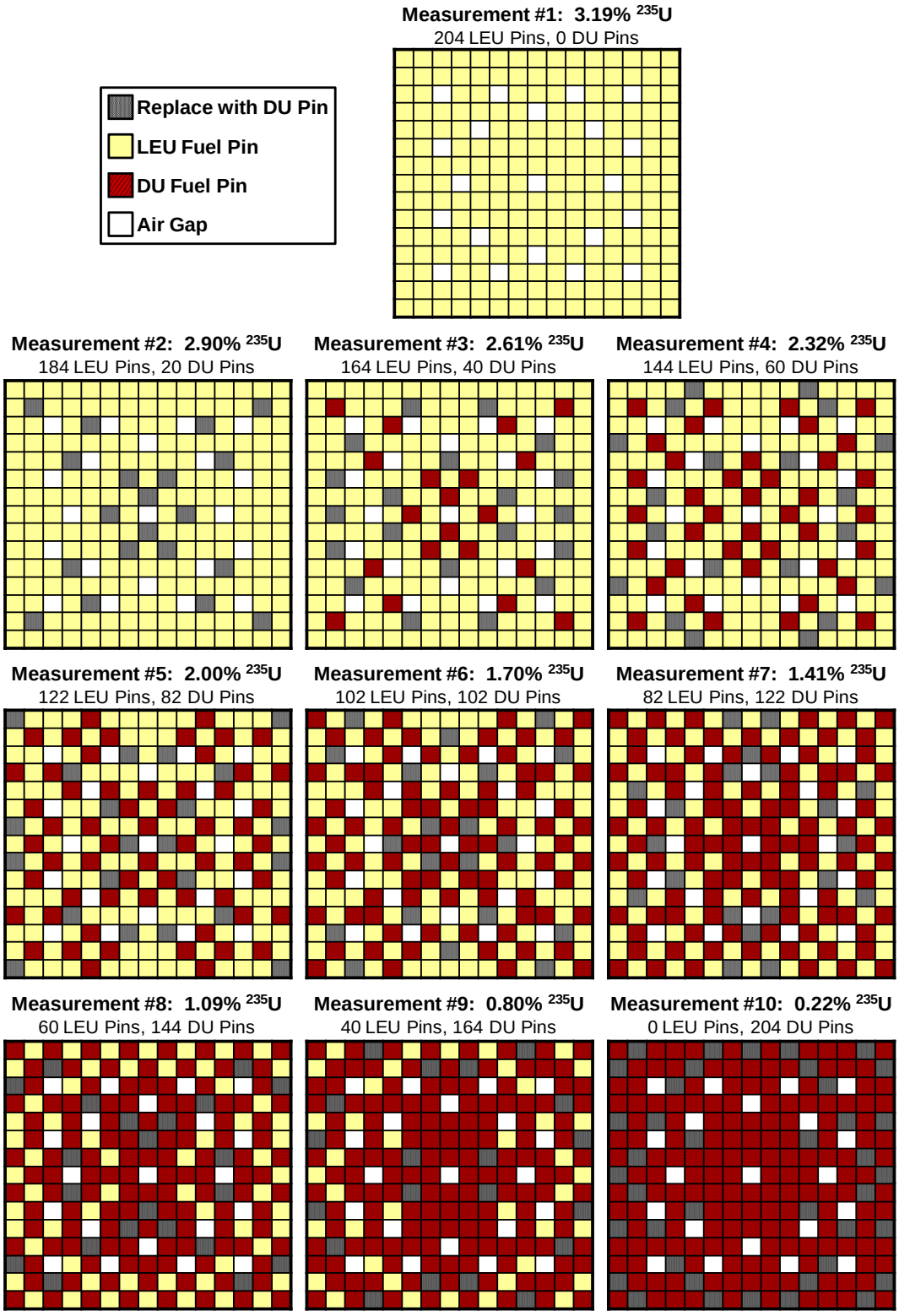

Fig. 6.5. Uniform pin removal configurations for measurements #1 – #10.

6.2.2. Sensitivity Analysis of SINRD to Region Defects

The purpose of the second set of SINRD measurements was to assess the sensitivity and penetrability of SINRD to region defects. LEU fuel pins were uniformly removed from 3 different regions of the assembly, assuming 4-quadrant symmetry, and replaced with DU pins. Region 1 consists of the second row of the fuel assembly, Region 2 consists of two rows in the middle of the assembly, and Region 3 consists of the remaining rows in the center of the assembly. These measurements were performed with the ^{252}Cf source located in polyethylene block behind the fuel assembly and in the center of the fuel assembly to determine how the source position affects the SINRD ratios.

For the first measurement, the fuel assembly was loaded with all LEU fuel pins (3.19% ^{235}U). The ^{252}Cf source was placed in the center of the fuel assembly. A minimum count time of 4-hrs was used for all measurements. After the measurement was completed, the ^{252}Cf source was removed and the count rates and uncertainties were recorded for the FFM, Gd, and Cd covered ^{235}U FCs and the count time and total counts were recorded for Bare ^{235}U FC. Next, 24 LEU fuel pins were uniformly removed from Region 1 and replaced with DU pins as shown in the *Measurement #1* configuration in Fig. 6.6. This fuel pin configuration was measured with the ^{252}Cf source located in the center of the assembly and in the poly block behind fuel assembly. This process was repeated for measurements #2 – #6 for both source positions using the fuel pin configurations shown in Fig. 6.6.

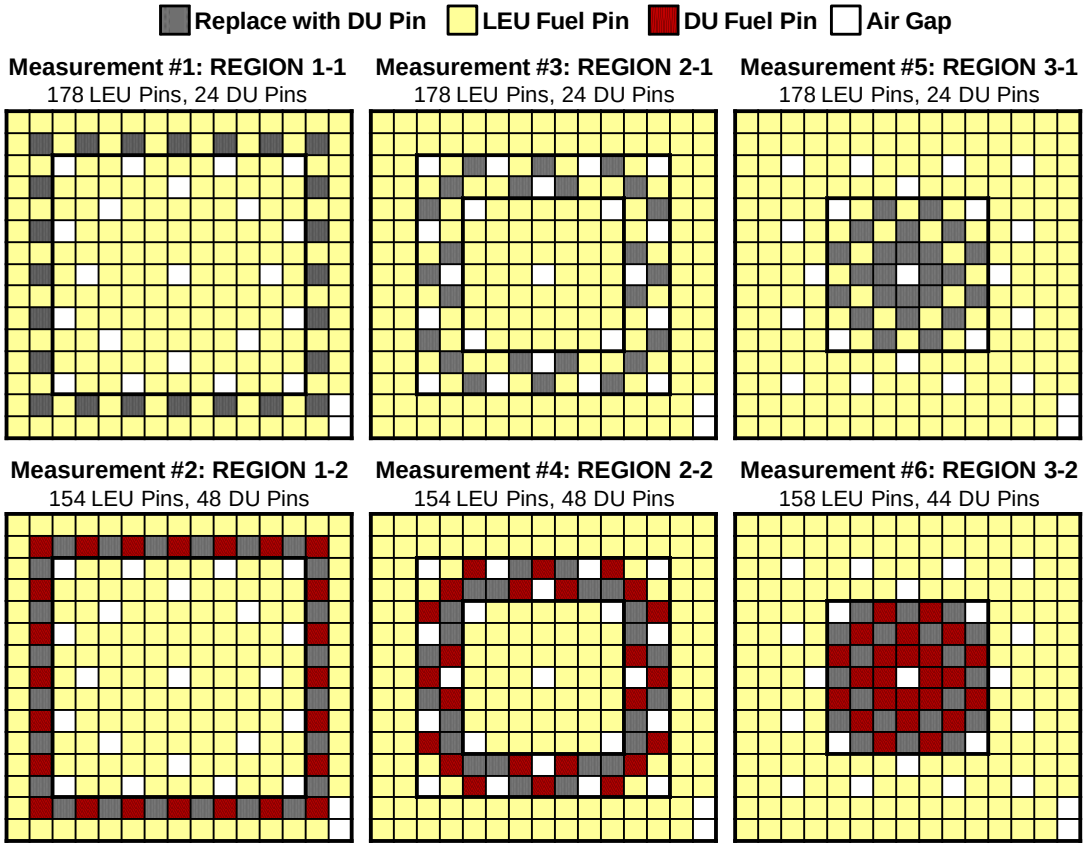

Fig. 6.6. Region defect pin removal configurations for measurements #1 – #6.

6.3. Comparison of Experimental Measurements to MCNPX Results

Two sets of measurements were performed in air with SINRD and benchmarked against results from MCNPX simulations of the experiment. The first set of SINRD measurements was analyzed to determine how well SINRD can measure the effective ^{235}U content in the PWR fresh LEU fuel assembly. For the second set of measurements, the sensitivity and penetrability of SINRD to region defects was assessed with the ^{252}Cf source located behind and in the center of the fuel assembly. The measured count rates and counts (Bare ^{235}U FC) for both sets of SINRD measurements are summarized in Table C.1 to Table C.6 of Appendix C.

6.3.1. Analysis of Results for Effective ^{235}U Measurements

Experimental results for the FFM / (Gd – Cd) and FFM / Gd ^{235}U FC ratios are compared to MCNPX results in Fig. 6.7. We find excellent agreement between the simulated and experimental results. Using the FFM / (Gd – Cd) ^{235}U FC ratio, increased the slope of the SINRD signature by 51%. These results were normalized to the case with all DU pins. This is important because any bias in the MCNPX results cancels out in the normalization. Thus, we see a negligible change between the MCNPX results and experimental measurements.

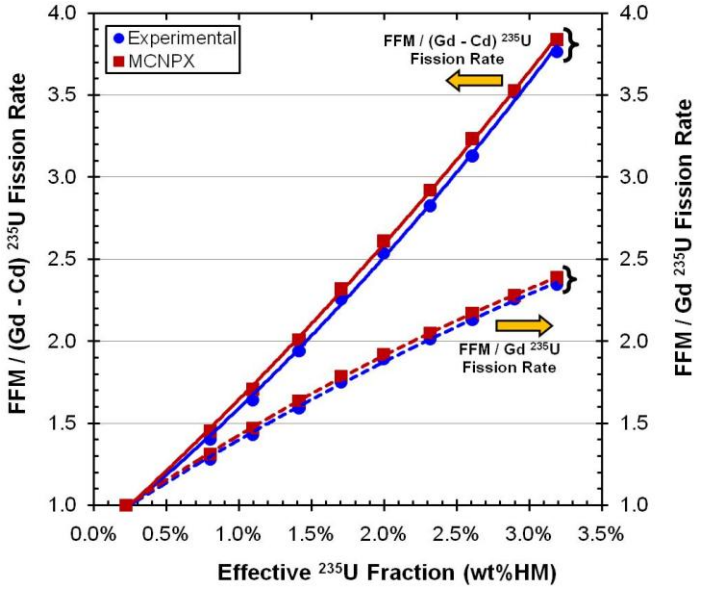

Fig. 6.7. Comparison of MCNPX and experimental results for FFM / (Gd – Cd) ^{235}U FC ratio and FFM / Gd ^{235}U FC ratio.

Examples of potential sources of bias not accounted for in the MCNPX simulations include: location of the ^{252}Cf source, geometry of the ^{252}Cf source, energy spectrum of the ^{252}Cf source, location of the FCs within the SINRD pod, actual thicknesses of Gd and Cd filters, extraneous materials, room return neutrons, and efficiency of detectors (e.g. no counts are thrown away in MCNPX). In regards to the SINRD detector efficiencies, it

should be noted that the measured count rate in the FFM was ~10x higher than the measured count rate in the Bare ^{235}U FC for the case with all LEU fuel pins (3.19% ^{235}U). This is attributed to the fact that the SINRD experiment was conducted in air. Compared to a fuel assembly in water, a much larger fraction of the neutrons born in the fuel pins on the outer rows of the assembly will contribute to the FFM fission rate and less will contribute to the Bare ^{235}U fission rate. Another potential source of bias error is the ^{252}Cf source distribution. In the MCNPX simulations, the ^{252}Cf source was modeled as a point source when in reality it is a volumetric source contained in an aluminum casing. The ^{252}Cf Watts spontaneous fission spectrum constants used in the simulations were taken from the MCNP5 manual. Modeling ^{252}Cf as a point source will add some uncertainty to the source distribution and the location of the ^{252}Cf source in the MCNPX models compared to the experiment.

To obtain a better understanding of how these sources of bias affect the SINRD ratios, the Calculated to Experimental ratio (C/E ratio) versus effective ^{235}U fraction is shown in Fig. 6.8 with (a) no normalization and (b) normalized to the case with all DU pins. The results are relatively constant for all the SINRD detector ratios. This confirms that the MCNPX model of SINRD is accurately simulating the physics of the experiment. For the normalized C/E ratios [Fig. 6.8(b)], the spread in all of the data points was less than 5% and in most cases less than 2.5%. However, the bias errors in the C/E ratios with no normalization [Fig. 6.8(a)] can be as large as ±15 – 20%. Thus, we expect the bias errors to dominate the uncertainty in the results. It is important to note that the level of bias is different for each SINRD detector ratio in Fig. 6.8(a) but cancels out in (b) when the results are normalized to the all DU case. Thus, in order to ensure that our SINRD ratios are insensitive to any potential sources of bias in the MCNPX results or measurements, SINRD requires calibration with a reference assembly of similar geometry.

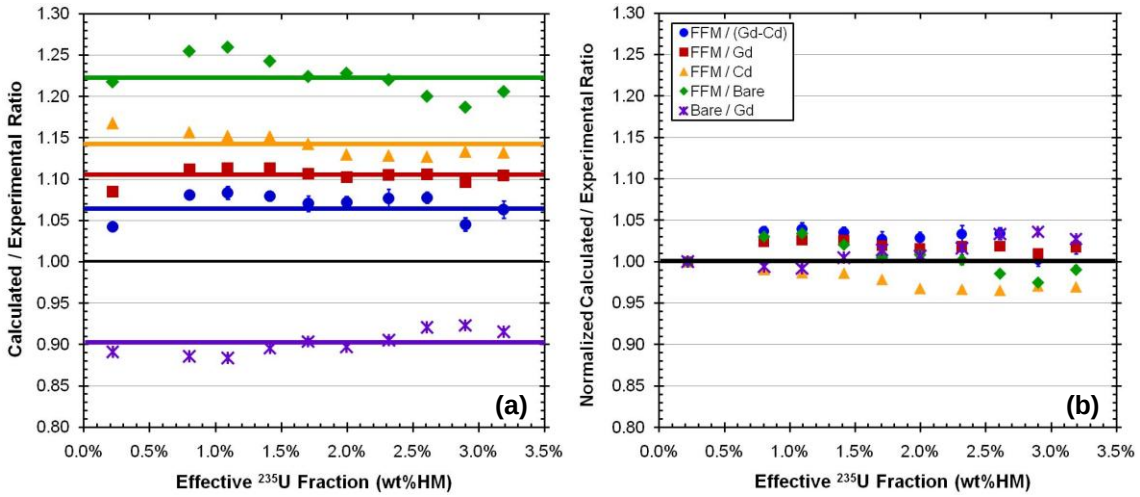

Fig. 6.8. Comparison of the C/E ratio versus effective ^{235}U fraction with (a) no normalization and (b) normalized to all DU case for different SINRD detector ratios.

In order to determine how potential sources of bias error affect each SINRD FC, the C/E ratio for individual detector count rates is shown in Fig. 6.9 with (a) no normalization and (b) normalized to the all DU case. The results are relatively constant for all SINRD detectors confirming that MCNPX is accurately simulating the physics of SINRD. Similar to the results shown in Fig. 6.8, the level of bias is different for each SINRD FC in Fig. 6.9(a) but cancels out in (b) when the results are normalized to the all DU case. Referring to Fig. 6.9(a), the C/E ratio is ~10% high for the FFM and ~10% low for the Bare ^{235}U FC. This effect may be attributed to the harder energy spectrum of the ^{252}Cf source distribution used in MCNPX compared to the actual source distribution due to the ^{252}Cf source being treated as a point source in the simulation. It is also important to note that the bias errors in the C/E ratios for each FC [Fig. 6.9(a)] ranged from ±10 – 13%. This is less than the bias errors in the SINRD ratios shown in Fig. 6.8(a) which ranged from ±15 – 20%.

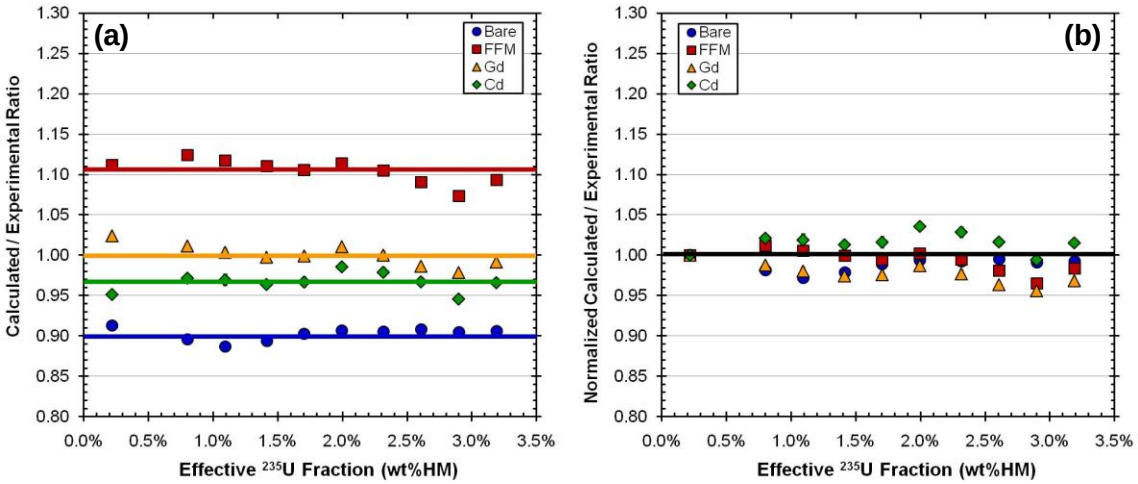

Fig. 6.9. Comparison of the C/E ratio for each SINRD FC versus effective ^{235}U fraction with (a) no normalization and (b) normalized to all DU case.

6.3.2. Sensitivity Analysis of SINRD for Region Defect Measurements

In order to assess the penetrability of SINRD to partial defects, the percent change in the SINRD ratios was calculated for Regions 1, 2, and 3 to determine if the diverted pins can be detected with a 3σ confidence level. The sensitivity of different SINRD ratios with 12% and 23% of the total pins removed from Regions 1, 2, and 3 are given in Table 6.2 and Table 6.3 with the ^{252}Cf source located in the center and back of the fuel assembly, respectively. The measured and MCNPX results are given in both tables. The values shown in bold correspond to the maximum positive and negative percent change in ratios that are within 3σ uncertainty for 12% and 23% pins removed from each region. The cells that are shaded gray correspond to the percent change in detector ratios that are not within 3σ uncertainty of an assembly with no diverted pins. The sensitivity results shown in Table 6.2 and Table 6.3 are summarized below:

- Good agreement between the experimental measurements and MCNPX results for both ^{252}Cf source positions.
- ^{252}Cf Source Located in Center of FA: FFM / Bare ^{235}U FC ratio is the most sensitive SINRD ratio for detecting pin diversions from Regions 1 – 3 within 3σ.

- This ratio is sensitive to reactivity changes in the fuel assembly due to changes in the concentration of thermal absorbers.
- The percent change in this ratio is positive for pin removal from Regions 1 – 3.
- All SINRD ratios have the highest sensitivity to pin removal in Region 1.

- ^{252}Cf Source Located Behind FA: FFM / (Gd – Cd) ^{235}U FC ratio is the most sensitive SINRD ratio for detecting pin diversions from Regions 1 – 3 within 3σ.
  - This ratio is sensitive to resonance absorption from ^{235}U within the (Gd – Cd) energy window.
  - The percent change in this ratio is positive for pin removal from Regions 1 – 3.
  - This ratio has nearly equal sensitivity to pin removal from Regions 1 – 3.

Table 6.2. Percent change in SINRD ratios with 12% and 23% fuel pins removed from Regions 1, 2, and 3 with ^{252}Cf source located in the center of assembly.

% Pin Defects	SINRD Ratios ^{252}Cf in CENTER of FA	REGION 1		REGION 2		REGION 3	
		Measured	*MCNPX*	*Measured*	*MCNPX*	*Measured*	*MCNPX*
12% Pin Defects (24 pins)	FFM / (Gd - Cd) ^{235}U	**8.59%**	**9.14%**	**7.31%**	**7.29%**	*-1.49%*	**-3.15%**
	FFM / Gd ^{235}U	2.81%	3.40%	2.53%	2.69%	1.27%	1.11%
	FFM / Bare ^{235}U	8.37%	8.99%	4.18%	5.07%	**3.53%**	**3.86%**
	Bare ^{235}U / Gd ^{235}U	-6.07%	-6.15%	-1.72%	-2.51%	**-2.34%**	-2.86%
	Bare ^{235}U / Cd ^{235}U	**-7.83%**	**-8.91%**	**-3.09%**	**-4.59%**	-1.63%	-1.18%
23% Pin Defects (46 pins)	FFM / (Gd - Cd) ^{235}U	**16.9%**	16.5%	**14.8%**	**13.0%**	*1.32%*	3.39%
	FFM / Gd ^{235}U	5.23%	6.58%	4.84%	5.15%	3.03%	3.43%
	FFM / Bare ^{235}U	15.6%	**17.1%**	9.52%	10.9%	**8.45%**	**8.74%**
	Bare ^{235}U / Gd ^{235}U	-12.4%	-12.8%	-5.20%	-6.44%	**-5.91%**	**-5.79%**
	Bare ^{235}U / Cd ^{235}U	**-16.7%**	**-18.6%**	**-8.50%**	**-10.5%**	-5.44%	-5.77%

Table 6.3. Percent change in SINRD ratios with 12% and 23% fuel pins removed from Regions 1, 2, and 3 with ^{252}Cf source located in the back of assembly.

% Pin Defects	SINRD Ratios ^{252}Cf in BACK of FA	REGION 1		REGION 2		REGION 3	
		Measured	*MCNPX*	*Measured*	*MCNPX*	*Measured*	*MCNPX*
12% Pin Defects (24 pins)	FFM / (Gd - Cd) ^{235}U	**11.1%**	10.5%	**11.6%**	**9.62%**	**11.1%**	**10.7%**
	FFM / Gd ^{235}U	5.81%	5.68%	6.42%	5.45%	6.43%	6.03%
	FFM / Bare ^{235}U	11.0%	**11.2%**	9.30%	8.82%	8.89%	8.52%
	Bare ^{235}U / Gd ^{235}U	-5.83%	-6.22%	-3.17%	-3.70%	-2.69%	-2.73%
	Bare ^{235}U / Cd ^{235}U	**-10.1%**	**-10.3%**	**-7.29%**	**-7.15%**	**-6.38%**	**-6.62%**
23% Pin Defects (46 pins)	FFM / (Gd - Cd) ^{235}U	19.7%	19.8%	**20.7%**	**19.7%**	**23.2%**	**21.3%**
	FFM / Gd ^{235}U	10.8%	11.2%	12.0%	11.5%	13.2%	12.5%
	FFM / Bare ^{235}U	**21.1%**	**21.4%**	19.4%	18.5%	20.0%	18.7%
	Bare ^{235}U / Gd ^{235}U	-13.2%	-13.3%	-9.36%	-8.71%	-8.37%	-7.46%
	Bare ^{235}U / Cd ^{235}U	**-22.2%**	**-22.6%**	**-18.0%**	**-17.2%**	**-18.2%**	**-16.3%**

Fig. 6.10 shows the C/E ratio versus diversion case with the ^{252}Cf source located behind the assembly with (a) no normalization and (b) normalized to the DU case. The results are relatively constant for all the SINRD detector ratios. Similar to the results shown in Fig. 6.8 for uniform pin removal, the MCNPX model of SINRD is shown to accurately simulate the physics of the experiment for region based pin diversions.

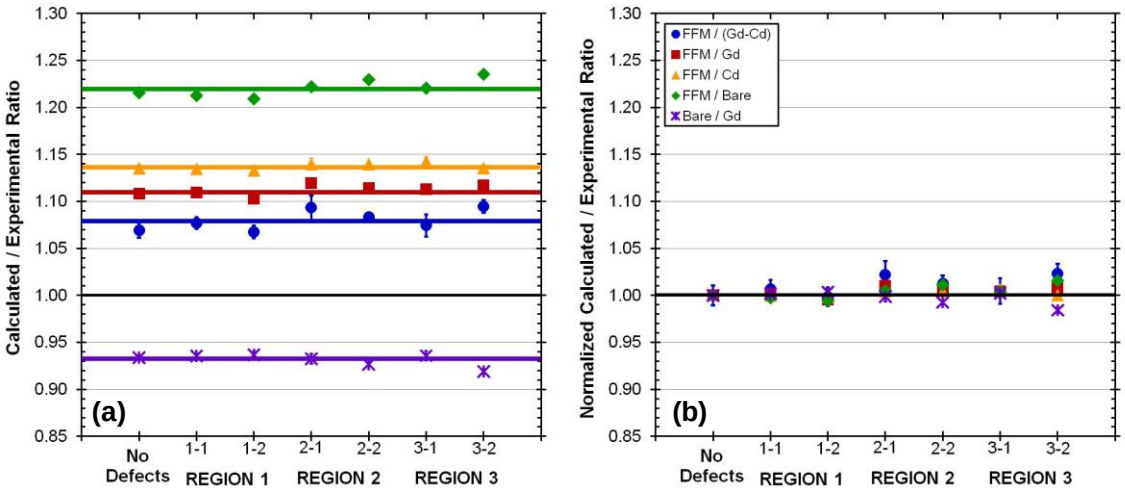

Fig. 6.10. C/E ratio versus diversion case with (a) no normalization and (b) normalized to all DU case with ^{252}Cf source located in back of fuel assembly.

6.3.2.1. Graphical Analysis of Partial Defects Results

The effect of removing fuel pins on the measured FFM / (Gd – Cd) ^{235}U FC ratio for each diversion case is shown in Fig. 6.11 with the ^{252}Cf source located in (a) the center and (b) the back of the fuel assembly. The solid line represents the case with no diversions; the dashed lines represent $\pm 3\sigma$ change in the SINRD ratio to account for systematic errors. It is important to note that the change in (Gd – Cd) SINRD ratio is uniform for all three regions when the ^{252}Cf source was located behind the assembly [Fig. 6.11(b)]. However, we do not see a uniform change when the source was located in the center of the assembly [Fig. 6.11(a)]. Furthermore, Region 3 pin diversions are not within $\pm 3\sigma$ of the no diversion signal when the ^{252}Cf source was located in the center of the assembly. Error propagations (Appendix B) were used to calculate the uncertainties in the percent change in the SINRD ratios for all diversion cases. The uncertainties in these ratios were less than 2% for both source positions. Thus, this type of measurement could show the departure from a reference fuel assembly with no defects.

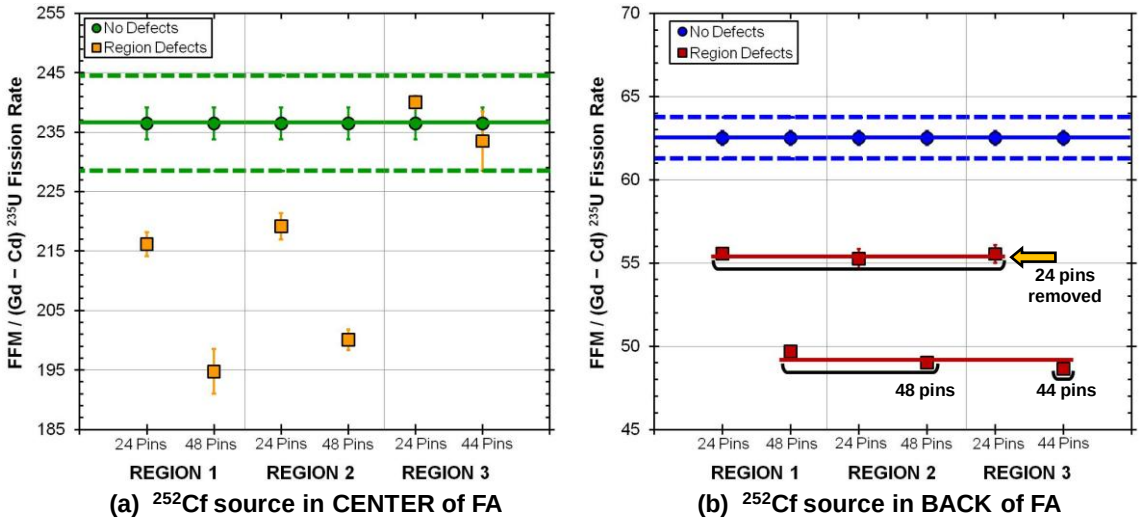

Fig. 6.11. Pin removal results for the measured FFM / (Gd – Cd) ^{235}U FC ratio as a function diversion case with ^{252}Cf source located in (a) center and (b) back of fuel assembly.

Fig. 6.12 shows the comparison of the measured FFM / (Gd – Cd) ^{235}U FC ratio with uniform pin removal and region pin removal versus effective ^{235}U enrichment with ^{252}Cf source located behind the fuel assembly. Since this SINRD ratio is not sensitive to the particular region of the fuel assembly from which pins were removed, we can see that there is a negligible change in the results (Fig. 6.12) for uniform versus region pin removal.

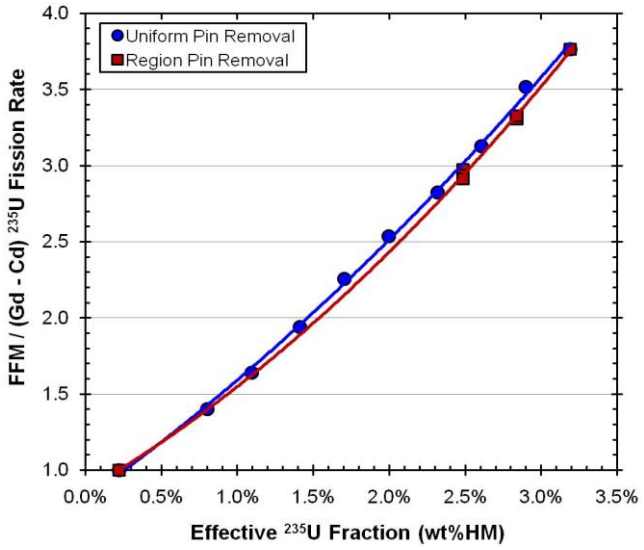

Fig. 6.12. Measured FFM / (Gd – Cd) ^{235}U FC ratio with uniform and region pin removal versus effective ^{235}U enrichment with ^{252}Cf source located behind fuel assembly.

6.3.2.2. *Statistical Analysis of Partial Defects Results*

Using the procedure described in section 5.2, the nondetection probability, β, was calculated for SINRD ratios with fuel pins removed from Regions 1, 2, and 3. The measured results for the mean ± 1σ and β are given in Table 6.4 for both source positions. The values for β that are greater than 20% have been shaded gray. The effect of 12% (24 pins) region defects on measured FFM / (Gd – Cd) ^{235}U probability distribution is shown in Fig. 6.13 with ^{252}Cf source located in (a) center and (b) back of fuel assembly. Based on the results for β, it is clear that placing the ^{252}Cf source behind

the fuel assembly improves both the sensitivity and penetrability of SINRD to pin diversions. This may be attributed to the importance of establishing a neutron slowing-down energy spectrum in the fuel assembly. When the ^{252}Cf source is located behind the assembly, the source neutrons are first moderated in the poly block and then travel the entire width of the assembly before entering the SINRD detector unit. In contrast, when the ^{252}Cf source is located in center of the assembly, the source neutrons only travel half the width of the assembly before entering the SINRD unit. Furthermore, only a fraction of the neutrons entering the SINRD unit will have neutron slowing-down energy spectrum from being reflected in the poly surrounding the fuel assembly.

Table 6.4. Mean ± 1σ and β for SINRD ratios with 12% fuel pins removed from Regions 1, 2, and 3 with ^{252}Cf source located in the center and back of assembly.

Source Location	SINRD Ratios	No Defects	REGION 1		REGION 2		REGION 3	
		Mean ± 1σ	*Mean ± 1σ*	*β*	*Mean ± 1σ*	*β*	*Mean ± 1σ*	*β*
CENTER of Assembly	FFM / (Gd - Cd) ^{235}U	236 ± 2.68	216 ± 2.03	0%	219 ± 2.21	0%	240 ± 1.06	*79%*
	FFM / Gd ^{235}U	48.6 ± 0.084	47.2 ± 0.073	0%	47.4 ± 0.081	0%	48.0 ± 0.030	0%
	FFM / Bare ^{235}U	61.2 ± 0.020	60.4 ± 0.016	0%	60.4 ± 0.019	0%	60.0 ± 0.016	0%
	Bare ^{235}U / Gd ^{235}U	2.42 ± 0.005	2.56 ± 0.004	0%	2.46 ± 0.005	0%	2.47 ± 0.002	0%
	Bare ^{235}U / Cd ^{235}U	3.04 ± 0.007	3.28 ± 0.006	0%	3.14 ± 0.006	0%	3.09 ± 0.003	0%
BACK of Assembly	FFM / (Gd - Cd) ^{235}U	62.5 ± 0.417	55.5 ± 0.298	0%	55.2 ± 0.589	0%	55.5 ± 0.548	0%
	FFM / Gd ^{235}U	24.7 ± 0.053	23.3 ± 0.043	0%	23.2 ± 0.084	0%	23.2 ± 0.078	0%
	FFM / Bare ^{235}U	41.0 ± 0.012	40.2 ± 0.017	0%	39.9 ± 0.018	0%	39.7 ± 0.017	0%
	Bare ^{235}U / Gd ^{235}U	2.57 ± 0.006	2.72 ± 0.007	0%	2.65 ± 0.011	0%	2.64 ± 0.010	0%
	Bare ^{235}U / Cd ^{235}U	4.25 ± 0.012	4.68 ± 0.014	0%	4.56 ± 0.023	0%	4.52 ± 0.020	0%

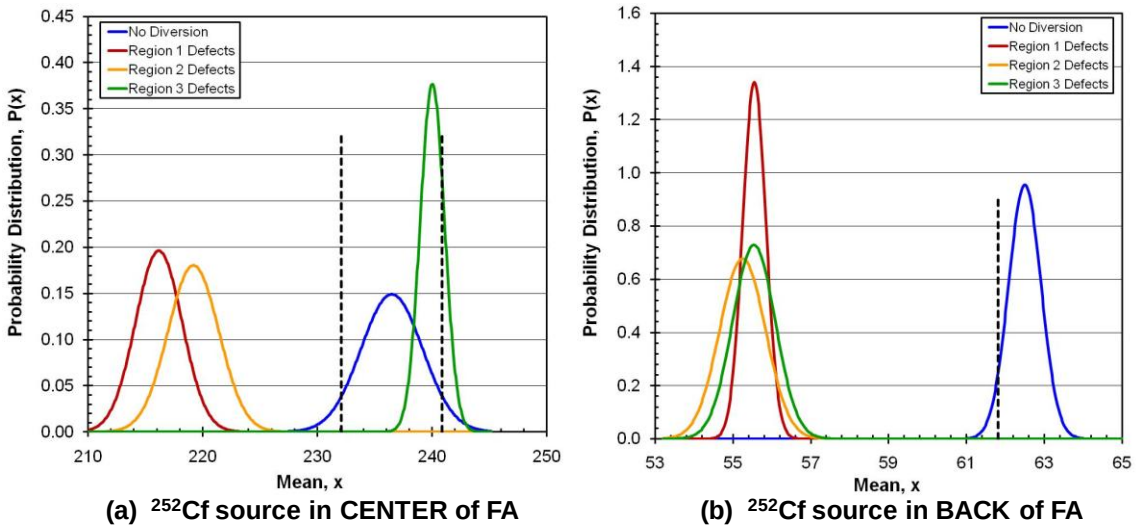

Fig. 6.13. Effect of region defects on measured FFM / (Gd – Cd) ^{235}U probability distribution versus mean with ^{252}Cf source located in (a) center and (b) back of fuel assembly.

The percent change in the FFM / (Gd – Cd) ^{235}U fission rate ratio versus percent reduction in ^{235}U mass is shown in Fig. 6.14 with ^{252}Cf source located in (a) center and (b) back of fuel assembly. The solid lines represent experimental results and the dashed lines represent MCNPX results. The average depth from the outer surface of the PWR 15x15 assembly is 2.1-cm for Region 1, 4.2-cm for Region 2 and 7.7-cm for Region 3. When the ^{252}Cf source was located in the center of the assembly, the sensitivity to pin removal is highest in Region 1 and lowest in Region 3. Similar to the results shown in Fig. 5.8 for PWR fresh fuel in water (section 5.2), there exists a combination of fuel pins from Regions 2 and 3 that could result in 0% percent change in FFM / (Gd – Cd) ^{235}U FC ratio [Fig. 6.14(a)]. Thus, the percent change in another ratio, such as Bare / Cd ^{235}U FC ratio, must be used in conjunction with FFM / (Gd – Cd) ^{235}U FC ratio such that the removal of pins from Regions 2 and 3 could be detected. In contrast, when the ^{252}Cf source was located behind the assembly, the sensitivity to partial defects is uniform for all regions. Furthermore, it is important to note that for 25% reduction in ^{235}U mass we see approximately a 25% change in the FFM / (Gd – Cd) ^{235}U FC ratio [Fig. 6.14(b)].

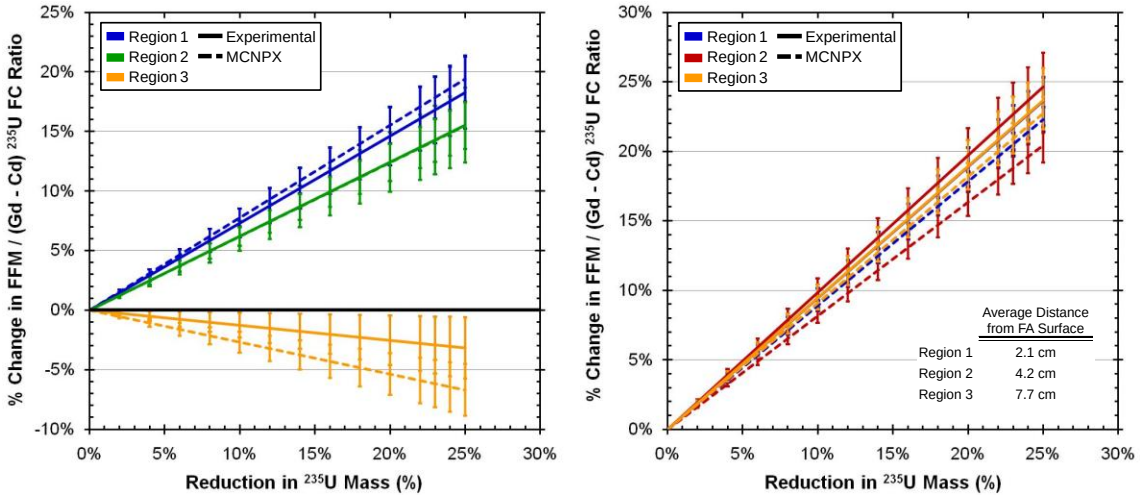

(a) ^{252}Cf source in CENTER of FA **(b) ^{252}Cf source in BACK of FA**

Fig. 6.14. Sensitivity to partial defects: % change in FFM / (Gd – Cd) ^{235}U FC ratio versus % reduction in ^{235}U mass with ^{252}Cf source located in (a) center and (b) back of fuel assembly.

6.4. Summary of Fresh Fuel Measurements with SINRD

We have performed two sets experimental measurements with SINRD in air using the LANL PWR 15x15 fresh LEU fuel assembly. These measurements were benchmarked against results from MCNPX simulations of the experiment. In the first set of SINRD measurements, we varied the effective enrichment of the fuel assembly from 3.19% to 0.22% ^{235}U by uniformly removing LEU fuel pins and replacing them with DU pins. In the second set of measurements, the sensitivity and penetrability of SINRD to region defects was assessed by removing LEU fuel pins from three different radial regions and replacing them with DU pins. These measurements were performed with the ^{252}Cf source located in the center and behind the fuel assembly (in a poly block) to determine how the source position affects the SINRD ratios. The results from MCNPX simulations showed similar behavior as the measured data for all cases. Based on the region defect results, we concluded that placing the ^{252}Cf source behind the fuel assembly significantly improves both the sensitivity and penetrability of SINRD to pin diversions.

The C/E ratio was analyzed for each detector and different SINRD ratios to obtain a better understanding of the sources of bias in the MCNPX results and how they affect the SINRD ratios. For all SINRD FCs and ratios, the C/E ratio was constant. This confirms that the MCNPX model of SINRD is accurately simulating the physics of the experiment. By normalizing the results to the case with all DU pins, the C/E ratio goes to 1.0 within ±5% for all ratios. This is because any bias in the MCNPX results cancels out in the normalization. Thus, in order to ensure our detector ratios are insensitive to any potential sources of bias in MCNPX results or measurements, SINRD requires calibration with a reference assembly of similar geometry. Also, we found that for verifying the ^{235}U content and partial defects for a PWR fresh fuel assembly in air, SINRD is highly effective when using the FFM / (Gd – Cd) ^{235}U FC ratio compared to a DU reference standard with the ^{252}Cf source located in back of the assembly.

7. ANALYSIS OF BWR 9X9 FRESH FUEL ASSEMBLY

We have also simulated BWR 9x9 fresh LEU and MOX fuel assemblies in water in order to gain a better understanding of the physics of the SINRD measurement technique for a smaller fuel assembly. The BWR fresh fuel cases are expected to have a higher sensitivity to pin removal because the assembly is smaller and the individual fuel pins are larger. Similar to the PWR fresh fuel simulations described in section 5, the ^{235}U enrichment was varied from 1.0 to 5.0 wt% ^{235}U for fresh LEU fuel and the Pu loading was varied from 2.0 to 10 wt% Pu for fresh MOX fuel. Spontaneous fission neutrons from ^{238}U (LEU fuel) and ^{240}Pu (MOX fuel) were used to self-interrogate the fresh fuel pins in the MCNPX simulations of SINRD. The specifications used to model the BWR 9x9 fuel assembly are given in Table 7.1.

Table 7.1. Specifications for BWR 9x9 fresh fuel assembly.

Assembly Data		
Lattice geometry		9 x 9 (square)
Assembly width (outer)		13.5 cm
Duct Thickness		0.25 cm
Fuel pin pitch		1.44 cm
Number of fuel pins		74 (8 Part-Length)
Inter-Assembly Gap		1.49 cm
Moderator		Light Water
Fuel Pin Data		
Fuel material		UO_2 / MOX
Cladding material		Zircaloy-2
Fissile Content	LEU Fuel	0.2% – 5% ^{235}U
	MOX Fuel	0% – 5.5% ^{239}Pu
Fuel pellet density		10.01 g/cm^3
Fuel pellet diameter		0.975 cm
Outer pin diameter		1.118 cm
Cladding Thickness		0.071 cm
Active Fuel Height		371 cm
Partial Pin Fuel Height		244 cm

7.1. BWR LEU and MOX Fresh Fuel Results

The same detector configuration was used for both PWR and BWR fuel assemblies. The only modification was that the width of the SINRD detector unit was set to the width of the fuel assembly being measured (13.5-cm for BWR and 21.4-cm for PWR). The FFM / Gd ^{235}U FC ratio is compared to the FFM / (Gd – Cd) ^{235}U FC ratio versus ^{235}U (LEU fuel) and ^{239}Pu (MOX fuel) fraction in Fig. 7.1(a) and (b), respectively. It is important to note that we have normalized the results to the ratio with all DU fuel pins. Using the (Gd – Cd) ^{235}U fission rate in the SINRD detector ratio, increased the slope of the SINRD signature by 54% for fresh LEU fuel and by 74% for fresh MOX fuel. The slope of the SINRD signature for BWR fresh MOX fuel is approximately 73% greater than for fresh LEU fuel. This is primarily due to the fact that the ^{239}Pu fission cross-section is an order of magnitude larger than the ^{235}U fission cross-section within the (Gd – Cd) absorption cutoff energy window.

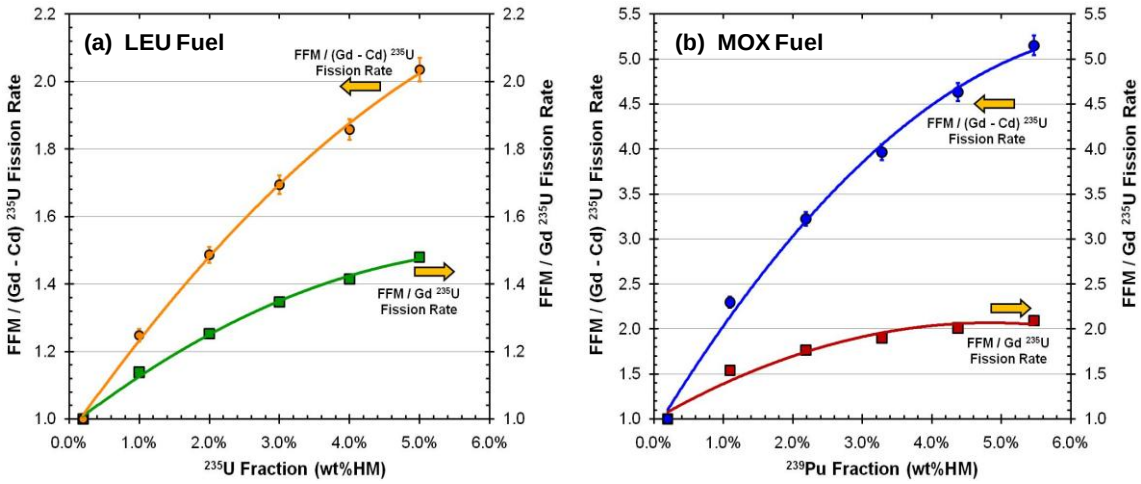

Fig. 7.1. Comparison of the FFM / Gd ^{235}U to FFM / (Gd – Cd) ^{235}U FC ratios for BWR fresh (a) LEU and (b) MOX fuel.

The FFM / (Gd – Cd) ^{235}U FC ratio was optimized for measuring the fissile content in LWR fresh fuel assemblies. Comparison of the SINRD detector ratio signature for

BWR 9x9 FA versus PWR 17x17 FA is shown in Fig. 7.2 for fresh (a) LEU and (b) MOX fuel. These results were not normalized to the case with all DU pins. For BWR fresh fuel, the slope of the (Gd – Cd) ^{235}U FC ratio was essentially unchanged for LEU fuel and decreased by 10% at high ^{239}Pu fractions for MOX fuel compared to PWR fresh fuel. Thus, based on the results shown in Fig. 7.2, the optimized (Gd – Cd) SINRD ratio is largely insensitive to the type of fuel assembly being measured. This may be attributed to the fact that the source strength and geometric coupling between SINRD and the fuel assembly cancels in the FC ratio.

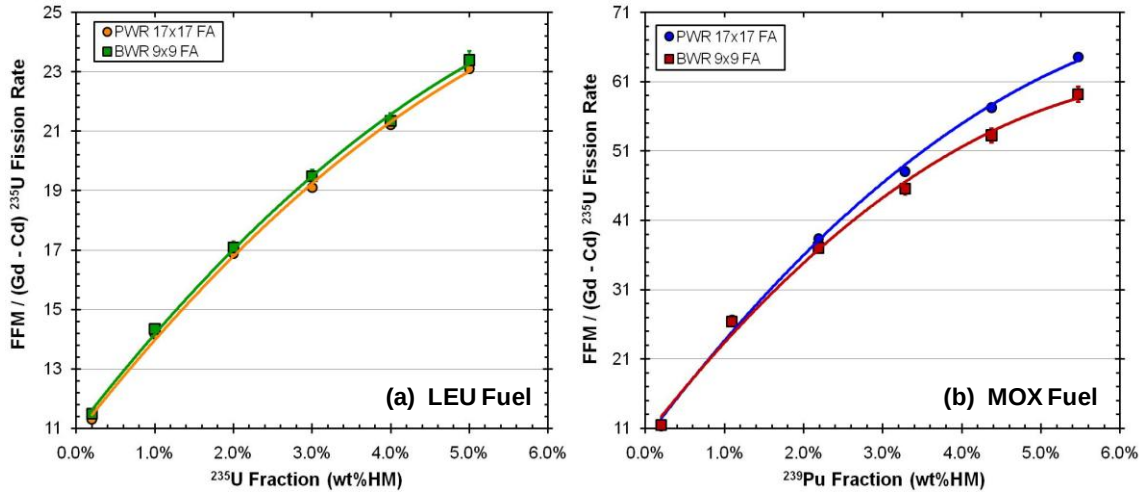

Fig. 7.2. Comparison of FFM / (Gd – Cd) ^{235}U FC ratio in PWR 17x17 FA versus BWR 9x9 FA for fresh (a) LEU and (b) MOX fuel.

7.2. Sensitivity of SINRD to Pin Removal in BWR Fuel Assembly

To assess the sensitivity and penetrability of SINRD, partial defects were modeled in BWR 9x9 fresh LEU (3% ^{235}U) and MOX (6% Pu) fuel assemblies. We have uniformly removed 4 and 18 fuel pins (5% and 24% of the pins, respectively) from two different radial regions of the assembly and replaced them with DU pins. The fuel pin removal locations of partial defects for Regions 1 and 2 are shown in Fig. 7.3. Region 1 consists of the second row from the outer surface of assembly and Region 2 consists of

rows in the center of the assembly. The average depth from the outer surface is 2.16-cm for Region 1 and 5.75-cm for Region 2.

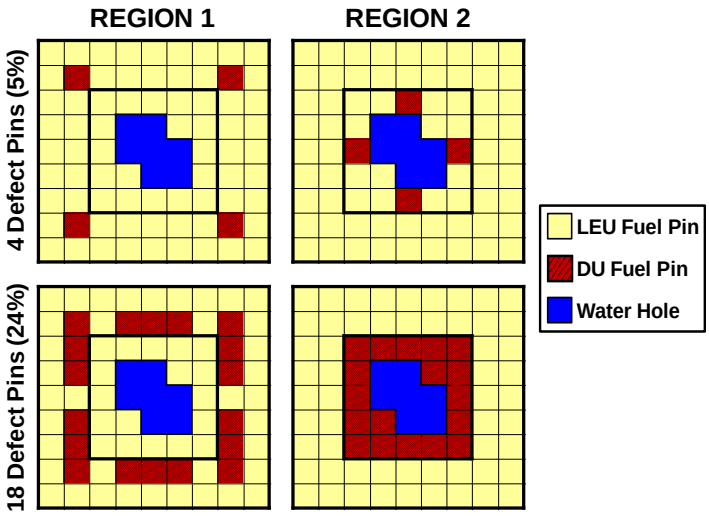

Fig. 7.3. Fuel pin removal locations of defects for Regions 1 and 2 in BWR 9x9 assembly where red pin locations represent fuel pins that were removed and blue locations are water holes.

The sensitivity of different SINRD detector ratios with 5% and 24% of the total number of pins removed from Regions 1 and 2 are given in Table 7.2 for BWR fresh LEU and MOX fuel. The percent change in the SINRD ratios was calculated for each region to determine if the diverted pins can be detected within 3σ confidence level. The values shown in bold correspond to the maximum positive and negative percent change in ratios that are within 3σ uncertainty for 5% and 24% pins removed from each region. The cells that are shaded gray correspond to the percent in change detector ratios that are not within 3σ uncertainty of an assembly with no diverted pins. The sensitivity results shown in Table 7.2 are summarized below:

- All SINRD ratios have the highest sensitivity to pin removal in Region 1.
- 5% Pin Defects: FFM / Bare ^{235}U FC ratio is the most sensitive SINRD ratio for detecting pin diversions within 3σ from Regions 1 and 2.

- This ratio is sensitive to reactivity changes in the fuel assembly due to changes in the concentration of thermal absorbers.
- The percent change in this ratio is positive for pin removal from Regions 1 – 2.

- 24% Pin Defects: Bare / Cd ^{235}U FC ratio is the most sensitive SINRD ratio for detecting pin diversions within 3σ from Regions 1 and 2.
  - This ratio is proportional to $p_{th} \cdot P_{TL}$ and inversely proportional to $p_{cut}^{Cd} \cdot P_{EL}^{Cd}$.
  - Thus, Bare / Cd ^{235}U FC ratio is sensitive to changes in the concentration of thermal absorbers relative to resonance absorbers in the fuel assembly.
  - The percent change in this ratio is negative for pin removal from Regions 1 – 2.

Table 7.2. Percent change in SINRD ratios with 5% and 24% fuel pins removed from Regions 1 and 2 for BWR fresh LEU and MOX fuel.

% Pin Defects	SINRD Ratios *BWR Fresh Fuel*	REGION 1		REGION 2	
		LEU	***MOX***	***LEU***	***MOX***
5% Pin Defects (4 pins)	FFM / (Gd - Cd) ^{235}U	*4.06%*	*4.75%*	*1.16%*	*1.53%*
	FFM / Gd ^{235}U	3.02%	2.63%	*0.86%*	*0.40%*
	FFM / Bare ^{235}U	**7.25%**	**7.14%**	**4.06%**	**3.41%**
	Bare ^{235}U / Gd ^{235}U	-4.56%	-4.86%	-3.34%	-3.11%
	Bare ^{235}U / Cd ^{235}U	***-5.50%***	**-5.74%**	**-3.60%**	**-3.55%**
24% Pin Defects (18 pins)	FFM / (Gd - Cd) ^{235}U	10.2%	17.0%	*-0.03%*	*-0.11%*
	FFM / Gd ^{235}U	5.34%	6.30%	-2.46%	*-2.49%*
	FFM / Bare ^{235}U	**15.8%**	**18.0%**	**6.11%**	**7.01%**
	Bare ^{235}U / Gd ^{235}U	-12.4%	-14.3%	-9.14%	-10.2%
	Bare ^{235}U / Cd ^{235}U	**-17.6%**	**-20.0%**	**-11.4%**	**-11.2%**

Error propagations (Appendix B) were used to calculate the uncertainties in the percent change in the SINRD ratios for all diversion cases. The uncertainties in these ratios were between 0.2% – 1.2% for count times of 30 minutes and 1.5 hours for BWR fresh LEU and MOX fuel, respectively. In practice, SINRD would require the use of an external ^{252}Cf source to measure a BWR fresh LEU fuel assembly. Thus, the count time of 30 minutes used for fresh LEU fuel represents the expected count time if a 1.0E+07

n/s ^{252}Cf source was used. This type of measurement could show the departure from a reference fuel assembly with no defects. The uncertainties in the SINRD ratios are higher for BWR fresh fuel assembly because the mass of the fuel is smaller. Thus, the expected count rates are lower. The count time was chosen to maximize the number of ratios that are within 3σ uncertainty of an assembly with no diverted pins.

7.2.1. Graphical Analysis of Partial Defects Results

Next, a graphical analysis of the partial defects results was performed. We chose to use the FFM / Bare ^{235}U FC ratio in this analysis because it was the most sensitive ratio for detecting 5% fuel pin diversions within 3σ from Regions 1 and 2. The effect of removing fuel pins on the FFM / Bare ^{235}U FC ratio for each diversion case is shown in Fig. 7.4 for BWR fresh (a) LEU and (b) MOX fuel. The solid line represents the signal from the no diversion case; the dashed lines represent ±2% change in the SINRD ratio to account for systematic errors. These results show that the SINRD ratio has the highest sensitivity to fuel pin diversions from Region 1. It is also important to note that all of the diversion cases are clearly outside of ±2% of the no diversion signal.

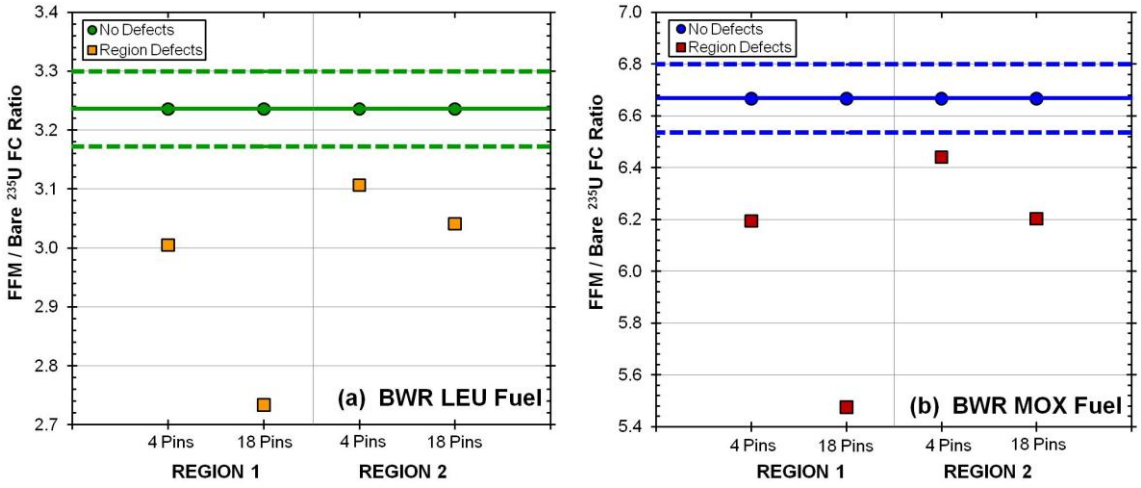

Fig. 7.4. Pin removal results for FFM / Bare ^{235}U FC ratio as a function diversion case for BWR fresh (a) LEU and (b) MOX fuel.

7.2.2. Statistical Analysis of Partial Defects Results

The procedure described in section 5.2 was used to calculate the nondetection probability, β, for SINRD ratios with 5% and 24% fuel pins removed from Regions 1 and 2. The results are given in Table 7.3 for BWR fresh LEU and MOX fuel. The values for β that are greater than 20% have been shaded gray for fresh LEU and MOX fuel. In general, β > 20% is considered a high nondetection probability and that ratio is not considered useful for detecting pin diversions. Referring to Table 7.3, it should be noted that for Region 2 defects, β for the FFM / Gd and FFM / (Gd – Cd) ^{235}U FC ratios increases when the percentage of pin defects was increased from 5% to 24%. For all other SINRD ratios, β decreases. This may be attributed to the fact that for both LEU and MOX fuel, removing 24% of the pins from Region 2 decreases the FFM by same amount as the (Gd – Cd). Thus, the sensitivity to pin removal cancels out in the ratio. The effect of 5% region defects on the FFM / Bare ^{235}U probability distribution is shown in Fig. 7.5 for BWR fresh (a) LEU and (b) MOX fuel. Similar to the PWR fresh fuel results (Fig. 5.7, section 5.2.2), the FFM / Bare ^{235}U FC ratio is the best ratio for detecting pin diversions.

Table 7.3. Mean ± 1σ and β for SINRD ratios with 5% fuel pins removed from Regions 1 and 2 for BWR fresh LEU and MOX fuel.

Fuel Type	SINRD Ratios	No Defects	REGION 1		REGION 2	
		Mean ± 1σ	***Mean ± 1σ***	***β***	***Mean ± 1σ***	***β***
LEU Fuel (3% ^{235}U)	FFM / (Gd - Cd) ^{235}U	19.5 ± 0.211	18.7 ± 0.199	1.3%	19.3 ± 0.210	*72%*
	FFM / Gd ^{235}U	8.79 ± 0.036	8.52 ± 0.035	0%	8.71 ± 0.036	*33%*
	FFM / Bare ^{235}U	3.19 ± 0.009	2.95 ± 0.008	0%	3.06 ± 0.008	0%
	Bare ^{235}U / Gd ^{235}U	2.76 ± 0.013	2.88 ± 0.013	0%	2.85 ± 0.013	0%
	Bare ^{235}U / Cd ^{235}U	5.03 ± 0.029	5.30 ± 0.030	0%	5.21 ± 0.030	0%
MOX Fuel (6% Pu)	FFM / (Gd - Cd) ^{235}U	45.6 ± 1.134	43.4 ± 1.073	*39%*	44.9 ± 1.138	*85%*
	FFM / Gd ^{235}U	12.4 ± 0.066	12.1 ± 0.066	0%	12.4 ± 0.068	*81%*
	FFM / Bare ^{235}U	6.62 ± 0.027	6.14 ± 0.025	0%	6.39 ± 0.026	0%
	Bare ^{235}U / Gd ^{235}U	1.87 ± 0.012	1.97 ± 0.013	0%	1.93 ± 0.013	0%
	Bare ^{235}U / Cd ^{235}U	2.58 ± 0.018	2.72 ± 0.020	0%	2.67 ± 0.019	0%

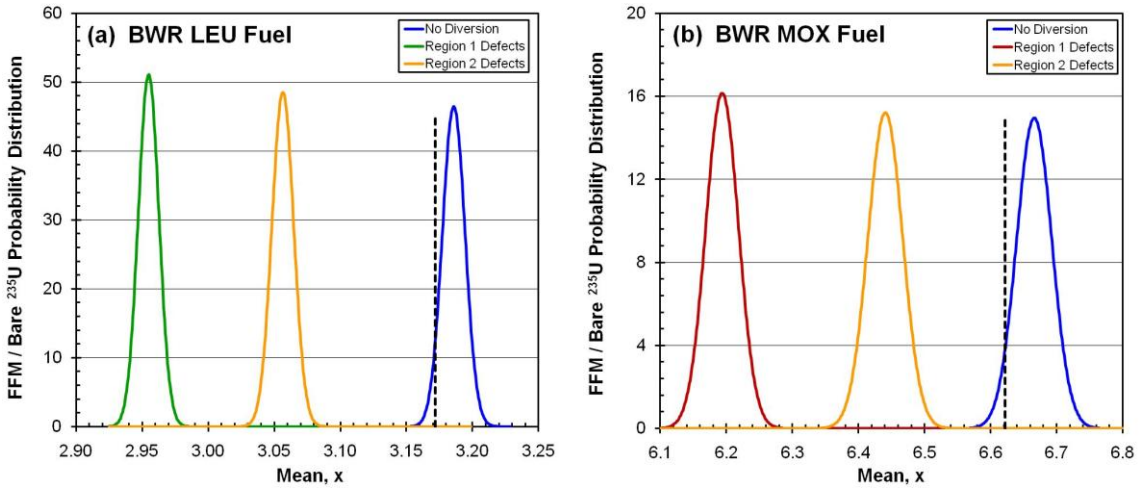

Fig. 7.5. Effect of region defects on FFM / Bare ^{235}U probability distribution versus mean for BWR fresh (a) LEU and (b) MOX fuel.

The percent change in (a) FFM / Bare ^{235}U FC ratio and (b) Bare / Cd ^{235}U FC ratio versus the percentage of pins removed is shown in Fig. 7.6 for BWR fresh LEU and MOX fuel. Using the diversion results for 5% and 24% partial defects, the average percent change in the SINRD ratio per fuel pin removed was calculated for each region and then multiplied by an increasing number of fuel pins. For both SINRD ratios, the sensitivity to pin removal is highest in Region 1. In contrast to the results shown for PWR fresh fuel in water (Fig. 5.8), no combination of fuel pins from Regions 1 and 2 could result in 0% percent change in FFM / Bare ^{235}U FC ratio.

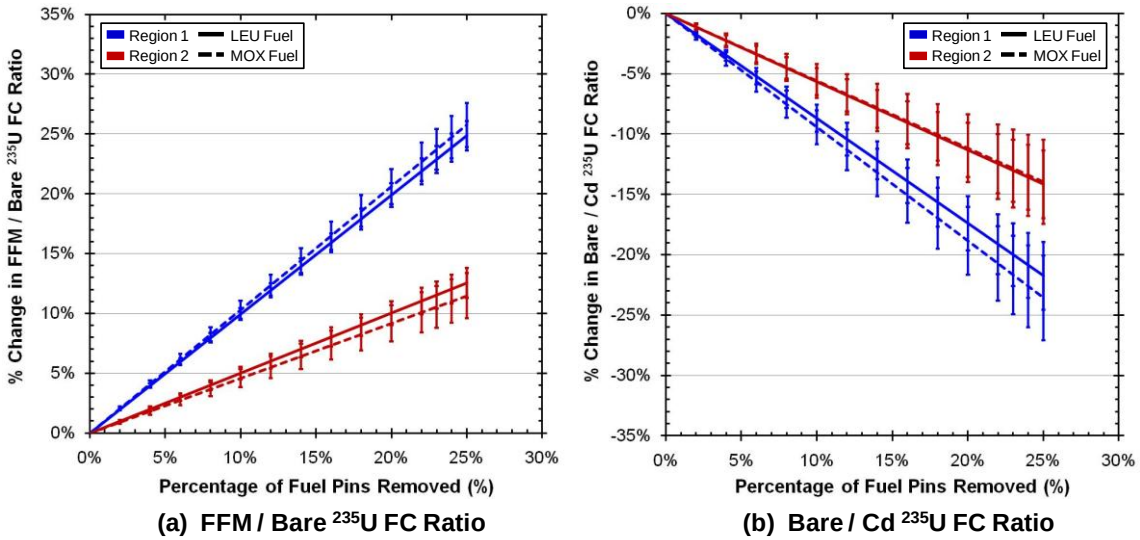

Fig. 7.6. Sensitivity to partial defects: % change in (a) FFM / Bare ^{235}U FC ratio and (b) Bare / Cd ^{235}U FC ratio versus % of fuel pins removed for BWR fresh LEU and MOX fuel**.**

To obtain a better understanding of the sensitivity of the SINRD ratios to region defects, the percent change in (a) Bare ^{235}U, (b) FFM ^{235}U, (c) Gd ^{235}U, and (d) Cd ^{235}U fission rates versus the percentage of pins removed is shown in Fig. 7.7 for BWR fresh LEU and MOX fuel. In contrast the results shown in Fig. 7.6, all of the SINRD FCs have the highest sensitivity of to pin removal from Region 2 (center). This may be attributed to the fact that the multiplication is highest in the center of the assembly.

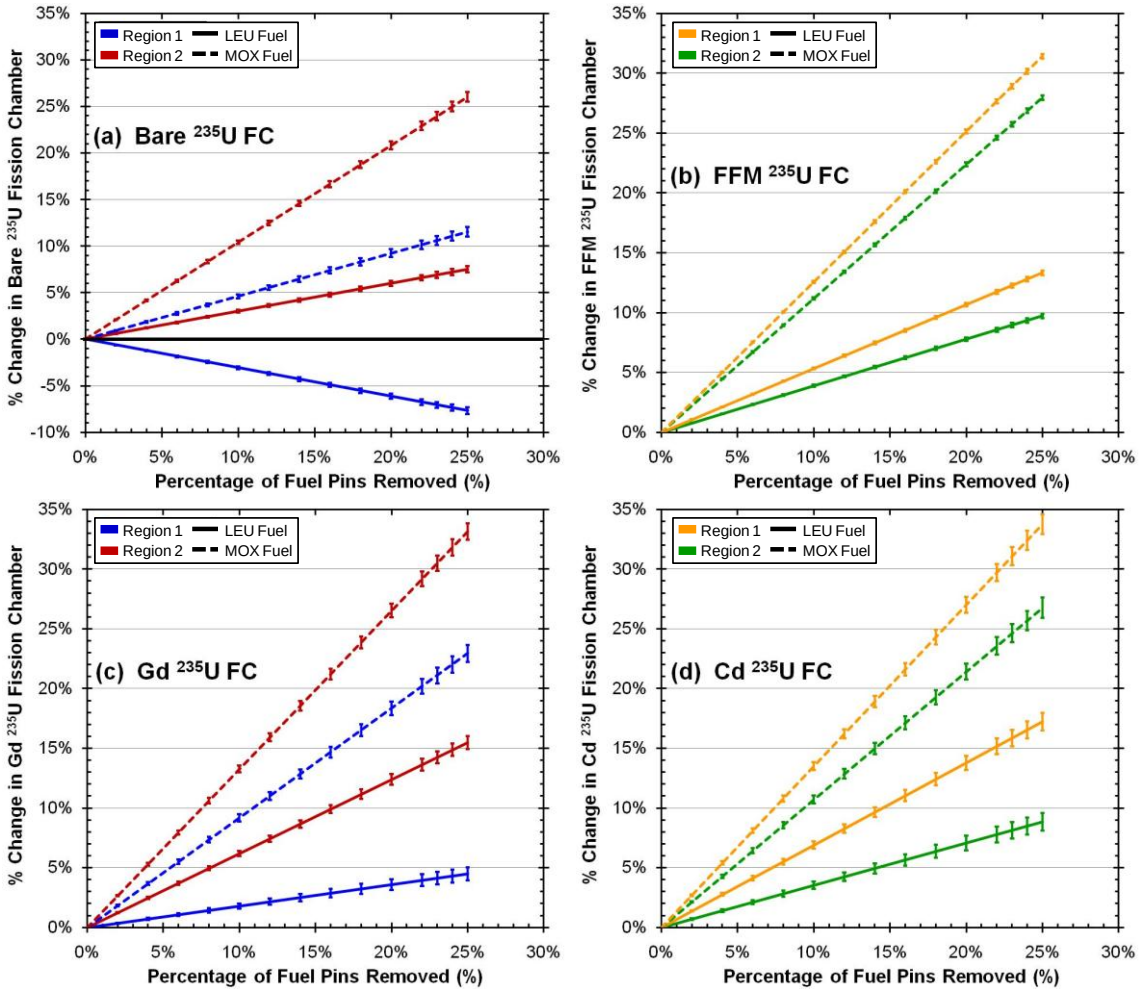

Fig. 7.7. Percent change in (a) Bare ^{235}U, (b) FFM ^{235}U, (c) Gd ^{235}U, and (d) Cd ^{235}U fission rates versus % of fuel pins removed for BWR fresh LEU and MOX fuel.

7.3. Summary of BWR Fresh Fuel Results

We have simulated the change in the FFM / (Gd – Cd) covered ^{235}U FC ratio for BWR 9x9 fresh LEU and MOX fuel assemblies. This ratio is sensitive to the fissile content in both LEU and MOX fuel assemblies and has not saturated for fissile loadings up to 6%. The slope of the SINRD signature for BWR fresh MOX fuel is approximately 73% greater than for BWR fresh LEU fuel. This is primarily due to the fact that the ^{239}Pu fission cross-section is an order of magnitude larger than the ^{235}U fission cross-section within the (Gd – Cd) absorption cutoff energy window (0.13 eV – 1.25 eV). For BWR

fresh fuel, the slope of the (Gd – Cd) ^{235}U FC ratio increased by 0.8% for LEU fuel and decreased by 10% for MOX fuel compared to PWR fresh fuel. Thus, the optimized FFM / (Gd – Cd) ^{235}U FC ratio is not sensitive to the type of fuel assembly being measured. This may be attributed to the fact that the source strength and geometric coupling between SINRD and the fuel assembly cancels in the ratio.

The sensitivity and penetrability of SINRD was assessed by modeling partial defects in BWR 9x9 fresh LEU and MOX fuel assemblies. The percent change in the SINRD ratios was calculated for Regions 1 and 2 to determine if the diverted pins can be detected with a 3σ confidence level. The uncertainties in these ratios were between 0.2% – 1.2% for count times of 30 minutes and 1.5 hours for BWR fresh LEU and MOX fuel, respectively. Thus, this type of measurement could show the departure from a reference fuel assembly with no defects. A statistical analysis was also performed to obtain a better understanding of how the uncertainty in the SINRD ratios in affects the ability to detect pin diversions. Similar to results for PWR fresh fuel in water, the FFM / Bare ^{235}U FC ratio is best ratio for detecting pin diversions.

8. ANALYSIS OF PWR 17X17 SPENT FUEL ASSEMBLY

The use of SINRD to quantify the fissile content in spent fuel and detect possible diversion scenarios was analyzed for PWR 17x17 spent LEU and MOX fuel assemblies. First, we calculated the isotopic composition of the spent fuel assemblies over the burnup range of 0 to 50-GWd/MTU (in 10-GWd increments). Then, we simulated SINRD's response to each spent fuel assembly in water with and without 2200-ppm of boron. In the MCNPX simulations of SINRD, spontaneous fission neutrons from ^{244}Cm were used to self-interrogate the spent fuel pins. The fuel burnup and initial enrichment were varied to observe how SINRD's response changes as a function of ^{235}U, ^{239}Pu, and ^{240}Pu content in the fuel. The SINRD detector configuration was optimized for PWR spent LEU and MOX fuel assemblies based on the concentration of ^{239}Pu relative to ^{240}Pu. The same specifications for a PWR 17x17 fuel assembly given in Table 5.1 for the fresh fuel simulations were also used for the spent fuel simulations.

8.1. Calculation of PWR Spent Fuel Isotopics

TransLAT was used to calculate the isotopic composition of PWR spent LEU and spent MOX fuel over the burnup range of 0 to 50-GWd/MTU. TransLAT is a three-dimensional lattice physics code with burnup capability. This code uses two- and three-dimensional multi-group integral transport theory methods and cross-section data based on ENDF/B-VI evaluation for its calculations [29]. The primary purpose for using TransLAT versus other burnup codes, such as Origen 2.2 or SCALE 5.1, was to calculate the spent fuel isotopic fractions as a function of fuel pin radius. This is needed in order to account for the large spatial gradient of higher actinide buildup across the fuel pellet. Using TransLAT, we modeled a PWR pin cell with 20 radial fuel regions. The radius of each fuel region was determined using an exponential transform. The PWR operating parameters (power density, temperature, pressure, etc.) used in TransLAT were obtained from the OECD/NEA Burnup Credit Benchmark Phase IV-B for a PWR 17x17 spent MOX fuel assembly [42].

The ^{239}Pu concentration as a function of fuel radius for PWR spent LEU and MOX fuel is shown in Fig. 8.1(a) and (b), respectively. These results clearly show the large spatial gradient of ^{239}Pu across the fuel pellet. To determine how this gradient affects our SINRD ratios, we modeled 1, 2, and 4 radial fuel regions in each fuel pin in spent LEU and MOX fuel assemblies. Since TransLAT uses integral transport theory methods for burnup calculations, a large number of radial regions were needed to accurately account for spatial self-shielding effects in the fuel; however, this is not needed in MCNPX. Therefore, we reduced the number of radial regions from 20 to a maximum of 4 to minimize the complexity of our MCNPX simulations. The spatial gradient of ^{239}Pu across the fuel pellet was used to determine the radius of each fuel region. The locations of the fuel regions are labeled in Fig. 8.1 for a total of 2 (a) and 4 (b) radial regions.

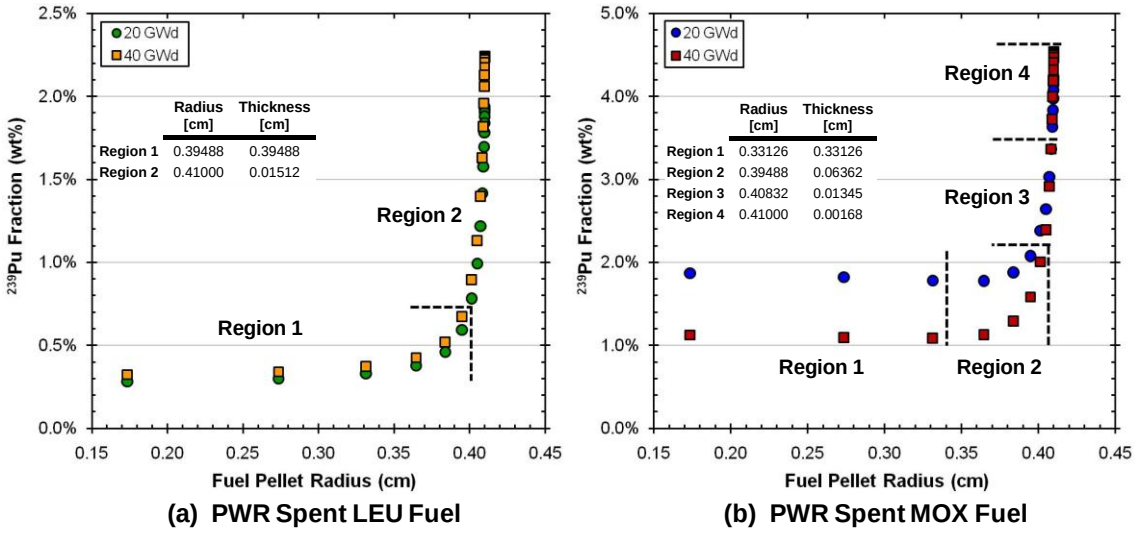

Fig. 8.1. ^{239}Pu fraction versus fuel pellet radius in PWR spent (a) LEU and (b) MOX fuel.

The sensitivity of the FFM / (Gd – Cd) ^{235}U FC ratio versus number of radial fuel regions is shown in Fig. 8.2 for PWR spent (a) LEU and (b) MOX fuel with 2200-ppm boron in water. Comparing the results for 1 versus 4 radial fuel regions, the maximum change in the SINRD ratio was 1.3% for LEU spent fuel and 7.5% for MOX spent fuel.

In order to minimize the computational time required for our MCNPX simulations, only one fuel region was modeled for PWR spent fuel. Appendix D contains an example TransLAT input deck for PWR spent LEU fuel with burnup of 40-GWd/MTU, 4% ^{235}U IE, and cooling time of 5-yrs.

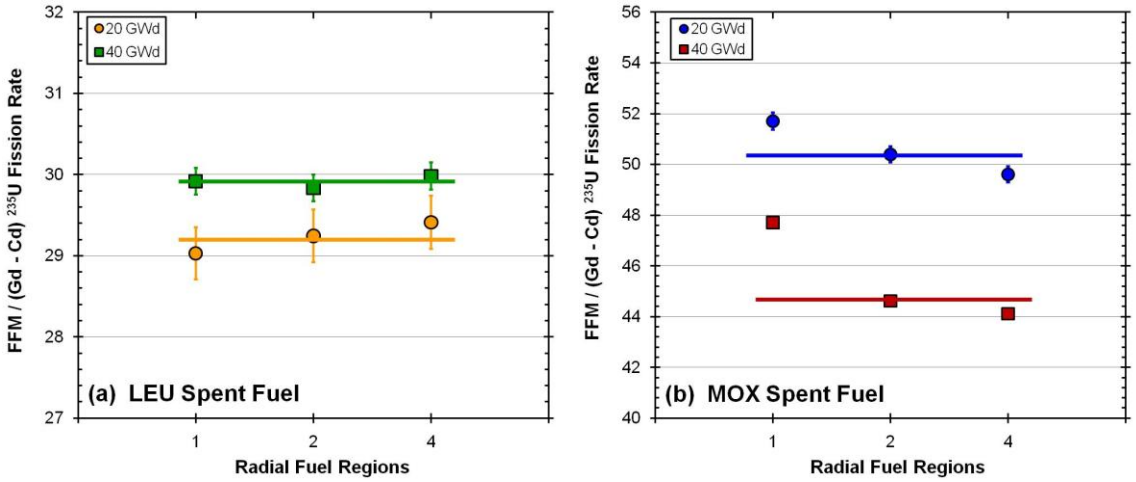

Fig. 8.2. Sensitivity of FFM / (Gd – Cd) ^{235}U FC ratio to the number of radial fuel regions for PWR spent (a) LEU and (b) MOX fuel with 2200-ppm boron in water.

8.2. PWR Spent LEU Fuel Assembly

In PWR spent LEU fuel, the primary isotopes of significance to SINRD are ^{235}U, ^{239}Pu, ^{240}Pu and ^{241}Pu. All of these isotopes have a large absorption resonance within the (Gd – Cd) cut-off energy window. Thus, the fission rate in Gd and Cd ^{239}Pu FCs is a function of the resonance absorption from all of these isotopes in spent fuel. The sensitivity of SINRD to a particular isotope is based on the magnitude of its cross-section and its concentration in spent fuel relative to the other isotopes. The sensitivity of SINRD to different combinations of filters and monitors was analyzed to determine the optimum configuration that maximized the FC ratio signature for measuring ^{239}Pu and ^{235}U in LEU spent fuel. We varied initial fuel enrichment from 4% to 5% ^{235}U to determine the sensitivity of SINRD to changes in the distribution of Pu isotopics in spent

fuel. The cooling time was fixed at 5-yrs. The calculated spent fuel isotopics for PWR spent LEU fuel are given in Table E.1 of Appendix E.

8.2.1. Optimized SINRD Ratios ^{239}Pu Measurements

To optimize the SINRD signature for measuring ^{239}Pu, we have used the 4% ^{235}U IE, 5-yrs cooled, LEU spent fuel as the base case. The effect of adding a Hf filter inside the Gd filter was investigated to determine if the absorption of low energy neutrons by ^{240}Pu was decreasing our detector ratio signature. The transmitted flux through a 2-mm Hf filter relative to the ^{240}Pu (n,γ) cross-section and buildup of plutonium isotopics in PWR spent LEU fuel is shown in Fig. 8.3(a) and (b), respectively.

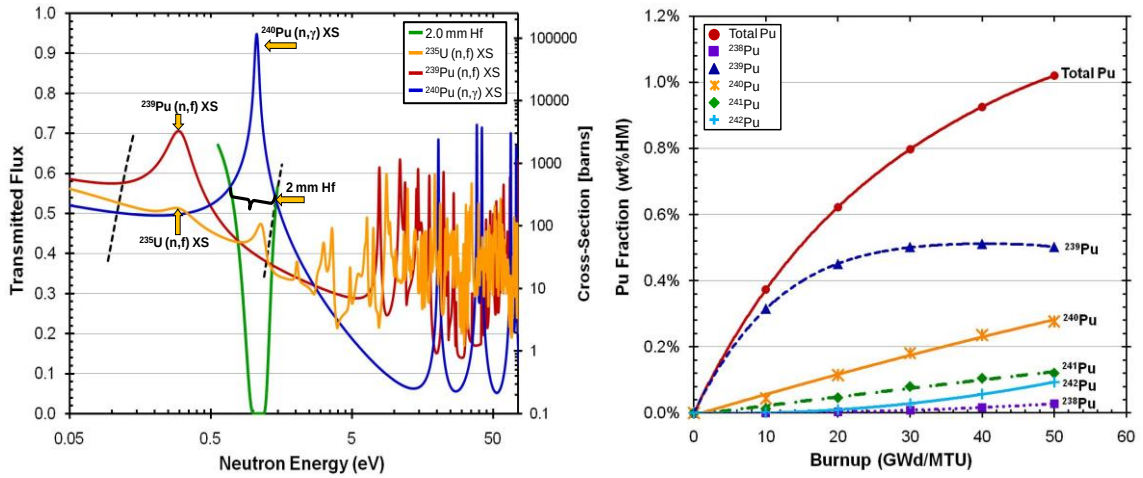

(a) Transmitted flux through 2.0 mm Hf **(b) Plutonium Isotopics versus Burnup**

Fig. 8.3. (a) Transmitted flux through 2-mm Hf relative to ^{240}Pu (n,γ) cross-section, (b) buildup of Pu isotopics in PWR spent LEU fuel (4% ^{235}U IE, 5-yrs cooled).

The effect of using 2-mm Hf on FFM / (Gd – Cd) ^{239}Pu FC ratio to maximize the SINRD FC ratio signature for measuring ^{239}Pu is shown in Fig. 8.4. These results have been normalized to the fresh fuel case (4% ^{235}U IE). In Fig. 8.4(a), the ^{239}Pu fraction in LEU spent fuel is compared to the FFM / (Gd+Hf – Cd) ^{239}Pu FC ratio as a function of burnup with no Hf and 2-mm Hf. It should be noted that the results for the SINRD ratio

closely follow the curve for the ^{239}Pu fraction in LEU spent fuel over the burnup range of 0 – 50 GWd/MTU. Fig. 8.4(b) shows the FFM / (Gd+Hf – Cd) ^{239}Pu FC ratio versus ^{239}Pu fraction in LEU spent fuel with no Hf and 2-mm Hf. Adding 2-mm Hf to the Gd ^{239}Pu FC increased the slope of the SINRD signature by 12%. This is due to the fact that the Hf filter absorbs the majority of neutrons in the same energy region as the ^{240}Pu (n,γ) resonance reducing the ^{240}Pu effect on the SINRD ratio. The purpose for plotting the (Gd+Hf – Cd) ^{239}Pu FC ratio results versus burnup in Fig. 8.4(a) and ^{239}Pu fraction in Fig. 8.4(b) was to illustrate that similarity of the curves in (a) translates to linear curves in (b) when the ratio was plotted versus ^{239}Pu fraction. One can also observe the effect of ^{240}Pu on the results with no Hf in Fig. 8.4(a) by the slight increase in the signal at 50-GWd/MTU. This is due to the fact that ^{240}Pu increases with higher burnup [Fig. 8.3(b)].

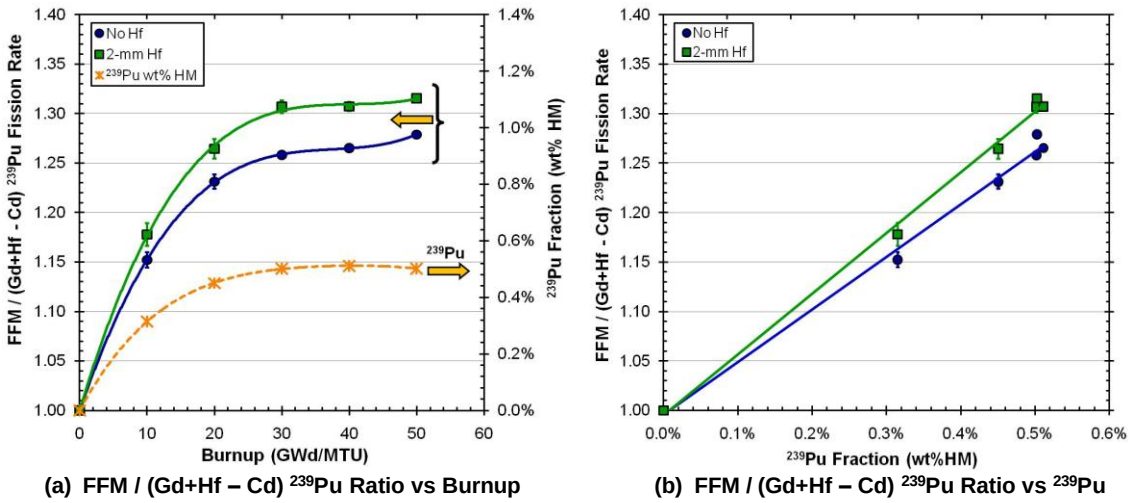

(a) FFM / (Gd+Hf – Cd) ^{239}Pu Ratio vs Burnup **(b) FFM / (Gd+Hf – Cd) ^{239}Pu Ratio vs ^{239}Pu**

Fig. 8.4. Optimized SINRD ratio for ^{239}Pu: FFM / (Gd+Hf – Cd) ^{239}Pu FC ratio versus (a) burnup and (b) ^{239}Pu wt%HM with no Hf and 2-mm Hf.

It is important to note that we normalized the results to the fresh fuel case because in practice SINRD could be calibrated using a fresh fuel assembly. The error bars shown on all results represent the calculated uncertainties in the SINRD detector ratios obtained via error propagations of expected counting statistics (see Appendix B). In Table 8.1, the

expected count rates in the SINRD FCs are given for a 40-GWd/MTU PWR spent LEU fuel assembly (4% IE, 5-yrs cooled). The use of 2-mm Hf in the Gd ^{239}Pu FC reduced the count rate by 43%. The effect of using Gd and Cd ^{235}U FCs compared to ^{239}Pu FCs decreased the count rates in the Gd FC by 61% and Cd FC by 9%. Using error propagations, the lower count rates in the Gd and Cd ^{235}U FCs increased the relative uncertainty in the FFM / (Gd – Cd) ^{235}U FC ratio by 68% compared to using ^{239}Pu FCs. This effect was further compounded by the 43% decrease in the slope of the SINRD ratio when all ^{235}U FCs were used. It should be noted that the (α,n) contribution to the total neutron emission rate from the assembly was not accounted for in these count rates. Thus, the expected count rates are somewhat conservative.

Table 8.1. Expected count rates in SINRD FCs from a 40-GWd PWR spent LEU fuel assembly (4% IE, 5-yrs cooled).

SINRD Detectors	PWR Spent LEU Fuel [cps]*	
	No Boron	***2200ppm Boron***
Bare ^{235}U	710 ± 0.544	378 ± 0.397
FFM ^{235}U	2532 ± 1.027	1811 ± 0.869
Gd ^{235}U	249 ± 0.322	165 ± 0.262
Cd ^{235}U	148 ± 0.248	104 ± 0.209
Gd ^{239}Pu	635 ± 0.514	412 ± 0.414
Gd+Hf ^{239}Pu	365 ± 0.390	240 ± 0.316
Cd ^{239}Pu	163 ± 0.261	116 ± 0.220

** Neutron source strength of 1.75E+08 n/s for BU = 40-GWd*

Next, the sensitivity of the FFM / (Gd+Hf – Cd) ^{239}Pu FC ratio to the addition of 2200-ppm boron to water was examined. The results are shown in Fig. 8.5 for (a) 4% ^{235}U and (b) 5% ^{235}U IE spent LEU fuel. It is important to note that adding 2200-ppm boron to water changed the SINRD signature by less than 5% for both cases. This change is negligible compared to the effect of boron on gross neutron methods [22] because SINRD is sensitive to the ^{239}Pu content in spent fuel which is not affected by

adding boron to the water. Furthermore, the FFM / Bare ^{235}U FC ratio can be used to verify the concentration of boron in the water.

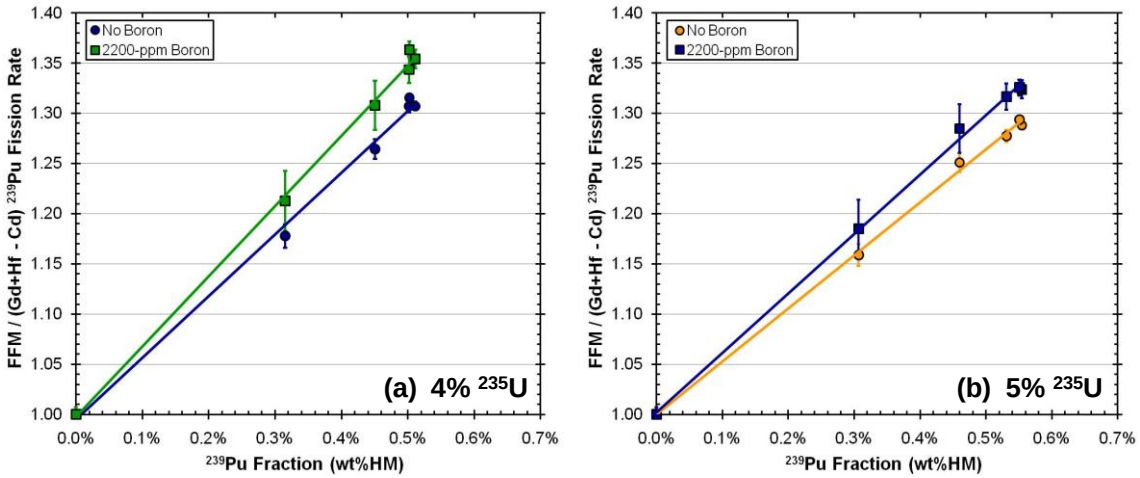

Fig. 8.5. Effect of adding 2200-ppm boron to water on the FFM / (Gd+Hf – Cd) ^{239}Pu FC ratio versus ^{239}Pu fraction in (a) 4% ^{235}U and (b) 5% ^{235}U IE spent LEU fuel.

The effect of using all ^{235}U FCs on the SINRD detector ratio signature was also examined to determine if the ^{239}Pu content in PWR spent LEU fuel could still be accurately quantified. The FFM / (Gd+Hf – Cd) ^{239}Pu FC ratio is compared to the FFM / (Gd – Cd) ^{235}U FC ratio versus ^{239}Pu fraction in Fig. 8.6(a) and (b), respectively. The results shown are for the case with 2200-ppm boron in water. The use of all ^{235}U FCs decreased the slope of the SINRD signature by a factor of 2 for both 4% and 5% ^{235}U IE spent LEU fuel. However, it is important to note that the FFM / (Gd – Cd) ^{235}U FC ratio still linearly tracks the ^{239}Pu content in PWR spent LEU fuel. It should also be noted that for both cases the SINRD ratio is slightly sensitive to the initial fuel enrichment.

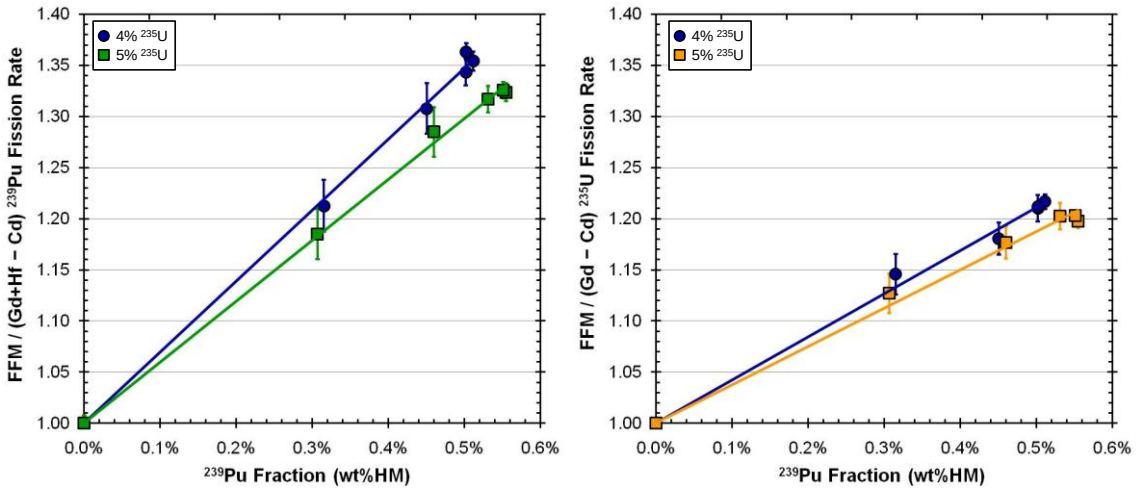

Fig. 8.6. Comparison of (a) FFM / (Gd+Hf – Cd) ^{239}Pu FC ratio to (b) FFM / (Gd – Cd) ^{235}U FC ratio versus ^{239}Pu fraction with 2200-ppm boron in water.

8.2.2. Use of SINRD to Measure ^{235}U

We have also investigated the use of SINRD to quantify the ^{235}U content in LEU spent fuel. The ability to measure ^{235}U using SINRD is important to verifying the burnup and initial enrichment of the fuel. In addition, this ability can be used in conjunction with the SINRD ratio for ^{239}Pu to more accurately determine the fissile content of the spent fuel assembly. To determine which SINRD ratio is best for quantifying ^{235}U, seven different ratios are shown in Fig. 8.7 versus ^{235}U fraction with no boron in water. These results were normalized to the fresh fuel case. The ratios shown in Fig. 8.7(a) have the FFM FC in the denominator and in Fig. 8.7(b) the Bare FC is in the denominator. It is important to note that the ^{235}U fraction shown on the x-axis in Fig. 8.7 is decreasing from left to right corresponding to burnup. Based on these results, we can see that the (Gd – Cd) ^{235}U / Bare ^{235}U FC ratio [Fig. 8.7(b)] is the only ratio that linearly tracks the ^{235}U content in PWR spent LEU fuel.

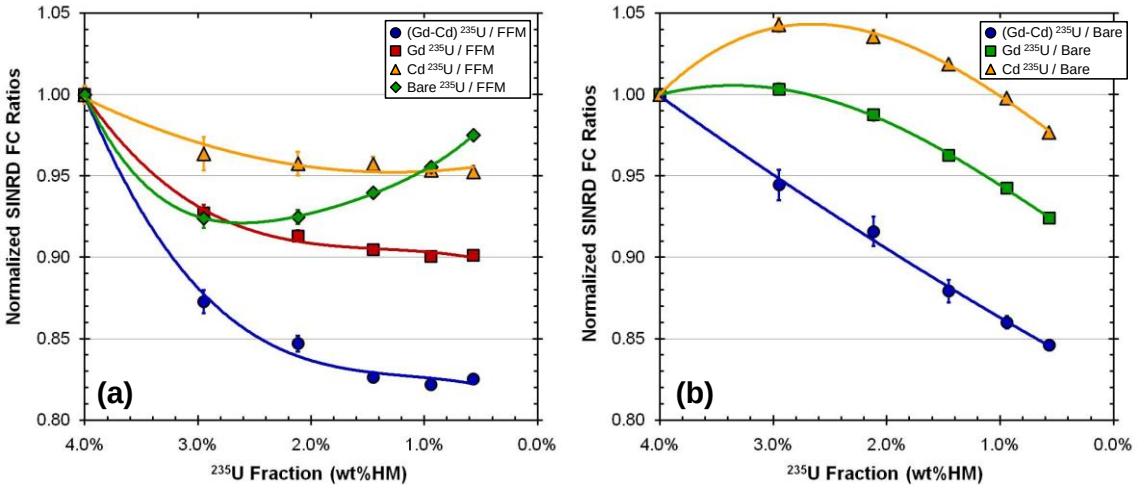

Fig. 8.7. Comparison of different SINRD ratios versus ^{235}U fraction in PWR spent LEU fuel with 4% IE and no boron in water.

In order to determine if resonance absorption by ^{239}Pu within the (Gd – Cd) energy window is contributing to our SINRD signature, the (Gd – Cd) ^{235}U / Bare ^{235}U FC ratio is shown in Fig. 8.8 versus (a) ^{235}U fraction and (b) ^{235}U + ^{239}Pu fraction. These results are shown with no boron and 2200-ppm boron in water to assess the sensitivity of this ratio boron. Similar to previous results, the addition of 2200-ppm boron to water had a small effect (<5%) on the SINRD signature which can be corrected for as discussed in previous section. Comparing the results shown in Fig. 8.8, there is a linear correlation between the (Gd – Cd) ^{235}U / Bare ^{235}U FC ratio versus only ^{235}U and versus ^{235}U + ^{239}Pu in LEU spent fuel. To better understand the underlying physics of this SINRD ratio, Fig. 8.9(a) shows the neutron flux multiplied by neutron energy, $E \cdot \phi(E)$, at burnups of 10, 30, and 50-GWd relative to Gd and Cd cut-off energies with no boron in water. In Fig. 8.9(b), the ^{235}U and ^{239}Pu fission cross-sections versus neutron energy are shown relative to Gd and Cd cut-off energies. The results in Fig. 8.9(a) show that the resonance absorption within the (Gd – Cd) energy window (indicated by black arrow) increases as the fuel burnup increases due to the buildup of ^{239}Pu. This indicates that ^{239}Pu absorption within the (Gd – Cd) energy window is contributing to our SINRD signature and thus should be accounted for.

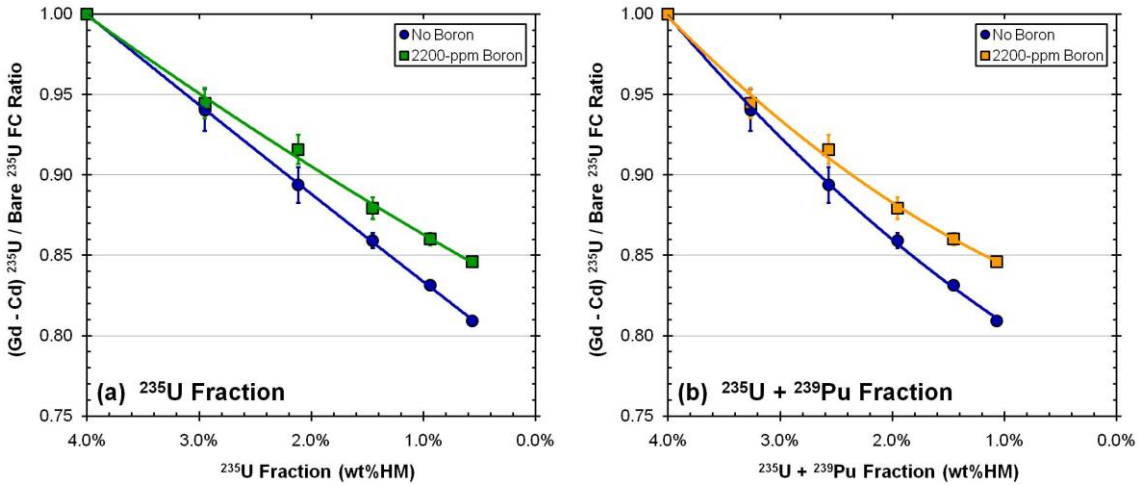

Fig. 8.8. (Gd – Cd) ^{235}U / Bare ^{235}U FC ratio versus (a) ^{235}U fraction and (b) ^{235}U + ^{239}Pu fraction in BWR spent LEU fuel with no boron and 2200-ppm boron in water.

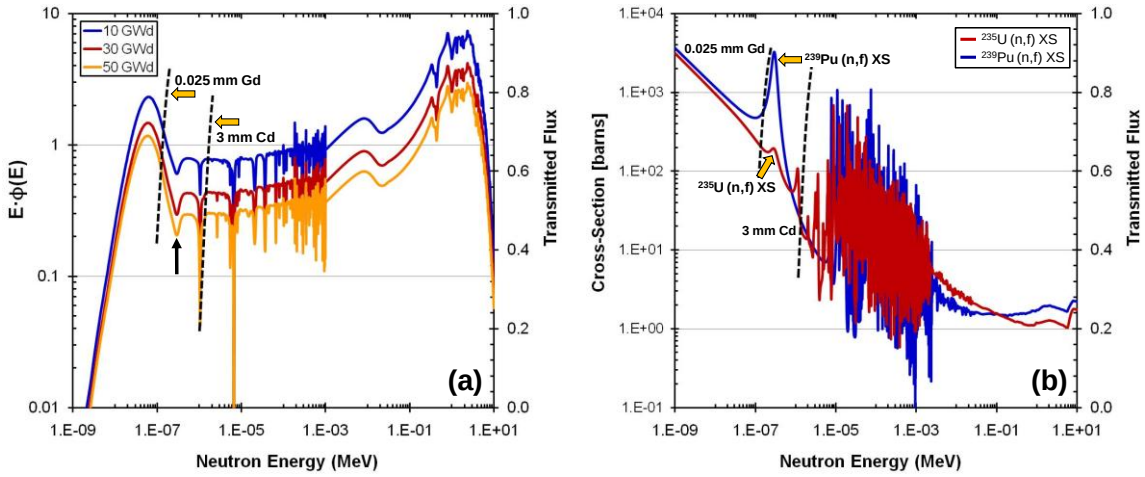

Fig. 8.9. Comparison of (a) E·ϕ(E) at burnups of 10, 30, and 50-GWd and (b) ^{235}U and ^{239}Pu fission cross-sections versus neutron energy relative to Gd and Cd cut-off energies.

Next, the effect of varying the initial ^{235}U IE on the (Gd – Cd) ^{235}U / Bare ^{235}U FC ratio was analyzed. The results are shown Fig. 8.10 versus ^{235}U + ^{239}Pu fraction in PWR spent LEU fuel with no boron and 2200-ppm boron in water. In contrast to previous results, these results were not normalized to the fresh fuel case. Varying the initial ^{235}U IE, changed the SINRD ratio by less than 5% over burnup range of 0 to 50-GWd/MTU.

For both 4% and 5% ^{235}U IE, the SINRD ratio linearly tracks the ^{235}U + ^{239}Pu content spent LEU fuel. It should be noted that the slope of the SINRD FC ratio signature for measuring ^{235}U + ^{239}Pu using all ^{235}U FCs decreased by a factor of 9.6 compared to the slope for measuring ^{239}Pu using ^{239}Pu FCs. This may be attributed to the fact that the ^{239}Pu fission cross-section is an order of magnitude larger than the ^{235}U fission cross-section within the (Gd – Cd) energy window. As a result, ^{239}Pu FCs have a higher sensitivity to ^{239}Pu resonance absorption in spent fuel.

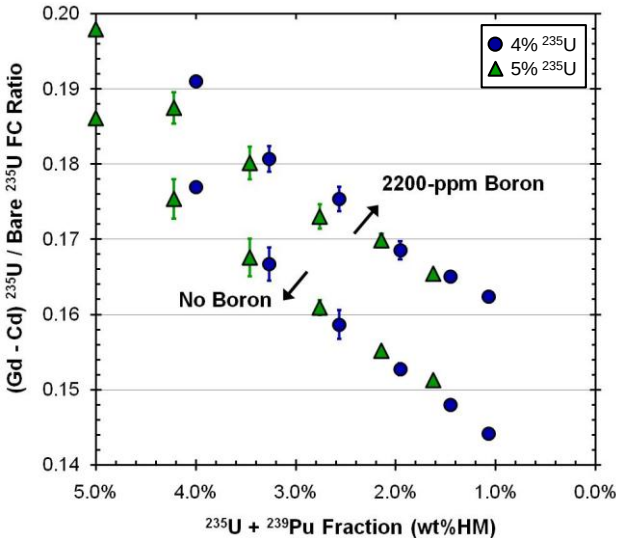

Fig. 8.10. Effect of varying IE on (Gd – Cd) ^{235}U / Bare ^{235}U FC ratio versus ^{235}U + ^{239}Pu fraction in PWR spent LEU fuel with and without boron in water.

8.3. PWR Spent MOX Fuel Assembly

In order to better understand the physics of the SINRD technique, we have also simulated the use of SINRD to measure the ^{239}Pu and ^{240}Pu content in a PWR 17x17 spent MOX fuel assembly. The initial enrichment was varied from 6% to 4% Pu to determine the sensitivity of SINRD to variations in the distribution of plutonium isotopics in MOX spent fuel. The cooling time was fixed at 5-yrs. We believe that SINRD technique will work better for a PWR assembly with spent MOX fuel because

the ^{239}Pu concentration is significantly larger and the ^{235}U concentration is significantly smaller (<0.15 wt%HM) compared to PWR spent LEU fuel. It should also be noted that since the ^{235}U fraction is so small in PWR spent MOX fuel, we did not try to quantify it. The calculated spent fuel isotopics for PWR spent MOX fuel is given in Table E.2 of Appendix E.

8.3.1. Optimized SINRD Ratios for ^{239}Pu Measurements

To optimize the SINRD signature for measuring ^{239}Pu, we have used the 6% Pu IE spent MOX fuel (5-yrs cooled) with no boron in water as the base case. The effect of adding a Hf filter inside the Gd filter was investigated to determine how the absorption of low energy neutrons by ^{240}Pu affects our SINRD ratios. The transmitted flux through a 1-mm Hf filter relative to the ^{240}Pu (n,γ) cross-section and the buildup of Pu isotopics in PWR spent MOX fuel is shown in Fig. 8.11(a) and (b), respectively.

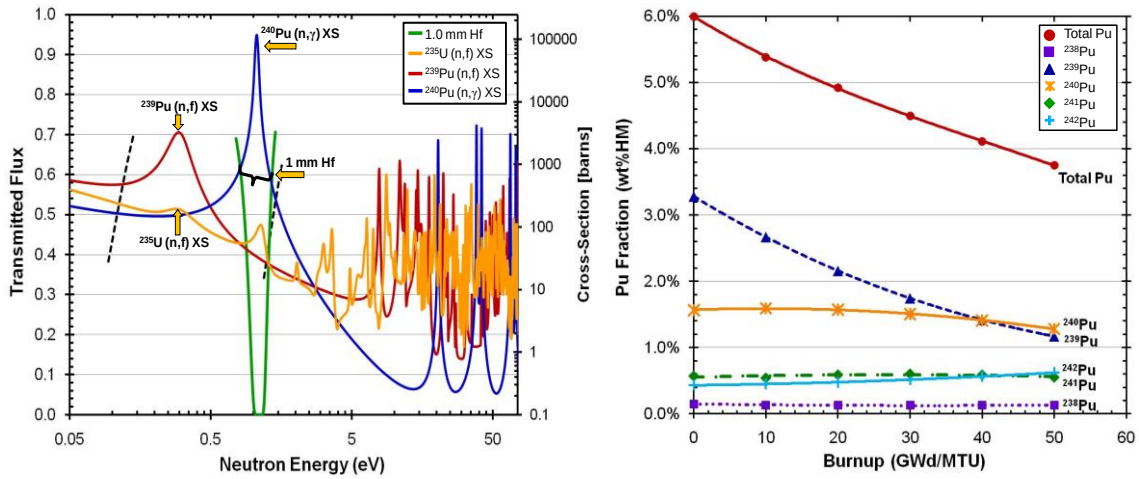

Fig. 8.11. (a) Transmitted flux through 1-mm Hf relative to ^{240}Pu (n,γ) cross-section, (b) buildup of Pu isotopics in PWR spent MOX fuel (6% Pu IE, 5-yrs cooled).

The effect of using all ^{235}U FCs on the FFM / (Gd+Hf – Cd) FC ratio versus ^{239}Pu fraction is shown in Fig. 8.12 with no boron in water. These results were normalized to

the fresh fuel case. It is important to note that the ^{239}Pu fraction shown on the x-axis in Fig. 8.12 is decreasing from left to right corresponding to burnup. For instance, the last data point on the right at 1.2% ^{239}Pu corresponds to a burnup of 50-GWd. The use of Hf increased the SINRD signature by 8% using ^{239}Pu FCs and by 51% using all ^{235}U FCs. This is attributed to the fact the Hf filter absorbs the majority of neutrons in the same energy region as the ^{240}Pu (n,γ) resonance reducing the ^{240}Pu effect on the SINRD ratio. It is also important to note that adding 1-mm Hf to the ^{235}U FC ratio [Fig. 8.12(b)] also significantly increased the linearity of the results. This is important because it indicates that the addition of Hf to our SINRD ratio enables us to track the ^{239}Pu concentration in spent MOX fuel more accurately.

Since the concentration of ^{240}Pu relative to ^{239}Pu is significant in PWR spent MOX fuel, we hypothesized that the parasitic absorption of low energy neutrons by ^{240}Pu would dominate within the (Gd – Cd) energy window. To test this hypothesis, the FFM / (Gd – Cd) FC ratio is shown in Fig. 8.13 as a function of (a) ^{239}Pu and (b) ^{240}Pu fractions. These results clearly show that without Hf our SINRD ratio is proportional to the ^{240}Pu content in spent MOX fuel not the ^{239}Pu content confirming our hypothesis.

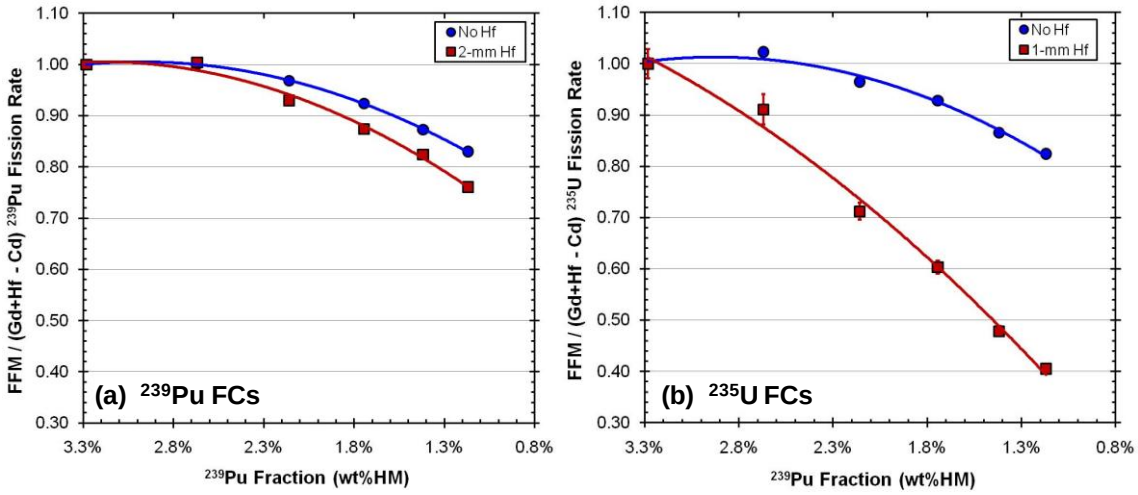

Fig. 8.12. Comparison of FFM / (Gd+Hf – Cd) FC ratio using (a) ^{239}Pu FCs and (b) all ^{235}U FCs versus ^{239}Pu fraction with no boron in water.

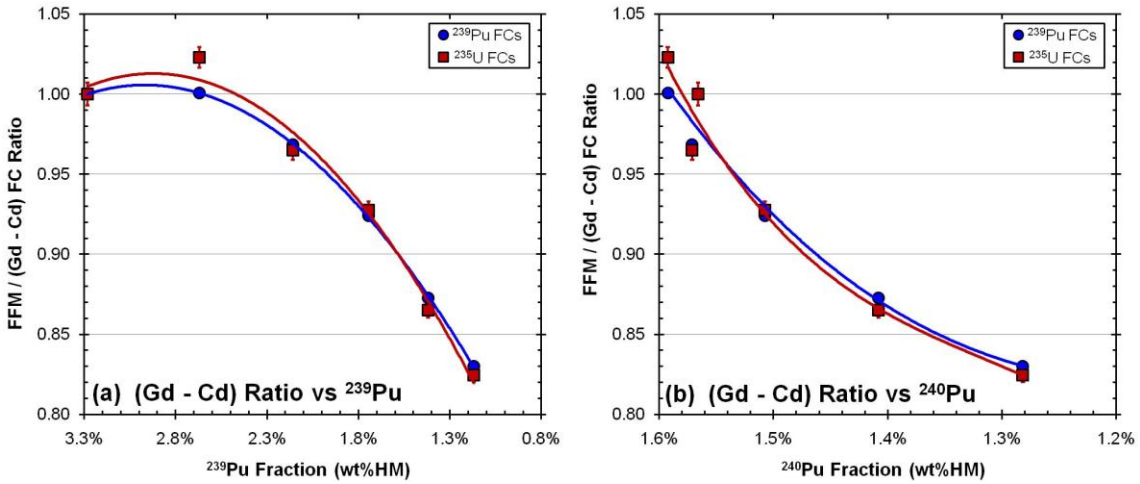

Fig. 8.13. Comparison of FFM / (Gd – Cd) FC ratio versus (a) ^{239}Pu and (b) ^{240}Pu fractions using both ^{239}Pu and ^{235}U FCs with no Hf and no boron in water.

Similar to the results shown for LEU spent fuel, we have normalized the results to the fresh fuel case because in practice SINRD could be calibrated using a fresh fuel assembly. It should also be noted that the error bars shown on all results represent the calculated uncertainties in the SINRD detector ratios obtained via error propagations of expected counting statistics (see Appendix B). The expected count rates in the SINRD FCs are given in Table 8.2 for a PWR spent MOX fuel assembly with 40-GWd/MTU burnup (6% Pu, 5-yrs cooled). The use of Hf in the Gd ^{239}Pu and ^{235}U FCs reduced the count rate by 40% and 23%, respectively. The effect of using Gd and Cd ^{235}U FCs compared to ^{239}Pu FCs decreased the count rates in the Gd FC by 53% and Cd FC by 8%. Using error propagations, the lower count rates in the Gd+Hf and Cd ^{235}U FCs increased the relative uncertainty in the FFM / (Gd+Hf – Cd) ^{235}U FC ratio by 80% compared to using ^{239}Pu FCs; however, it is important to note that using all ^{235}U FCs increased the slope of the SINRD signature by 60%. It should be noted that these count rates are conservative because the (α,n) contribution to the total neutron emission rate from the assembly was not accounted for.

Table 8.2. Expected count rates in SINRD FCs from a 40-GWd PWR spent MOX fuel assembly (6% Pu, 5-yrs cooled).

SINRD Detectors	PWR Spent MOX Fuel [cps]*	
	No Boron	***2200ppm Boron***
Bare ^{235}U	9364 ± 3.950	6044 ± 3.174
FFM ^{235}U	56236 ± 9.681	42916 ± 8.457
Gd ^{235}U	4504 ± 2.740	3311 ± 2.349
Gd+Hf ^{235}U	3452 ± 2.399	2563 ± 2.067
Cd ^{235}U	3152 ± 2.292	2411 ± 2.005
Gd ^{239}Pu	9758 ± 5.703	7002 ± 4.831
Gd+Hf ^{239}Pu	5826 ± 4.407	4243 ± 3.761
Cd ^{239}Pu	3421 ± 3.377	2608 ± 2.948

** Neutron source strength of 3.8E+09 n/s for BU = 40-GWd*

The FFM / (Gd+Hf – Cd) ^{235}U FC ratio was optimized for determining ^{239}Pu in PWR spent MOX fuel for the base case (6% Pu, 5-yrs cooled, no boron) using 1-mm Hf. Next, the effect of adding 2200-ppm boron to the water on our optimized SINRD ratio was examined. The results are shown in Fig. 8.14 versus ^{239}Pu fraction for (a) 6% Pu and (b) 4% Pu IE spent MOX fuel. These results were normalized to the fresh fuel case. The addition of 2200-ppm boron to the water increased the slope of the SINRD detector ratio by 18% for 6% Pu IE and by 7% for 4% Pu IE spent MOX fuel. Compared to PWR spent LEU fuel, the boron effect is approximately a factor of 2 greater for spent MOX fuel. However, it should be noted that the effect of boron on our SINRD ratio for spent MOX fuel is still considerably lower than for gross neutron methods [22].

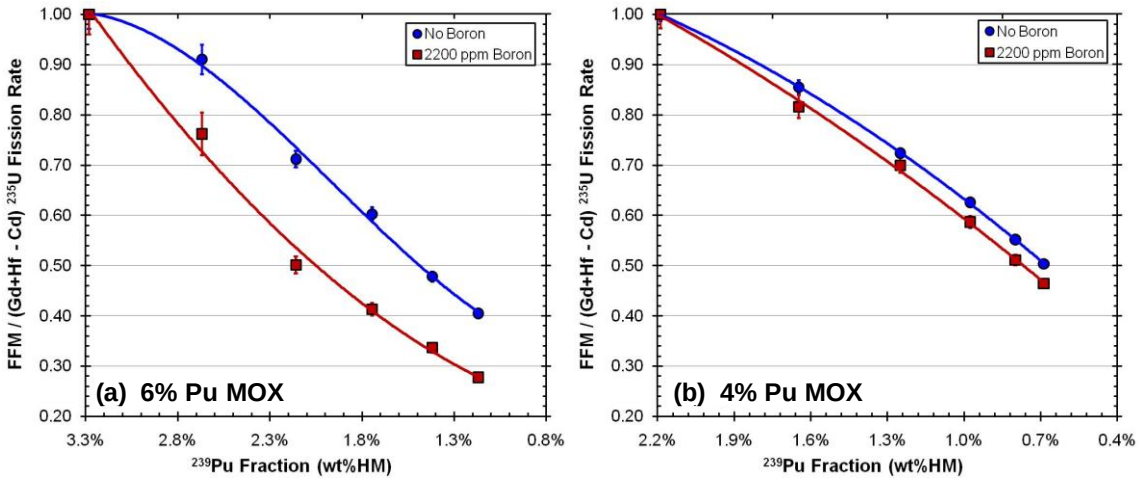

Fig. 8.14. Effect of adding 2200-ppm boron to water on the FFM / (Gd+Hf – Cd) ^{235}U FC ratio versus ^{239}Pu fraction in (a) 6% Pu and (b) 4% Pu IE spent MOX fuel.

8.3.2. Use of SINRD to Measure ^{240}Pu

We have also investigated using the SINRD detector ratio, with and without Hf, to quantify ^{240}Pu in PWR spent MOX fuel. Fig. 8.15 shows the (Gd+Hf – Cd) / (Gd – Cd) ^{235}U FC ratio versus ^{240}Pu / ^{239}Pu fraction in (a) 6% Pu and (b) 4% Pu IE spent MOX fuel with and without 2200-ppm boron in water. It is important to note that the SINRD detector configuration would have to be modified to include additional Gd covered ^{235}U FC (no Hf) to measure the ^{240}Pu content. In addition, since the results are plotted versus ^{240}Pu / ^{239}Pu fraction another SINRD ratio must be used to obtain the ^{240}Pu fraction. This SINRD ratio must be able to clearly distinguish 6% Pu from 4% Pu spent MOX fuel or accurately measure the ^{239}Pu fraction.

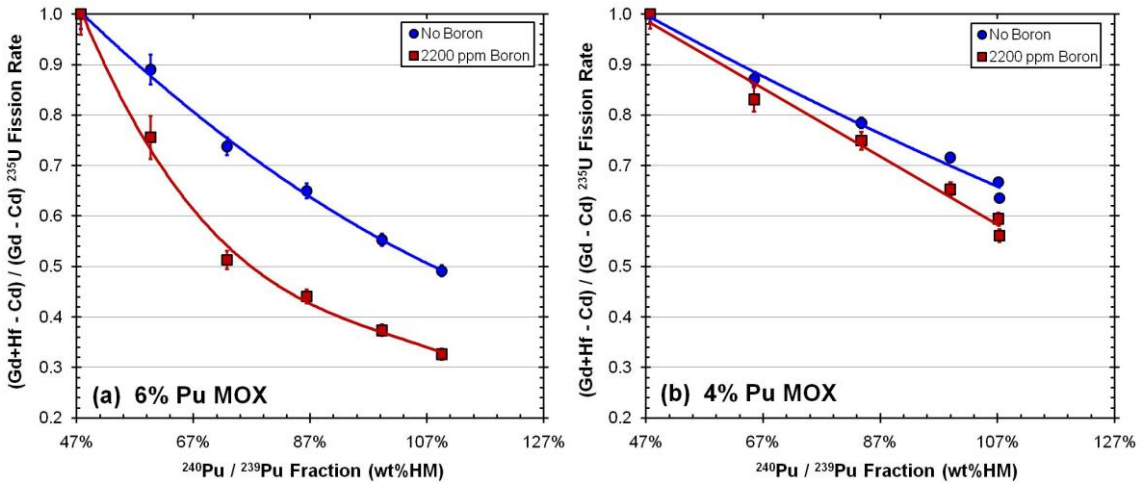

Fig. 8.15. Effect of adding 2200-ppm boron to water on the (Gd+Hf – Cd) / (Gd – Cd) ^{235}U FC ratio versus ^{240}Pu / ^{239}Pu fraction in (a) 6% Pu and (b) 4% Pu IE spent MOX fuel.

8.4. Analysis of SINRD for Possible Diversion Scenarios

In general, there are two different models for the diversion of fissile material from a fuel assembly. The first is to misdeclare the burnup of the assembly, and the second is to remove fuel pins and to replace them with DU or iron pins. In the first model, the fissile material distribution is the same as for the calibration standard (no pin removal); however, for the second diversion model, the location of the pin diversion will affect the measured response based on the penetrability of the verification method. It is important to note that only ^{235}U FCs were used in this analysis. The following safeguards detection requirements were used to assess the sensitivity of SINRD to diversion scenarios:

- Independent of the Operator's declaration of:
  - burnup, initial enrichment, cooling time, and boron concentration
- Sensitive to fuel pin removal over entire burnup range.
- Able to distinguish fresh and 1-cycle MOX fuel from 3- and 4-cycle LEU fuel.
- Recognize that the IAEA will likely need to use all ^{235}U fission chambers.

8.4.1. Verification of Burnup

In PWR 17x17 spent LEU and MOX fuel assemblies, the ^{244}Cm neutron emission rate is approximately 1.8E+08 n/s and 3.8E+09 n/s, respectively, for burnup of 40-GWd. These source terms are further amplified by a factor of 2 – 3 by neutron multiplication in the assembly in water. For spent LEU fuel, this high neutron source term provides adequate counting statistics in the fission chambers to give better than 1% precision in a few minutes for the ratios. This is even further decreased for PWR spent MOX fuel.

8.4.1.1. PWR Spent LEU Fuel

We have investigated the use of SINRD to verify the burnup of a PWR spent LEU fuel assembly. The ^{235}U and ^{244}Cm fraction versus burnup are shown in Fig. 8.16(a). In Fig. 8.16(b), the Gd ^{235}U / Bare ^{235}U FC ratio and FFM fission rate as a function of burnup is shown for the diversion scenario where the burnup is misdeclared low. These results were normalized to the fresh fuel case. Since the ^{239}Pu content increases with burnup in LEU spent fuel, a proliferator is more likely to misdeclare the burnup low. Comparison of the results in Fig. 8.16 (a) to (b), clearly shows that the FFM fission rate is directly proportional to the ^{244}Cm fraction and the Gd ^{235}U / Bare ^{235}U FC ratio is proportional to the ^{235}U fraction over the burnup range of 0 – 50-GWd/MTU.

The fact that ^{235}U fraction decreases as a function of burnup, whereas the ^{244}Cm fraction increases enables us to verify the burnup of the PWR spent LEU assembly because the proliferator can only get one of these curves right. For instance in Fig. 8.16(b), we show the case where the burnup is misdeclared low. The solid black line indicates the actual burnup of the assembly which is 36-GWd and the solid black arrows point to the expected measured values at this burnup. The misdeclared burnup (20-GWd) is shown by the black dotted line. The dotted green and blue lines correspond to the expected measured values at the lower burnup. It should be noted that when the burnup is misdeclared the expected measured values move in opposite directions. Thus, comparing a set of measurements where the burnup is misdeclared to a reference measurement with known burnup would clearly indicate an anomaly in the declaration.

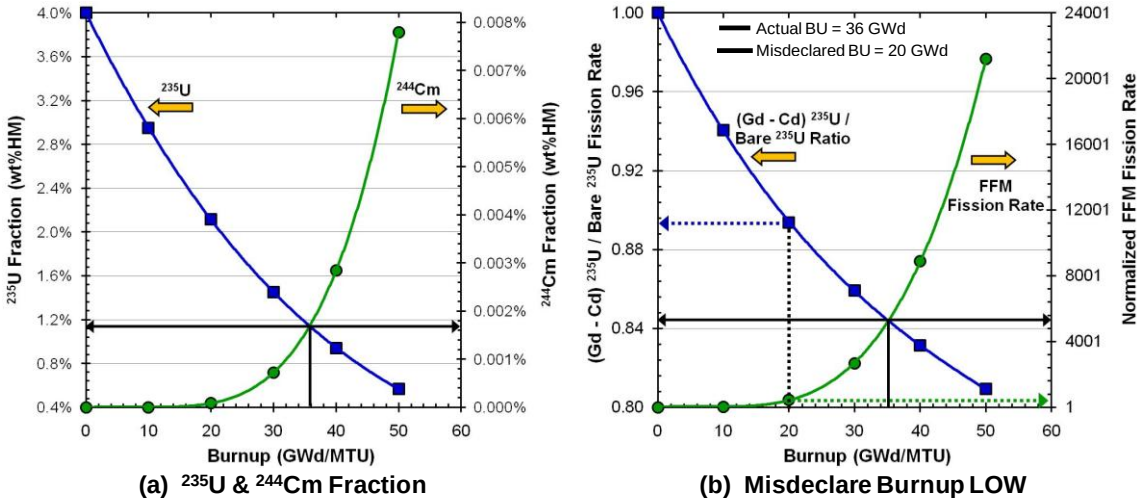

Fig. 8.16. Comparison of (a) ^{235}U and ^{244}Cm fraction to (b) the Gd ^{235}U / Bare ^{235}U FC ratio and FFM fission rate versus burnup for diversion scenario where burnup is misdeclared low.

8.4.1.2. PWR Spent MOX Fuel

Next, the use of SINRD to verify the burnup of a PWR spent MOX fuel assembly was examined. Fig. 8.17(a) shows the ^{239}Pu and ^{244}Cm fraction as a function of burnup. The FFM / (Gd+Hf – Cd) ^{235}U FC ratio and FFM fission rate versus burnup is shown in Fig. 8.17(b) for the diversion scenario where the burnup is misdeclared high. In contrast to LEU spent fuel, the ^{239}Pu content decreases with burnup in MOX spent fuel. Thus, a proliferator is more likely to misdeclare the burnup high. It should be noted that all ^{235}U FCs and 1-mm Hf were used in the FFM / (Gd+Hf – Cd) detector ratio.

Comparison of Fig. 8.17 (a) to (b), clearly shows that the FFM / (Gd+Hf – Cd) ^{235}U FC ratio and FFM fission rate are directly proportional to the ^{239}Pu and ^{244}Cm fractions, respectively. Similar to the PWR spent LEU case, our ability to verify the burnup of the assembly is based on the fact that ^{239}Pu fraction decreases, whereas the ^{244}Cm fraction increases as a function of burnup. Thus, a proliferator who misdeclared the burnup of the assembly could only get one of these curves right because the expected measured values move in opposite directions.

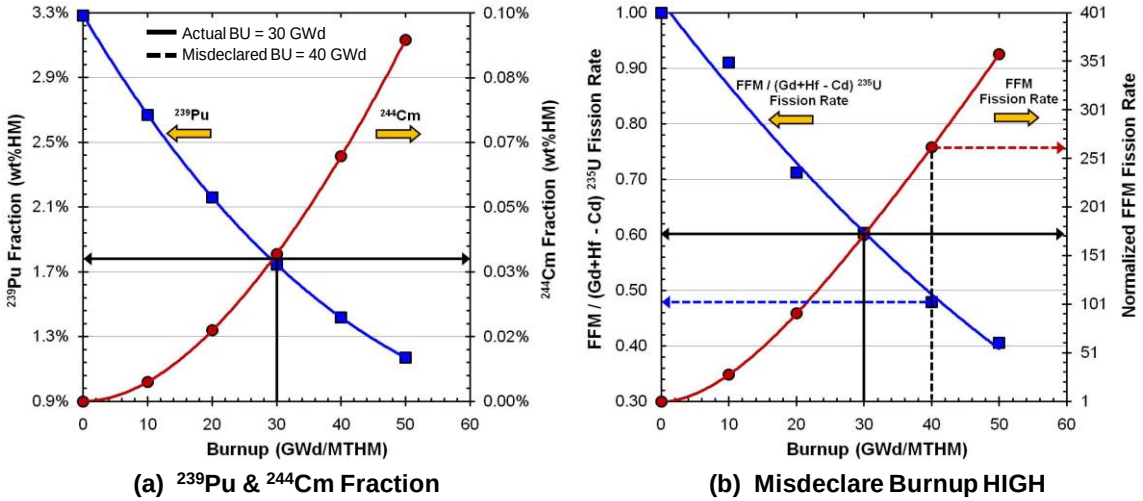

Fig. 8.17. Comparison of (a) ^{239}Pu and ^{244}Cm fraction to (b) the FFM / (Gd+Hf – Cd) ^{235}U FC ratio and FFM fission rate versus burnup for diversion scenario where burnup is misdeclared high.

8.4.2. Sensitivity to PWR Spent MOX Fuel versus Spent LEU Fuel

Another advantage of the SINRD method is that it can easily distinguish between a 1-cycle spent MOX fuel assembly and 3- and 4-cycles spent LEU fuel assemblies. In contrast to many existing verification methods which use gross neutron measurements, the SINRD method uses detector ratios which are sensitive to the plutonium content in the spent fuel. In Fig. 8.18, the FFM / (Gd+Hf – Cd) ^{235}U FC ratio versus burnup is shown for PWR spent LEU and MOX fuel using 1-mm Hf with (a) no boron and (b) 2200-ppm boron in water. Comparing the results shown in Fig. 8.18, the SINRD FC ratio is ~7x higher for 10-GWd spent MOX fuel than for 40-GWd spent LEU fuel with no boron and ~9x higher with 2200-ppm boron in water.

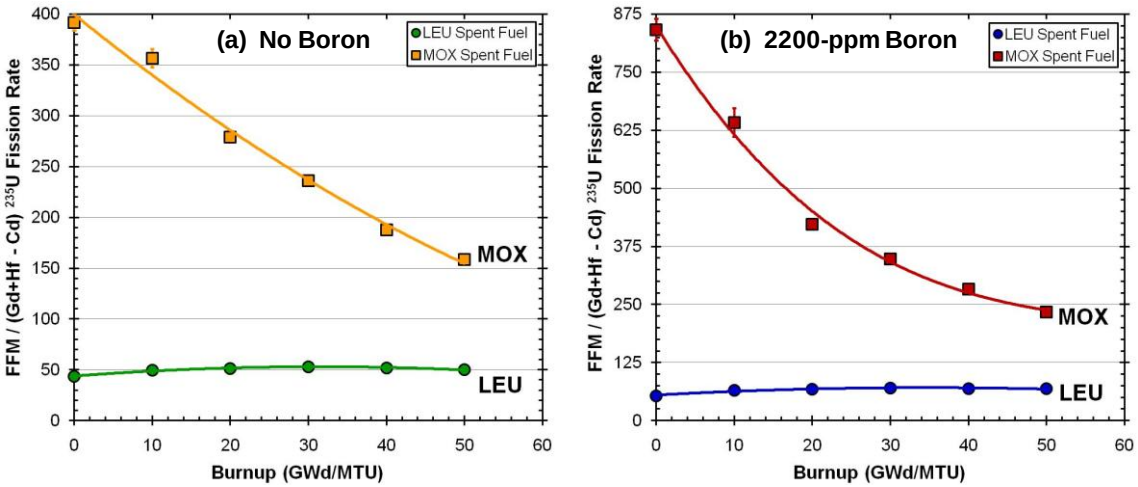

Fig. 8.18. Comparison of FFM / (Gd+Hf – Cd) ^{235}U FC ratio for PWR spent LEU and MOX fuel with (a) no boron and (b) 2200-ppm boron in water.

8.4.3. Sensitivity of SINRD to Pin Removal

The sensitivity and penetrability of SINRD was assessed by modeling partial defects in PWR 17x17 spent LEU (4% ^{235}U IE) and MOX (6% Pu IE) fuel assemblies. Partial defects were modeled for fuel burnups of 10-GWd and 40-GWd using the same pin removal locations that were used in the PWR fresh fuel simulations. The locations of partial defects are shown in Fig. 8.19 for convenience.

To assess the penetrability of SINRD to partial defects, the percent change in the SINRD ratios was calculated for each region to determine if the diverted pins can be detected within 3σ uncertainty. The count times used for the diversion cases are given in Table 8.3. These count times are conservative because they only reflect the different concentrations of ^{244}Cm in PWR spent LEU and MOX fuel.

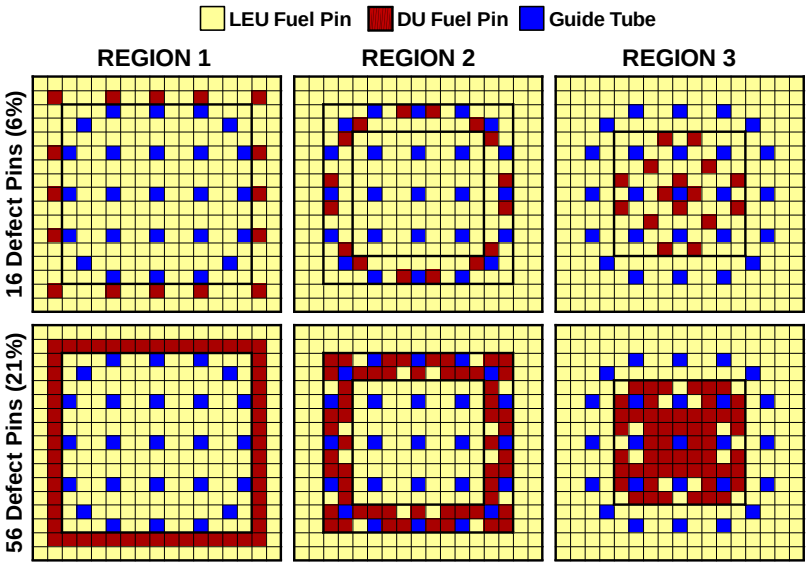

Fig. 8.19. Fuel pin removal locations of defects for Regions 1 – 3 in PWR 17x17 assembly where red pin locations are fuel pins that were removed and blue locations are guide tube holes.

Table 8.3. Count times used to detect fuel pin diversions within 3σ uncertainty.

Fuel Type	Burnup [GWd]	Count Time for Diversion Cases	
		No Boron	***2200-ppm Boron***
LEU Spent Fuel (4% ^{235}U)	10	2.5 hours	2.0 hours
	40	20 minutes	15 minutes
MOX Spent Fuel (6% Pu)	10	30 minutes	30 minutes
	40	5 minutes	5 minutes

The sensitivity of different SINRD ratios with 6% and 21% of the total number of pins removed from Regions 1 – 3 are given in Table 8.4 and Table 8.5 for PWR spent LEU and MOX fuel, respectively. The values shown in bold correspond to the maximum positive and negative percent change in ratios that are within 3σ uncertainty for 6% and 21% pins removed from each region. The cells that are shaded gray correspond to the percent in change detector ratios that are not within 3σ uncertainty of an assembly with no diverted pins.

Table 8.4. Percent change in SINRD ratios with 6% and 21% fuel pins removed from Regions 1, 2, and 3 for PWR spent LEU fuel (no Hf).

Region Defects	Burnup	SINRD Ratios *PWR Spent LEU*	REGION 1		REGION 2		REGION 3	
			No boron	*2200-ppm*	*No boron*	*2200-ppm*	*No boron*	*2200-ppm*
6% Pin Defects (16 pins)	***10 GWd***	FFM / (Gd - Cd) ^{235}U	*5.14%*	*4.75%*	*1.31%*	*0.81%*	*-1.91%*	*-2.37%*
		FFM / Bare ^{235}U	**7.23%**	**6.57%**	**2.12%**	*1.27%*	*-1.36%*	*-1.89%*
		Bare ^{235}U / Gd ^{235}U	-4.65%	*-4.31%*	*-1.81%*	*-1.45%*	*0.05%*	*0.22%*
		Bare ^{235}U / Cd ^{235}U	**-6.44%**	*-5.82%*	*-2.53%*	*-2.06%*	*0.47%*	*0.64%*
	40 GWd	FFM / (Gd - Cd) ^{235}U	5.52%	4.85%	2.36%	*0.12%*	**-1.90%**	*-2.70%*
		FFM / Bare ^{235}U	**7.96%**	**6.29%**	**3.14%**	**1.66%**	-1.21%	-1.57%
		Bare ^{235}U / Gd ^{235}U	-5.60%	-3.97%	-2.70%	-1.83%	*-0.24%*	*-0.14%*
		Bare ^{235}U / Cd ^{235}U	**-7.73%**	**-5.44%**	**-4.05%**	**-1.98%**	*0.06%*	*0.42%*
21% Pin Defects (56 pins)	***10 GWd***	FFM / (Gd - Cd) ^{235}U	18.0%	15.9%	*4.99%*	*2.10%*	*-8.63%*	*-11.4%*
		FFM / Bare ^{235}U	**24.8%**	**19.9%**	**9.42%**	**4.64%**	-6.54%	-9.48%
		Bare ^{235}U / Gd ^{235}U	-19.6%	-13.9%	-9.06%	*-5.21%*	*-0.17%*	*1.22%*
		Bare ^{235}U / Cd ^{235}U	**-28.5%**	**-20.2%**	**-12.2%**	*-6.82%*	*1.07%*	*2.94%*
	40 GWd	FFM / (Gd - Cd) ^{235}U	19.8%	18.0%	6.61%	3.23%	**-9.09%**	**-11.2%**
		FFM / Bare ^{235}U	**25.2%**	**20.0%**	**11.2%**	**5.62%**	-4.93%	-8.71%
		Bare ^{235}U / Gd ^{235}U	-19.2%	-12.8%	-10.8%	-6.06%	-1.74%	*0.90%*
		Bare ^{235}U / Cd ^{235}U	**-29.1%**	**-19.9%**	**-15.1%**	**-8.22%**	*-0.27%*	**2.63%**

Table 8.5. Percent change in SINRD ratios with 6% and 21% fuel pins removed from Regions 1, 2, and 3 for PWR spent MOX fuel (1-mm Hf).

Region Defects	Burnup	SINRD Ratios *PWR Spent MOX*	REGION 1		REGION 2		REGION 3	
			No boron	*2200-ppm*	*No boron*	*2200-ppm*	*No boron*	*2200-ppm*
6% Pin Defects (16 pins)	***10 GWd***	FFM / (Gd+Hf - Cd) ^{235}U	**35.6%**	**39.8%**	**20.1%**	*7.64%*	*-9.28%*	*-6.16%*
		FFM / Bare ^{235}U	8.75%	7.22%	2.21%	1.69%	-0.91%	-1.46%
		Bare ^{235}U / Gd+Hf ^{235}U	-6.43%	-4.95%	-1.75%	-1.84%	*0.09%*	*0.37%*
		Bare ^{235}U / Cd ^{235}U	**-9.15%**	**-6.78%**	**-2.99%**	**-2.08%**	**0.47%**	*0.50%*
	40 GWd	FFM / (Gd+Hf - Cd) ^{235}U	**22.0%**	**25.1%**	**8.64%**	**9.97%**	*-1.34%*	*2.76%*
		FFM / Bare ^{235}U	9.71%	7.36%	2.73%	1.99%	-0.74%	**-1.83%**
		Bare ^{235}U / Gd+Hf ^{235}U	-6.91%	-5.18%	-2.29%	-2.07%	*-0.18%*	*0.25%*
		Bare ^{235}U / Cd ^{235}U	**-9.39%**	**-7.20%**	**-3.17%**	**-2.79%**	*-0.14%*	-0.03%
21% Pin Defects (56 pins)	***10 GWd***	FFM / (Gd+Hf - Cd) ^{235}U	**65.0%**	**71.4%**	**36.4%**	**41.1%**	*0.24%*	*-6.18%*
		FFM / Bare ^{235}U	29.0%	24.3%	9.75%	5.31%	**-4.82%**	**-7.49%**
		Bare ^{235}U / Gd+Hf ^{235}U	-26.2%	-19.7%	-8.76%	-5.37%	**0.61%**	1.54%
		Bare ^{235}U / Cd ^{235}U	**-36.6%**	**-27.4%**	**-11.7%**	**-7.44%**	*0.40%*	**1.55%**
	40 GWd	FFM / (Gd+Hf - Cd) ^{235}U	**51.8%**	**55.6%**	**28.0%**	**26.6%**	*-0.03%*	**-10.7%**
		FFM / Bare ^{235}U	30.1%	24.5%	11.5%	6.24%	**-4.75%**	-7.85%
		Bare ^{235}U / Gd+Hf ^{235}U	-26.7%	-19.7%	-10.7%	-6.69%	**0.47%**	1.63%
		Bare ^{235}U / Cd ^{235}U	**-37.7%**	**-28.0%**	**-14.7%**	**-9.2%**	*0.07%*	**1.88%**

It should be emphasized that all ^{235}U FCs were used to obtain these results where no Hf was used for spent LEU fuel and 1-mm Hf was used for spent MOX fuel. It is important to note that for PWR spent LEU fuel assembly with burnup of 10-GWd none of the SINRD ratios can detect 6% pin diversions within *3σ* in Region 3. If the count time was increased to 6.5-hrs with no boron and 8-hrs with 2200-ppm boron in water, then only the FFM / Bare ^{235}U FC ratio could detect 6% pin diversions within *3σ* in Region 3. A summary of the results shown in Table 8.4 and Table 8.5 is given below:

- All SINRD ratios have the highest sensitivity to pin removal in Region 1.
- FFM / Bare ^{235}U FC ratio is the most sensitive SINRD ratio for detecting fuel pin diversions from Regions 1 – 3 within *3σ*.
  - This ratio is sensitive to reactivity changes in the fuel assembly due to changes in the concentration of thermal absorbers.
  - The percent change in this ratio is positive for pin removal from Regions 1 (outer) and 2 (middle) and negative for pin removal from Region 3 (center).
- Region 3 has higher sensitivity than Region 2 when 2200-ppm boron is added to the water for the cases with 21% partial defects.
  - This may be attributed to the boron in the water "hardening" the neutron energy spectrum which reduces the multiplication of the assembly.

8.4.3.1. Graphical Analysis of Partial Defects Results

In Fig. 8.20, the fuel pin removal results for FFM / Bare ^{235}U FC ratio as a function diversion case are shown for PWR spent (a) LEU and (b) MOX fuel with fuel burnup of 40-GWd and 2200-ppm boron in water. The solid line represents the signal from the case with no diversions; the dashed lines represent ±1% change in the SINRD ratio to account for systematic errors. We chose to use the FFM / Bare ^{235}U FC ratio in this analysis because it was the most sensitive ratio for detecting fuel pin diversions within *3σ* from Regions 1 – 3. These results show that the SINRD ratio has the highest sensitivity to fuel pin diversions from Region 1. The diversion of 16 pins from Regions 2 and 3 are the only cases that are not clearly within ±1% of the no diversion signal.

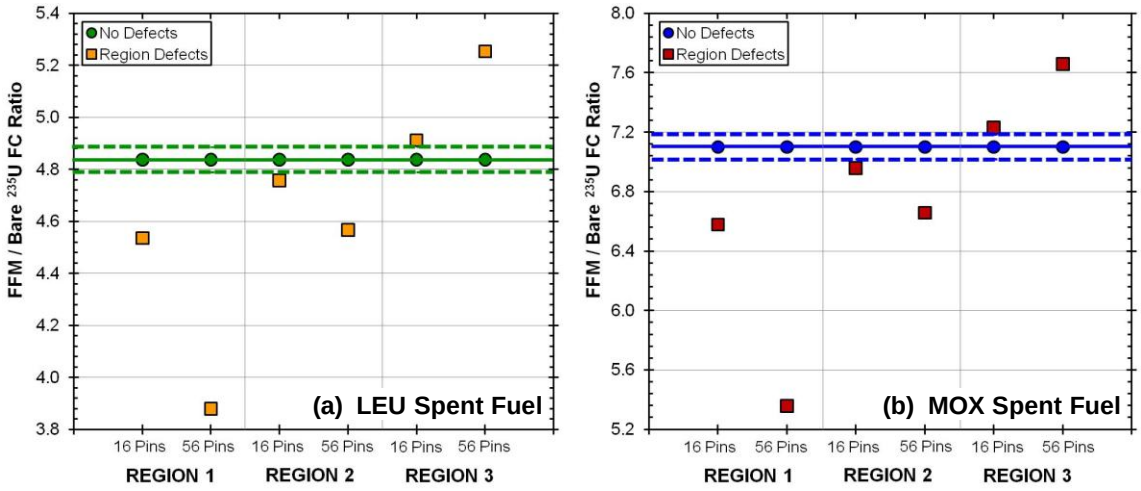

Fig. 8.20. Pin removal results for FFM / Bare ^{235}U FC ratio as a function diversion case for 40-GWd PWR spent (a) LEU and (b) MOX fuel with 2200-ppm boron in water.

8.4.3.2. Statistical Analysis of Partial Defects Results

Using the procedure described in section 5.2, the nondetection probability, β, was calculated for SINRD ratios with 6% of the fuel pins removed from Regions 1 – 3 where α = 5%. The effect of 6% region defects on the FFM / Bare ^{235}U probability distribution is shown in Fig. 8.21 for PWR spent (a) LEU and (b) MOX fuel. These results are shown for PWR spent fuel with burnup of 40-GWd and 2200-ppm boron in water. In Table 8.6 and Table 8.7, the mean ± 1σ and β are given for different SINRD ratios with 6% fuel pins removed from Regions 1 – 3 for PWR spent LEU and MOX fuel, respectively. If β > 20%, the results were shaded gray for LEU and MOX fuel. The purpose for highlighting these results was to show the SINRD ratios that are not considered useful for detecting pin diversions because the β is too high. Based on the results for β, it is clear that the FFM / Bare ^{235}U FC ratio is best ratio for detecting pin diversions.

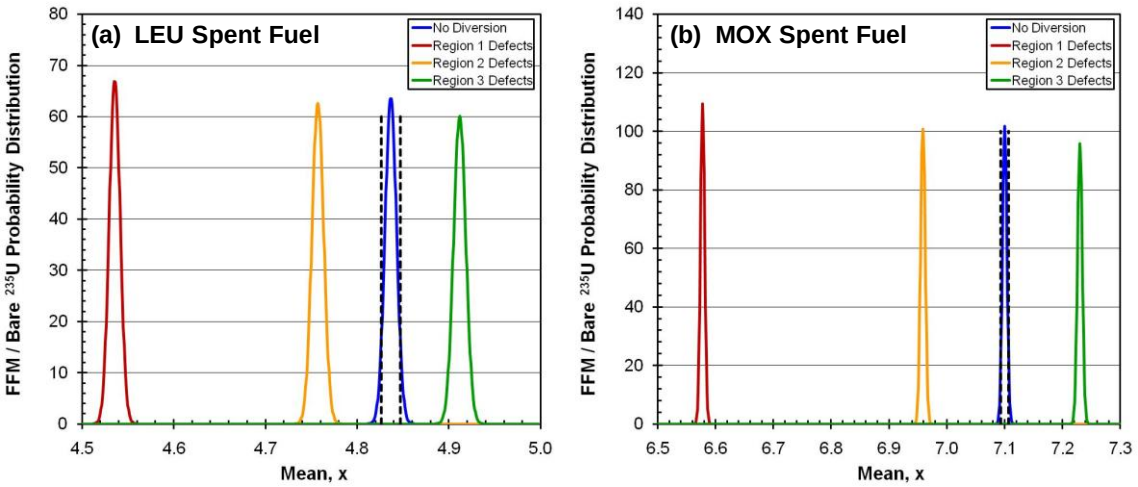

Fig. 8.21. Effect of 6% region defects on FFM / Bare ^{235}U probability distribution versus mean for 40-GWd PWR spent (a) LEU and (b) MOX fuel with 2200-ppm boron in water.

Table 8.6. Mean ± 1σ and β for PWR spent LEU fuel with 6% of fuel pins removed from Regions 1 – 3.

Burnup	Water	SINRD Ratios *PWR Spent LEU*	No Defects	REGION 1		REGION 2		REGION 3	
			Mean ± 1σ	***Mean ± 1σ***	***β***	***Mean ± 1σ***	***β***	***Mean ± 1σ***	***β***
10 GWd	***No boron***	FFM / (Gd - Cd) ^{235}U	23.8 ± 0.499	22.5 ± 0.480	*20%*	23.5 ± 0.514	*84%*	24.2 ± 0.548	*75%*
		FFM / Bare ^{235}U	3.84 ± 0.019	3.57 ± 0.018	0%	3.76 ± 0.019	0%	3.90 ± 0.020	14%
		Bare ^{235}U / Cd ^{235}U	4.41 ± 0.044	4.69 ± 0.049	0%	4.52 ± 0.048	*21%*	4.39 ± 0.047	*87%*
	2200-ppm	FFM / (Gd - Cd) ^{235}U	28.2 ± 1.092	26.8 ± 1.047	*67%*	27.9 ± 1.123	*92%*	28.8 ± 1.190	*83%*
		FFM / Bare ^{235}U	4.95 ± 0.042	4.62 ± 0.040	0%	4.89 ± 0.044	*57%*	5.04 ± 0.046	*30%*
		Bare ^{235}U / Cd ^{235}U	3.47 ± 0.057	3.67 ± 0.063	4%	3.54 ± 0.061	*65%*	3.44 ± 0.060	*88%*
40 GWd	***No boron***	FFM / (Gd - Cd) ^{235}U	24.9 ± 0.099	24 ± 0.093	0%	24.3 ± 0.098	0%	25.4 ± 0.105	0%
		FFM / Bare ^{235}U	3.57 ± 0.003	3.28 ± 0.003	0%	3.45 ± 0.003	0%	3.61 ± 0.003	0%
		Bare ^{235}U / Cd ^{235}U	4.80 ± 0.009	5.17 ± 0.010	0%	4.99 ± 0.009	0%	4.80 ± 0.009	*89%*
	2200-ppm	FFM / (Gd - Cd) ^{235}U	29.9 ± 0.189	28 ± 0.180	0%	29.9 ± 0.195	*92%*	30.7 ± 0.205	0.7%
		FFM / Bare ^{235}U	4.79 ± 0.006	4.49 ± 0.006	0%	4.71 ± 0.006	0%	4.86 ± 0.007	0%
		Bare ^{235}U / Cd ^{235}U	3.62 ± 0.009	3.82 ± 0.010	0%	3.69 ± 0.010	0%	3.61 ± 0.010	*50%*

Table 8.7. Mean ± 1σ and β for PWR spent MOX fuel with 6% of fuel pins removed from Regions 1 – 3.

Burnup	Water	SINRD Ratios *PWR Spent MOX*	No Defects	REGION 1		REGION 2		REGION 3	
			Mean ± 1σ	***Mean ± 1σ***	***β***	***Mean ± 1σ***	***β***	***Mean ± 1σ***	***β***
10 GWd	***No boron***	FFM / (Gd+Hf - Cd) ^{235}U	362 ± 9.170	233 ± 3.980	0%	289 ± 6.059	0%	395 ± 11.32	5.1%
		FFM / Bare ^{235}U	6.91 ± 0.004	6.31 ± 0.004	0%	6.76 ± 0.004	0%	6.97 ± 0.004	0%
		Bare ^{235}U / Cd ^{235}U	2.57 ± 0.003	2.80 ± 0.003	0%	2.64 ± 0.003	0%	2.55 ± 0.003	0%
	2200-ppm	FFM / (Gd+Hf - Cd) ^{235}U	641 ± 34.82	386 ± 13.25	0%	592 ± 30.85	*61%*	681 ± 40.58	*67%*
		FFM / Bare ^{235}U	7.91 ± 0.006	7.34 ± 0.006	0%	7.78 ± 0.006	0%	8.03 ± 0.006	0%
		Bare ^{235}U / Cd ^{235}U	2.24 ± 0.003	2.40 ± 0.003	0%	2.29 ± 0.003	0%	2.23 ± 0.003	1.3%
40 GWd	***No boron***	FFM / (Gd+Hf - Cd) ^{235}U	187 ± 2.039	146 ± 1.304	0%	171 ± 1.761	0%	190 ± 2.151	*65%*
		FFM / Bare ^{235}U	6.01 ± 0.003	5.42 ± 0.002	0%	5.84 ± 0.003	0%	6.05 ± 0.003	0%
		Bare ^{235}U / Cd ^{235}U	2.97 ± 0.002	3.25 ± 0.003	0%	3.06 ± 0.003	0%	2.97 ± 0.003	*49%*
	2200-ppm	FFM / (Gd+Hf - Cd) ^{235}U	284 ± 5.307	212 ± 3.116	0%	255 ± 4.454	0%	276 ± 5.141	*57%*
		FFM / Bare ^{235}U	7.10 ± 0.004	6.58 ± 0.004	0%	6.96 ± 0.004	0%	7.23 ± 0.004	0%
		Bare ^{235}U / Cd ^{235}U	2.51 ± 0.002	2.69 ± 0.003	0%	2.58 ± 0.003	0%	2.51 ± 0.003	*90%*

Using the diversion results for 6% and 21% partial defects, the average percent change in the SINRD ratio per fuel pin removed was calculated for each region and then multiplied by an increasing number of fuel pins. The sensitivity of two different SINRD detector ratios to the removal of fuel pins is shown in Fig. 8.22 for 10-GWd and 40-GWd PWR spent fuel with 2200-ppm boron in water. Fig. 8.22(a) and (c) show the percent change in the FFM / Bare ^{235}U FC ratio versus the percentage of pins removed for PWR spent LEU and MOX fuel, respectively. In Fig. 8.22(b) and (d), the percent change in the Bare / Cd ^{235}U FC ratio versus the percentage of pins removed is shown for PWR spent LEU and MOX fuel, respectively.

For both SINRD ratios, the sensitivity to pin removal is highest in Region 1 (outer surface of assembly). Based on these results, it should be noted that there exists a combination of fuel pins from Regions 2 and 3 that could result in 0% percent change in FFM / Bare ^{235}U FC ratio; however, the results shown in Fig. 8.22(b) and (d) go in the opposite direction as the results shown in (a) and (c). Thus, the percent change in the Bare / Cd ^{235}U FC ratio could be used in conjunction with the percent change in FFM / Bare ^{235}U FC ratio such that the removal of pins from Regions 2 and 3 could be detected.

Furthermore, it should be emphasized that based on the results shown in Fig. 8.22, we can conclude that the SINRD detector ratios are sensitive over the entire burnup range. The only dependence the SINRD ratios have on the source term is the count time required to achieve a percent change in the ratio that is greater than 3σ. This dependence is only significant for LEU spent fuel at a burnup of 10-GWd because the ^{244}Cm concentration is so low.

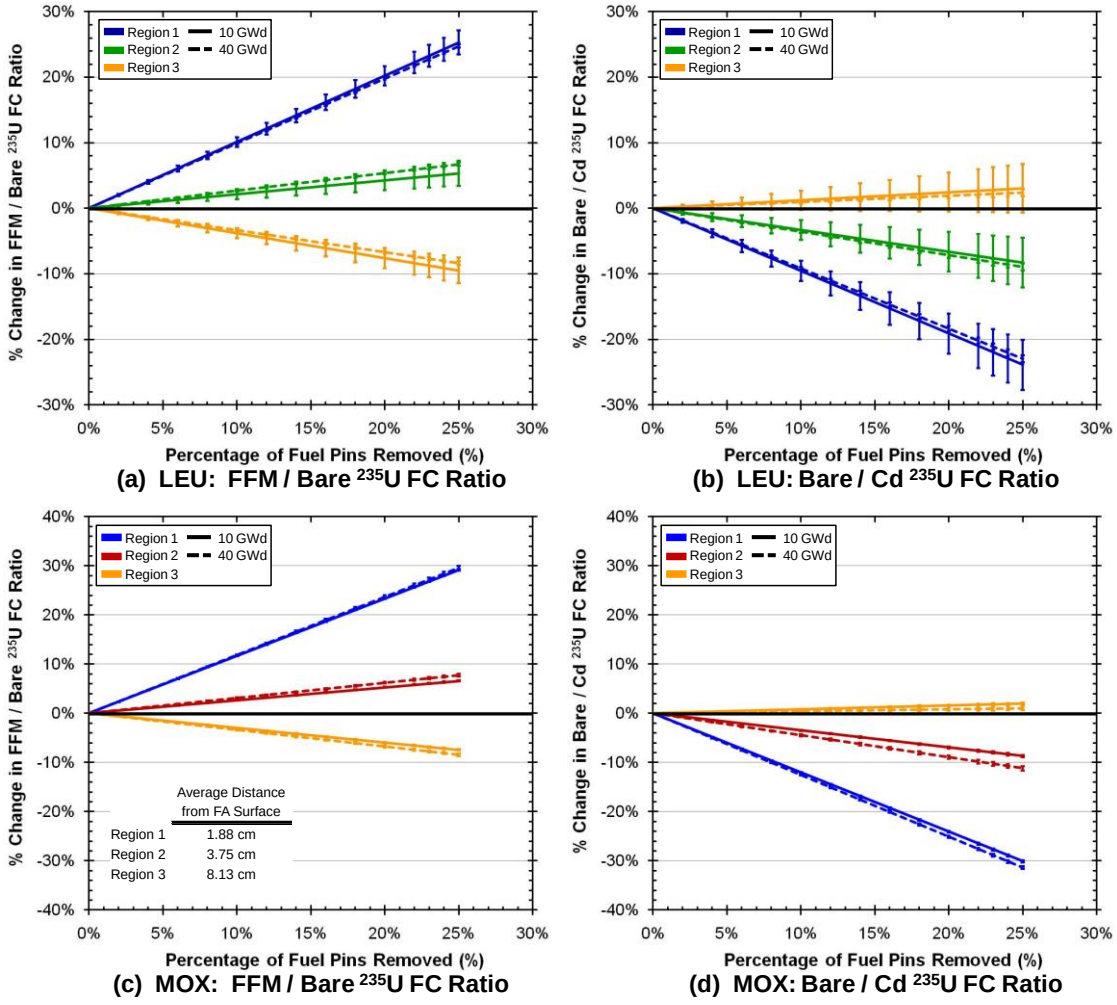

Fig. 8.22. Percent change in (a) and (c) FFM / Bare ^{235}U FC ratio to (b) and (d) Bare / Cd ^{235}U FC ratio versus % of pins removed for PWR spent LEU and MOX fuel, respectively.

To obtain a better understanding of the sensitivity of the SINRD ratios to pin removal from the assembly, the percent change in (a) Bare ^{235}U, (b) FFM ^{235}U, (c) Gd ^{235}U, and (d) Cd ^{235}U fission rates versus the percentage of pins removed is shown in Fig. 8.23 for PWR spent LEU and MOX fuel. These results are shown for the spent fuel case with burnup of 40-GWd and 2200-ppm boron in water. In contrast the results shown in Fig. 8.22, all of the SINRD FCs except the FFM have the highest sensitivity of to pin removal from Region 3 (center). This may be attributed to the fact that the multiplication is highest in the center of the assembly. The FFM is simply a fast-neutron flux monitor that measures the neutron source emission rate. In order for a neutron to contribute to the fission rate in the FFM, it must have energy greater than 3.8-keV or else it will be absorbed in the B_4C. Thus, the FFM has the highest sensitivity to pin removal from Region 1 because the majority of neutrons that contribute to the FFM fission rate were likely born in Region 1.

Error propagations (Appendix B) were used to calculate the uncertainties in the percent change in the SINRD ratios for all diversion cases. The uncertainties in the FFM / Bare ^{235}U FC ratio were between 0.1% – 1.5% for PWR spent LEU and MOX fuel using the count times given in Table 8.3. Thus, this type of measurement could show the departure from a reference fuel assembly with no defects.

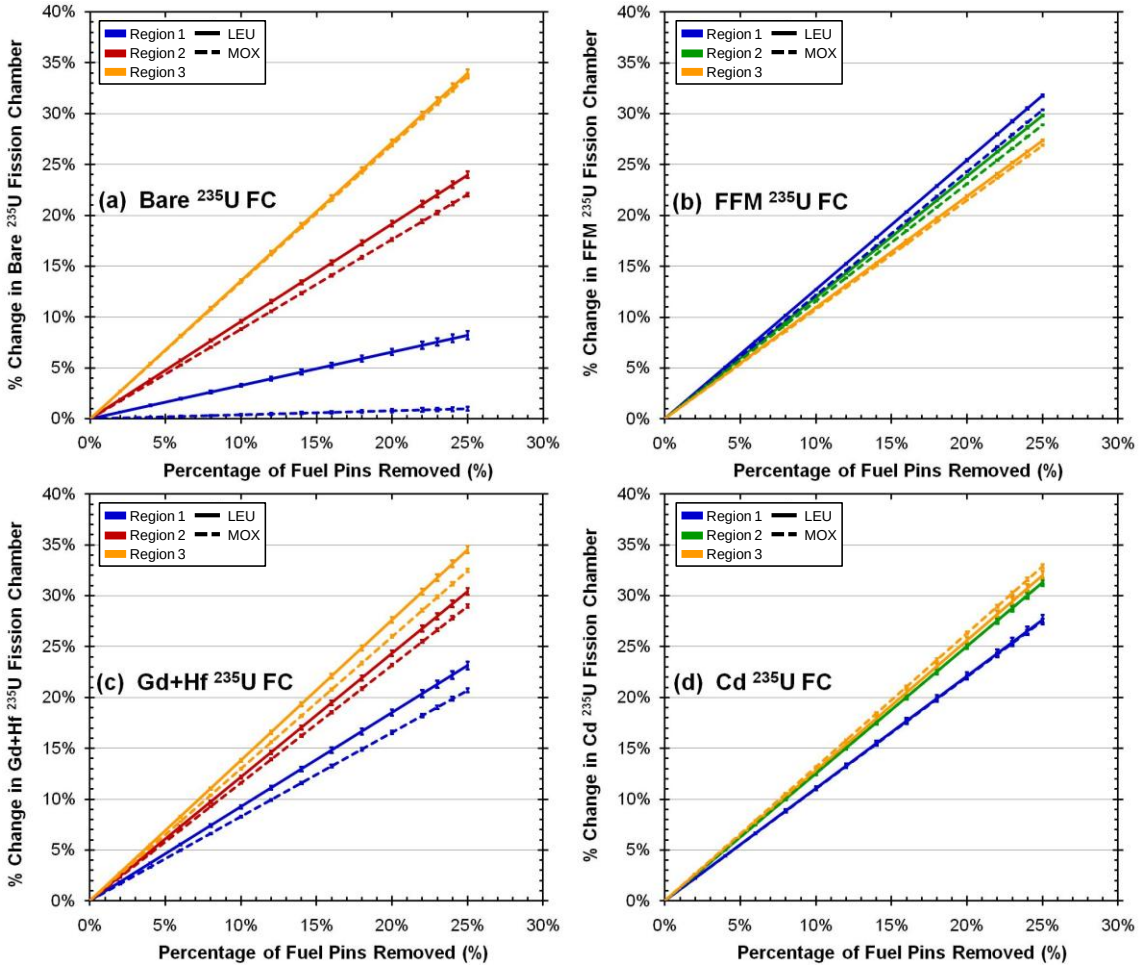

Fig. 8.23. Percent change in (a) Bare ^{235}U, (b) FFM ^{235}U, (c) Gd+Hf ^{235}U, and (d) Cd ^{235}U FCs versus % of fuel pins removed for 40-GWd PWR spent LEU and MOX fuel with 2200-ppm boron.

8.5. Summary of PWR Spent Fuel Results

We have simulated the change in different SINRD detector ratios over a burnup range of 0 – 50-GWd using MCNPX. For a PWR spent LEU fuel assembly, the FFM / (Gd+Hf – Cd) ^{239}Pu FC ratio was optimized for determining ^{239}Pu using 2-mm Hf. This ratio is proportional to the ^{239}Pu mass in the assembly over the burnup range of 0 to 50-GWd. Due to the fact that the IAEA will likely need to use all ^{235}U FCs, the FFM / (Gd – Cd) ^{235}U FC ratio was also examined to determine if the ^{239}Pu content could still be quantified. The use of all ^{235}U FCs decreased the slope of the SINRD signature by a factor of 2 for both 4% and 5% ^{235}U IE spent LEU fuel; however, it is important to note

that this SINRD ratio still linearly tracks the ^{239}Pu content in PWR spent LEU fuel. For a PWR spent MOX fuel assembly, the FFM / (Gd+Hf – Cd) ^{235}U FC ratio was optimized for determining ^{239}Pu using 1-mm Hf. This ratio is directly proportional to the ^{239}Pu mass in the assembly over burnup range of 0 to 50-GWd. For instance, a 20% change in the ^{239}Pu mass results in a 20% change in the SINRD ratio.

The sensitivity and penetrability of SINRD was assessed by modeling partial defects in PWR 17x17 spent LEU and MOX fuel assemblies. It is important to note that all ^{235}U FCs were used in this analysis. The percent change in the SINRD ratios was calculated for Regions 1 – 3 to determine if the diverted pins can be detected within 3σ. The nondetection probability, β, was also calculated in order to better understand how the uncertainty in the SINRD ratios affects the ability to detect pin diversions. Based on the results from these calculations, the FFM / Bare ^{235}U FC ratio is best ratio for detecting pin diversions. The uncertainty in this ratio ranged from 0.1% to 1.5% for PWR spent LEU and MOX fuel. Thus, this type of measurement could show the departure from a reference fuel assembly with no defects.

The purpose of the PWR spent fuel simulations was to assess the ability of SINRD to quantify the fissile content in spent fuel and the sensitivity of SINRD to possible diversion scenarios. We have concluded that SINRD provides a number of improvements over current IAEA verification methods. These improvements include:

1) SINRD provides absolute measurements of burnup independent of the operator's declaration.
2) SINRD is sensitive to pin removal over the entire burnup range and can verify the diversion of 6% of fuel pins within 3σ from PWR spent LEU and MOX fuel.
3) SINRD is insensitive to the boron concentration in the water and the initial fuel enrichment and can therefore be used at multiple spent fuel storage facilities.
4) The calibration of SINRD at one reactor facility carries over to reactor sites in different countries because it uses the ratio of FCs that are not facility dependent.
5) SINRD can distinguish fresh and 1-cycle spent MOX fuel from 3- and 4-cycles spent LEU fuel without using reactor burnup codes.

9. ANALYSIS OF BWR 9X9 SPENT FUEL ASSEMBLY

We have also simulated the use of SINRD to quantify the fissile content in spent fuel and detect possible diversion scenarios for BWR 9x9 spent LEU and MOX fuel assemblies with 0%, 40%, and 70% void fractions (VF)[‡]. This required first calculating the isotopic composition of the spent fuel assemblies at each VF over burnup range of 0 to 50-GWd/MTU (in 10-GWd increments). Then, SINRD's response to each spent fuel assembly in water was simulated. Spontaneous fission neutrons from ^{244}Cm were used to self-interrogate the spent fuel pins in the MCNPX simulations of SINRD. We varied the fuel burnup, void fraction, and initial enrichment to observe how SINRD's response changes as a function of ^{235}U, ^{239}Pu, and ^{240}Pu content in the fuel. The SINRD detector configuration was optimized for BWR spent LEU and MOX fuel based on the concentration of ^{239}Pu relative to ^{240}Pu. The same specifications given in Table 7.1 for a BWR 9x9 fresh fuel assembly were used for the spent fuel simulations.

In contrast to a PWR, the light water coolant in a BWR is allowed to boil as it is circulated from the bottom to the top of the reactor. This results in the formation of vapor bubbles or voids in the upper region of a BWR. Voids displace part of the coolant and lower its density which in turn reduces the reactivity of the core [43]. Since voids form in the upper region of a BWR, the moderating power is highest in the bottom region of the core (0% VF). Accounting for the different void fractions in a BWR is important to SINRD because it significantly affects the fuel burnup and thus the spent fuel isotopics we are trying to measure.

9.1. Calculation of BWR Spent Fuel Isotopics

TransLAT was used to calculate the isotopic composition of BWR spent LEU and MOX fuel over the burnup range of 10 to 50-GWd/MTU for 0%, 40%, and 70% void fractions [29]. The BWR operating parameters (power density, fuel temperature, etc.) used in TransLAT were obtained from the OECD/NEA Burnup Credit Benchmark Phase

[‡] *Void fraction* is defined as the volume of vapor divided by the total volume of the steam-water mixture.

III-B for BWR spent LEU fuel assemblies [44]. A BWR pin cell was modeled with 20 radial fuel regions. The radius of each fuel region was determined using an exponential transform. In a BWR core, individual fuel assemblies are separated by control blades with a water gap in between the assembly and the blade. For a BWR 9x9 fuel assembly, the inter-assembly gap is ~1.5-cm. To account for the additional moderation from the water gap surrounding the assembly, we increased the pitch of the BWR pin cell proportionally.

The ^{239}Pu concentration as a function of fuel radius for BWR spent LEU and MOX fuel is shown in Fig. 9.1(a) and (b), respectively. These results clearly show the large spatial gradient of ^{239}Pu across the fuel pellet. To determine how this gradient affects our SINRD ratios, we modeled 1, 2, and 4 radial fuel regions in BWR spent LEU and MOX fuel. Since TransLAT uses integral transport theory methods for burnup calculations, a large number of radial regions were needed to accurately account for spatial self-shielding effects in the fuel; however, this is not needed in MCNPX. Therefore, we reduced the number of radial regions from 20 to a maximum of 4 to minimize the complexity of our MCNPX simulations. The spatial gradient of ^{239}Pu across the fuel pellet was used to determine the radius of each fuel region. The locations of the fuel regions are labeled in Fig. 9.1 for a total of 2 (a) and 4 (b) radial regions.

Fig. 9.2 shows the FFM / (Gd+Hf – Cd) ^{235}U FC ratio versus number of radial fuel regions for 40-GWd BWR spent (a) LEU fuel with no Hf and (b) MOX fuel with 1-mm Hf. The maximum change in the SINRD ratio from using 1, 2, and 4 radial fuel regions was 2% for LEU spent fuel and 5% for MOX spent fuel. These results are consistent with the results for PWR spent LEU and MOX fuel. Thus, to minimize the computational time required for our MCNPX simulations, only one fuel region was modeled for BWR spent fuel. Appendix D contains an example TransLAT input deck for BWR spent MOX fuel with burnup of 40-GWd, 6% Pu IE, and 5-yrs cooled.

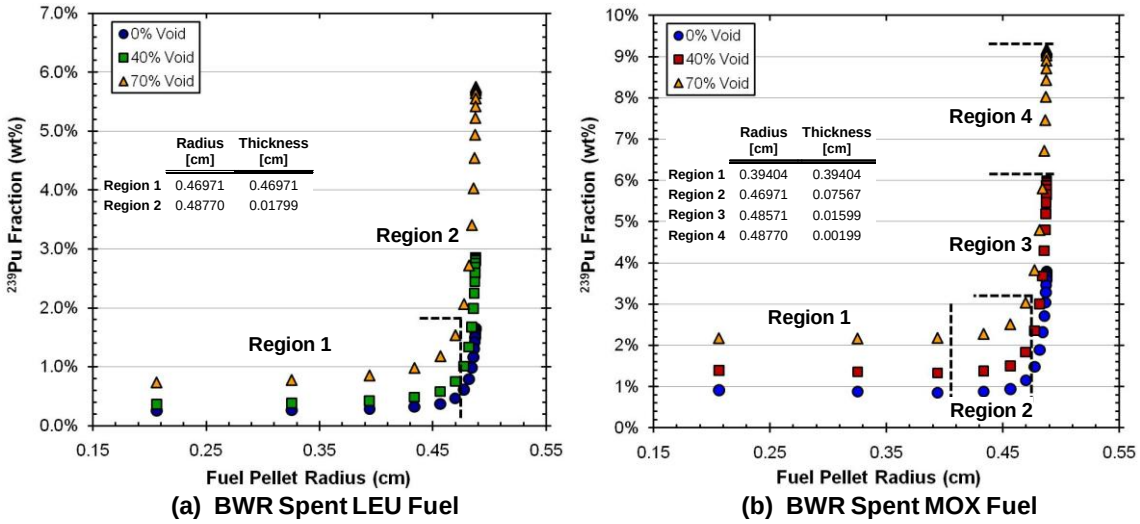

Fig. 9.1. ^{239}Pu fraction versus fuel pellet radius in BWR spent (a) LEU and MOX fuel (40-GWd).

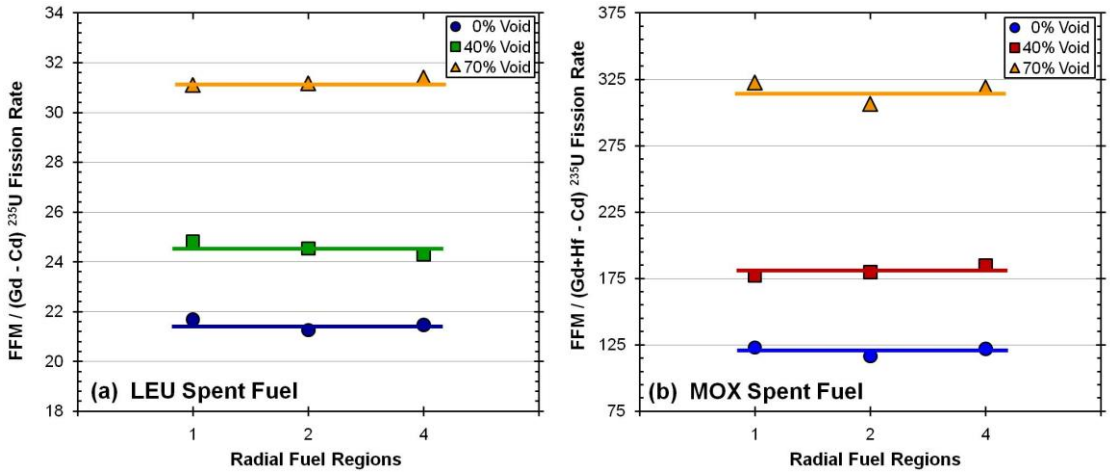

Fig. 9.2. Sensitivity of FFM / (Gd – Cd) ^{235}U FC ratio to the number of radial fuel regions for BWR spent (a) LEU and (b) MOX fuel with 40-GWd burnup.

9.2. BWR Spent LEU Fuel Assembly

The use of different SINRD ratios was analyzed to determine the optimum ratio that maximized the SINRD signature for measuring ^{239}Pu and ^{235}U in a BWR 9x9 spent LEU FA with 0%, 40%, and 70% void fractions. We varied the initial enrichment from 3% to 4.5% ^{235}U to assess the sensitivity of SINRD to changes in the distribution of Pu

isotopics. The cooling time was fixed at 5-yrs. The calculated spent fuel isotopics for BWR spent LEU fuel are given in Table E.3 to Table E.5 of Appendix E.

9.2.1. Optimized SINRD Ratios ^{239}Pu Measurements

The SINRD detector ratio signature was optimized for measuring ^{239}Pu in BWR spent LEU fuel using 3% ^{235}U IE, 5-yrs cooled, and no void fraction as the base case. To determine how the absorption of low energy neutrons by ^{240}Pu affects the SINRD FC ratio, a 2-mm Hf filter was added inside the Gd filter. The transmitted flux through a 2-mm Hf filter relative to the ^{240}Pu (n,γ) cross-section and buildup of Pu isotopics in spent LEU fuel are shown in Fig. 9.3(a) and (b), respectively.

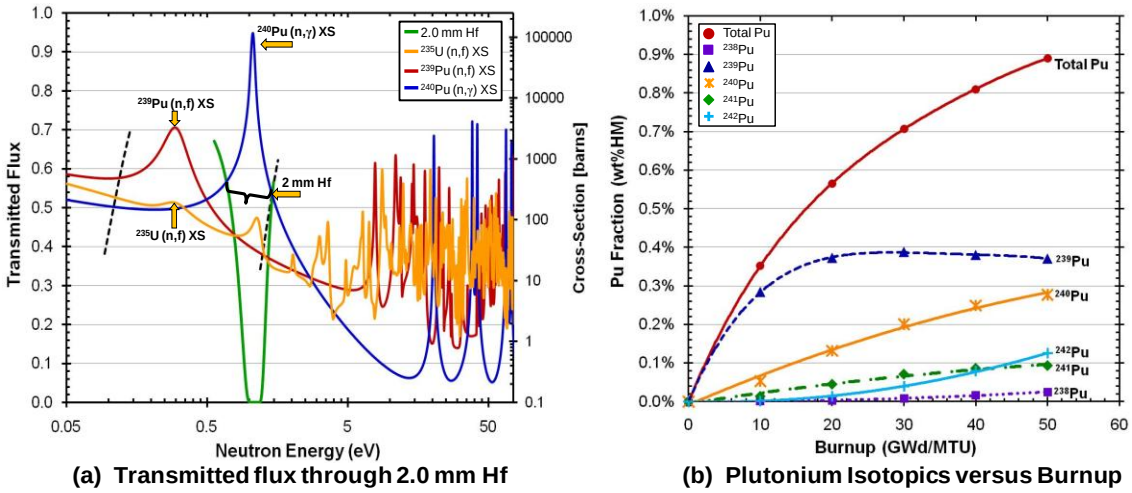

(a) Transmitted flux through 2.0 mm Hf **(b) Plutonium Isotopics versus Burnup**

Fig. 9.3. (a) Transmitted flux through 2-mm Hf relative to ^{240}Pu (*n,γ*) cross-section, (b) buildup of Pu isotopics in BWR spent LEU fuel (No Void, 3% ^{235}U IE, 5-yrs cooled).

In Fig. 9.4, the effect of using 2-mm Hf on FFM / (Gd – Cd) ^{239}Pu FC ratio is shown as a function of (a) burnup and (b) ^{239}Pu fraction. These results have been normalized to the fresh fuel case (3% IE). Adding 2-mm Hf to the Gd ^{239}Pu FC increased the slope of the SINRD signature by 6%. This is because the Hf filter absorbs the majority of neutrons in the same energy region as the ^{240}Pu (n,γ) resonance reducing the ^{240}Pu effect on the SINRD ratio.

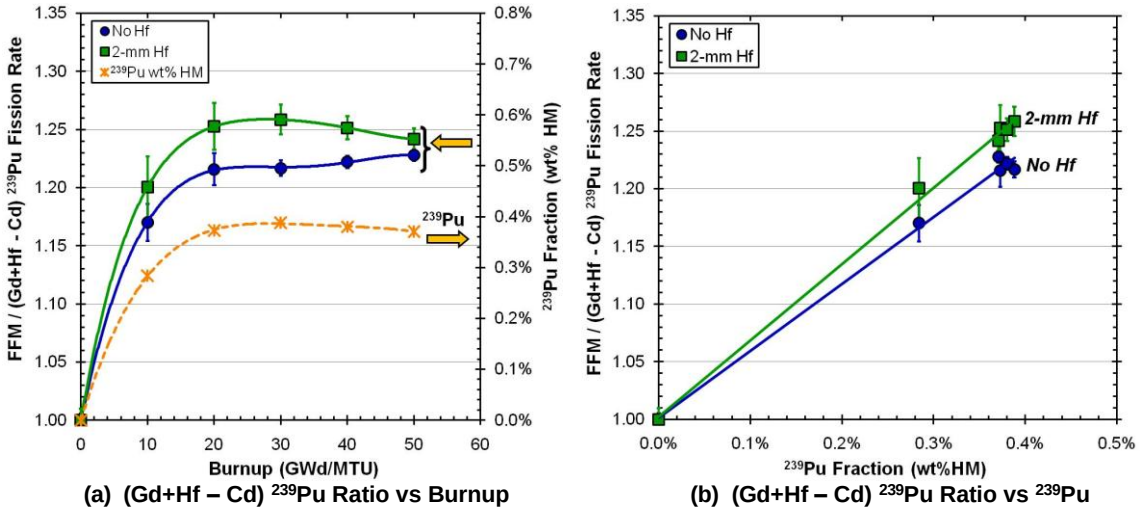

Fig. 9.4. Optimized SINRD ratio for ^{239}Pu: FFM / (Gd+Hf – Cd) ^{239}Pu FC ratio versus (a) burnup and (b) ^{239}Pu wt%HM with no Hf and 2-mm Hf.

Referring to Fig. 9.4(a), it is important to note that the results for the SINRD ratio with 2-mm Hf closely follow the curve for the ^{239}Pu fraction in LEU spent fuel over the burnup range of 0 – 50-GWd. However, when no Hf is used the SINRD ratio continues to increase with burnup even though the ^{239}Pu fraction decreases for burnups >30-GWd. The purpose for plotting the (Gd+Hf – Cd) ^{239}Pu FC ratio results versus burnup in Fig. 9.4(a) and ^{239}Pu fraction in (b) was to illustrate that similarity of the curves in (a) translates to linear curves in (b) when the SINRD ratio was plotted versus ^{239}Pu fraction.

In BWR spent LEU fuel, the relative concentrations of ^{235}U, ^{239}Pu, and ^{240}Pu change significantly for different void fractions. As a result, we have examined the effect of void fractions on the FFM / (Gd+Hf – Cd) ^{239}Pu FC ratio using ^{239}Pu FCs with 2-mm Hf and all ^{235}U FCs with no Hf. The results are shown in Fig. 9.5 for (a) 0%, (b) 40% and (c) 70% void fractions in BWR spent LEU fuel with 3% ^{235}U IE. For no void fraction, the use of all ^{235}U FCs not only decreased the SINRD signature but the results no longer linearly track the ^{239}Pu fraction. This negative effect on our SINRD signature may be attributed to the fact that the concentration of ^{235}U relative to ^{239}Pu is large at low fuel burnups (≤ 30-GWd) and nearly equal at high burnups. As a result, the competing effects from the burnup of ^{235}U and buildup ^{239}Pu are wiping out our signature. Thus, all

^{235}U FCs cannot be used to quantify ^{239}Pu in BWR spent LEU fuel with no void fraction. Referring to Fig. 9.5(b) and (c), the results for 40% and 70% void fractions clearly show that all ^{235}U FCs can be used to determine the ^{239}Pu content in spent LEU fuel. The ability to use all ^{235}U FCs to measure ^{239}Pu in BWR spent fuel with 40% and 70% VFs may be attributed to the fact that the amount of ^{239}Pu relative ^{235}U is much higher and that the buildup of ^{239}Pu does not saturate over burnup range of 0 to 50-GWd/MTU.

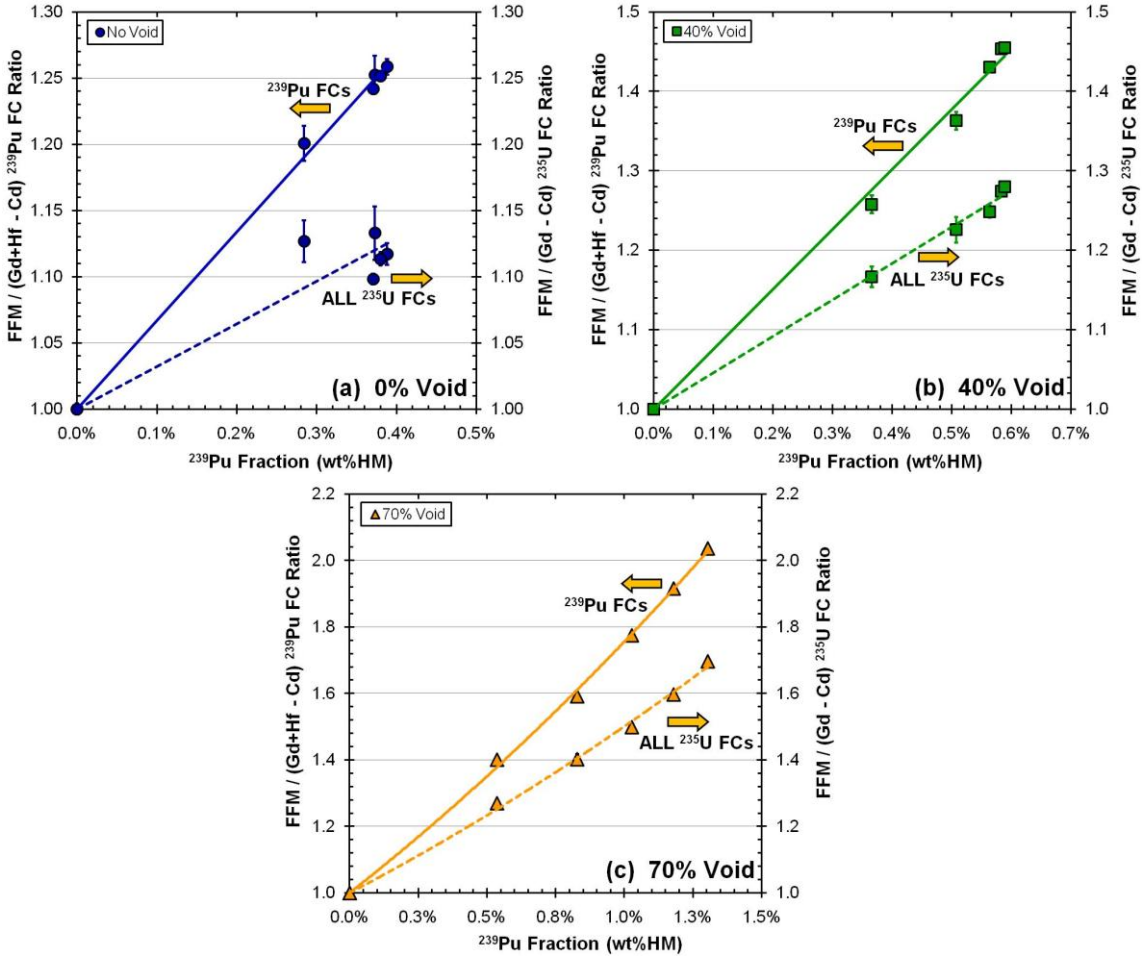

Fig. 9.5. Effect of using all ^{235}U FCs on the FFM / (Gd+Hf – Cd) FC ratio versus ^{239}Pu fraction in BWR spent LEU fuel (3% IE) with (a) 0%, (b) 40% and (c) 70% void fractions.

It should be emphasized that these results have been normalized to the fresh fuel case because in practice SINRD could be calibrated using a fresh fuel assembly. It is also important to note that the error bars shown on all results represent the calculated uncertainties in the SINRD ratios obtained via error propagations of expected counting statistics (see Appendix B). The expected count rates in the SINRD FCs are given in Table 9.1 for a BWR spent LEU fuel assembly with 40-GWd burnup (3% IE, 5-yrs cooled). The use of Hf in the Gd ^{239}Pu and ^{235}U FCs reduced the count rate by 44% and 24%, respectively. The effect of using Gd and Cd ^{235}U FCs compared to ^{239}Pu FCs decreased the count rates in the Gd FC by 59% (no Hf) and Cd FC by 10%. Using error propagations, the lower count rates in the Gd and Cd ^{235}U FCs increased the relative uncertainty in the FFM / (Gd – Cd) ^{235}U FC ratio by 67% compared to using ^{239}Pu FCs. It is important to note that this increase in the relative uncertainty is significant because using all ^{235}U FCs also decreased the slope of the SINRD signature. It should also be noted that these count rates are somewhat conservative because the (α,n) contribution to the total neutron emission rate from the assembly was not accounted for. However, the (α,n) contribution is small compared to the spontaneous fission contribution to the total neutron emission rate, especially at higher burnups.

Table 9.1. Expected count rates in SINRD FCs for 40-GWd BWR spent LEU fuel.

SINRD Detectors	BWR Spent LEU Fuel [cps]*		
	No Void	***40% Void***	***70% Void***
Bare ^{235}U	308 ± 0.29	415 ± 0.34	489 ± 0.37
FFM ^{235}U	896 ± 0.50	1451 ± 0.63	2280 ± 0.80
Gd ^{235}U	95 ± 0.16	145 ± 0.20	207 ± 0.24
Gd+Hf ^{235}U	72 ± 0.14	110 ± 0.17	158 ± 0.21
Cd ^{235}U	54 ± 0.12	86 ± 0.15	134 ± 0.19
Gd ^{239}Pu	241 ± 0.26	358 ± 0.32	479 ± 0.36
Gd+Hf ^{239}Pu	134 ± 0.19	199 ± 0.24	271 ± 0.27
Cd ^{239}Pu	60 ± 0.13	96 ± 0.16	148 ± 0.20

* *Neutron source terms: 9.3E+07 n/s, 1.4E+08 n/s, 1.9E+08 n/s for 0% VF, 40% VF, and 70% VF, respectively.*

The sensitivity of our SINRD detector ratio signature to initial enrichment was also investigated using ^{239}Pu FCs and all ^{235}U FCs. The FFM / (Gd+Hf – Cd) ^{239}Pu FC ratio is compared to the FFM / (Gd – Cd) ^{235}U FC ratio versus ^{239}Pu fraction in Fig. 9.6(a) and (b), respectively, for 3% and 4.5% ^{235}U IE. These results were not normalized to the fresh fuel case. The maximum change in the SINRD ratio from varying the IE was 7.5% for the case with no void and all ^{235}U FCs; however, the sensitivity to IE decreases as the void fraction increases. Referring to Fig. 9.6(b) for all ^{235}U FCs, the large scatter in the results for 0% and 40% void fractions confirms our conclusion that ^{239}Pu FCs are needed to accurately measure the ^{239}Pu content in BWR spent LEU fuel at low void fractions.

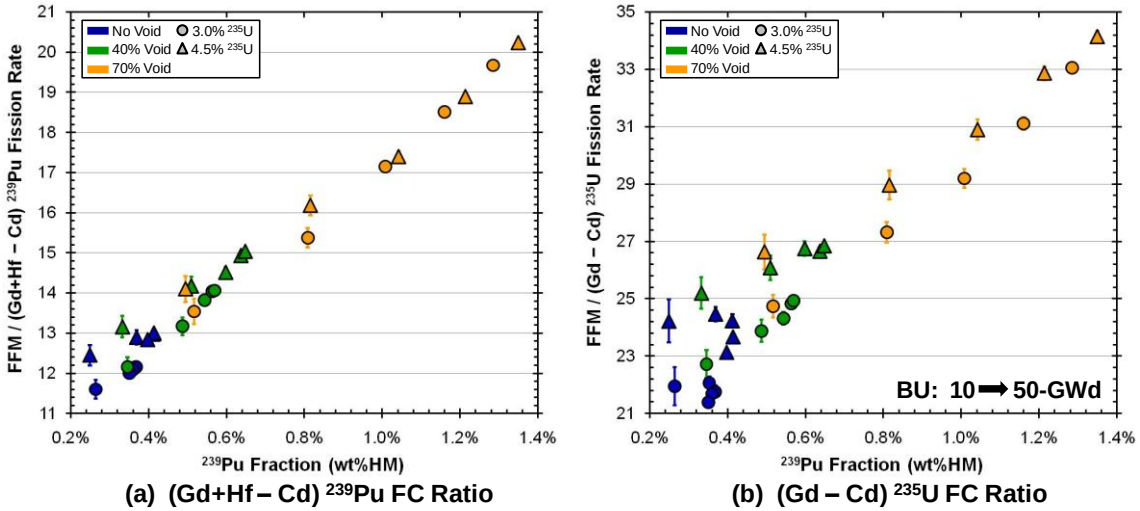

Fig. 9.6. Comparison of (a) FFM / (Gd+Hf – Cd) ^{239}Pu FC ratio to (b) FFM / (Gd – Cd) ^{235}U FC ratio versus ^{239}Pu fraction for BWR spent LEU fuel with 3% and 4.5% ^{235}U IE.

The FFM / (Gd+Hf – Cd) ^{239}Pu FC ratio was optimized for measuring ^{239}Pu in both BWR and PWR spent LEU fuel assemblies by using a 2-mm Hf filter. Comparison of the optimized SINRD ratio for ^{239}Pu is shown in Fig. 9.7 using (a) ^{239}Pu FCs (2-mm Hf) and (b) all ^{235}U FCs (no Hf) for BWR (3% IE, no void) and PWR (4% IE, no boron) spent LEU fuel. These results were normalized to the fresh fuel case. The results for the (Gd+Hf – Cd) ^{239}Pu FC ratio increased by 5.6% for PWR spent LEU fuel compared to

BWR spent LEU fuel. This was expected because the ^{239}Pu fraction is higher in PWR spent fuel. Thus, if ^{239}Pu FCs are used, the optimized (Gd+Hf – Cd) SINRD ratio is not sensitive to the type of fuel assembly being measured. This may be attributed to the fact that the source strength and geometric coupling between SINRD and the fuel assembly cancels in the FC ratio. It is important to note, however, that the sensitivity of our SINRD ratio to the fuel assembly type is significant when all ^{235}U FCs are used.

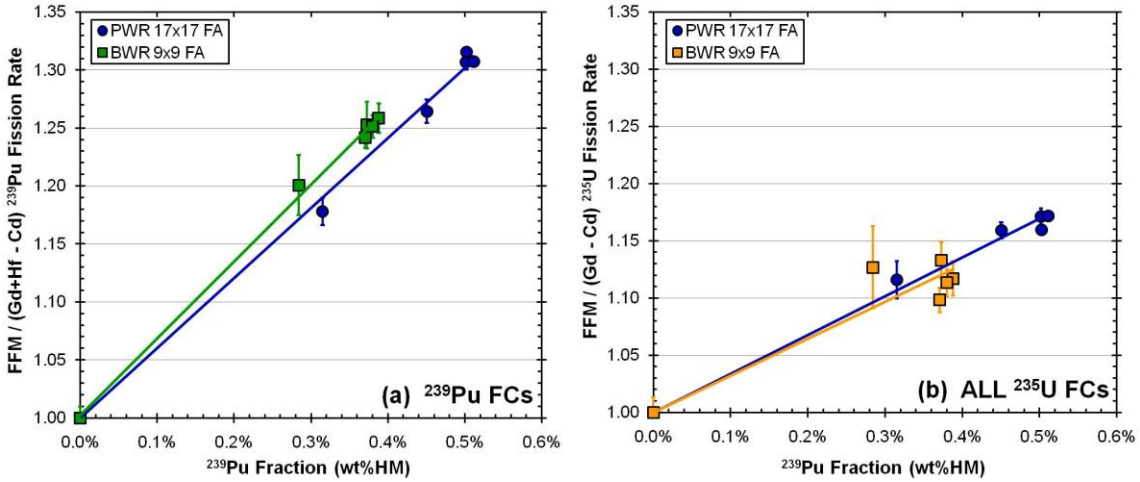

Fig. 9.7. Comparison of optimized SINRD ratio for ^{239}Pu using (a) ^{239}Pu FCs (2-mm Hf) and (b) all ^{235}U FCs (no Hf) for BWR (3% IE, no void) and PWR (4% IE, no boron) spent LEU fuel.

9.2.2. SINRD Results for ^{235}U Measurements

The use of SINRD to quantify ^{235}U in BWR spent LEU fuel was also investigated. The capability to measure ^{235}U using SINRD is important to verifying the burnup and initial enrichment of spent fuel. In Fig. 9.8, seven different SINRD ratios are shown versus ^{235}U fraction for the case with 3% IE and no void fraction to determine which ratio is best for quantifying ^{235}U. These results were normalized to the fresh fuel case. The ratios shown in Fig. 9.8(a) have the FFM FC in the denominator and in Fig. 9.8(b) the Bare FC is in the denominator. It should be noted that all ^{235}U FCs were used in all of the SINRD ratios. Similar to results for PWR spent LEU fuel, we can see that the (Gd

– Cd) ^{235}U / Bare ^{235}U FC ratio [Fig. 9.8(b)] is the only ratio that linearly tracks ^{235}U in BWR spent LEU fuel.

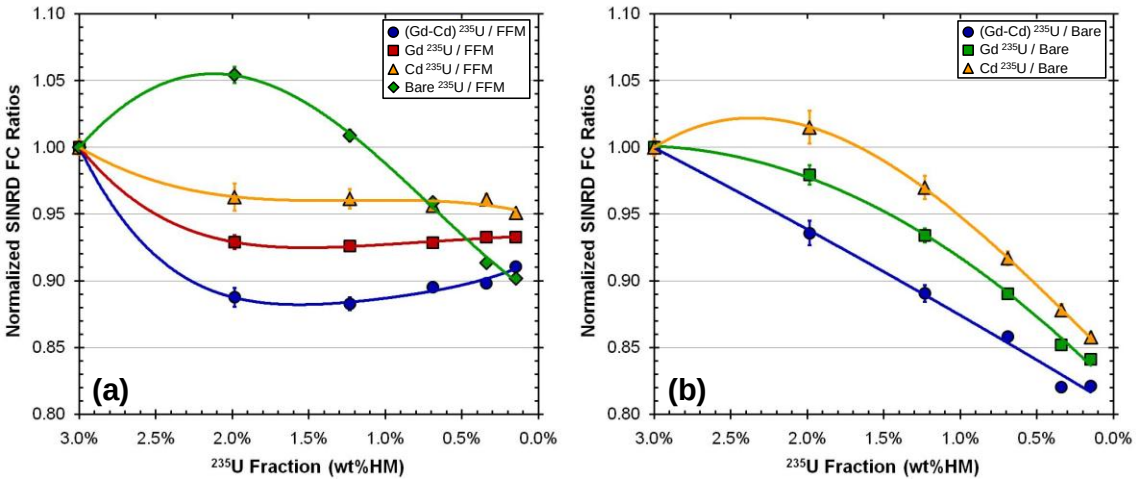

Fig. 9.8. Comparison of different SINRD ratios versus ^{235}U fraction in BWR spent LEU fuel with 3% IE and no void fraction.

In order to determine if resonance absorption by ^{239}Pu within the (Gd – Cd) energy window is contributing to our SINRD signature, the (Gd – Cd) ^{235}U / Bare ^{235}U FC ratio is shown in Fig. 9.9 versus (a) ^{235}U fraction and (b) ^{235}U + ^{239}Pu fraction. These results are shown with 0%, 40%, and 70% void fractions to assess the sensitivity of this ratio different void fractions. It is important to note the change in the slope of the (Gd – Cd) ^{235}U / Bare ^{235}U FC ratio for different void fractions when plotted versus only ^{235}U compared to ^{235}U + ^{239}Pu in LEU spent fuel. These results show that the effect of ^{239}Pu on our SINRD ratio increases as the void fraction increases. This was expected because the concentration of ^{239}Pu in BWR spent LEU fuel increases by a factor of 3 from 0% to 70% void fraction. Thus, the ability to quantify ^{235}U decreases as the void fraction increases due to the competing effects of the burnup of ^{235}U and buildup of ^{239}Pu.

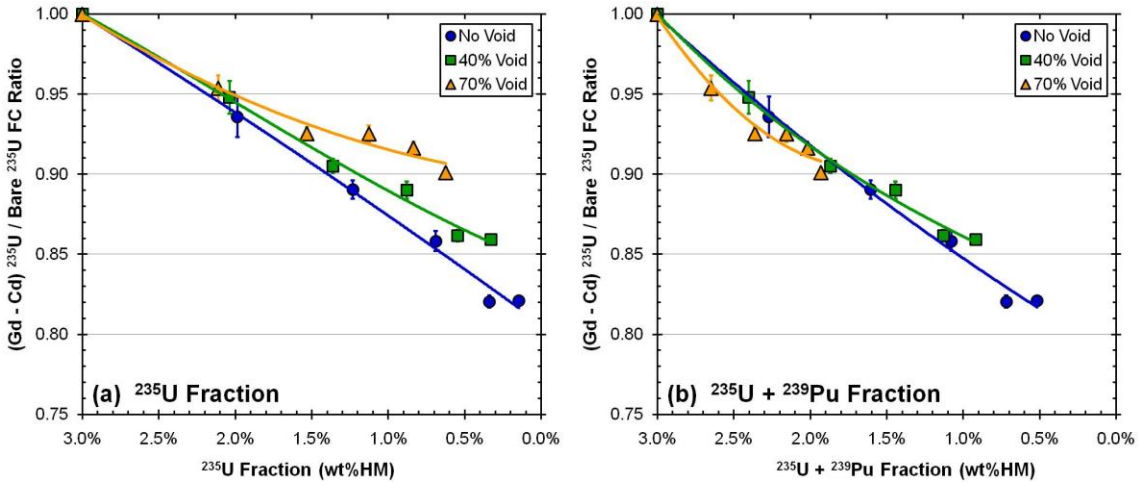

Fig. 9.9. (Gd – Cd) ^{235}U / Bare ^{235}U FC ratio versus (a) ^{235}U fraction and (b) ^{235}U + ^{239}Pu fraction in BWR spent LEU fuel with 3% IE for different void fractions.

To obtain a better understanding of the physics of this SINRD ratio, Fig. 9.10 shows the neutron flux multiplied by neutron energy, $E \cdot \phi(E)$, at burnups of 10, 30, and 50-GWd relative to Gd and Cd cut-off energies for 3% IE BWR spent LEU fuel with (a) 0% VF and (b) 70% VF. Comparing the results shown in Fig. 9.10, we see that the depression in the neutron flux within the (Gd – Cd) energy window (indicated by black arrow) increases as the burnup increases and is noticeably larger for the case with 70% VF. This depression in the flux is from ^{235}U and ^{239}Pu resonance absorption which increases with burnup due to the buildup of ^{239}Pu. The depression is larger for spent LEU fuel with 70% VF [Fig. 9.10(b)] compared to (a) with 0% VF because the ^{239}Pu content is a factor of 3 greater. These results show that ^{239}Pu resonance absorption within the (Gd – Cd) energy window is contributing to our SINRD signature, especially at high void fractions, and thus should be accounted for.

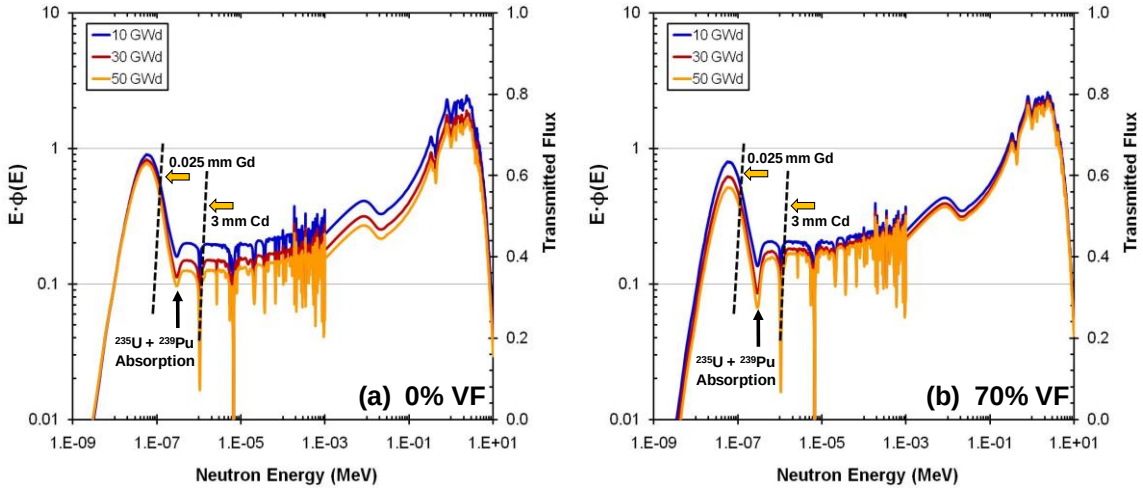

Fig. 9.10. Comparison of E·ϕ(E) at burnups of 10, 30, and 50-GWd versus neutron energy relative to Gd and Cd cut-off energies for BWR spent LEU fuel with (a) 0% VF and (b) 70% VF.

The effect of varying the initial ^{235}U IE from 3% to 4.5% on the (Gd – Cd) ^{235}U / Bare ^{235}U FC ratio was also analyzed. The results are shown in Fig. 9.11 versus ^{235}U + ^{239}Pu fraction in BWR spent LEU fuel for different void fractions. In contrast to previous results, these results were not normalized to the fresh fuel case. Varying the initial ^{235}U IE, changed the SINRD ratio by less than 5% over burnup range of 0 to 50-GWd/MTU and thus, is not sensitive to this parameter. For both 3% and 4.5% ^{235}U IE, the SINRD ratio linearly tracks the ^{235}U + ^{239}Pu content in BWR spent LEU fuel with 0%, 40%, and 70% void fractions. It should be noted that the slope of the SINRD FC ratio signature for determining ^{235}U + ^{239}Pu using all ^{235}U FCs decreased by a factor of ~9 for 0% VF, ~13 for 40% VF and ~16 for 70% VF compared to the slope for measuring ^{239}Pu using ^{239}Pu FCs. This effect is attributed to the fact that the ^{239}Pu fission cross-section is an order of magnitude larger than ^{235}U within the (Gd – Cd) energy window. As a result, ^{239}Pu FCs have a higher sensitivity to ^{239}Pu resonance absorption in spent fuel.

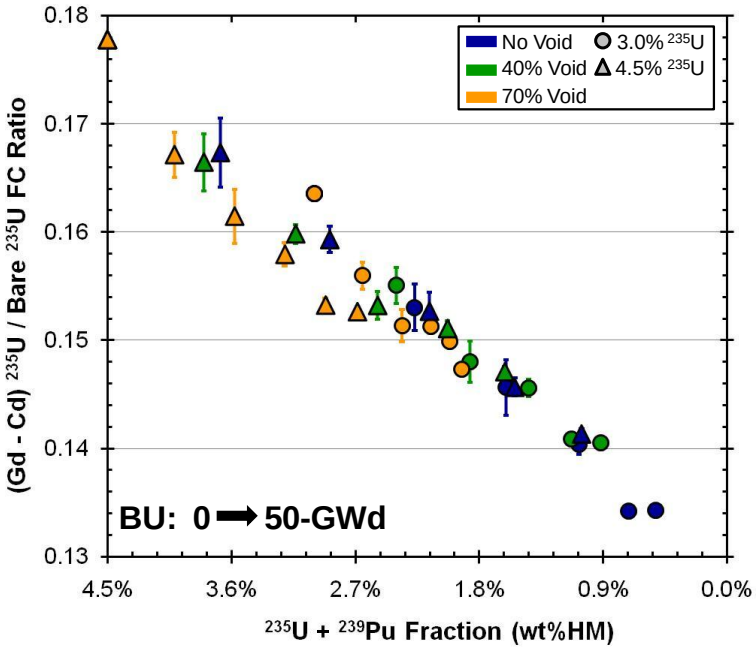

Fig. 9.11. Comparison of (Gd – Cd) ^{235}U / Bare ^{235}U FC ratio versus ^{235}U + ^{239}Pu fraction in BWR spent LEU fuel with 3% and 4.5% ^{235}U IE.

Fig. 9.12 shows the (Gd – Cd) ^{235}U / Bare ^{235}U FC ratio versus ^{235}U + ^{239}Pu fraction for different ^{235}U IE in BWR 9x9 FA (no void) and PWR 17x17 FA (no boron). These results were not normalized to the fresh fuel case. Comparing the results for PWR and BWR spent LEU fuel, we see that the SINRD ratio is directly proportional to the ^{235}U + ^{239}Pu content over burnup range of 0 to 50-GWd/MTU for all cases. Thus, our SINRD ratio for quantifying the ^{235}U + ^{239}Pu content in spent fuel is insensitive to the type of fuel assembly being measured. This is an important characteristic because it means that SINRD does need separate calibration curves in order to verify BWR (no void) and PWR (no boron) spent fuel assemblies.

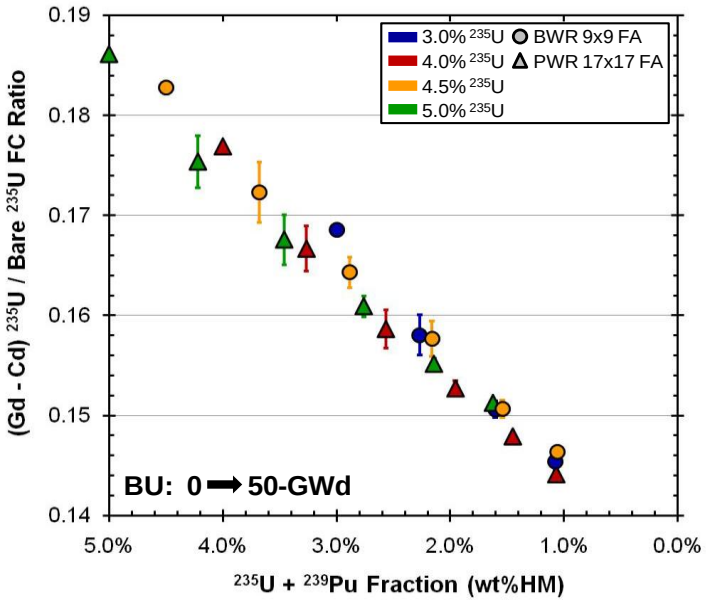

Fig. 9.12. Comparison of (Gd – Cd) ^{235}U / Bare ^{235}U FC ratio versus ^{235}U + ^{239}Pu fraction for different ^{235}U IE in BWR 9x9 FA (0% VF) and PWR 17x17 FA (no boron).

9.3. BWR Spent MOX Fuel Assembly

We also investigated the use of SINRD to measure the ^{239}Pu and ^{240}Pu content in a BWR 9x9 spent MOX fuel assembly with 0%, 40%, and 70% void fractions. The initial fuel enrichment was varied from 6% to 4% Pu to better understand the physics of the SINRD technique for different distributions of Pu isotopics in MOX spent fuel. The cooling time was fixed at 5-yrs. It should also be noted that since the ^{235}U fraction is less than <0.1% in spent MOX fuel, we did not try to quantify it. The calculated spent fuel isotopics for BWR spent MOX fuel are given in Table E.6 – Table E.8 of Appendix E.

9.3.1. Optimized SINRD Ratios for ^{239}Pu Measurements

We have optimized the SINRD signature for measuring ^{239}Pu using 6% Pu IE spent MOX fuel (5-yrs cooled) with no void fraction as the base case. The effect of adding a Hf filter inside the Gd filter was analyzed to determine how the absorption of low energy neutrons by ^{240}Pu affects our SINRD detector ratio signature. The transmitted flux through a 1-mm Hf filter relative to the ^{240}Pu (n,γ) cross-section and buildup of Pu isotopics in PWR spent MOX fuel is shown in Fig. 9.13(a) and (b), respectively.

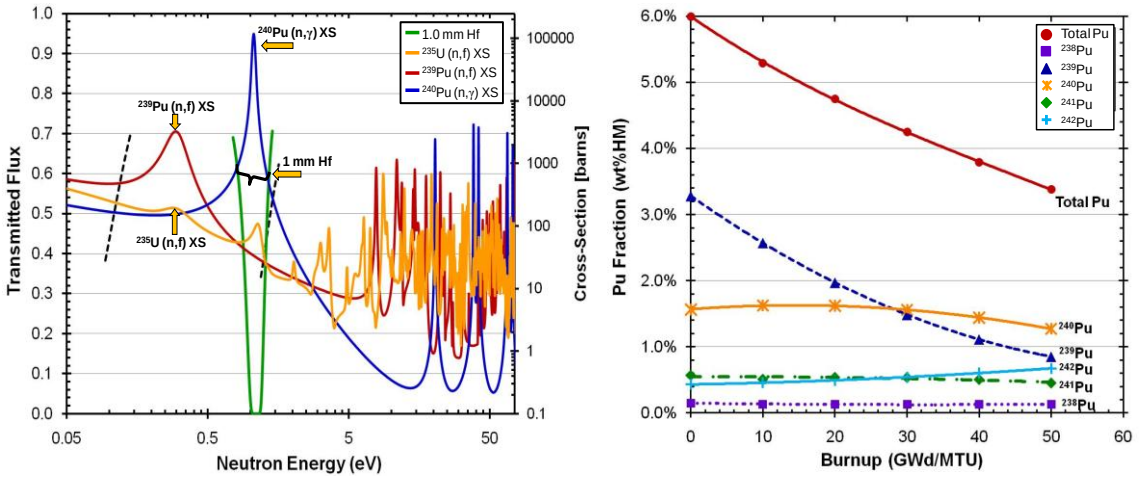

Fig. 9.13. (a) Transmitted flux through 1-mm Hf relative to ^{240}Pu (n,γ) cross-section, (b) buildup of Pu isotopics in PWR spent MOX fuel (no void, 6% Pu IE, 5-yrs cooled).

The effect of using all ^{235}U FCs on the FFM / (Gd+Hf – Cd) FC ratio versus ^{239}Pu fraction is shown in Fig. 9.14 with no void fraction. These results were normalized to the fresh fuel case. Using all ^{235}U FCs with 1-mm Hf increased the slope of the SINRD signature by 47% compared to using ^{239}Pu FCs with 3-mm Hf. Furthermore, adding 1-mm Hf to the ^{235}U FC ratio also greatly increased the linearity of the results. This is important because it indicates that the use of Hf has reduced the effect of ^{240}Pu on our SINRD ratio signature enabling us to quantify the ^{239}Pu content in BWR spent MOX fuel more accurately. This is consistent with the results for PWR spent MOX fuel.

The expected count rates in the SINRD FCs are given in Table 9.2 for a BWR spent MOX fuel assembly with 40-GWd burnup (6% Pu, 5-yrs cooled). The use of Hf in the Gd ^{239}Pu and ^{235}U FCs reduced the count rate by 44% and 22%, respectively. The effect of using Gd and Cd ^{235}U FCs compared to ^{239}Pu FCs decreased the count rates in the Gd FC by 53% and Cd FC by 8%. Using error propagations, the lower count rates in the Gd+Hf and Cd ^{235}U FCs increased the relative uncertainty in the FFM / (Gd+Hf – Cd) ^{235}U FC ratio by ~73% compared to using ^{239}Pu FCs for 0% and 40% VF; however, it is important to note that using all ^{235}U FCs increased the slope of the SINRD signature by

~57% for 0% and 40% VF. It should also be noted that these count rates did not accounted for the (α,n) contribution to the total neutron emission rate from the assembly.

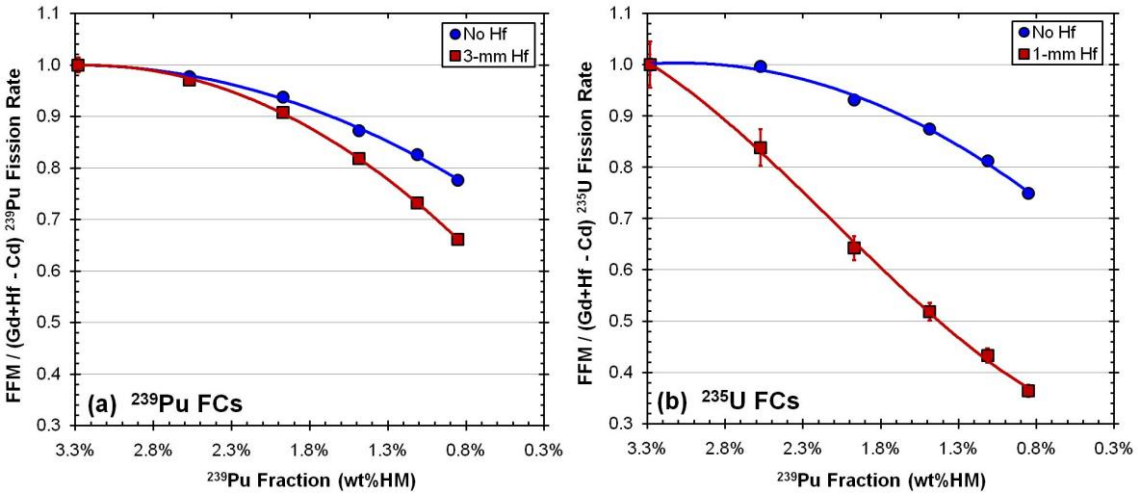

Fig. 9.14. Comparison of FFM / (Gd+Hf – Cd) FC ratio using (a) ^{239}Pu FCs and (b) ALL ^{235}U FCs versus ^{239}Pu fraction with no void fraction.

Table 9.2. Expected count rates in SINRD FCs for 40-GWd BWR spent MOX fuel.

SINRD Detectors	BWR Spent MOX Fuel [cps]*		
	0% Void	*40% Void*	*70% Void*
Bare ^{235}U	2342 ± 1.14	3062 ± 1.30	3565 ± 1.41
FFM ^{235}U	12409 ± 2.63	18626 ± 3.22	25083 ± 3.73
Gd ^{235}U	1052 ± 0.76	1502 ± 0.91	1916 ± 1.03
Gd+Hf ^{235}U	817 ± 0.67	1169 ± 0.81	1500 ± 0.91
Cd ^{235}U	716 ± 0.63	1064 ± 0.77	1422 ± 0.89
Gd ^{239}Pu	2319 ± 1.39	3187 ± 1.63	3903 ± 1.80
Gd+Hf ^{239}Pu	1339 ± 1.06	1855 ± 1.24	2297 ± 1.38
Cd ^{239}Pu	788 ± 0.81	1162 ± 0.98	1528 ± 1.13

* *Neutron source terms: 1.2E+09 n/s, 1.6E+09 n/s, 2.0E+09 n/s for 0% VF, 40% VF, and 70% VF, respectively.*

Next, we examined how void fraction and initial enrichment affect our SINRD ratio for determining ^{239}Pu. The results are shown in Fig. 9.15 for (a) 6% Pu and (b) 4% Pu IE

spent MOX fuel. These results were normalized to the fresh fuel case. The change in our optimized SINRD ratio was less than 5% for spent MOX fuel with 0% and 40% void fractions. It is important to note that our SINRD ratio tracks the ^{239}Pu content linearly in BWR spent MOX fuel with 0% and 40% void fractions; however, for the case with 70% void fraction, this ratio no longer tracks ^{239}Pu content spent MOX fuel.

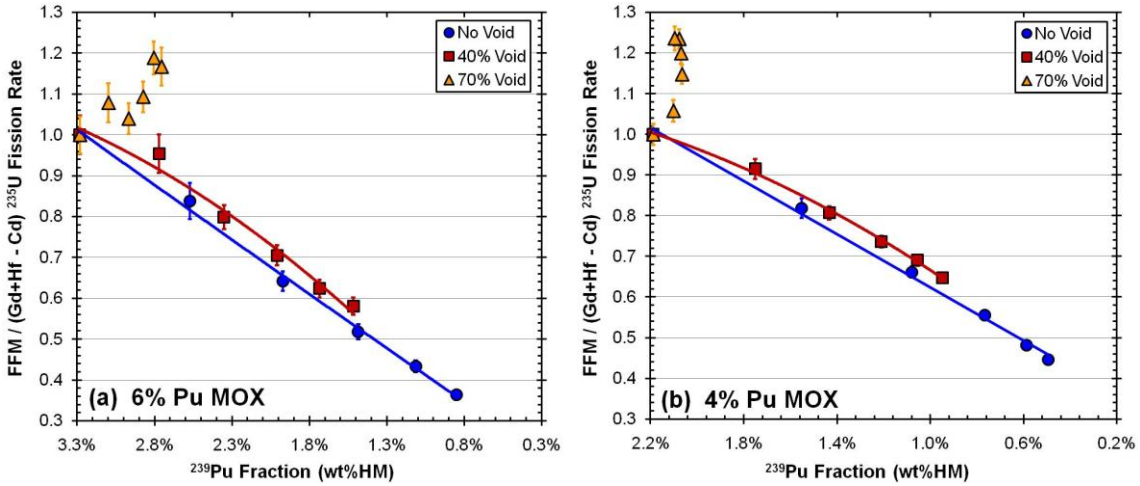

Fig. 9.15. Effect of void fraction on the FFM / (Gd+Hf – Cd) ^{235}U FC ratio versus ^{239}Pu fraction in BWR spent MOX fuel for (a) 6% Pu and (b) 4% Pu IE.

In Fig. 9.16, the FFM / (Gd+Hf – Cd) ^{235}U FC ratio versus ^{239}Pu fraction is shown with no normalization for BWR spent MOX fuel. Similar to the results shown in Fig. 9.15, we see that our optimized SINRD linearly tracks the ^{239}Pu content in spent MOX fuel with 0% and 40% void fractions but not for the case with 70% void fraction.

The optimized SINRD ratio for measuring ^{239}Pu for BWR (no void) and PWR (no boron) spent MOX fuel is shown in Fig. 9.17 for (a) 6% Pu and (b) 4% Pu IE. These results were normalized to the fresh fuel case. Comparing the results for PWR and BWR spent MOX fuel, the SINRD ratio changed by less than 3% for both 6% Pu and 4% Pu IE. Thus, the optimized SINRD ratio for measuring ^{239}Pu in spent MOX fuel is insensitive to the type of fuel assembly being measured. This is an important

characteristic because it means that SINRD does need separate calibration curves in order to verify BWR (no void) and PWR (no boron) spent fuel assemblies.

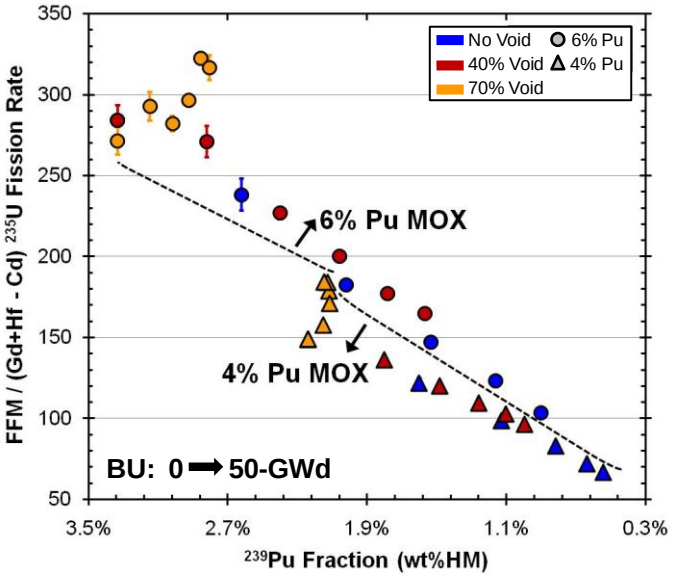

Fig. 9.16. FFM / (Gd+Hf – Cd) ^{235}U FC ratio versus ^{239}Pu fraction with no normalization for BWR spent MOX fuel with 6% and 4% Pu IE.

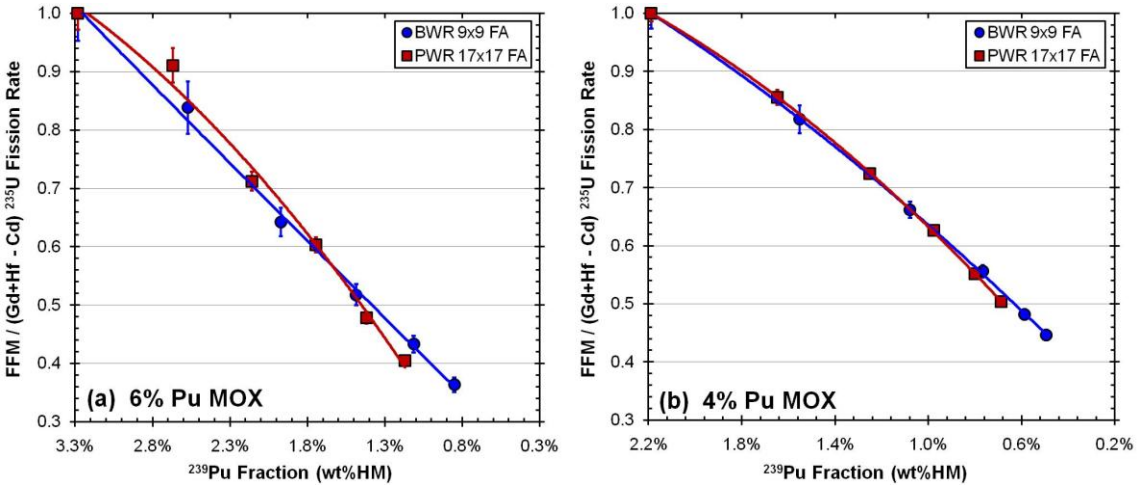

Fig. 9.17. Comparison of FFM / (Gd+Hf – Cd) ^{235}U FC ratio for BWR and PWR spent MOX fuel with IE of (a) 6% Pu and (b) 4% Pu.

9.3.2. Use of SINRD to Measure ^{240}Pu

We have also investigated using the SINRD detector ratio, with and without Hf, to quantify ^{240}Pu in BWR spent MOX fuel. The (Gd+Hf – Cd) / (Gd – Cd) ^{235}U FC ratio versus ^{240}Pu / ^{239}Pu fraction is shown in Fig. 9.18 for (a) 6% Pu and (b) 4% Pu IE spent MOX fuel for different void fractions. It is important to note that the SINRD detector configuration would have to be modified to include an additional Gd ^{235}U FC (no Hf) to determine the ^{240}Pu content. Since the results are plotted versus ^{240}Pu / ^{239}Pu fraction another SINRD ratio must be used to obtain the ^{240}Pu fraction. This SINRD ratio must be able to clearly distinguish BWR spent MOX fuel with 6% Pu IE from 4% Pu IE or accurately quantify the ^{239}Pu fraction.

The (Gd+Hf – Cd) / (Gd – Cd) ^{235}U FC ratios for BWR and PWR spent MOX fuel assemblies are compared in Fig. 9.19 for (a) 6% Pu and (b) 4% Pu IE. Based on these results, the SINRD ratio for determining the ^{240}Pu / ^{239}Pu fraction changed by less than 5% for BWR and PWR spent MOX fuel with 6% Pu and 4% Pu IE. Similar to the ^{239}Pu results shown in the previous section, the SINRD ratio for quantifying the ^{240}Pu / ^{239}Pu fraction in spent MOX fuel is insensitive to the type of fuel assembly being measured.

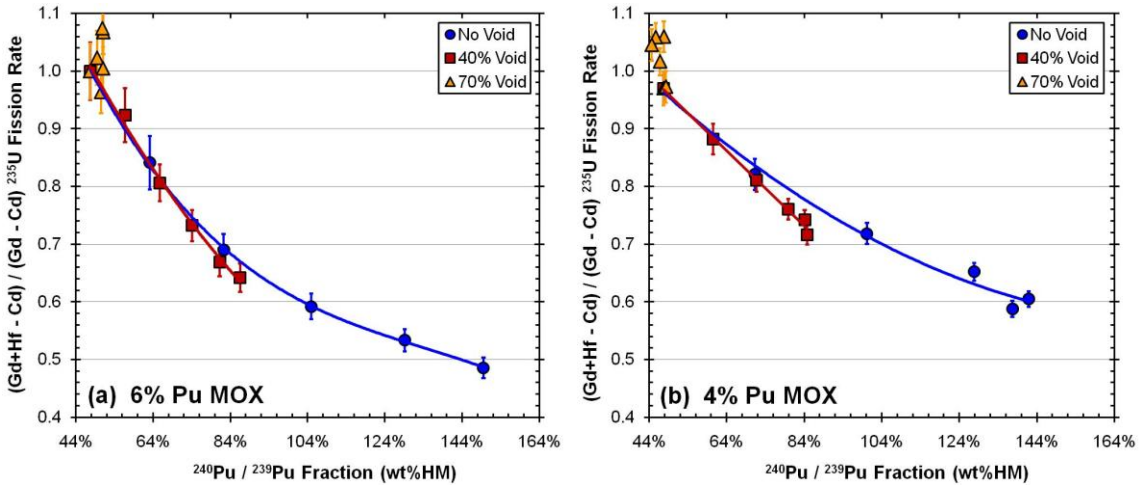

Fig. 9.18. Effect of void fraction on the (Gd+Hf – Cd) / (Gd – Cd) ^{235}U FC ratio versus ^{240}Pu / ^{239}Pu fraction in (a) 6% Pu and (b) 4% Pu IE spent MOX fuel.

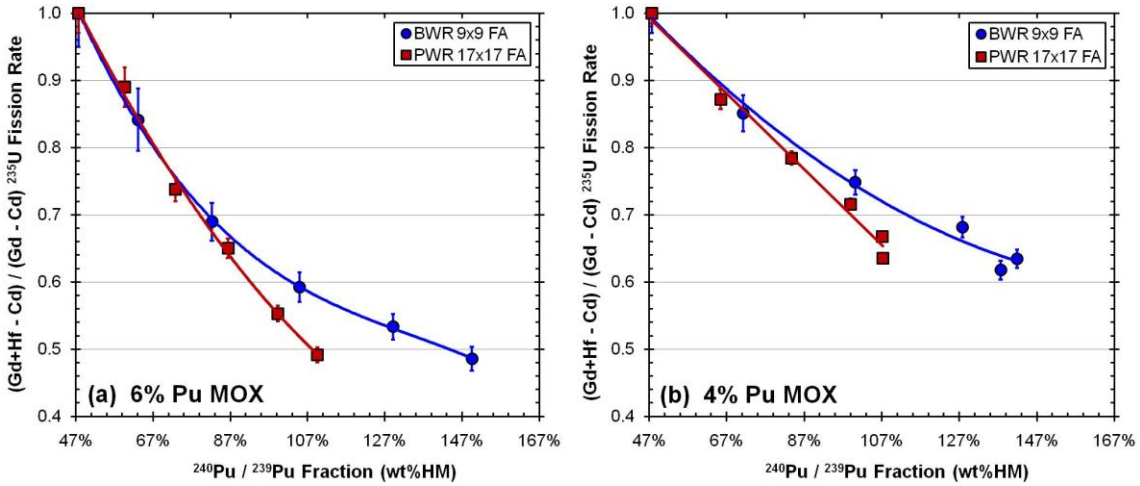

Fig. 9.19. Comparison of (Gd+Hf – Cd) / (Gd – Cd) ^{235}U FC ratio for BWR and PWR spent MOX fuel with IE of (a) 6% Pu and (b) 4% Pu.

9.4. Analysis of Possible Diversion Scenarios for BWR

The sensitivity of SINRD to possible diversion scenarios was assessed for BWR spent LEU and MOX fuel assemblies with void fractions of 0%, 40%, and 70%. The initial fuel enrichment was fixed at 3% ^{235}U for spent LEU fuel and 6% Pu for spent MOX fuel. It is also important to note that only ^{235}U FCs were used in SINRD. We used the following safeguards detection requirements to evaluate SINRD for this analysis:

- Independent of the Operator's declaration of:
  - burnup, initial enrichment, cooling time, and void fraction
- Sensitive to fuel pin removal over entire burnup range.
- Able to distinguish fresh and 1-cycle MOX fuel from 3- and 4-cycle LEU fuel.
- Recognize that IAEA may prefer to use all ^{235}U fission chambers.

9.4.1. Verification of Burnup

In BWR 9x9 spent LEU and MOX fuel assemblies, the ^{244}Cm neutron emission rate is approximately 9.3E+07 n/s and 1.2E+09 n/s, respectively, for burnup of 40-GWd with no void fraction. These source terms are further amplified by a factor of 2 – 3 by neutron multiplication in the assembly when in water. For spent LEU fuel, this high neutron source term provides adequate counting statistics in the fission chambers to give

better than 1% precision in a few minutes for the SINRD ratios. This count time is decreased even further for spent MOX fuel.

9.4.1.1. BWR Spent LEU Fuel

The use of SINRD to verify the burnup of a BWR spent LEU fuel assembly was investigated. In Fig. 9.20, the ^{235}U and ^{244}Cm fractions are compared to the (Gd – Cd) ^{235}U / Bare ^{235}U FC ratio and FFM fission rate versus burnup for the diversion scenario where the burnup is misdeclared low. Since the ^{239}Pu content increases with burnup in LEU spent fuel, a proliferator is more likely to misdeclare the burnup low. Comparison of the results in Fig. 9.20 (a) to (b), clearly shows that the FFM fission rate is directly proportional to ^{244}Cm and that the (Gd – Cd) ^{235}U / Bare ^{235}U FC ratio is proportional to ^{235}U in LEU spent fuel over the burnup range of 0 – 50-GWd/MTU.

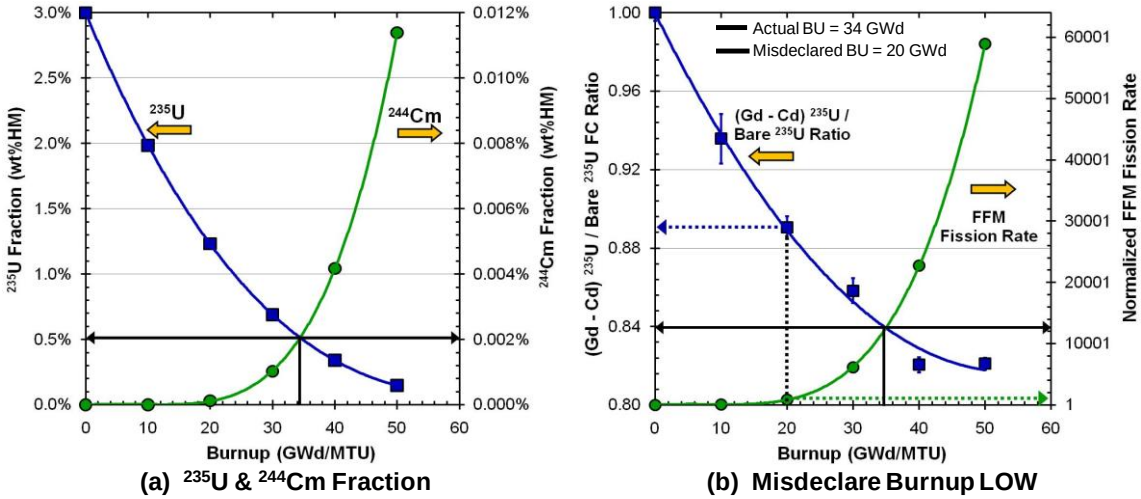

Fig. 9.20. Comparison of (a) ^{235}U and ^{244}Cm fraction to (b) the (Gd – Cd) ^{235}U / Bare ^{235}U FC ratio and FFM fission rate versus burnup for diversion scenario where burnup is misdeclared low.

The fact that ^{235}U fraction decreases as a function of burnup, whereas the ^{244}Cm fraction increases enables us to verify the burnup of the BWR spent LEU assembly because the proliferator can only get one of these curves right. Referring to Fig. 9.20(b), the solid black line indicates the actual burnup of the assembly (34-GWd) and the solid

black arrows point to the expected measured values at this burnup. The misdeclared burnup (20-GWd) is shown by the black dotted line. The dotted green and blue lines correspond to the expected measured values for the misdeclared burnup. When the burnup is misdeclared, the expected measured values move in opposite directions. Thus, comparing a set of measurements where the burnup is misdeclared to a reference measurement with known burnup would clearly indicate an anomaly in the declaration.

9.4.1.2. BWR Spent MOX Fuel

Next, the use of SINRD to verify the burnup of a BWR spent MOX fuel assembly with no void fraction was examined. Fig. 9.21(a) shows the ^{239}Pu and ^{244}Cm fraction as a function of burnup. The FFM / (Gd+Hf – Cd) ^{235}U FC ratio and FFM fission rate versus burnup is shown in Fig. 9.21(b) for the diversion scenario where the burnup is misdeclared high. In contrast to LEU spent fuel, the ^{239}Pu content decreases with burnup in MOX spent fuel. Thus, a proliferator is more likely to misdeclare the burnup high.

Comparison of Fig. 9.21 (a) to (b), clearly shows that the FFM / (Gd+Hf – Cd) ^{235}U FC ratio and FFM fission rate are directly proportional to the ^{239}Pu and ^{244}Cm fractions, respectively. Similar to the BWR spent LEU case, our ability to verify the burnup of the assembly is based on the fact that ^{239}Pu fraction decreases, whereas the ^{244}Cm fraction increases as a function of burnup. Thus, a proliferator who misdeclared the burnup of the assembly could only get one of these curves right because the expected measured values move in opposite directions. It should be noted that all ^{235}U FCs and 1-mm Hf were used in the FFM / (Gd+Hf – Cd) detector ratio.

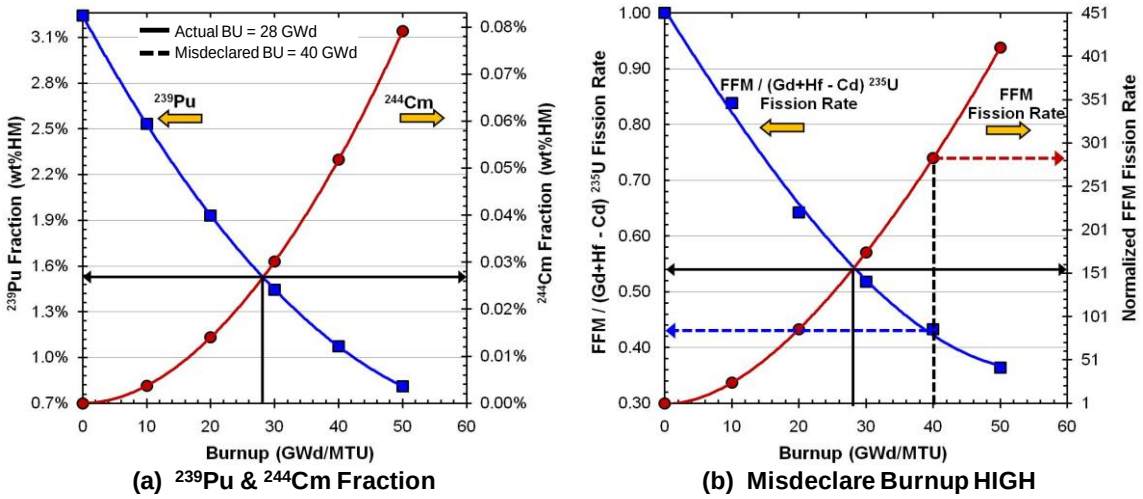

Fig. 9.21. Comparison of (a) ^{239}Pu and ^{244}Cm fraction to (b) the FFM / (Gd+Hf – Cd) ^{235}U FC ratio and FFM fission rate versus burnup for diversion scenario where burnup is misdeclared high.

9.4.2. Sensitivity to BWR Spent MOX Fuel versus Spent LEU Fuel

Using the SINRD ratios for measuring ^{239}Pu in BWR spent fuel, a 1-cycle spent MOX assembly can easily be distinguished from 3- and 4-cycles spent LEU fuel assemblies. This ability is based on the fact that SINRD uses detector ratios that are sensitive to the ^{239}Pu content in the spent fuel. Comparing a 1-cycle spent MOX to 3- and 4-cycles spent LEU fuel assemblies, the ^{239}Pu content is considerably different whereas the gross neutron emission rate is nearly equivalent. Fig. 9.22 shows the FFM / (Gd+Hf – Cd) ^{235}U FC ratio using 1-mm Hf versus burnup for BWR spent LEU and MOX fuel with (a) 0% and (b) 40% void fractions. Comparing the results shown in Fig. 9.22, the SINRD FC ratio is ~5x higher for 10-GWd spent MOX fuel than for 40-GWd spent LEU fuel with 0% void and ~4.4x higher with 40% void.

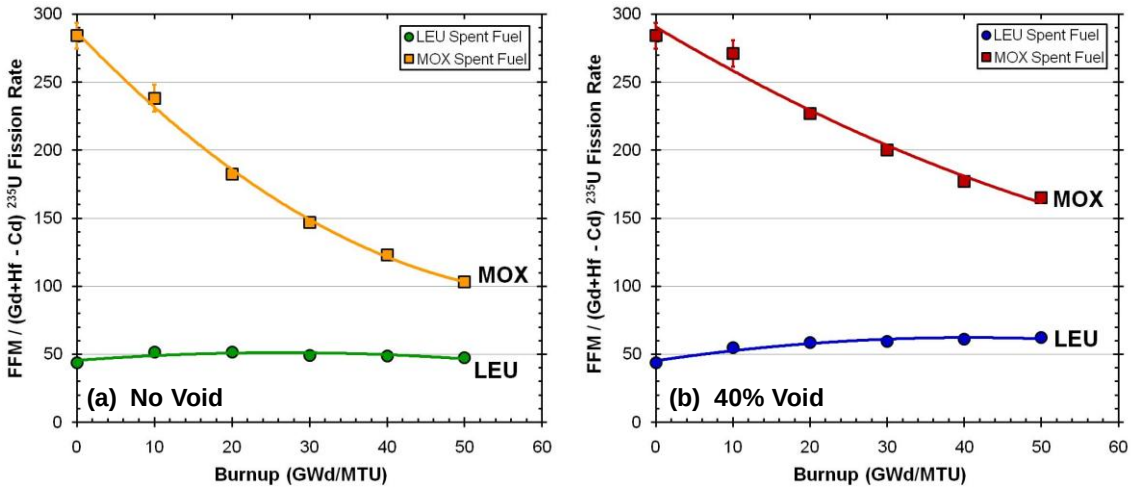

Fig. 9.22. Comparison of FFM / (Gd+Hf – Cd) ^{235}U FC ratio for BWR spent LEU and MOX fuel with (a) 0% and (b) 40% void fractions.

9.4.3. Sensitivity of SINRD to Pin Removal

The sensitivity and penetrability of SINRD was assessed by modeling partial defects in BWR 9x9 spent LEU (3% ^{235}U IE) and MOX (6% Pu IE) fuel assemblies. Partial defects were modeled for fuel burnups of 10-GWd and 40-GWd using the same pin removal locations that were used in the BWR fresh fuel simulations. The locations of partial defects are shown in Fig. 9.23 for convenience.

To assess the penetrability of SINRD to partial defects, the percent change in the SINRD ratios was calculated for each region to determine if the diverted pins can be detected within 3σ uncertainty. The count times used for the diversion cases are given in Table 9.3. These count times are somewhat conservative because the contribution to the total neutron emission rate from (α,n) neutrons was not accounted for.

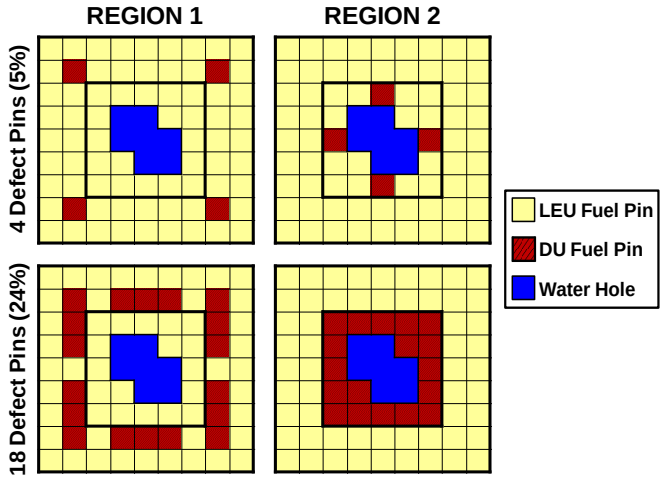

Fig. 9.23. Fuel pin removal locations of defects for Regions 1 and 2 in BWR 9x9 assembly where red pin locations are fuel pins that were removed and blue locations are water holes.

Table 9.3. Count times used to detect pin diversions within 3σ uncertainty for BWR spent fuel.

Fuel Type	Burnup [GWd/MTU]	Count Times for Diversion Cases		
		No Void	***40% Void***	***70% Void***
LEU Spent Fuel (3% ^{235}U)	10	5 hours	4.5 hours	4.5 hours
	40	20 minutes	10 minutes	10 minutes
MOX Spent Fuel (6% Pu)	10	30 minutes	30 minutes	30 minutes
	40	15 minutes	15 minutes	5 minutes

The sensitivity of different SINRD ratios with 5% and 24% of the total number of pins removed from Regions 1 – 2 are given in Table 9.4 and Table 9.5 for BWR spent LEU and MOX fuel, respectively. The values shown in bold correspond to the maximum positive and negative percent change in ratios that are within 3σ uncertainty for 5% and 24% pins removed from each region. The cells that are shaded gray correspond to the percent in change detector ratios that are not within 3σ uncertainty of a spent fuel assembly with no diverted pins. It should be emphasized that all ^{235}U FCs were used to obtain these results where no Hf was used for spent LEU fuel and 1-mm Hf was used for spent MOX fuel.

Table 9.4. Percent change in SINRD ratios with 5% and 24% fuel pins removed from Regions 1 and 2 for BWR spent LEU fuel (no Hf).

Region Defects	Burnup	SINRD Ratios *BWR Spent LEU*	REGION 1			REGION 2		
			0% Void	*40% Void*	*70% Void*	*0% Void*	*40% Void*	*70% Void*
5% Pin Defects (4 pins)	***10 GWd***	FFM / (Gd - Cd) ^{235}U	*2.13%*	*2.35%*	*3.21%*	*-0.59%*	*0.70%*	*-0.16%*
		FFM / Bare ^{235}U	**4.49%**	**4.85%**	**4.67%**	*1.07%*	1.53%	0.75%
		Bare ^{235}U / Gd ^{235}U	*-3.51%*	*-3.56%*	-3.21%	*-1.81%*	*-1.86%*	*-1.14%*
		Bare ^{235}U / Cd ^{235}U	*-4.32%*	*-4.25%*	**-4.38%**	*-1.91%*	*-2.62%*	*-1.30%*
	40 GWd	FFM / (Gd - Cd) ^{235}U	2.87%	**5.20%**	4.13%	*0.92%*	*1.71%*	*1.10%*
		FFM / Bare ^{235}U	**3.76%**	4.60%	**4.84%**	0.86%	1.24%	0.97%
		Bare ^{235}U / Gd ^{235}U	-2.38%	-2.50%	-3.01%	-1.13%	-1.35%	-1.35%
		Bare ^{235}U / Cd ^{235}U	**-3.54%**	**-4.73%**	**-4.29%**	**-2.07%**	**-2.62%**	**-2.17%**
24% Pin Defects (18 pins)	***10 GWd***	FFM / (Gd - Cd) ^{235}U	*9.03%*	*9.10%*	11.3%	*-1.60%*	*-1.28%*	*0.72%*
		FFM / Bare ^{235}U	**15.6%**	**14.3%**	**14.7%**	**4.58%**	**5.01%**	**5.33%**
		Bare ^{235}U / Gd ^{235}U	-13.8%	-11.8%	-11.5%	-8.84%	-9.09%	-8.77%
		Bare ^{235}U / Cd ^{235}U	**-18.8%**	**-16.4%**	**-17.1%**	**-10.7%**	**-11.0%**	**-11.6%**
	40 GWd	FFM / (Gd - Cd) ^{235}U	9.03%	11.5%	12.7%	*-0.30%*	*1.68%*	*0.83%*
		FFM / Bare ^{235}U	**12.9%**	**14.8%**	**16.3%**	**4.21%**	**5.67%**	**6.73%**
		Bare ^{235}U / Gd ^{235}U	-10.1%	-11.5%	-12.9%	-7.66%	-8.52%	-10.0%
		Bare ^{235}U / Cd ^{235}U	**-14.9%**	**-17.4%**	**-18.2%**	**-10.1%**	**-11.6%**	**-12.1%**

Table 9.5. Percent change in SINRD ratios with 5% and 24% fuel pins removed from Regions 1 and 2 for BWR spent MOX fuel (1-mm Hf).

Region Defects	Burnup	SINRD Ratios *BWR Spent MOX*	REGION 1			REGION 2		
			0% Void	*40% Void*	*70% Void*	*0% Void*	*40% Void*	*70% Void*
5% Pin Defects (4 pins)	***10 GWd***	FFM / (Gd+Hf - Cd) ^{235}U	*12.4%*	*11.7%*	*8.70%*	*11.5%*	*11.3%*	*6.86%*
		FFM / Bare ^{235}U	3.87%	4.55%	4.41%	1.00%	0.94%	0.56%
		Bare ^{235}U / Gd+Hf ^{235}U	-2.79%	-3.42%	-3.31%	-1.37%	-0.96%	-0.76%
		Bare ^{235}U / Cd ^{235}U	**-3.78%**	**-4.24%**	**-3.80%**	**-2.39%**	**-1.83%**	**-1.21%**
	40 GWd	FFM / (Gd+Hf - Cd) ^{235}U	**9.39%**	**12.7%**	**21.9%**	**3.90%**	**4.28%**	**16.3%**
		FFM / Bare ^{235}U	4.66%	4.80%	4.28%	0.82%	1.36%	0.50%
		Bare ^{235}U / Gd+Hf ^{235}U	-3.18%	-2.92%	-2.46%	-1.00%	-1.50%	*-0.27%*
		Bare ^{235}U / Cd ^{235}U	**-4.40%**	**-4.21%**	**-3.87%**	**-1.59%**	**-1.98%**	**-1.31%**
24% Pin Defects (18 pins)	***10 GWd***	FFM / (Gd+Hf - Cd) ^{235}U	**37.9%**	**40.8%**	**41.7%**	**24.1%**	**21.0%**	**24.8%**
		FFM / Bare ^{235}U	15.7%	16.1%	15.1%	5.00%	5.22%	4.55%
		Bare ^{235}U / Gd+Hf ^{235}U	-13.1%	-13.3%	-12.6%	-7.27%	-7.87%	-7.57%
		Bare ^{235}U / Cd ^{235}U	**-17.8%**	**-18.0%**	**-16.9%**	**-10.1%**	**-10.0%**	**-9.89%**
	40 GWd	FFM / (Gd+Hf - Cd) ^{235}U	**30.6%**	**31.0%**	**47.2%**	**16.1%**	**16.9%**	**30.6%**
		FFM / Bare ^{235}U	17.1%	16.9%	15.7%	7.08%	6.47%	5.10%
		Bare ^{235}U / Gd+Hf ^{235}U	-14.4%	-14.8%	-12.0%	-9.77%	-9.12%	-7.26%
		Bare ^{235}U / Cd ^{235}U	**-20.5%**	**-19.5%**	**-16.9%**	**-13.1%**	**-11.7%**	**-10.0%**

It is important to note that for a BWR spent LEU fuel assembly with burnup of 10-GWd none of the SINRD ratios can detect 5% pin diversions within *3σ* in Region 2. If the count time was increased to 40-hrs for 0% void, 12-hrs for 40% void, and 25-hrs for 70%, then only the FFM / Bare ^{235}U FC ratio could detect 5% pin diversions within *3σ* in Region 2. A summary of the results shown in Table 9.4 and Table 9.5 is given below:

- All SINRD ratios have the highest sensitivity to pin removal in Region 1.
- For BWR spent LEU fuel, the FFM / Bare ^{235}U FC ratio is the most sensitive SINRD ratio for detecting fuel pin diversions within *3σ* from Regions 1 and 2.
  - This ratio is sensitive to reactivity changes in the fuel assembly due to changes in the concentration of thermal absorbers.
  - The percent change in this ratio is positive for pin removal from Regions 1 – 2.
- For BWR spent MOX fuel, the Bare / Cd ^{235}U FC ratio is the most sensitive SINRD ratio for detecting fuel pin diversions within *3σ* from Regions 1 and 2.
  - This ratio is proportional to $p_{th} \cdot P_{TL}$ and inversely proportional to $p_{cut}^{Cd} \cdot P_{EL}^{Cd}$.
  - Thus, Bare / Cd ^{235}U FC ratio is sensitive to changes in the concentration of thermal absorbers relative to resonance absorbers in the fuel assembly.
  - The percent change in this ratio is negative for pin removal from Regions 1 – 2.

9.4.3.1. Graphical Analysis of Partial Defects Results

The fuel pin removal results for Bare / Cd ^{235}U FC ratio as a function diversion case are shown in Fig. 9.24 for BWR spent (a) LEU and (b) MOX fuel with burnup of 40-GWd and no void fraction. The solid line represents the signal from the case with no diversions; the dashed lines represent ±1% change in the SINRD ratio to account for systematic errors. We chose to use the Bare / Cd ^{235}U FC ratio in this analysis because for spent fuel with 40-GWd burnup it was the most sensitive ratio for detecting fuel pin diversions within *3σ* from Regions 1 and 2. These results show that the SINRD ratio has the highest sensitivity to fuel pin diversions from Region 1. The diversion of 4 pins (5% of total number of pins) from Region 2 for MOX spent fuel is the only case that is not clearly within ±1% of the no diversion signal.

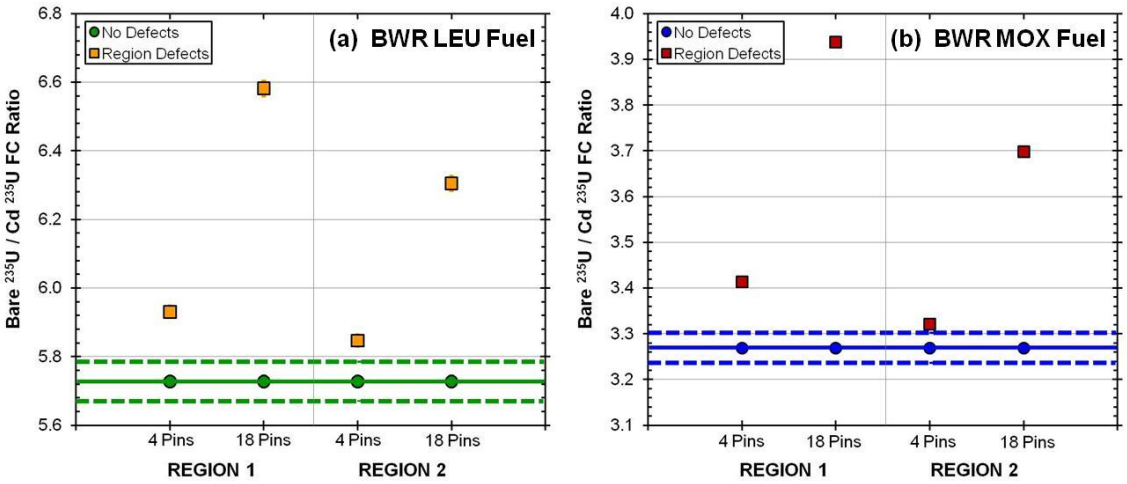

Fig. 9.24. Pin removal results for Bare / Cd ^{235}U FC ratio as a function diversion case for 40-GWd BWR spent (a) LEU and (b) MOX fuel with no void fraction.

9.4.3.2. Statistical Analysis of Partial Defects Results

The nondetection probability, β, was calculated for SINRD ratios with 4 fuel pins removed from Regions 1 and 2 where α = 5%. Fig. 9.25 shows the effect of 5% region defects on the Bare / Cd ^{235}U probability distribution for BWR spent (a) LEU and (b) MOX fuel. These results are shown for spent fuel with burnup of 40-GWd and no void fraction. In Table 9.6 and Table 9.7, the mean ± 1σ and β are given for SINRD ratios with no diversion and 5% fuel pins removed from Regions 1 – 2 for BWR spent LEU and MOX fuel, respectively. If β > 20%, the results were shaded gray for LEU and MOX fuel. The purpose for highlighting these results was to show the SINRD ratios that are not considered useful for detecting pin diversions because the β is too high. Based on the results for β, it is clear that the FFM / Bare ^{235}U FC ratio is the best ratio for detecting pin diversions from a 10-GWd/MTU BWR spent LEU fuel assembly. This is because the FFM / Bare ^{235}U FC ratio has the lowest uncertainty of all the SINRD ratios. Minimizing the uncertainty is especially important for spent LEU fuel at low burnups (<20-GWd) because neutron source term is very low. However, for a BWR spent MOX fuel assembly, the Bare / Cd ^{235}U FC ratio is the best ratio for detecting pin diversions.

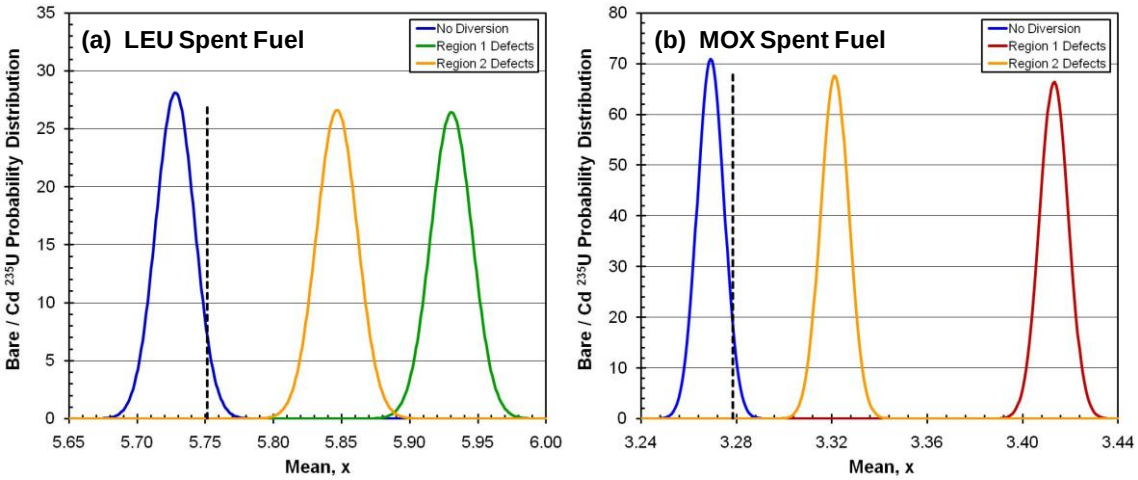

Fig. 9.25. Effect of 5% region defects on Bare / Cd ^{235}U probability distribution versus mean for BWR spent (a) LEU and (b) MOX fuel with 40-GWd and no void fraction.

Table 9.6. Mean ± 1σ and β for BWR spent LEU fuel with 5% of fuel pins removed from Regions 1 and 2.

Burnup	Void Fraction	SINRD Ratios	No Defects	REGION 1		REGION 2	
			Mean ± 1σ	*Mean ± 1σ*	*β*	*Mean ± 1σ*	*β*
10-GWd	*0% Void*	FFM / (Gd - Cd) ^{235}U	21.7 ± 0.651	21.2 ± 0.649	*83%*	21.8 ± 0.681	*92%*
		FFM / Bare ^{235}U	3.36 ± 0.024	3.21 ± 0.023	0%	3.32 ± 0.024	*55%*
		Bare ^{235}U / Cd ^{235}U	4.94 ± 0.074	5.16 ± 0.080	13%	5.04 ± 0.079	*64%*
	40% Void	FFM / (Gd - Cd) ^{235}U	22.7 ± 0.573	22.2 ± 0.569	*76%*	22.5 ± 0.585	*91%*
		FFM / Bare ^{235}U	3.54 ± 0.021	3.37 ± 0.020	0%	3.49 ± 0.021	17%
		Bare ^{235}U / Cd ^{235}U	4.70 ± 0.058	4.90 ± 0.062	4%	4.82 ± 0.062	*32%*
	70% Void	FFM / (Gd - Cd) ^{235}U	24.8 ± 0.462	24.0 ± 0.451	*47%*	24.9 ± 0.480	*93%*
		FFM / Bare ^{235}U	3.85 ± 0.016	3.67 ± 0.015	0%	3.82 ± 0.016	*43%*
		Bare ^{235}U / Cd ^{235}U	4.34 ± 0.037	4.53 ± 0.039	0%	4.40 ± 0.039	*54%*
40-GWd	*0% Void*	FFM / (Gd - Cd) ^{235}U	21.5 ± 0.127	20.9 ± 0.125	0%	21.3 ± 0.129	*53%*
		FFM / Bare ^{235}U	2.91 ± 0.004	2.80 ± 0.004	0%	2.89 ± 0.004	0%
		Bare ^{235}U / Cd ^{235}U	5.73 ± 0.017	5.93 ± 0.018	0%	5.85 ± 0.018	0%
	40% Void	FFM / (Gd - Cd) ^{235}U	24.9 ± 0.185	23.6 ± 0.173	0%	24.4 ± 0.184	*25%*
		FFM / Bare ^{235}U	3.50 ± 0.006	3.34 ± 0.005	0%	3.46 ± 0.006	0%
		Bare ^{235}U / Cd ^{235}U	4.80 ± 0.016	5.03 ± 0.017	0%	4.92 ± 0.017	0%
	70% Void	FFM / (Gd - Cd) ^{235}U	31.3 ± 0.226	30.0 ± 0.216	0%	30.9 ± 0.228	*55%*
		FFM / Bare ^{235}U	4.67 ± 0.007	4.45 ± 0.006	0%	4.63 ± 0.007	0%
		Bare ^{235}U / Cd ^{235}U	3.65 ± 0.010	3.81 ± 0.011	0%	3.73 ± 0.011	0%

Table 9.7. Mean ± 1σ and β for BWR spent MOX fuel with 5% of fuel pins removed from Regions 1 and 2.

Burnup	Void Fraction	SINRD Ratios	No Defects	REGION 1		REGION 2	
			Mean ± 1σ	*Mean ± 1σ*	*β*	*Mean ± 1σ*	*β*
10-GWd	*0% Void*	FFM / (Gd+Hf - Cd) ^{235}U	231 ± 8.949	202 ± 7.102	2.5%	204 ± 7.214	5.2%
		FFM / Bare ^{235}U	6.44 ± 0.009	6.19 ± 0.008	0%	6.37 ± 0.009	0%
		Bare ^{235}U / Cd ^{235}U	2.69 ± 0.006	2.79 ± 0.007	0%	2.75 ± 0.007	0%
	40% Void	FFM / (Gd+Hf - Cd) ^{235}U	259 ± 8.642	229 ± 6.991	1.1%	230 ± 7.017	1.6%
		FFM / Bare ^{235}U	6.66 ± 0.007	6.36 ± 0.007	0%	6.60 ± 0.007	0%
		Bare ^{235}U / Cd ^{235}U	2.61 ± 0.005	2.72 ± 0.005	0%	2.66 ± 0.005	0%
	70% Void	FFM / (Gd+Hf - Cd) ^{235}U	301 ± 9.300	275 ± 8.028	8.7%	280 ± 8.318	*26%*
		FFM / Bare ^{235}U	6.90 ± 0.006	6.60 ± 0.006	0%	6.86 ± 0.006	0%
		Bare ^{235}U / Cd ^{235}U	2.52 ± 0.004	2.62 ± 0.004	0%	2.55 ± 0.004	0%
40-GWd	*0% Void*	FFM / (Gd+Hf - Cd) ^{235}U	127 ± 1.176	115 ± 1.001	0%	122 ± 1.117	0.4%
		FFM / Bare ^{235}U	5.29 ± 0.003	5.05 ± 0.003	0%	5.25 ± 0.003	0%
		Bare ^{235}U / Cd ^{235}U	3.27 ± 0.003	3.41 ± 0.003	0%	3.32 ± 0.003	0%
	40% Void	FFM / (Gd+Hf - Cd) ^{235}U	173 ± 1.757	151 ± 1.390	0%	165 ± 1.656	0.3%
		FFM / Bare ^{235}U	6.10 ± 0.003	5.81 ± 0.003	0%	6.02 ± 0.003	0%
		Bare ^{235}U / Cd ^{235}U	2.86 ± 0.002	2.99 ± 0.003	0%	2.92 ± 0.002	0%
	70% Void	FFM / (Gd+Hf - Cd) ^{235}U	330 ± 9.426	258 ± 5.969	0%	276 ± 6.810	0%
		FFM / Bare ^{235}U	7.08 ± 0.005	6.77 ± 0.005	0%	7.04 ± 0.005	0%
		Bare ^{235}U / Cd ^{235}U	2.49 ± 0.003	2.59 ± 0.003	0%	2.52 ± 0.003	0%

Using the diversion results for 5% and 24% partial defects, the average percent change in the SINRD ratio per fuel pin removed was calculated for each region and then multiplied by an increasing number of fuel pins. The sensitivity of two different SINRD detector ratios to the removal of fuel pins is shown in Fig. 9.26 for burnups of 10-GWd and 40-GWd. Fig. 9.26(a) and (c) show the percent change in the FFM / Bare ^{235}U FC ratio versus the percentage of pins removed for BWR spent LEU and MOX fuel, respectively. In Fig. 9.26(b) and (d), the percent change in the Bare / Cd ^{235}U FC ratio versus the percentage of pins removed for BWR spent LEU and MOX fuel, respectively.

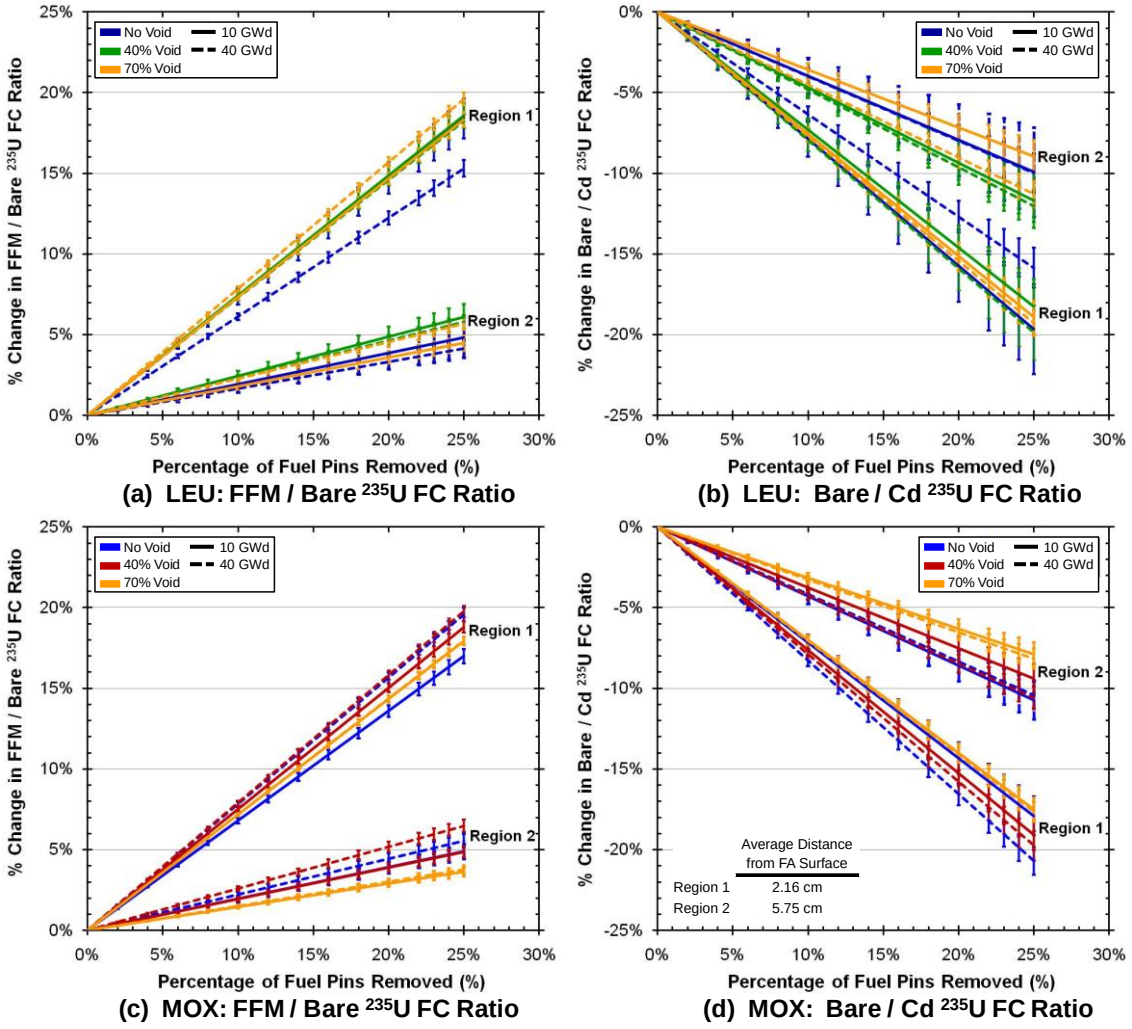

Fig. 9.26. Percent change in (a) and (c) FFM / Bare ^{235}U FC ratio to (b) and (d) Bare / Cd ^{235}U FC ratio versus % of pins removed for BWR spent LEU and MOX fuel with 0% VF, respectively.

For both SINRD ratios, the sensitivity to pin removal is highest in Region 1. In contrast to the results shown in Fig. 8.22 for PWR spent fuel, no combination of fuel pins from Regions 1 and 2 could result in 0% percent change in FFM / Bare ^{235}U FC ratio or Bare / Cd ^{235}U FC ratio for BWR spent fuel. Furthermore, it should be emphasized that based on the results shown in Fig. 9.26, we can conclude that the SINRD detector ratios are sensitive over the entire burnup range. The only dependence the SINRD ratios have on the source term is the count time required to achieve a percent

change in the ratio that is within than 3σ. This dependence is only significant for LEU spent fuel at a burnup of 10-GWd because the ^{244}Cm concentration is so low.

To obtain a better understanding of the sensitivity of the SINRD ratios to partial defects, the percent change in (a) Bare ^{235}U, (b) FFM ^{235}U, (c) Gd ^{235}U, and (d) Cd ^{235}U fission rates versus the percentage of pins removed is shown in Fig. 9.27 for BWR spent LEU and MOX fuel. These results are shown for BWR spent fuel with burnup of 40-GWd and no void fraction. In contrast to the results shown in Fig. 9.26, all of the SINRD FCs except the FFM have the highest sensitivity of to pin removal from Region 2 (center). This is attributed to the fact that the multiplication is highest in the center of the assembly. For both BWR spent LEU and MOX fuel assemblies, the sensitivity to pin removal from Regions 1 and 2 is approximately equal in the FFM ^{235}U FC.

Error propagations (Appendix B) were used to calculate the uncertainties in the percent change in the SINRD ratios for all diversion cases. These uncertainties were between 0.2% – 1% for the FFM / Bare ^{235}U FC ratio for spent LEU fuel and between 0.15% – 0.4% for the Bare / Cd ^{235}U FC ratio for spent MOX fuel using the count times given in Table 9.3. Thus, this type of measurement could show the departure from a reference fuel assembly with no defects.

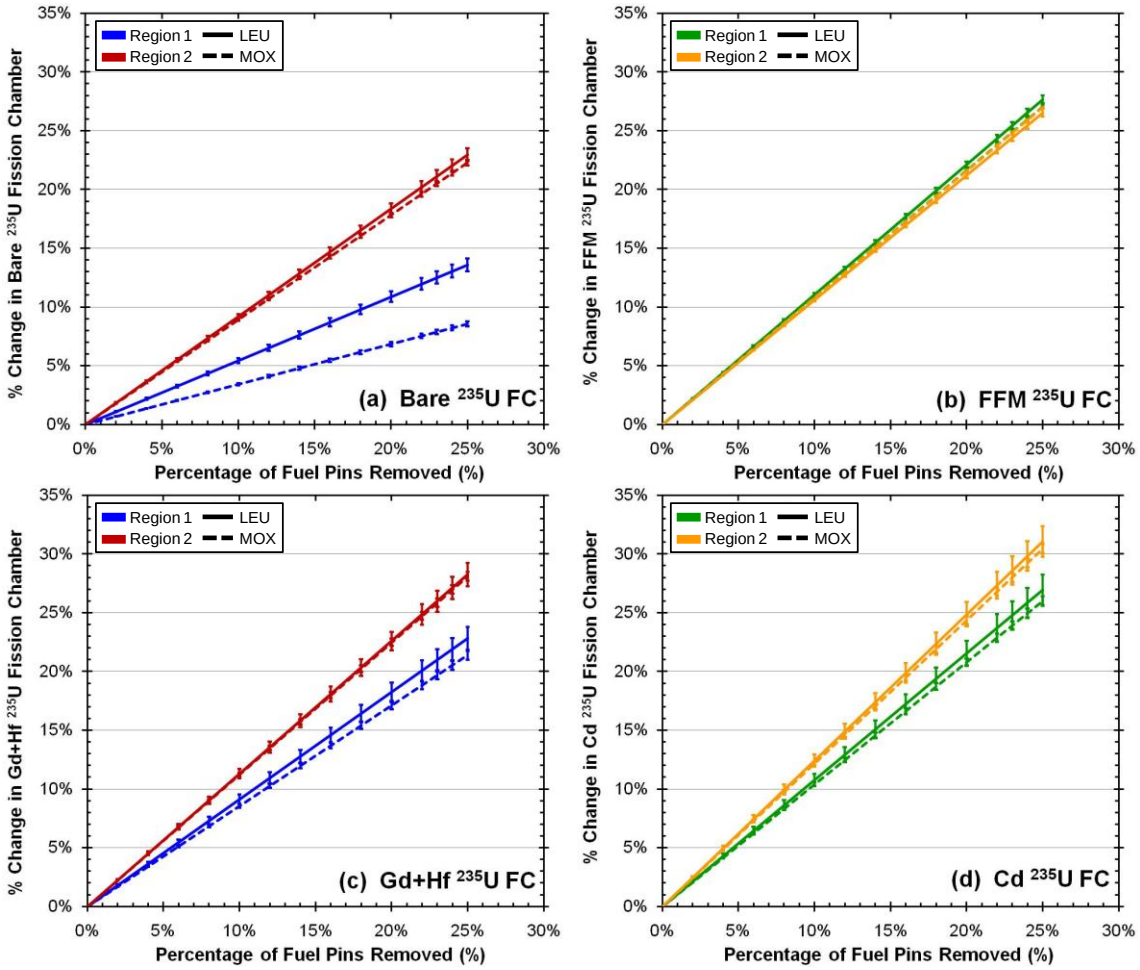

Fig. 9.27. Percent change in (a) Bare ^{235}U, (b) FFM ^{235}U, (c) Gd+Hf ^{235}U, and (d) Cd ^{235}U FCs versus % of fuel pins removed for 40-GWd BWR spent LEU and MOX fuel with 0% VF.

9.5. Summary of BWR Spent Fuel Results

We have simulated the change in different SINRD detector ratios over a burnup range of 0 – 50 GWd using MCNPX. For a BWR spent LEU fuel assembly with void fractions of 0%, 40%, and 70%, the FFM / (Gd+Hf – Cd) ^{239}Pu FC ratio was optimized for determining ^{239}Pu using 2-mm Hf. This SINRD ratio is proportional to the ^{239}Pu mass in the assembly over the burnup range of 0 to 50-GWd. Due to the fact that the IAEA will likely need all ^{235}U FCs, the use of the FFM / (Gd – Cd) ^{235}U FC ratio to determine ^{239}Pu was also investigated. All ^{235}U FCs cannot be used to quantify the ^{239}Pu content in BWR spent LEU fuel with 0% void fraction but can be used for 40% and 70% void

fractions. The ability to use all ^{235}U FCs to quantify ^{239}Pu in spent fuel with 40% and 70% void fractions may be attributed to the much larger amount of ^{239}Pu relative ^{235}U and that the ^{239}Pu content continues to increase over burnup range of 0 to 50-GWd. For a BWR spent MOX fuel assembly, the FFM / (Gd+Hf – Cd) ^{235}U FC ratio was optimized for determining ^{239}Pu using 1-mm Hf. This SINRD ratio is directly proportional to ^{239}Pu in spent MOX fuel with 0% and 40% void fractions; however, this ratio cannot be used to quantify ^{239}Pu in spent MOX fuel with 70% void fraction.

The sensitivity and penetrability of SINRD was assessed by modeling partial defects in BWR 9x9 spent LEU and MOX fuel assemblies. It is important to note that all ^{235}U FCs were used in this analysis. The percent change in the SINRD ratios was calculated for Regions 1 and 2 to determine if the diverted pins can be detected within 3σ. It should be noted that for a BWR spent LEU fuel assembly with burnup of 10-GWd none of the SINRD ratios can detect 5% pin diversions within 3σ in Region 2. The nondetection probability, β, was also calculated in order to better understand how the uncertainty in the SINRD ratios affects the ability to detect pin diversions. Based on the results from these calculations, the FFM / Bare ^{235}U FC ratio is the best ratio for detecting pin diversions from a BWR spent LEU fuel assembly. This is because the FFM / Bare ^{235}U FC ratio has the lowest uncertainty of all the SINRD ratios which is important for spent LEU fuel because neutron source term is very low at low burnups (<20-GWd). For a BWR spent MOX fuel assembly, the Bare / Cd ^{235}U FC ratio is the best ratio for detecting pin diversions. These uncertainties were between 0.2% – 1% for the FFM / Bare ^{235}U FC ratio for spent LEU fuel and between 0.15% – 0.4% for the Bare / Cd ^{235}U FC ratio for spent MOX fuel. Thus, this type of measurement could show the departure from a reference fuel assembly with no defects.

The purpose of the BWR spent fuel simulations was to assess the ability of SINRD to measure the fissile content in spent fuel and the sensitivity and penetrability of SINRD to partial defects in an assembly. Based on the results from these simulations, we have concluded that SINRD provides a number of improvements over current IAEA verification methods. These improvements include:

1) SINRD provides absolute measurements of burnup independent of the operator's declaration.
2) SINRD is sensitive to pin removal over the entire burnup range and can verify the diversion of 5% of fuel pins within 3σ from BWR spent LEU and MOX fuel.
3) SINRD is slightly sensitive (<5%) to the initial enrichment and type of FA and can therefore be used at multiple spent fuel storage facilities.
4) The calibration of SINRD at one reactor facility carries over to reactor sites in different countries because it uses the ratio of FCs that are not facility dependent.
5) SINRD can distinguish fresh and 1-cycle spent MOX fuel from 3- and 4-cycles spent LEU fuel without using reactor burnup codes.

10. CONCLUSIONS

The results from MCNPX simulations and experimental measurements were used to develop SINRD to improve existing nuclear safeguards and material accountability measurements for LWR fuel assemblies. The purpose of these simulations and measurements were to assess the following characteristics of SINRD: (1) ability to measure the fissile content in fresh and spent fuel and (2) sensitivity and penetrability of SINRD to the removal of fuel pins from an assembly. It is important to note that SINRD requires a calibration with a reference assembly of similar geometry. However, since this densitometry method uses ratios of different detectors, most of the systematic errors related to calibration and positioning cancel in the ratios. In addition, SINRD can be calibrated with a fresh fuel assembly because it is not sensitive to neutron absorbing fission products in spent fuel.

From the MCNPX simulations of LWR fresh LEU and MOX fuel assemblies, we have gained a better understanding of the physics of SINRD when only the ^{235}U (LEU fuel) or ^{239}Pu (MOX fuel) content is changing. In addition, experimental measurements were compared to the results from MCNPX simulations to obtain a better understanding of the sources of bias error in the MCNPX results. For all SINRD FCs and ratios, the C/E ratio was constant confirming that the MCNPX model of SINRD is accurately simulating the physics of the experiment. However, the bias error was as large as ±15 – 20% with no normalization. This was reduced to ±5% by normalizing the results to the case with all DU pins. Thus, in order to ensure that our SINRD ratios are insensitive to any potential sources of bias error, SINRD requires calibration with a reference assembly. From the fresh fuel simulations and measurements, we have established a valid computational model of SINRD for a fresh fuel assembly. This model was used as a basis for comparison to simulations of SINRD for LWR spent fuel assemblies.

The SINRD measurement technique was simulated for LWR spent LEU and spent MOX fuel assemblies in water over the burnup range of 0 – 50 GWd/MTU. PWR 17x17 spent fuel assemblies were simulated with and without 2200-ppm boron in water. BWR

9x9 spent fuel assemblies were simulated with 0%, 40% and 70% void fractions. The ability of SINRD to measure the fissile content in LWR spent fuel was assessed using Gd and Cd ^{239}Pu FCs, as well as, all ^{235}U FCs. In order to quantify the fissile content in LWR spent fuel, it is first necessary to verify the burnup and initial enrichment of the assembly using a known reference assembly for calibration. Then, the optimized SINRD ratios for ^{239}Pu and ^{235}U can be used in conjunction with burnup codes and MCNPX simulations to estimate the fissile content. Key conclusions regarding the use of SINRD to quantify the fissile content in LWR spent LEU and MOX fuel assemblies are summarized below:

- For spent LEU fuel, ^{239}Pu FCs are required to accurately quantify ^{239}Pu content.
  - Optimized SINRD ratio: FFM / (Gd+Hf – Cd) ^{239}Pu FC ratio using 2-mm Hf.
  - Exceptions: all ^{235}U FCs can be used to quantify ^{239}Pu in BWR spent LEU fuel with 40% and 70% VF.
- For spent MOX fuel, all ^{235}U FCs can be used to accurately quantify ^{239}Pu content.
  - Optimized SINRD ratio: FFM / (Gd+Hf – Cd) ^{235}U FC ratio using 1-mm Hf.
  - Exceptions: this ratio cannot be used to quantify ^{239}Pu in BWR spent MOX fuel with 70% void fraction.

The sensitivity of SINRD to possible diversion scenarios was also analyzed within the context of desired safeguards detection requirements. Only ^{235}U FCs were used in SINRD for this analysis. In Table 10.1, the performance of SINRD is compared to current IAEA verification methods for possible diversion scenarios. Based on the results from this analysis, we have concluded that SINRD provides a number of improvements over current IAEA verification methods. These improvements include:

1) SINRD provides absolute measurements of burnup independent of the operator's declaration.
2) SINRD is sensitive to pin removal over the entire burnup range and can verify the diversion of 6% of fuel pins within 3σ from LWR spent LEU and MOX fuel.
3) SINRD is slightly sensitive (<5%) to the boron concentration, initial enrichment, and type of FA and can therefore be used at multiple spent fuel storage facilities.

4) The calibration of SINRD at one reactor facility carries over to reactor sites in different countries because it uses the ratio of FCs that are not facility dependent.
5) SINRD can distinguish fresh and 1-cycle spent MOX fuel from 3- and 4-cycles spent LEU fuel without using reactor burnup codes.

Table 10.1. Comparison of SINRD to current IAEA spent fuel verification methods for possible diversion scenarios [3].

Possible Diversion Scenarios	IAEA Verification Methods			SINRD
	DCVD	***FDET***	***SMOPY***	
Replace entire LEU Fuel Assembly with Irradiated Dummy	NO	YES	YES	YES
Replace entire LEU Fuel Assembly with Unirradiated Dummy	YES	YES	YES	YES
50% Pin Removal from Spent Fuel Assembly with Pin Substitutions	NO	YES[(1)]	YES[(1)]	YES[(2)]
50% Pin Removal from Spent Fuel Assembly with NO Pin Substitutions	YES	YES[(1)]	YES[(1)]	YES[(2)]
3σ Detection Limit [% Pins Removed]	N/A	40%[(3)]	25%[(4)]	6%[(5)]
Diversion of Fresh MOX Assembly with Irradiated Spent LEU Assembly	NO	NO	YES[(6)]	YES[(7)]

(1) *Cannot detect long cooled assemblies with certain configurations of substituted pins. Verification measurement of cooling time is needed.*
(2) *Detection of fuel pin removal is **not** dependent on cooling time.*
(3) *Depends on IAEA records and operator's declaration of discharge date and initial enrichment and on the existence of calibration curve for different fuel assembly types* [36].
(4) *Based on numerical simulations for cases studied in IAEA report IAEA-SM-367/14/03* [37].
(5) *Based on MCNPX simulations for cases described in sections 8.4.3 and 9.4.3 of this dissertation*.
(6) *Requires the use of online burnup codes.*
(7) *Does **not** require the use of online burnup codes.*

In the LWR spent fuel simulations, we assumed that the spent fuel was homogeneously distributed throughout the assembly. In reality, the spent fuel isotopics will vary across the assembly due to variations in the neutron flux. It should be noted, however, that additional research on SINRD (not discussed in this dissertation) has been performed to support the NGSI spent fuel effort. In this research, SINRD was simulated

for a PWR 17x17 spent LEU fuel assembly with no boron and 2200-ppm boron in the water. MCNPX CINDER [45] was used calculate the spent fuel isotopics in every pin which accounted for variations in the isotopic concentrations across the assembly [46]. Comparing the SINRD results for PWR spent LEU fuel with burnup of 45-GWd/MTU, 5-yrs cooled, the FFM / (Gd+Hf – Cd) ^{239}Pu FC ratio changed by less than 3% with and without boron in the water and for both 4% and 5% ^{235}U IE. This is attributed to the fact that there is not a large variation in the ^{239}Pu content across the assembly. As a result, the spent fuel pins present an approximate uniform sample to the transmitted neutrons entering SINRD because the self-shielding effects are small for individual pins. Thus, we conclude that SINRD is insensitive to the distribution of spent fuel isotopics across the assembly.

A practical application of SINRD is to combine this technique with existing IAEA verification methods, such as the FDET or SMOPY. The similar design characteristics of SINRD and FDET are complementary to one another, which enables these detector systems to be easily combined and practically implemented. A schematic of the combined SINRD and FDET detector system is shown in Fig. 10.1. We have modified the shape of the FDET to make it symmetrical to SINRD and replaced the outer polyethylene shell with aluminum casing. In practice, both detector systems would be enclosed in 1/8” metal casing to make them water proof. Similarly, the same electronics package currently used for the fission chambers in the FDET would also be used for the SINRD detectors.

A disadvantage of using just the FDET to verify spent fuel is that it requires the use the operator’s declaration and the existence of calibration curves for different fuel assembly types. On the other hand, the FDET provides gross gamma measurements that can be used to verify cooling time. SINRD is advantageous because it uses ratios of FCs that are not facility dependent and provides absolute measurements of burnup independent of the operator’s declaration. Thus, the combined SINRD and FDET detector system provides a more robust verification method for spent fuel assemblies by increasing the overall sensitivity to possible diversion scenarios.

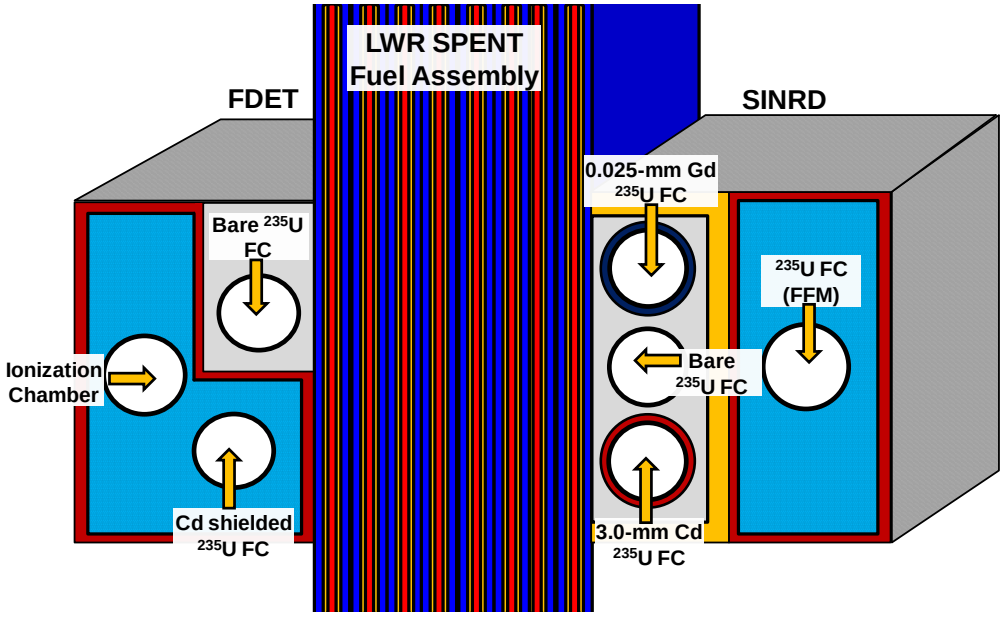

Fig. 10.1. Schematic of combined SINRD and FDET detector system.

Another possible design for spent fuel verification would be to use SINRD on both arms of the Fork and add an ionization chamber under the FFM for gross gamma measurements. Using a SINRD Fork with added ionization chambers would enhance the overall capabilities of SINRD by: improving counting statistics in the FCs, reducing the count time required to detect pin diversions within 3σ, and minimizing systematic errors from positioning. In addition, the added ionization chambers enable the cooling time of the assembly to be verified. The primary disadvantage of a SINRD Fork is the increase in the total cost of the instrument. This increase would be substantial if Gd and Cd covered ^{239}Pu FCs were used. Thus, in order to be economically viable, a SINRD Fork might need to use all ^{235}U FCs.

Future work includes performing additional verification measurements with SINRD in water using the reference PWR 15x15 fresh LEU fuel assembly available at LANL, measuring LWR spent fuel assemblies in water with international collaboration, and building a prototype combined SINRD + FDET for spent fuel measurements.

REFERENCES

[1] R. Hooper, The Changing Nature of Safeguards, International Atomic Energy Agency Bulletin Vol. 45, Issue 1, Vienna, Austria, June 2003.

[2] E.R. Edwards, A Review of Recent Studies of Nondestructive Assay Methods for Irradiated Nuclear Fuels, Nucl. Appl., 4 (1968) 245 – 259.

[3] Coordinated Technical Meeting on Spent Fuel Verification Methods, International Atomic Energy Agency Conference, Vienna, Austria, March 3 – 6, 2003.

[4] United States Department of Energy, Next Generation Safeguards Initiative, Annual Report FY2009, National Nuclear Security Administration, Office of Nonprolifeation and International Security (NA-24), Washington, DC (2009).

[5] S.J. Tobin, H.O. Menlove, M.T. Swinhoe, M.A. Schear, Next Generation Safeguards Initiative Research to Determine the Pu Mass in Spent Fuel Assemblies: Purpose, Approach, Constraints, Implementation, and Calibration, Nucl. Instr. and Meth. A (2010), doi:10.1016/j.nima.2010.09.064, in Press.

[6] M.L. Fensin, S.J. Tobin, N.P. Sandoval, M.T. Swinhoe, H.O. Menlove, A Monte Carlo Based Spent Fuel Analysis Safeguards Strategy Assessment, Proceedings of the Global 2009 Conference, Paris, France, September 6–11, 2009.

[7] S.J. Tobin, S.F. Demuth, M.L. Fensin, J.S. Hendricks, et al., Determination of Plutonium Content in Spent Fuel with NDA – Why an Integrated Approach? Proceedings of 49th Annual INMM Meeting, Nashville, TN, July 13 – 17, 2008.

[8] S.J. Tobin, W.S. Charlton, M.H. Ehinger, et al., Determining Plutonium in Spent Fuel with Nondestructive Assay Techniques, Proceedings of 31st Annual ESARDA Meeting, Vilnius, Lithuania, May 26 – 28, 2009.

[9] D.B. Pelowitz (Ed.), MCNPX User's Manual, Version 2.6.0, Los Alamos National Laboratory Report, LA-CP-07-1473, April 2008.

[10] H.O. Menlove, C.D. Tesche, M.M. Thorpe, R.B. Walton, A Resonance Self-Indication Technique for Isotopic Assay of Fissile Materials, Nucl. Appl., 6 (1969) 401 – 408.

[11] Nondestructive Assay of SEFOR Fuel Rods, Los Alamos National Laboratory Program Status Report April-June 1969, LA-4227-MS (1969).

[12] Neutron Self-Indication Assay of SEFOR Fuel Rods, Los Alamos National Laboratory Program Status Report July-September1969, LA-4315-MS (1969).

[13] A.M. LaFleur, W.S. Charlton, H.O. Menlove, M.T. Swinhoe, Nondestructive Measurements of Fissile Material Using Self-Indication Neutron Resonance Absorption Densitometry (SINRAD), Proceedings of 8th International Conference on Facility Operations – Safeguards Interface, Portland, OR, March 30 – April 4, 2008.

[14] A.M. LaFleur, W.S. Charlton, H.O. Menlove, M.T. Swinhoe, Development of Self-Interrogation Neutron Resonance Densitometry to Measure the Fissile Content in Nuclear Fuels, Los Alamos National Laboratory Report, LA-UR-09-08178, (ISPO-538) January 2010.

[15] A.M. LaFleur, W.S. Charlton, H.O. Menlove, M.T. Swinhoe, Development of Self-Interrogation Neutron Resonance Densitometry (SINRD) to Measure the ^{235}U and ^{239}Pu Content in a PWR 17x17 Spent Fuel Assembly, Proceedings of 31st Annual ESARDA Meeting, Vilnius, Lithuania, May 26 – 28, 2009.

[16] H.O. Menlove, J.E. Pieper, Neutron Collar Calibration for Assay of LWR Fuel Assemblies, Los Alamos National Laboratory Report, LA-10827-MS, March 1987.

[17] A.M. LaFleur, H.O. Menlove, S.Y. Lee, S.K. Ahn, Summary of Results from SINRD Fresh Fuel Measurements in Air, Los Alamos National Laboratory Report, LA-UR 10-06673, July 2010.

[18] M. Tarvainen, F. Lévai, T. Valentine, et al., NDA Techniques for Spent Fuel Verification and Radiation Monitoring, STUK-YTO-TR 133 (1997).

[19] D. Reily, N. Ensslin, H. Smith, S. Kreiner, Passive Nondestructive Assay of Nuclear Materials, United States Nuclear Regulatory Commission: NUREG/CR-5550, U.S. Government Printing Office, Washington, DC (1991). p. 530 – 549.

[20] H.R. Trellue, Neutronic and Logistic Proposal for Transmutation of Plutonium from Spent Nuclear Fuel as Mixed-Oxide Fuel in Light Water Reactors, Nucl. Tech. 147 (2004) 171 – 180.

[21] OECD Nuclear Energy Agency, The Economics of the Nuclear Fuel Cycle, Organization for Economic Co-operation and Development, Paris, France (1994).

[22] M.T. Swinhoe, H.O. Menlove, D.H. Beddingfield, A Survey of LWR Spent Fuel and Measurement Methods, Los Alamos National Laboratory Report, LA-UR-02-6996, August 2002.

[23] M. Tarvainen, F. Lévai, T. Valentine, M. Abhold, B. Moran, NDA Techniques for Spent Fuel Verification and Radiation Monitoring, STUK-YTO-TR 133, Finnish Support Programme to IAEA Safeguards, Helsinki, Finland, August 1997.

[24] OrigenARP. SCALE: A Modular Code System for Performing Standardized Computer Analyses for Licensing Evaluations, ORNL/TM-2005/39, Version 5.1, Vols. I-III, November 2006. Available from Radiation Safety Information Computational Center at Oak Ridge National Laboratory as CCC-732.

[25] D.D. Cobb, H.A. Dayem, R.J. Dietz, Preliminary Concepts: Safeguards for Spent Light-Water Reactor Fuels, Los Alamos National Laboratory Report, LA-7730-MS, June 1979.

[26] International Atomic Energy Agency, The Structure and Content of Agreements Between the Agency and States Required in Connection with the Treaty on the Non-Proliferation of Nuclear Weapons, INFCIRC/153 (Corrected), IAEA, Vienna, Austria (1972).

[27] International Atomic Energy Agency, IAEA Safeguards Glossary, IAEA/NVS/3, IAEA, Vienna, Austria (2002).

[28] International Atomic Energy Agency, Design Measures to Facilitate Implementation of Safeguards at Future Water Cooled Nuclear Power Plants, Safeguards Technical Reports Series No. 392, IAEA, Vienna, Austria (1998).

[29] TransFX Computer Software Manuals: Advanced Particle Transport Software Using Three-Dimensional Deterministic Methods in Arbitrary Geometry, Transware Enterprises, San Jose, CA (2001).

[30] OECD Nuclear Energy Agency, JANIS 3.0 User's Guide, Organization for Economic Co-operation and Development, Paris, France (2007).

[31] J.E. Doyle (Ed.), Nuclear Safeguards, Security and Nonproliferation, Elsevier Inc., Burlington, MA (2008) 102 – 104.

[32] J.D. Chen, A.F. Gerwing, R. Maxwell, et al, Field Test of a DCVD Using an Ixon Camera with a Lumogen-Coated EMCCD Detector, Canadian and Swedish Safeguards Support Programs Report, Task JNT A 704, CSSP Report 2004-01-03, SKI Report SKI-R-03/47, December 2003.

[33] J.D. Chen, A.F. Gerwing, R. Keeffe, M. Larsson, et al, Long-Cooled Spent Fuel Verification Using a Digital Cerenkov Viewing Device, International Atomic Energy Agency Report, IAEA-SM-367/14/07, Vienna, Austria (2007).

[34] J.D. Chen, D.A. Parcey, and R. Kosierv, Detection of Partial Defects using a Digital Cerenkov Viewing Device, International Atomic Energy Agency Report, IAEA-CN-184/338, Vienna, Austria (2009).

[35] H.O. Menlove, J. Phillips, et al. Apparatus for in situ Determination of Burnup, Cooling Time and Fissile Content of an Irradiated Nuclear Fuel Assembly in a Fuel Storage Pond, US Patent 4,510,117, Washington DC, April 9, 1985.

[36] A. Tiitta, J. Saarinen, M. Tarvainen, et al, Investigation on the Possibility to Use Fork Detector for Partial Defect Verification of Spent LWR Fuel Assemblies, Finnish Support Programme to IAEA Safeguards Report, Task JNT A 1071, STUK-YTO-TR 191, Helsinki, Finland, September 2002.

[37] A. Lebrun, M. Merelli, J-L. Szabo, et al, SMOPY a New NDA Tool for Safeguards of LEU and MOX Spent Fuel, International Atomic Energy Agency Report, IAEA-SM-367/14/03, Vienna, Austria, October 2003.

[38] J.R. Lamarsh, Introduction to Nuclear Engineering, Prentice-Hall, Inc., Upper Saddle River, NJ (2001). p.117

[39] MCNP – A General Monte Carlo N-Particle Transport Code, Version 5, Volume I: Overview and Theory, Los Alamos National Laboratory Report, LA-UR-03-1987, February 2008.

[40] H.O. Menlove, M.A. Marzo, S.G. de Almeida, M. Candida de Almeida, et al., In-Plant Test and Evaluation of the Neutron Collar for Verification of PWR Fuel Assemblies at Resende, Brazil, Los Alamos National Laboratory Report, LA-10562-MS, November 1985.

[41] G.E. Bosler, H.O. Menlove, J.K. Halbig, N. Nicholson, et al., Physical Inventory Verification Exercise at a Light-Water Reactor Facility, Los Alamos National Laboratory Report, LA-10695-MS (ISPO-248), April 1986.

[42] OECD Nuclear Energy Agency, Burnup Credit Benchmark Phase IV-B: Results and Analysis of MOX Fuel Depletion Calculations, Organization for Economic Co-operation and Development, NEA/NSC/DOC(2003)4, ISBN 92-64-02124-8, Paris, France (2003).

[43] M.M. El-Wakil, Nuclear Power Engineering, McGraw-Hill Book Company, Inc., New York (1962). p.276

[44] OECD Nuclear Energy Agency, Burnup Credit Benchmark Phase III-B: Burnup Calculations of BWR Fuel Assemblies for Storage and Transport, Organization for Economic Co-operation and Development, NEA/NSC/DOC(2002)2, JAERI-Research 2002-001, Paris, France (2002).

[45] D.B. Pelowitz, J.S. Hendricks, J.W. Durkee, et al., MCNPX 2.6 Extensions, Los Alamos National Laboratory Report, LA-UR-08-2216, April 2008.

[46] A.M. LaFleur, H.O. Menlove, S.J. Tobin, M.T. Swinhoe, Development of Self-Interrogation Neutron Resonance Densitometry to Measure the Fissile Content in PWR 17x17 Spent LEU Fuel, Los Alamos National Laboratory Report, LA-UR-09-08178, December 2010.

APPENDIX A

MCNPX INPUT DECKS FOR LWR FUEL ASSEMBLIES

A.1. PWR 17x17 Spent LEU Fuel Assembly

```
PWR 17x17 SPENT Fuel Assembly in Water (FFM-Bare)
c
c ****************************************
c  SINRD CELL CARDS
c ****************************************
c
c ALL U235 FC - 0.025mm NATURAL Gd & NO NATURAL Hf
c
c ** Bare U235 Fission Chamber **
100   0        -100                  imp:n=1
101  12 -19.1  -101 100              imp:n=1 $U235
102   2 -2.70  -102 101 +103 -104    imp:n=1
c
c ** B4C outer U235 Fission Chamber **
110   0        -110                  imp:n=1
111  12 -19.1  -111 110              imp:n=1 $U235
112   2 -2.70  -112 111 +103 -104    imp:n=1
c
c ** 0.025mm Gd covered U235 Fission Chamber **
200   0        -200                  imp:n=1
201  12 -19.1  -201 200              imp:n=1 $U235
202   2 -2.70  -202 201              imp:n=1
204  16 -7.90  -204 202 +205 -206    imp:n=1 $0.025mm Gd
c
c ** 3.00 mm Cd covered U235 Fission Chamber **
300   0        -300                  imp:n=1
301  12 -19.1  -301 300              imp:n=1 $U235
302   2 -2.70  -302 301              imp:n=1
303   3 -8.65  -303 302 +305 -306    imp:n=1 $3.00mm Cd
c
c ** Detector Pod **
400   2 -2.70  -400 #100 #101 #102 #200 #201 #202 #204
                #300 #301 #302 #303  imp:n=1  $Al BOX
401  14 -2.52  -401 400              imp:n=1  $1.0cm B4C Liner
402   4 -0.96  -403 #110 #111 #112   imp:n=1  $Poly BOX
403   3 -8.65  -402 403              imp:n=1  $Cd Liner
c
c ******************************************
c  PWR 17x17 SPENT LEU Fuel Assembly CELL CARDS
c ******************************************
c
c NO BORON - NO DEFECTS
c
c Initial enrichment = 4.0 wt% U235
c DENSITY of Spent Fuel = 10.4-g/cc (95%TD)
c
c
c ** SPENT LEU FUEL RODS **
500 40 -10.40   -501       u=1   imp:n=1 $SPENT Fuel, 40GWd
501  9  -6.55   -502  501  u=1   imp:n=1 $CLADDING
502 15  -1.00    502       u=1   imp:n=1 $WATER
c
c ** DU REGION DEFECTS **
600 20 -10.4538 -600       u=7   imp:n=1
601  0          -601  600  u=7   imp:n=1 $AIR GAP
602  9  -6.55   -602  601  u=7   imp:n=1 $CLADDING
603 15  -1.00    602       u=7   imp:n=1 $WATER
c
c ** GUIDE TUBES **
```

```
505 15  -1.00   -502       u=9   imp:n=1
506 15  -1.00    502       u=9   imp:n=1
c
510 0   -506  imp:n=1    lat=1 u=2 fill=-8:8 -8:8 0:0
                    1 1 1 1 1 1 1 1 1 1 1 1 1 1 1 1 1
                    1 1 1 1 1 1 1 1 1 1 1 1 1 1 1 1 1
                    1 1 1 1 1 9 1 1 9 1 1 9 1 1 1 1 1
                    1 1 1 9 1 1 1 1 1 1 1 1 1 9 1 1 1
                    1 1 1 1 1 1 1 1 1 1 1 1 1 1 1 1 1
                    1 1 9 1 1 9 1 1 9 1 1 9 1 1 9 1 1
                    1 1 1 1 1 1 1 1 1 1 1 1 1 1 1 1 1
                    1 1 1 1 1 1 1 1 1 1 1 1 1 1 1 1 1
                    1 1 9 1 1 9 1 1 9 1 1 9 1 1 9 1 1
                    1 1 1 1 1 1 1 1 1 1 1 1 1 1 1 1 1
                    1 1 1 1 1 1 1 1 1 1 1 1 1 1 1 1 1
                    1 1 9 1 1 9 1 1 9 1 1 9 1 1 9 1 1
                    1 1 1 1 1 1 1 1 1 1 1 1 1 1 1 1 1
                    1 1 1 9 1 1 1 1 1 1 1 1 1 9 1 1 1
                    1 1 1 1 1 9 1 1 9 1 1 9 1 1 1 1 1
                    1 1 1 1 1 1 1 1 1 1 1 1 1 1 1 1 1
                    1 1 1 1 1 1 1 1 1 1 1 1 1 1 1 1 1
511   0        -508 509      fill=2  imp:n=1
512   0        -509                  imp:n=1  $AIR GAP
c
998 15 -1.0    -999 508 509 401 402  imp:n=1  $Water
999 0  999  imp:n=0

c ******************************************
c SURFACE CARDS -- PWR 17x17 Fuel Assembly
c ******************************************
c
c ** SPENT FUEL PINS **
500 rcc 0  0 -200  0 0 400  0.4095
501 rcc 0  0 -200  0 0 400  0.4100 $SPENT FUEL
502 rcc 0  0 -200  0 0 400  0.4750 $CLADDING
c
c ** DU DEFECT FUEL PINS **
600 rcc 0  0 -200  0 0 400  0.4095 $DU
601 rcc 0  0 -200  0 0 400  0.4100 $AIR GAP
602 rcc 0  0 -200  0 0 400  0.4750 $CLADDING
c
c ** PWR 17x17 ASSEMBLY LATTICE **
506 rpp  -0.625  0.625  -0.625  0.625  -200 200
508 rpp -10.625 10.625 -10.625 10.625  -180 180
c
c *** AIR GAP b/n Assembly & Fission Chambers ***
509 rpp -10.625 10.625  10.626 10.725  -5.625 5.30
c
c ******************
c Fission chambers
c ******************
c
c ** Bare U235 Fission Chamber **
100 rcc  -9.325  12.395   0   18.650  0  0  1.169838
101 rcc  -9.325  12.395   0   18.650  0  0  1.170000
102 c/x  12.395  0  1.27
103 px   -9.425
104 px    9.425
c
c ** FFM U235 Fission Chamber **
110 rcc  -9.325  17.515   0   18.650  0  0  1.169838
111 rcc  -9.325  17.515   0   18.650  0  0  1.170000
112 c/x  17.515  0  1.27
```

```
c
c ** 0.025 mm Gd covered Fission Chamber **
200 rcc  -9.325  12.395   2.78   18.650  0  0  1.169838
201 rcc  -9.325  12.395   2.78   18.650  0  0  1.170000
202 rcc  -9.425  12.395   2.78   18.850  0  0  1.270000
204 c/x   12.395  2.78  1.27
205 px   -9.4275
206 px    9.4275
c
c ** 3.00 mm Cd covered Fission Chamber **
300 rcc  -9.325  12.395   -2.94   18.650  0  0  1.169838
301 rcc  -9.325  12.395   -2.94   18.650  0  0  1.170000
302 rcc  -9.425  12.395   -2.94   18.850  0  0  1.270000
303 c/x   12.395 -2.94 1.57
305 px   -9.620
306 px    9.620
c
c ** Aluminum box lined with 1.0-cm B4C **
400 rpp   -9.625   9.625  10.725  14.065  -4.625 4.30   $ Aluminum Box
401 rpp  -10.625  10.625  10.725  15.065  -5.625 5.30   $ 1.0 cm B4C
402 rpp  -10.625  10.625  15.065  19.965  -5.625 5.30   $ 1.0 mm Cd
403 rpp  -10.525  10.525  15.165  19.865  -5.525 5.20   $ Poly
c
999 rpp -25 25 -25 25 -201 201
c

c ***********************************************************
c  SOURCE DEFINITION
c ***********************************************************
MODE N
SDEF CEL=d1 EXT=d2 RAD=d3 AXS 0 0 1 ERG=d4
c
si1  l (500<510[-8 -8 0]<511) (500<510[-7 -8 0]<511) (500<510[-6 -8 0]<511)
       (500<510[-5 -8 0]<511) (500<510[-4 -8 0]<511) (500<510[-3 -8 0]<511)
       (500<510[-2 -8 0]<511) (500<510[-1 -8 0]<511) (500<510[ 0 -8 0]<511)
       (500<510[ 1 -8 0]<511) (500<510[ 2 -8 0]<511) (500<510[ 3 -8 0]<511)
       (500<510[ 4 -8 0]<511) (500<510[ 5 -8 0]<511) (500<510[ 6 -8 0]<511)
       (500<510[ 7 -8 0]<511) (500<510[ 8 -8 0]<511)
c
       (500<510[-8 -7 0]<511) (500<510[-7 -7 0]<511) (500<510[-6 -7 0]<511)
       (500<510[-5 -7 0]<511) (500<510[-4 -7 0]<511) (500<510[-3 -7 0]<511)
       (500<510[-2 -7 0]<511) (500<510[-1 -7 0]<511) (500<510[ 0 -7 0]<511)
       (500<510[ 1 -7 0]<511) (500<510[ 2 -7 0]<511) (500<510[ 3 -7 0]<511)
       (500<510[ 4 -7 0]<511) (500<510[ 5 -7 0]<511) (500<510[ 6 -7 0]<511)
       (500<510[ 7 -7 0]<511) (500<510[ 8 -7 0]<511)
c
       (500<510[-8 -6 0]<511) (500<510[-7 -6 0]<511) (500<510[-6 -6 0]<511)
       (500<510[-5 -6 0]<511) (500<510[-4 -6 0]<511) (500<510[-3 -6 0]<511)
       (500<510[-2 -6 0]<511) (500<510[-1 -6 0]<511) (500<510[ 0 -6 0]<511)
       (500<510[ 1 -6 0]<511) (500<510[ 2 -6 0]<511) (500<510[ 3 -6 0]<511)
       (500<510[ 4 -6 0]<511) (500<510[ 5 -6 0]<511) (500<510[ 6 -6 0]<511)
       (500<510[ 7 -6 0]<511) (500<510[ 8 -6 0]<511)
c
       (500<510[-8 -5 0]<511) (500<510[-7 -5 0]<511) (500<510[-6 -5 0]<511)
       (500<510[-5 -5 0]<511) (500<510[-4 -5 0]<511) (500<510[-3 -5 0]<511)
       (500<510[-2 -5 0]<511) (500<510[-1 -5 0]<511) (500<510[ 0 -5 0]<511)
       (500<510[ 1 -5 0]<511) (500<510[ 2 -5 0]<511) (500<510[ 3 -5 0]<511)
       (500<510[ 4 -5 0]<511) (500<510[ 5 -5 0]<511) (500<510[ 6 -5 0]<511)
       (500<510[ 7 -5 0]<511) (500<510[ 8 -5 0]<511)
c
       (500<510[-8 -4 0]<511) (500<510[-7 -4 0]<511) (500<510[-6 -4 0]<511)
       (500<510[-5 -4 0]<511) (500<510[-4 -4 0]<511) (500<510[-3 -4 0]<511)
       (500<510[-2 -4 0]<511) (500<510[-1 -4 0]<511) (500<510[ 0 -4 0]<511)
```

```
      (500<510[ 1 -4 0]<511) (500<510[ 2 -4 0]<511) (500<510[ 3 -4 0]<511)
      (500<510[ 4 -4 0]<511) (500<510[ 5 -4 0]<511) (500<510[ 6 -4 0]<511)
      (500<510[ 7 -4 0]<511) (500<510[ 8 -4 0]<511)
c
      (500<510[-8 -3 0]<511) (500<510[-7 -3 0]<511) (500<510[-6 -3 0]<511)
      (500<510[-5 -3 0]<511) (500<510[-4 -3 0]<511) (500<510[-3 -3 0]<511)
      (500<510[-2 -3 0]<511) (500<510[-1 -3 0]<511) (500<510[ 0 -3 0]<511)
      (500<510[ 1 -3 0]<511) (500<510[ 2 -3 0]<511) (500<510[ 3 -3 0]<511)
      (500<510[ 4 -3 0]<511) (500<510[ 5 -3 0]<511) (500<510[ 6 -3 0]<511)
      (500<510[ 7 -3 0]<511) (500<510[ 8 -3 0]<511)
c
      (500<510[-8 -2 0]<511) (500<510[-7 -2 0]<511) (500<510[-6 -2 0]<511)
      (500<510[-5 -2 0]<511) (500<510[-4 -2 0]<511) (500<510[-3 -2 0]<511)
      (500<510[-2 -2 0]<511) (500<510[-1 -2 0]<511) (500<510[ 0 -2 0]<511)
      (500<510[ 1 -2 0]<511) (500<510[ 2 -2 0]<511) (500<510[ 3 -2 0]<511)
      (500<510[ 4 -2 0]<511) (500<510[ 5 -2 0]<511) (500<510[ 6 -2 0]<511)
      (500<510[ 7 -2 0]<511) (500<510[ 8 -2 0]<511)
c
      (500<510[-8 -1 0]<511) (500<510[-7 -1 0]<511) (500<510[-6 -1 0]<511)
      (500<510[-5 -1 0]<511) (500<510[-4 -1 0]<511) (500<510[-3 -1 0]<511)
      (500<510[-2 -1 0]<511) (500<510[-1 -1 0]<511) (500<510[ 0 -1 0]<511)
      (500<510[ 1 -1 0]<511) (500<510[ 2 -1 0]<511) (500<510[ 3 -1 0]<511)
      (500<510[ 4 -1 0]<511) (500<510[ 5 -1 0]<511) (500<510[ 6 -1 0]<511)
      (500<510[ 7 -1 0]<511) (500<510[ 8 -1 0]<511)
c
      (500<510[-8  0 0]<511) (500<510[-7  0 0]<511) (500<510[-6  0 0]<511)
      (500<510[-5  0 0]<511) (500<510[-4  0 0]<511) (500<510[-3  0 0]<511)
      (500<510[-2  0 0]<511) (500<510[-1  0 0]<511) (500<510[ 0  0 0]<511)
      (500<510[ 1  0 0]<511) (500<510[ 2  0 0]<511) (500<510[ 3  0 0]<511)
      (500<510[ 4  0 0]<511) (500<510[ 5  0 0]<511) (500<510[ 6  0 0]<511)
      (500<510[ 7  0 0]<511) (500<510[ 8  0 0]<511)
c
      (500<510[-8  1 0]<511) (500<510[-7  1 0]<511) (500<510[-6  1 0]<511)
      (500<510[-5  1 0]<511) (500<510[-4  1 0]<511) (500<510[-3  1 0]<511)
      (500<510[-2  1 0]<511) (500<510[-1  1 0]<511) (500<510[ 0  1 0]<511)
      (500<510[ 1  1 0]<511) (500<510[ 2  1 0]<511) (500<510[ 3  1 0]<511)
      (500<510[ 4  1 0]<511) (500<510[ 5  1 0]<511) (500<510[ 6  1 0]<511)
      (500<510[ 7  1 0]<511) (500<510[ 8  1 0]<511)
c
      (500<510[-8  2 0]<511) (500<510[-7  2 0]<511) (500<510[-6  2 0]<511)
      (500<510[-5  2 0]<511) (500<510[-4  2 0]<511) (500<510[-3  2 0]<511)
      (500<510[-2  2 0]<511) (500<510[-1  2 0]<511) (500<510[ 0  2 0]<511)
      (500<510[ 1  2 0]<511) (500<510[ 2  2 0]<511) (500<510[ 3  2 0]<511)
      (500<510[ 4  2 0]<511) (500<510[ 5  2 0]<511) (500<510[ 6  2 0]<511)
      (500<510[ 7  2 0]<511) (500<510[ 8  2 0]<511)
c
      (500<510[-8  3 0]<511) (500<510[-7  3 0]<511) (500<510[-6  3 0]<511)
      (500<510[-5  3 0]<511) (500<510[-4  3 0]<511) (500<510[-3  3 0]<511)
      (500<510[-2  3 0]<511) (500<510[-1  3 0]<511) (500<510[ 0  3 0]<511)
      (500<510[ 1  3 0]<511) (500<510[ 2  3 0]<511) (500<510[ 3  3 0]<511)
      (500<510[ 4  3 0]<511) (500<510[ 5  3 0]<511) (500<510[ 6  3 0]<511)
      (500<510[ 7  3 0]<511) (500<510[ 8  3 0]<511)
c
      (500<510[-8  4 0]<511) (500<510[-7  4 0]<511) (500<510[-6  4 0]<511)
      (500<510[-5  4 0]<511) (500<510[-4  4 0]<511) (500<510[-3  4 0]<511)
      (500<510[-2  4 0]<511) (500<510[-1  4 0]<511) (500<510[ 0  4 0]<511)
      (500<510[ 1  4 0]<511) (500<510[ 2  4 0]<511) (500<510[ 3  4 0]<511)
      (500<510[ 4  4 0]<511) (500<510[ 5  4 0]<511) (500<510[ 6  4 0]<511)
      (500<510[ 7  4 0]<511) (500<510[ 8  4 0]<511)
c
      (500<510[-8  5 0]<511) (500<510[-7  5 0]<511) (500<510[-6  5 0]<511)
      (500<510[-5  5 0]<511) (500<510[-4  5 0]<511) (500<510[-3  5 0]<511)
      (500<510[-2  5 0]<511) (500<510[-1  5 0]<511) (500<510[ 0  5 0]<511)
```

```
       (500<510[ 1  5 0]<511) (500<510[ 2  5 0]<511) (500<510[ 3  5 0]<511)
       (500<510[ 4  5 0]<511) (500<510[ 5  5 0]<511) (500<510[ 6  5 0]<511)
       (500<510[ 7  5 0]<511) (500<510[ 8  5 0]<511)
c
       (500<510[-8  6 0]<511) (500<510[-7  6 0]<511) (500<510[-6  6 0]<511)
       (500<510[-5  6 0]<511) (500<510[-4  6 0]<511) (500<510[-3  6 0]<511)
       (500<510[-2  6 0]<511) (500<510[-1  6 0]<511) (500<510[ 0  6 0]<511)
       (500<510[ 1  6 0]<511) (500<510[ 2  6 0]<511) (500<510[ 3  6 0]<511)
       (500<510[ 4  6 0]<511) (500<510[ 5  6 0]<511) (500<510[ 6  6 0]<511)
       (500<510[ 7  6 0]<511) (500<510[ 8  6 0]<511)
c
       (500<510[-8  7 0]<511) (500<510[-7  7 0]<511) (500<510[-6  7 0]<511)
       (500<510[-5  7 0]<511) (500<510[-4  7 0]<511) (500<510[-3  7 0]<511)
       (500<510[-2  7 0]<511) (500<510[-1  7 0]<511) (500<510[ 0  7 0]<511)
       (500<510[ 1  7 0]<511) (500<510[ 2  7 0]<511) (500<510[ 3  7 0]<511)
       (500<510[ 4  7 0]<511) (500<510[ 5  7 0]<511) (500<510[ 6  7 0]<511)
       (500<510[ 7  7 0]<511) (500<510[ 8  7 0]<511)
c
       (500<510[-8  8 0]<511) (500<510[-7  8 0]<511) (500<510[-6  8 0]<511)
       (500<510[-5  8 0]<511) (500<510[-4  8 0]<511) (500<510[-3  8 0]<511)
       (500<510[-2  8 0]<511) (500<510[-1  8 0]<511) (500<510[ 0  8 0]<511)
       (500<510[ 1  8 0]<511) (500<510[ 2  8 0]<511) (500<510[ 3  8 0]<511)
       (500<510[ 4  8 0]<511) (500<510[ 5  8 0]<511) (500<510[ 6  8 0]<511)
       (500<510[ 7  8 0]<511) (500<510[ 8  8 0]<511)
c
sp1                    1 1 1 1 1 1 1 1 1 1 1 1 1 1 1 1 1
                       1 1 1 1 1 1 1 1 1 1 1 1 1 1 1 1 1
                       1 1 1 1 1 0 1 1 0 1 1 0 1 1 1 1 1
                       1 1 1 0 1 1 1 1 1 1 1 1 1 0 1 1 1
                       1 1 1 1 1 1 1 1 1 1 1 1 1 1 1 1 1
                       1 1 0 1 1 0 1 1 0 1 1 0 1 1 0 1 1
                       1 1 1 1 1 1 1 1 1 1 1 1 1 1 1 1 1
                       1 1 1 1 1 1 1 1 1 1 1 1 1 1 1 1 1
                       1 1 0 1 1 0 1 1 0 1 1 0 1 1 0 1 1
                       1 1 1 1 1 1 1 1 1 1 1 1 1 1 1 1 1
                       1 1 1 1 1 1 1 1 1 1 1 1 1 1 1 1 1
                       1 1 0 1 1 0 1 1 0 1 1 0 1 1 0 1 1
                       1 1 1 1 1 1 1 1 1 1 1 1 1 1 1 1 1
                       1 1 1 0 1 1 1 1 1 1 1 1 1 0 1 1 1
                       1 1 1 1 1 0 1 1 0 1 1 0 1 1 1 1 1
                       1 1 1 1 1 1 1 1 1 1 1 1 1 1 1 1 1
                       1 1 1 1 1 1 1 1 1 1 1 1 1 1 1 1 1
c
si2   40    $Fuel Length
sp2  -21 0
si3  0 0.41 $Fuel Radius
sp3  -21 1
c
c Cm244 WATTS FISSION SPECTRUM CONSTANTS
sp4 -3 0.906 3.848
c
c *********************************************************
c  TALLIES -- FISSION RATE Gd & Cd Fission Chambers
c *********************************************************
c
c
fc4 Bare U235 FC (THERMAL FLUX)
f4:n 101
fm4 -1 12 -6
sd4 1
c
fc14 B4C U235 FC (FFM)
f14:n 111
```

```
fm14 -1 12 -6
sd14 1
c
fc44 TOTAL FISSION RATE in SINRD FLUX MONITORS
f44:n (101 111)
fm44 -1 12 -6
sd44  1
c
c ******************************************************************************
NPS 3.0E+08
CUT:n 2j 0 0
FCL:n 1j 1 2j 1 27j
WWG 44 0
WWP:n 5 3 5 0 -1
MESH  geom=rec ref 0 0 0 origin -26 -26 -202
      imesh -11 11 26  iints 3  5  3
      jmesh -11 11 12.4 13.8 16.2 17.5 18.8 26  jints 3 5 1 1 1 1 1 1
      kmesh -30 -10 -4.25 -1.47 1.39 4.07 10 30 202 kints 1 1 1 1 1 1 1 1 1
c ******************************************************************************
c
c
c ***********************************************************
c  MATERIAL CARDS
c ***********************************************************
c
c  Material 2 is Aluminum (density = 2.70 g/cc)
m2    13027.70c 1.0
c
c  Material 3 is NATURAL Cadmium (density = 8.65 g/cc)
m3    48106 0.01250
      48108 0.00890
      48110 0.12490
      48111 0.12800
      48112 0.24130
      48113 0.12220
      48114 0.28730
      48116 0.07490
      nlib=.70c
c
c  Material 4 is polyethylene (CH2)
m4    1001.70c 2.0
      6000.70c 1.0
mt4   poly.60t
c
c  Material 5 is Fresh UO2 Fuel - 4.0 wt% U235 (10.4 g/cc)
m5       8016 -0.118534632
        92235 -0.035258615
        92238 -0.846206753
        nlib=.70c
c
c  Material 6 is Fresh UO2 Fuel - 5.0 wt% U235 (10.4 g/cc)
m6       8016 -0.118534632
        92235 -0.044073268
        92238 -0.837392099
        nlib=.70c
c
c  Material 9 is Zircaloy 2 (density = 6.55 g/cc)
m9    26054 7.8122E-06   $ Fuel Cladding
      26056 1.2245E-04
      26057 2.8278E-06
      26058 3.7633E-07
      40090 1.9889E-02
      40091 4.3373E-03
```

```
      40092 6.6297E-03
      40094 6.7186E-03
      40096 1.0824E-03
      24050 2.9656E-06
      24052 5.7189E-05
      24053 6.4848E-06
      24054 1.6142E-06
      nlib=.70c
c
c  Material 12 is U235 in Fission Chamber - 93% U235 (19.1 g/cc)
m12      92235 0.93
         92238 0.07
         nlib=.70c
c
c  Material 13 is Pu239 in Fission Chamber - 94% Pu239 (19.8 g/cc)
m13      94239 0.94
         94240 0.06
         nlib=.70c
c
c  Material 14 is Boron Carbide (1.0 cm)
m14      5010 4.0
         6000 1.0
         nlib=.70c
c
c  Material 15 is Water -- NO boron
m15      1001.70c 2.0
         8016.70c 1.0
mt15     lwtr.10t
c
c  Material 16 is NATURAL Gadolinium (density = 7.9 g/cc)
m16      64152 0.0020
         64154 0.0218
         64155 0.1480
         64156 0.2047
         64157 0.1565
         64158 0.2484
         64160 0.2186
         nlib=.70c
c
c  Material 18 is Fresh MOX Fuel - 6 wt% Pu (density = 10.4 g/cc)
m18      8016 -0.118422235
        92235 -0.001657366
        92238 -0.827025733
        94238 -0.001322359
        94239 -0.028933383
        94240 -0.013805529
        94241 -0.005024827
        94242 -0.003808568
        nlib=.70c
c
c  Material 19 is NATURAL Hf (density = -13.31 g/cm3)
m19      72174 0.00162
         72176 0.05206
         72177 0.18606
         72178 0.27297
         72179 0.13629
         72180 0.35100
         nlib=.70c
c
c  Material 20 is Fresh DU Fuel - 0.20 wt% U235
m20      8016 -0.118534632
        92235 -0.001762931
        92238 -0.879702437
```

```
        nlib=.70c
c
c  Material 21 is Fresh MOX Fuel, 8 wt% Pu (density = 10.4 g/cc)
m21      8016 -0.118407764
        92235 -0.001622130
        92238 -0.809442727
        94238 -0.001763174
        94239 -0.038578477
        94240 -0.018407674
        94241 -0.006699879
        94242 -0.005078174
        nlib=.70c
c
c  Material 22 is Fresh MOX Fuel, 4 wt% Pu (density = 10.4 g/cc)
m22      8016 -0.118422235
        92235 -0.001692629
        92238 -0.844622025
        94238 -0.000881573
        94239 -0.019288922
        94240 -0.009203686
        94241 -0.003349884
        94242 -0.002539046
        nlib=.70c
c
c  Material 40 is PWR Spent LEU Fuel - 4% U235 - BU = 40GWd
m40     92234 -8.1358E-06
        92235 -8.2656E-03
        92236 -4.6557E-03
        92238 -8.4585E-01
        93237 -4.0652E-04
        94238 -1.4673E-04
        94239 -4.4910E-03
        94240 -2.0727E-03
        94241 -9.2225E-04
        94242 -4.9867E-04
        95241 -2.8054E-04
        95243 -9.7823E-05
        96242 -6.8212E-09
        96244 -2.5020E-05
        42095 -8.3880E-04
        43099 -8.6238E-04
        44101 -8.4822E-04
        45103 -5.0184E-04
        46105 -4.0890E-04
        47109 -7.6381E-05
        54131 -4.6385E-04
        55133 -1.2503E-03
        55135 -4.1071E-04
        55137 -1.1807E-03
        59141 -1.2294E-03
        60143 -8.5741E-04
        60145 -7.4480E-04
        62147 -2.3158E-04
        62149 -2.4484E-06
        62150 -3.0723E-04
        62151 -1.1407E-05
        62152 -1.3688E-04
        63153 -1.2198E-04
        64155 -9.0916E-06
        64156 -8.3341E-05
        8016 -1.2170E-01
        nlib=.70c
print
```

A.2. BWR 9x9 Spent MOX Fuel Assembly

```
BWR 9x9 SPENT Fuel Assembly in Water (FFM-Bare)
c
c ****************************************
c  SINRD CELL CARDS
c ****************************************
c
c ALL U235 FC - 0.025mm NATURAL Gd & NO NATURAL Hf
c
c ** Bare U235 Fission Chamber **
100   0        -100                  imp:n=1
101  12 -19.1  -101 100              imp:n=1 $U235
102   2 -2.70  -102 101 +103 -104    imp:n=1
c
c ** B4C outer U235 Fission Chamber **
110   0        -110                  imp:n=1
111  12 -19.1  -111 110              imp:n=1 $U235
112   2 -2.70  -112 111 +103 -104    imp:n=1
c
c ** 0.025mm Gd covered U235 Fission Chamber **
200   0        -200                  imp:n=1
201  12 -19.1  -201 200              imp:n=1 $U235
202   2 -2.70  -202 201              imp:n=1
204  16 -7.90  -204 202 +205 -206    imp:n=1 $0.025mm Gd
c
c ** 3.00 mm Cd covered U235 Fission Chamber **
300   0        -300                  imp:n=1
301  12 -19.1  -301 300              imp:n=1 $U235
302   2 -2.70  -302 301              imp:n=1
303   3 -8.65  -303 302 +305 -306    imp:n=1 $3.00mm Cd
c
c ** Detector Pod **
400   2 -2.70  -400 #100 #101 #102 #200 #201 #202 #204
                #300 #301 #302 #303  imp:n=1  $Al BOX
401  14 -2.52  -401 400              imp:n=1  $1.0cm B4C Liner
402   4 -0.96  -403 #110 #111 #112   imp:n=1  $Poly BOX
403   3 -8.65  -402 403              imp:n=1  $Cd Liner
c
c ******************************************
c  BWR 9x9 SPENT MOX Fuel Assembly CELL CARDS
c ******************************************
c
c 0% VOID FRACTION - NO DEFECTS
c
c Initial enrichment = 6.0 wt% Pu
c DENSITY of Spent Fuel = 10.012-g/cc (91%TD)
c
c *** RADIAL FUEL Regions (4) ***
c
c  SPENT MOX FUEL RODS
500 40 -10.0120 -503       u=1   imp:n=1 $SPENT Fuel, 40GWd
501  9  -6.55   -504  503  u=1   imp:n=1 $CLADDING
502 15  -1.00    504       u=1   imp:n=1 $WATER
c
c  DU REGION DEFECTS
600 20 -10.4538 -503       u=7   imp:n=1
602  9  -6.55   -504  503  u=7   imp:n=1 $CLADDING
603 15  -1.00    504       u=7   imp:n=1 $WATER
c
c  LARGE WATER RODS
```

```
604 15  -1.00   -504       u=9   imp:n=1
605 15  -1.00    504       u=9   imp:n=1
c
800 0   -700  imp:n=1    lat=1 u=2 fill=-4:4 -4:4 0:0
                    1 1 1 1 1 1 1 1 1
                    1 1 1 1 1 1 1 1 1
                    1 1 1 1 1 1 1 1 1
                    1 1 1 9 9 1 1 1 1
                    1 1 1 9 9 9 1 1 1
                    1 1 1 1 9 9 1 1 1
                    1 1 1 1 1 1 1 1 1
                    1 1 1 1 1 1 1 1 1
                    1 1 1 1 1 1 1 1 1
801   0        -701            fill=2    imp:n=1
802   9  -6.55 -702 701 704              imp:n=1  $Duct
803   0        -704                      imp:n=1  $AIR Gap
c
998 15 -1.0    -999 701 702 704 401 402  imp:n=1  $Water
999 0  999  imp:n=0

c ****************************************
c SURFACE CARDS -- PWR 17x17 Fuel Assembly
c ****************************************
c
c *** (4) RADIAL FUEL Regions ***
c
c  TOTAL LENGTH Fuel Rods
500 rcc 0  0 -179.375  0 0 358.75  0.3940376
501 rcc 0  0 -179.375  0 0 358.75  0.4697124
502 rcc 0  0 -179.375  0 0 358.75  0.4857073
503 rcc 0  0 -179.375  0 0 358.75  0.4877000
504 rcc 0  0 -179.375  0 0 358.75  0.5590 $CLADDING
c
c  PART LENGTH Fuel Rods
600 rcc 0  0 -114.30  0 0 228.60  0.3940376
601 rcc 0  0 -114.30  0 0 228.60  0.4697124
602 rcc 0  0 -114.30  0 0 228.60  0.4857073
603 rcc 0  0 -114.30  0 0 228.60  0.4877000
605 rcc 0  0 -114.30  0 0 228.60  0.5590 $CLADDING
c
c  BWR 9x9 LATTICE Structure & Assembly Duct
700 rpp  -0.736  0.736  -0.736  0.736  -179.375 179.375
701 rpp  -6.624  6.624  -6.624  6.624  -159.375 159.375   $ Fuel Assembly
702 rpp  -6.751  6.751  -6.751  6.751  -159.375 159.375   $ Duct
c
c *** AIR GAP b/n Assembly & Fission Chambers ***
704 rpp  -6.751  6.751   6.752  6.852  -5.625 5.3
c
c *************************
c  SINRD Fission chambers
c *************************
c
c ** Bare U235 Fission Chamber **
100 rcc  -5.450  8.522   0   10.90  0  0  1.16984
101 rcc  -5.450  8.522   0   10.90  0  0  1.17000
102 c/x   8.522  0  1.27
103 px   -5.55
104 px    5.55
c
c ** B4C (outer) U235 Fission Chamber **
110 rcc  -5.450  13.642   0   10.90  0  0  1.16984
111 rcc  -5.450  13.642   0   10.90  0  0  1.17000
112 c/x  13.642  0  1.27
```

```
c
c ** 0.025 mm Gd covered Fission Chamber **
200 rcc  -5.450  8.522   2.78   10.90  0  0  1.16984
201 rcc  -5.450  8.522   2.78   10.90  0  0  1.17000
202 rcc  -5.550  8.522   2.78   11.10  0  0  1.27000
204 c/x   8.522  2.78    1.2725
205 px   -5.5525
206 px    5.5525
c
c ** 3.00 mm Cd covered Fission Chamber **
300 rcc  -5.450  8.522   -2.94   10.90  0  0  1.16984
301 rcc  -5.450  8.522   -2.94   10.90  0  0  1.17000
302 rcc  -5.550  8.522   -2.94   11.10  0  0  1.27000
303 c/x   8.522 -2.94     1.57
305 px   -5.75
306 px    5.75
c
c ** Aluminum box lined with 1.0-cm B4C **
400 rpp  -5.751  5.751   6.852  10.192  -4.625 4.300   $ Aluminum Box
401 rpp  -6.751  6.751   6.852  11.192  -5.625 5.300   $ 1.0 cm B4C
402 rpp  -6.751  6.751  11.192  16.092  -5.625 5.300   $ 1.0 mm Cd
403 rpp  -6.651  6.651  11.292  15.992  -5.525 5.200   $ Poly
c
999 rpp -25 25 -25 25 -181 181
c

c ***********************************************************
c  SOURCE DEFINITION
c ***********************************************************
MODE N
SDEF CEL=d1 EXT=d2 RAD=d3 AXS 0 0 1 ERG=d4
c
si1  l (500<800[-4 -4 0]<801) (500<800[-3 -4 0]<801) (500<800[-2 -4 0]<801)
       (500<800[-1 -4 0]<801) (500<800[ 0 -4 0]<801) (500<800[ 1 -4 0]<801)
       (500<800[ 2 -4 0]<801) (500<800[ 3 -4 0]<801) (500<800[ 4 -4 0]<801)
c
       (500<800[-4 -3 0]<801) (500<800[-3 -3 0]<801) (500<800[-2 -3 0]<801)
       (500<800[-1 -3 0]<801) (500<800[ 0 -3 0]<801) (500<800[ 1 -3 0]<801)
       (500<800[ 2 -3 0]<801) (500<800[ 3 -3 0]<801) (500<800[ 4 -3 0]<801)
c
       (500<800[-4 -2 0]<801) (500<800[-3 -2 0]<801) (500<800[-2 -2 0]<801)
       (500<800[-1 -2 0]<801) (500<800[ 0 -2 0]<801) (500<800[ 1 -2 0]<801)
       (500<800[ 2 -2 0]<801) (500<800[ 3 -2 0]<801) (500<800[ 4 -2 0]<801)
c
       (500<800[-4 -1 0]<801) (500<800[-3 -1 0]<801) (500<800[-2 -1 0]<801)
       (500<800[-1 -1 0]<801) (500<800[ 0 -1 0]<801) (500<800[ 1 -1 0]<801)
       (500<800[ 2 -1 0]<801) (500<800[ 3 -1 0]<801) (500<800[ 4 -1 0]<801)
c
       (500<800[-4  0 0]<801) (500<800[-3  0 0]<801) (500<800[-2  0 0]<801)
       (500<800[-1  0 0]<801) (500<800[ 0  0 0]<801) (500<800[ 1  0 0]<801)
       (500<800[ 2  0 0]<801) (500<800[ 3  0 0]<801) (500<800[ 4  0 0]<801)
c
       (500<800[-4  1 0]<801) (500<800[-3  1 0]<801) (500<800[-2  1 0]<801)
       (500<800[-1  1 0]<801) (500<800[ 0  1 0]<801) (500<800[ 1  1 0]<801)
       (500<800[ 2  1 0]<801) (500<800[ 3  1 0]<801) (500<800[ 4  1 0]<801)
c
       (500<800[-4  2 0]<801) (500<800[-3  2 0]<801) (500<800[-2  2 0]<801)
       (500<800[-1  2 0]<801) (500<800[ 0  2 0]<801) (500<800[ 1  2 0]<801)
       (500<800[ 2  2 0]<801) (500<800[ 3  2 0]<801) (500<800[ 4  2 0]<801)
c
       (500<800[-4  3 0]<801) (500<800[-3  3 0]<801) (500<800[-2  3 0]<801)
       (500<800[-1  3 0]<801) (500<800[ 0  3 0]<801) (500<800[ 1  3 0]<801)
       (500<800[ 2  3 0]<801) (500<800[ 3  3 0]<801) (500<800[ 4  3 0]<801)
```

```
c
       (500<800[-4  4 0]<801) (500<800[-3  4 0]<801) (500<800[-2  4 0]<801)
       (500<800[-1  4 0]<801) (500<800[ 0  4 0]<801) (500<800[ 1  4 0]<801)
       (500<800[ 2  4 0]<801) (500<800[ 3  4 0]<801) (500<800[ 4  4 0]<801)
c
sp1                1 1 1 1 1 1 1 1
                   1 1 1 1 1 1 1 1
                   1 1 1 1 1 1 1 1
                   1 1 1 0 0 1 1 1
                   1 1 1 0 0 0 1 1
                   1 1 1 1 0 0 1 1
                   1 1 1 1 1 1 1 1
                   1 1 1 1 1 1 1 1
                   1 1 1 1 1 1 1 1
si2   40    $Fuel Length
sp2  -21 0
si3  0 0.4877 $Fuel Radius
sp3  -21 1
c
c Cm244 WATTS FISSION SPECTRUM CONSTANTS
sp4 -3 0.906 3.848
c
c ***********************************************************
c  TALLIES -- FISSION RATE Bare & FFM Fission Chambers
c ***********************************************************
c
c
fc4 Bare U235 FC (THERMAL FLUX)
f4:n 101
fm4 -1 12 -6
sd4 1
c
fc14 B4C U235 FC (FFM)
f14:n 111
fm14 -1 12 -6
sd14 1
c
fc44 TOTAL FLUX in SINRD FLUX MONITORS
f44:n (101 111)
fm44 -1 12 -6
sd44  1
c
c ****************************************************************************
NPS 3.5E+08
CUT:n 2j 0 0
FCL:n 1j 1 2j 1 27j
WWG 44 0
WWP:n 5 3 5 0 -1
MESH geom=rec ref 0 0 0 origin -26 -26 -182
     imesh -7 7 26  iints 2  5  2
     jmesh -7 7 8.5 9.9 12.3 13.6 15 26 jints 2 5 1 1 1 1 1 1
     kmesh -30 -10 -4.25 -1.47 1.39 4.07 10 30 182 kints 1 1 1 1 1 1 1 1 1
c ****************************************************************************
c
c
c ***********************************************************
c  MATERIAL CARDS
c ***********************************************************
c
c  Material 2 is Aluminum (density = 2.70 g/cc)
m2    13027.66c 1.0
c
c  Material 3 is NATURAL Cadmium (density = 8.65 g/cc)
```

```
m3    48106 0.01250
      48108 0.00890
      48110 0.12490
      48111 0.12800
      48112 0.24130
      48113 0.12220
      48114 0.28730
      48116 0.07490
      nlib=.66c
c
c  Material 4 is polyethylene (CH2)
m4    1001.66c 2.0
      6000.66c 1.0
mt4   poly.60t
c
c  Material 5 is Fresh UO2 Fuel - 4 wt% U235
m5     8016 -0.118534632
      92234 -0.000240509
      92235 -0.035258615
      92238 -0.845966244
      nlib=.66c
c
c  Material 6 is Fresh UO2 Fuel - 3 wt% U235
m6      8016 -0.118521432
       92234 -0.000238128
       92235 -0.026448814
       92238 -0.854791626
       nlib=.66c
c
c  Material 9 is Zircaloy 2
m9    26054 7.8122E-06   $ Fuel Cladding
      26056 1.2245E-04
      26057 2.8278E-06
      26058 3.7633E-07
      40090 1.9889E-02
      40091 4.3373E-03
      40092 6.6297E-03
      40094 6.7186E-03
      40096 1.0824E-03
      24050 2.9656E-06
      24052 5.7189E-05
      24053 6.4848E-06
      24054 1.6142E-06
      nlib=.66c
c
c  Material 12 is U235 in Fission Chamber (93% U235)
m12      92235 0.93
         92238 0.07
         nlib=.66c
c
c  Material 13 is Pu239 in Fission Chamber (94% Pu239)
m13      94239 0.94
         94240 0.06
         nlib=.66c
c
c  Material 14 is Boron Carbide (1.0 cm)
m14      5010 4.0
         6000 1.0
         nlib=.66c
c
c  Material 15 is Water -- NO boron
m15      1001.66c 2.0
         8016.66c 1.0
```

```
mt15     lwtr.60t
c
c  Material 16 is NATURAL Gadolinium (density = 7.9 g/cc)
m16      64152 0.0020
         64154 0.0218
         64155 0.1480
         64156 0.2047
         64157 0.1565
         64158 0.2484
         64160 0.2186
         nlib=.66c
c
c  Material 17 is Fresh MOX Fuel, 8 wt% Pu (density = 10.021 g/cc)
m17      8016 -0.118407764
        92235 -0.001622130
        92238 -0.809442727
        94238 -0.001763174
        94239 -0.038578477
        94240 -0.018407674
        94241 -0.006699879
        94242 -0.005078174
        nlib=.66c
c
c  Material 18 is Fresh MOX Fuel - 6 wt% Pu (density = 10.021 g/cc)
m18      8016 -0.118422235
        92235 -0.001657366
        92238 -0.827025733
        94238 -0.001322359
        94239 -0.028933383
        94240 -0.013805529
        94241 -0.005024827
        94242 -0.003808568
        nlib=.66c
c
c  Material 19 is NATURAL Hf (density = -13.31 g/cm3)
m19      72174 0.00162
         72176 0.05206
         72177 0.18606
         72178 0.27297
         72179 0.13629
         72180 0.35100
         nlib=.66c
c
c  Material 20 is Fresh DU Fuel - 0.20 a/o U235
m20    8016 0.666666
      92235 0.000667
      92238 0.332668
      nlib=.66c
c
c  Material 40 is BWR Spent MOX Fuel - 6% Pu - NO VOID - BU = 40GWd
m40     92234.66c -7.4964E-05
        92235.66c -7.4560E-04
        92236.66c -1.8135E-04
        92238.66c -8.2910E-01
        93237.66c -1.1077E-04
        94238.66c -1.1328E-03
        94239.66c -9.7862E-03
        94240.66c -1.2636E-02
        94241.66c -4.4468E-03
        94242.66c -5.3113E-03
        95241.66c -1.7160E-03
        95243.66c -1.1860E-03
        96242.66c -6.7048E-08
```

```
        96244.66c -4.5523E-04
        42095.50c -6.5227E-04
        43099.66c -8.4886E-04
        44101.50c -9.0658E-04
        45103.66c -8.2908E-04
        46105.66c -8.3800E-04
        47109.66c -2.1135E-04
        54131.66c -5.4747E-04
        55133.66c -1.2618E-03
        55135.60c -7.7036E-04
        55137.60c -1.1732E-03
        59141.50c -1.1066E-03
        60143.50c -8.1268E-04
        60145.50c -6.3992E-04
        62147.66c -2.4927E-04
        62149.66c -3.1836E-06
        62150.49c -3.0015E-04
        62151.50c -1.9377E-05
        62152.49c -1.8757E-04
        63153.66c -1.6750E-04
        64155.66c -1.3241E-05
        64156.66c -1.1051E-04
        8016.66c -1.2147E-01
print
```

APPENDIX B

ERROR PROPAGATIONS FOR SINRD RATIOS

B.1. Count Rates in SINRD Detectors

The count rate in detector (*i*) was calculated using the following equation where the subscript *i* = FFM ^{235}U, Bare ^{235}U, Gd covered, or Cd covered ^{235}U (or ^{239}Pu) fission chambers corresponding to the particular detector on which fission rate was tallied in MCNPX. The superscript *k* = ^{238}U, ^{240}Pu, or ^{244}Cm corresponding to the spontaneous fission source in fresh LEU fuel, fresh MOX fuel, or spent fuel, respectively.

$$CR_i = m_{SF}^k \cdot y_{SF}^k \cdot MCNPX\ \ Tally_i \tag{B.1}$$

where m_{SF}^k is the mass of the self-interrogating spontaneous fission source (*k*) in fuel, y_{SF}^k is the spontaneous fission yield of the self-interrogating spontaneous source (*k*) in fuel and $MCNPX\ Tally_i$ is the fission rate tally in detector (*i*) from MCNPX output.

Assuming a count time, t_C, the total number of counts in detector (*i*) and the corresponding standard deviation the counts were calculated using the following equations:

$$\begin{aligned} C_i &= CR_i \cdot t_C = m_{SF}^k \cdot y_{SF}^k \cdot MCNPX\ \ Tally_i \cdot t_C \\ \sigma_i &= \sqrt{C_i} \end{aligned} \tag{B.2}$$

Using the total number of counts calculated for each detector, six different detector ratios and corresponding standard deviations were calculated from the following equations (B.3) – (B.8):

$$1)\ R_1 = \frac{C_{FFM}}{C_{Bare}},\ \sigma_{R1} = \frac{C_{FFM}}{C_{Bare}}\sqrt{\left(\frac{\sigma_{FFM}}{C_{FFM}}\right)^2 + \left(\frac{\sigma_{Bare}}{C_{Bare}}\right)^2} \tag{B.3}$$

$$2)\ R_2 = \frac{C_{FFM}}{C_{Gd-Cd}},\ \sigma_{R2} = \frac{C_{FFM}}{C_{Gd-Cd}}\sqrt{\left(\frac{\sigma_{FFM}}{C_{FFM}}\right)^2 + \left(\frac{\sigma_{Gd-Cd}}{C_{Gd-Cd}}\right)^2} \tag{B.4}$$

$$3)\ R_3 = \frac{C_{FFM}}{C_{Gd}},\ \sigma_{R3} = \frac{C_{FFM}}{C_{Gd}}\sqrt{\left(\frac{\sigma_{FFM}}{C_{FFM}}\right)^2 + \left(\frac{\sigma_{Gd}}{C_{Gd}}\right)^2} \tag{B.5}$$

$$4)\ R_4 = \frac{C_{FFM}}{C_{Cd}},\ \sigma_{R4} = \frac{C_{FFM}}{C_{Cd}}\sqrt{\left(\frac{\sigma_{FFM}}{C_{FFM}}\right)^2 + \left(\frac{\sigma_{Cd}}{C_{Cd}}\right)^2} \tag{B.6}$$

$$5)\ R_5 = \frac{C_{Bare}}{C_{Gd}},\ \sigma_{R5} = \frac{C_{Bare}}{C_{Gd}}\sqrt{\left(\frac{\sigma_{Bare}}{C_{Bare}}\right)^2 + \left(\frac{\sigma_{Gd}}{C_{Gd}}\right)^2} \tag{B.7}$$

$$6)\ R_6 = \frac{C_{Bare}}{C_{Cd}},\ \sigma_{R6} = \frac{C_{Bare}}{C_{Cd}}\sqrt{\left(\frac{\sigma_{Bare}}{C_{Bare}}\right)^2 + \left(\frac{\sigma_{Cd}}{C_{Cd}}\right)^2} \tag{B.8}$$

B.2. Sensitivity to Partial Defects

Next, fuel rods were uniformly removed from Regions 1, 2, and 3 of the assembly and the six detector ratios given above were recalculated. The perturbed detector ratio, *D*, resulting from the uniform removal of fuel rods is given in Eq. (B.9):

$$D_x^{(n)} = \frac{C_i^{(n)}}{C_j^{(n)}},\ \sigma_{D(x,n)} = \frac{C_i^{(n)}}{C_j^{(n)}}\sqrt{\left(\frac{\sigma_i^{(n)}}{C_i^{(n)}}\right)^2 + \left(\frac{\sigma_j^{(n)}}{C_j^{(n)}}\right)^2} \tag{B.9}$$

where $n = 1, 2, 3$, corresponding to the region from which fuel rods were removed from the assembly and $x = 1,\ldots, 6$, corresponding to the six detector ratios given in Eq. (B.3) – (B.8). The subscript *i* corresponds to the detector used in the numerator of the six ratios where *i* = FFM ^{235}U or Bare ^{235}U FCs. The subscript *j* corresponds to the detector used in the denominator of the six ratios where *j* = Bare ^{235}U, Gd or Cd ^{235}U (or ^{239}Pu) FCs.

To assess the sensitivity of each region in the assembly to the uniform removal of fuel pins, the percent-difference, *P*, between the detector ratio, *R* (no defects), and the detector ratio, *D* (partial defects), and corresponding standard deviations were calculated for each region (*n*) using the following equations:

$$P_x^{(n)} = \frac{R_x^{(n)} - D_x^{(n)}}{R_x^{(n)}} \times 100$$

$$let\ A = R_x^{(n)} - D_x^{(n)}\ \ and\ \ \sigma_A = \sqrt{\left(\sigma_{R(x,n)}\right)^2 + \left(\sigma_{D(x,n)}\right)^2} \tag{B.10}$$

$$\Rightarrow \sigma_{P(x,n)} = \frac{A_x^{(n)}}{R_x^{(n)}} \sqrt{\left(\frac{\sigma_{A(x,n)}}{A_x^{(n)}}\right)^2 + \left(\frac{\sigma_{R(x,n)}}{R_x^{(n)}}\right)^2}$$

APPENDIX C
MEASURED COUNT RATES FOR SINRD FRESH FUEL EXPERIMENT IN AIR

C.1. Uniform Fuel Pin Removal

Table C.1. Measured count rates in SINRD fission chambers for uniform pin removal. The cells highlighted in gray represent background measurements.

Effective wt% ^{235}U	Count Time [s]	Count Rates in SINRD Fission Chambers [cps]							
		Bare FC*	1-σ	FFM	1-σ	Gd FC	1-σ	Cd FC	1-σ
0.22%	230040	37.98	0.019	67.70	0.017	6.396	0.005	2.344	0.003
0.80%	55170	27.19	0.019	80.84	0.035	5.959	0.009	2.502	0.006
1.09%	19080	23.33	0.033	86.70	0.066	5.721	0.019	2.560	0.012
1.41%	55170	19.91	0.018	91.84	0.041	5.445	0.010	2.610	0.007
1.70%	19530	17.42	0.028	95.85	0.072	5.170	0.017	2.628	0.011
2.00%	55170	15.38	0.016	97.88	0.042	4.893	0.009	2.583	0.007
2.32%	19410	13.98	0.025	101.3	0.078	4.753	0.015	2.607	0.007
2.61%	97290	12.67	0.011	104.8	0.033	4.650	0.007	2.644	0.005
2.90%	56640	11.89	0.014	108.4	0.044	4.538	0.009	2.694	0.007
3.19%	55740	11.09	0.013	106.9	0.043	4.318	0.009	2.608	0.007
3.19%	*55680*	*0.001*	*0.000*	*0.022*	*0.001*	*0.000*	*0.000*	*0.000*	*0.000*

** Count rate in Bare ^{235}U FC was calculated manually using data in Table C.2.*

Table C.2. Measured counts in Bare ^{235}U FC for uniform pin removal. The cells highlighted in gray represent background measurements.

Effective wt% ^{235}U	Count Time [seconds]	Bare FC [counts]	Standard Deviation
0.22%	99999	3797605	1949
0.80%	78332	2130098	1459
1.09%	21934	511650	715
1.41%	62310	1240760	1114
1.70%	21953	382305	618
2.00%	62035	954361	977
2.32%	22368	312738	559
2.61%	99999	1267085	1126
2.90%	63670	757258	870
3.19%	64114	710871	843
3.19%	*62790*	*56*	*7*

C.2. Region Fuel Pin Removal

Table C.3. Measured count rates in SINRD fission chambers for region pin removal with ^{252}Cf source located in back of fuel assembly in poly block.

Count Time [s]	Region #	Count Rates in SINRD Fission Chambers [cps]							
		Bare FC*	1-σ	FFM	1-σ	Gd FC	1-σ	Cd FC	1-σ
55740	3.19%	11.088	0.013	106.87	0.043	4.318	0.009	2.608	0.007
74850	1 - 1	12.109	0.024	103.88	0.037	4.456	0.008	2.586	0.006
55680	1 - 2	13.436	0.014	101.05	0.042	4.600	0.009	2.566	0.007
18930	2 - 1	11.887	0.023	103.92	0.075	4.487	0.016	2.606	0.012
216810	2 - 2	13.253	0.012	101.86	0.021	4.702	0.005	2.624	0.003
22500	3 - 1	11.953	0.021	104.97	0.066	4.533	0.015	2.643	0.011
53280	3 - 2	13.043	0.014	101.65	0.043	4.703	0.009	2.613	0.007

** Count rate in Bare ^{235}U FC was calculated manually using data in Table C.4.*

Table C.4. Measured counts in Bare ^{235}U FC for region pin removal with ^{252}Cf source located in back of fuel assembly in poly block.

Count Time [seconds]	Region #	Bare FC [counts]	Standard Deviation
64114	3.19%	710871	843
21672	1 - 1	262420	512
64470	1 - 2	866206	931
22171	2 - 1	263554	513
99999	2 - 2	1325248	1151
26097	3 - 1	311941	559
62220	3 - 2	811556	901

Table C.5. Measured count rates in SINRD fission chambers for region pin removal with ^{252}Cf source located in center of fuel assembly.

Count Time [s]	Region #	Count Rates in SINRD Fission Chambers [cps]							
		Bare FC*	1-σ	FFM	1-σ	Gd FC	1-σ	Cd FC	1-σ
54300	3.19%	15.46	0.015	310.7	0.077	6.394	0.011	5.080	0.010
66420	1 - 1	16.80	0.014	309.3	0.068	6.549	0.010	5.118	0.009
12870	1 - 2	18.27	0.034	307.5	0.155	6.692	0.023	5.113	0.020
55050	2 - 1	16.04	0.015	308.8	0.075	6.520	0.011	5.111	0.009
66030	2 - 2	16.95	0.014	306.7	0.068	6.647	0.010	5.114	0.009
347790	3 - 1	15.87	0.013	307.7	0.030	6.413	0.004	5.131	0.004
15240	3 - 2	16.43	0.029	303.5	0.137	6.432	0.021	5.132	0.018

** Count rate in Bare ^{235}U FC was calculated manually using data in Table C.6.*

Table C.6. Measured counts in Bare ^{235}U FC for region pin removal with ^{252}Cf source located in center of fuel assembly.

Count Time [seconds]	Region #	Bare FC [counts]	Standard Deviation
67832	3.19%	1048813	1024
82172	1 - 1	1380334	1175
15646	1 - 2	285826	535
67525	2 - 1	1082911	1041
81517	2 - 2	1381342	1175
99999	3 - 1	1587115	1260
19141	3 - 2	314533	561

APPENDIX D

TRANSLAT INPUT DECKS FOR LWR SPENT FUEL ASSEMBLIES

D.1. PWR 17x17 Spent LEU Fuel Assembly

Table D.1. Summary of reactor parameters used in TransLAT input decks for a PWR pin cell (LEU fuel).

PWR Pin Cell Data	
Fuel Pin Pitch	1.25 cm
Fuel Material	UO_2
^{235}U Enrichment	4 wt%HM ^{235}U
Expanded Pellet Density	10.4 g/cm^3
Fuel Pellet Radius	0.410 cm
Outer Pin Radius	0.475 cm
Cladding Material	Zircaloy-2 (6.55 g/cm^3)
Cladding Thickness	0.065 cm
Moderator	Light Water (1.0 g/cm^3)
Operating Parameters	
Power Density	34 MW/MTU
Fuel Temperature	900 K
Clad Temperature	620 K
Moderator Temperature	575 K
Coolant Pressure	2175 psia
Burnup Range	10 – 50 GWd/MTU
Decay Time	5 yrs

```
*FN p=punch_4_LEU40_PWR\r
*FN   r=res_4_LEU40_PWR.r
TTL PWR 17x17 SPENT LEU Fuel - 4% U235 - 40-GWd
! ****************************
!  INTEGRATION PARAMETERS
! ****************************
CON:0
TRP:N MOCS2D
TRP:G OFF
!
! ****************************
!  OPERATING STATE CONDITIONS
! ****************************
SYS PD=34 TF=900 TC=620 TM=575 PR=2175
DOP ON
!
! ****************************
!  FIXED BUCKLING OPTION
! ****************************
FUM 1,1,1.0E-8
!
! ****************************
!  MATERIAL DATA
! ****************************
FUE:FUEL 10.400 4.000 ICHN=92 MATTYP=1 TAVE=TF/
MAT:CLAD  6.55  40000=100.0 TAVE=TC /
MAT:COOL  0. 1001=6.6691E-2 8016=3.3346E-2 TAVE=TM /
MOD:1 0.0/ LIGHT WATER COOLANT
!
GEO:1
'PC', 22 /
  'RPP','COOL',1,1,0.6250/
  'RCC','CLAD',1,1,0.4750/
  'RCC','FUEL',1,1,0.4100/
  'RCC','FUEL',1,1,0.409988134/
  'RCC','FUEL',1,1,0.409979431/
  'RCC','FUEL',1,1,0.409964347/
  'RCC','FUEL',1,1,0.409938203/
  'RCC','FUEL',1,1,0.409892887/
  'RCC','FUEL',1,1,0.409814344/
  'RCC','FUEL',1,1,0.409678209/
  'RCC','FUEL',1,1,0.409442252/
  'RCC','FUEL',1,1,0.409033280/
  'RCC','FUEL',1,1,0.408324427/
  'RCC','FUEL',1,1,0.407095805/
  'RCC','FUEL',1,1,0.404966294/
  'RCC','FUEL',1,1,0.401275311/
  'RCC','FUEL',1,1,0.394877904/
  'RCC','FUEL',1,1,0.383789580/
  'RCC','FUEL',1,1,0.364570708/
  'RCC','FUEL',1,1,0.331259540/
  'RCC','FUEL',1,1,0.273522858/
  'RCC','FUEL',1,1,0.173450579/
/
LAT
+PC:1
 4*0.0/
/
MAP
'MAPS',1/
```

```
     1,1,1/
     1,1,'PC:1'/
/
EDR
       'M5R', 'PC:1.2'/
       'FR1', 'PC:1.3'/
       'FR2', 'PC:1.4'/
       'FR3', 'PC:1.5'/
       'FR4', 'PC:1.6'/
       'FR5', 'PC:1.7'/
       'FR6', 'PC:1.8'/
       'FR7', 'PC:1.9'/
       'FR8', 'PC:1.10'/
       'FR9', 'PC:1.11'/
       'FR10', 'PC:1.12'/
       'FR11', 'PC:1.13'/
       'FR12', 'PC:1.14'/
       'FR13', 'PC:1.15'/
       'FR14', 'PC:1.16'/
       'FR15', 'PC:1.17'/
       'FR16', 'PC:1.18'/
       'FR17', 'PC:1.19'/
       'FR18', 'PC:1.20'/
       'FR19', 'PC:1.21'/
       'FR20', 'PC:1.22'/
/
! PRI
! 1/
! 20,2,2,2/
! /
!
! ****************************
!  BURNUP
! ****************************
BUR BUMAX=40.0/
PUN:20 0,2,0,2,1,0,0/
RES new 40BUR
STA
RES old 40DCY 40BUR
 0, 40.0 /
!
! ************************************************************
TTL PWR 17x17 SPENT LEU Fuel - 4% U235 - 40-GWd - DECAY 5 years
! ************************************************************
!  INTEGRATION PARAMETERS
! ****************************
CON:0
TRP:N MOCS2D
TRP:G OFF
SYS PD=0 TF=900 TC=620 TM=575 PR=2175
DOP ON
PUN:20 0,2,0,2,0/
PRI
 1/
 20,2,2,2/
/
BUR LTIME=1 /
    50*876/
STA
RES old 40DCY1 40DCY
```

```
 0, -72035.2941 /
!
! ************************************************************
TTL MCNP PWR 17x17 SPENT LEU Fuel - 4% U235 - 40-GWd
! ************************************************************
!  INTEGRATION PARAMETERS
! ****************************
CON:0
TRP:N MOCS2D
TRP:G OFF
SYS PD=0 TF=900 TC=620 TM=575 PR=2175
DOP ON
PUN:20 0,2,0,2,0/
PRI
 1/
 20,2,2,2/
/
STA
```

D.2. BWR 9x9 Spent MOX Fuel Assembly

Table D.2. Summary of reactor parameters used in TransLAT input decks for a BWR pin cell (MOX fuel).

BWR Pin Cell Data	
Fuel Pin Pitch	1.7128 cm
Fuel Material	MOX
Pu Loading	6 wt%HM Pu (3.28% ^{239}Pu)
Expanded Pellet Density	10.012 g/cm^3
Fuel Pellet Radius	0.4877 cm
Outer Pin Radius	0.5590 cm
Cladding Material	Zircaloy-2 (6.55 g/cm^3)
Cladding Thickness	0.071 cm
Operating Parameters	
Power Density	25.6 MW/MTU
Fuel Temperature	900 K
Clad Temperature	559 K
Moderator Temperature	559 K
Burnup Range	10 – 50 GWd/MTU
Decay Time	5 yrs
Moderator (Light Water) Data	
No Void	0.7398 g/cm^3
40% Void	0.4585 g/cm^3
70% Void	0.2475 g/cm^3

```
*FN p=punch_6_MOX40\r
*FN   r=res_6_MOX40.r
TTL BWR 9x9 SPENT MOX Fuel 6% Pu - NO VOID - 40-GWD
! ****************************
!  INTEGRATION PARAMETERS
! ****************************
CON:0
TRP:N MOCS2D
TRP:G OFF
!
! ****************************
!  OPERATING STATE CONDITIONS
! ****************************
SYS PD=25.6 TF=900 TC=559 TM=559
DOP ON
!
! ****************************
!  FIXED BUCKLING OPTION
! ****************************
FUM 1,1,1.0E-8
!
! *****************
! MATERIAL DATA
! *****************
MAT:FUEL 10.012   92235=0.165737 92238=82.70257 \
                  94238=0.132236 94239=2.893338 94240=1.380553 94241=0.502483 \
                  94242=0.380857 8016=11.842223 TAVE=TF ICHN=92 MATTYP=1 /
MAT:CLAD  6.55  40000=100.0 TAVE=TC /
MOD:1 0.0/ LIGHT WATER COOLANT with 0% VOID FRACTION
!
GEO:1
'PC', 22 /
  'RPP','MOD',1,1,0.8563964/
  'RCC','CLAD',1,1,0.5590/
  'RCC','FUEL',1,1,0.4877/
  'RCC','FUEL',1,1,0.487686256/
  'RCC','FUEL',1,1,0.487675904/
  'RCC','FUEL',1,1,0.487657961/
  'RCC','FUEL',1,1,0.487626862/
  'RCC','FUEL',1,1,0.487572958/
  'RCC','FUEL',1,1,0.487479530/
  'RCC','FUEL',1,1,0.487317596/
  'RCC','FUEL',1,1,0.487036922/
  'RCC','FUEL',1,1,0.486550444/
  'RCC','FUEL',1,1,0.485707254/
  'RCC','FUEL',1,1,0.484245793/
  'RCC','FUEL',1,1,0.481712711/
  'RCC','FUEL',1,1,0.477322239/
  'RCC','FUEL',1,1,0.469712440/
  'RCC','FUEL',1,1,0.456522733/
  'RCC','FUEL',1,1,0.433661633/
  'RCC','FUEL',1,1,0.394037562/
  'RCC','FUEL',1,1,0.325359022/
  'RCC','FUEL',1,1,0.206321736/
/
LAT
+PC:1
 4*0.0/
/
MAP
```

```
'MAPS',1/
     1,1,1/
     1,1,'PC:1'/
/
EDR
       'M5R', 'PC:1.2'/
       'FR1', 'PC:1.3'/
       'FR2', 'PC:1.4'/
       'FR3', 'PC:1.5'/
       'FR4', 'PC:1.6'/
       'FR5', 'PC:1.7'/
       'FR6', 'PC:1.8'/
       'FR7', 'PC:1.9'/
       'FR8', 'PC:1.10'/
       'FR9', 'PC:1.11'/
       'FR10', 'PC:1.12'/
       'FR11', 'PC:1.13'/
       'FR12', 'PC:1.14'/
       'FR13', 'PC:1.15'/
       'FR14', 'PC:1.16'/
       'FR15', 'PC:1.17'/
       'FR16', 'PC:1.18'/
       'FR17', 'PC:1.19'/
       'FR18', 'PC:1.20'/
       'FR19', 'PC:1.21'/
       'FR20', 'PC:1.22'/
/
! PRI
! 1/
! 20,2,2,2/
! /
!
! ****************************
!  BURNUP
! ****************************
BUR BUMAX=40.0/
PUN:20 0,2,0,2,1,0,0/
!
RES new 40BUR
STA
RES old 40DCY 40BUR
 0, 40.0 /
!
! ************************************************************
TTL BWR 9x9 SPENT MOX Fuel - 6% Pu - 40-GWD - DECAY 5 years
! ************************************************************
!  INTEGRATION PARAMETERS
! ****************************
CON:0
TRP:N MOCS2D
TRP:G OFF
SYS PD=0 TF=900 TC=559 TM=559
DOP ON
PUN:20 0,2,0,2,0/
PRI
 1/
 20,2,2,2/
/
!
BUR LTIME=1 /
```

```
    50*876/
STA
!
RES old 40DCY1 40DCY
 0, -81300 /
!
! ************************************************************
TTL MCNP BWR 9x9 SPENT MOX Fuel ISOTOPICS - 6% Pu - 40-GWD
! ************************************************************
!  INTEGRATION PARAMETERS
! ****************************
CON:0
TRP:N MOCS2D
TRP:G OFF
SYS PD=0 TF=900 TC=559 TM=559
DOP ON
PUN:20 0,2,0,2,0/
PRI
 1/
 20,2,2,2/
/
STA
```

APPENDIX E

SPENT FUEL ISOTOPICS FOR LWR FUEL ASSEMBLIES

E.1. PWR 17x17 Spent Fuel Assembly

Table E.1. Average isotopic composition of PWR spent LEU fuel (4% ^{235}U, 5-yrs cooled).

Isotope	PWR Spent LEU Fuel: Average Weight Fraction [wt%]				
	10 GWd	*20 GWd*	*30 GWd*	*40 GWd*	*50 GWd*
^{234}U	8.31E-07	2.18E-06	4.54E-06	8.14E-06	1.28E-05
^{235}U	2.60E-02	1.86E-02	1.28E-02	8.27E-03	4.99E-03
^{236}U	1.71E-03	3.01E-03	3.98E-03	4.66E-03	5.06E-03
^{238}U	8.47E-01	8.47E-01	8.47E-01	8.46E-01	8.45E-01
^{237}Np	5.53E-05	1.56E-04	2.78E-04	4.07E-04	5.27E-04
^{238}Pu	4.04E-06	2.47E-05	7.15E-05	1.47E-04	2.44E-04
^{239}Pu	2.77E-03	3.96E-03	4.41E-03	4.49E-03	4.41E-03
^{240}Pu	3.90E-04	1.00E-03	1.59E-03	2.07E-03	2.43E-03
^{241}Pu	1.09E-04	4.04E-04	7.02E-04	9.22E-04	1.06E-03
^{242}Pu	9.40E-06	8.17E-05	2.47E-04	4.99E-04	8.17E-04
^{241}Am	3.02E-05	1.17E-04	2.09E-04	2.81E-04	3.24E-04
^{243}Am	4.02E-07	7.75E-06	3.65E-05	9.78E-05	1.94E-04
^{242}Cm	8.13E-11	1.03E-09	3.44E-09	6.82E-09	1.02E-08
^{244}Cm	1.81E-08	7.96E-07	6.29E-06	2.50E-05	6.84E-05
^{95}Mo	2.34E-04	4.51E-04	6.52E-04	8.39E-04	1.01E-03
^{99}Tc	2.34E-04	4.57E-04	6.67E-04	8.62E-04	1.04E-03
^{101}Ru	2.11E-04	4.24E-04	6.37E-04	8.48E-04	1.06E-03
^{103}Rh	1.39E-04	2.74E-04	3.97E-04	5.02E-04	5.86E-04
^{105}Pd	6.55E-05	1.60E-04	2.76E-04	4.09E-04	5.55E-04
^{109}Ag	8.37E-06	2.58E-05	4.91E-05	7.64E-05	1.06E-04
^{131}Xe	1.48E-04	2.77E-04	3.82E-04	4.64E-04	5.22E-04
^{133}Cs	3.44E-04	6.69E-04	9.72E-04	1.25E-03	1.50E-03
^{135}Cs	1.12E-04	2.18E-04	3.18E-04	4.11E-04	4.99E-04
^{137}Cs	2.99E-04	5.95E-04	8.89E-04	1.18E-03	1.47E-03
^{141}Pr	3.20E-04	6.31E-04	9.34E-04	1.23E-03	1.52E-03
^{143}Nd	3.03E-04	5.46E-04	7.31E-04	8.57E-04	9.25E-04
^{145}Nd	2.14E-04	4.09E-04	5.86E-04	7.45E-04	8.85E-04
^{147}Sm	8.51E-05	1.50E-04	1.99E-04	2.32E-04	2.51E-04
^{149}Sm	2.63E-06	2.62E-06	2.54E-06	2.45E-06	2.36E-06
^{150}Sm	6.75E-05	1.45E-04	2.27E-04	3.07E-04	3.83E-04
^{151}Sm	7.77E-06	9.40E-06	1.06E-05	1.14E-05	1.21E-05
^{152}Sm	3.56E-05	7.36E-05	1.07E-04	1.37E-04	1.63E-04
^{153}Eu	1.64E-05	4.49E-05	8.16E-05	1.22E-04	1.62E-04
^{155}Gd	1.26E-06	2.97E-06	5.68E-06	9.09E-06	1.27E-05
^{156}Gd	4.88E-06	1.67E-05	4.07E-05	8.33E-05	1.51E-04
^{16}O	1.19E-01	1.20E-01	1.21E-01	1.22E-01	1.23E-01

Table E.2. Average isotopic composition of PWR spent MOX fuel (6% Pu, 5-yrs cooled).

Isotope	PWR Spent MOX Fuel: Average Weight Fraction [wt%]				
	10 GWd	*20 GWd*	*30 GWd*	*40 GWd*	*50 GWd*
^{234}U	5.39E-05	5.78E-05	6.22E-05	6.68E-05	7.11E-05
^{235}U	1.42E-03	1.19E-03	9.86E-04	7.96E-04	6.25E-04
^{236}U	5.67E-05	1.06E-04	1.48E-04	1.83E-04	2.11E-04
^{238}U	8.27E-01	8.27E-01	8.26E-01	8.26E-01	8.26E-01
^{237}Np	3.28E-05	6.46E-05	9.47E-05	1.22E-04	1.47E-04
^{238}Pu	1.17E-03	1.12E-03	1.11E-03	1.13E-03	1.15E-03
^{239}Pu	2.35E-02	1.90E-02	1.53E-02	1.25E-02	1.03E-02
^{240}Pu	1.40E-02	1.38E-02	1.33E-02	1.24E-02	1.13E-02
^{241}Pu	4.76E-03	5.19E-03	5.31E-03	5.17E-03	4.83E-03
^{242}Pu	3.93E-03	4.19E-03	4.54E-03	4.97E-03	5.43E-03
^{241}Am	1.44E-03	1.69E-03	1.82E-03	1.83E-03	1.74E-03
^{243}Am	3.87E-04	7.12E-04	9.96E-04	1.25E-03	1.49E-03
^{242}Cm	1.18E-08	3.22E-08	5.14E-08	6.62E-08	7.54E-08
^{244}Cm	4.41E-05	1.61E-04	3.34E-04	5.54E-04	8.17E-04
^{95}Mo	1.69E-04	3.33E-04	4.94E-04	6.50E-04	8.01E-04
^{99}Tc	2.25E-04	4.39E-04	6.44E-04	8.38E-04	1.02E-03
^{101}Ru	2.29E-04	4.55E-04	6.79E-04	8.98E-04	1.11E-03
^{103}Rh	2.53E-04	4.75E-04	6.66E-04	8.26E-04	9.56E-04
^{105}Pd	2.12E-04	4.20E-04	6.25E-04	8.26E-04	1.02E-03
^{109}Ag	5.95E-05	1.13E-04	1.61E-04	2.05E-04	2.44E-04
^{131}Xe	1.74E-04	3.18E-04	4.35E-04	5.28E-04	6.00E-04
^{133}Cs	3.39E-04	6.58E-04	9.60E-04	1.24E-03	1.51E-03
^{135}Cs	2.11E-04	4.06E-04	5.87E-04	7.53E-04	9.04E-04
^{137}Cs	3.01E-04	5.98E-04	8.92E-04	1.18E-03	1.47E-03
^{141}Pr	2.77E-04	5.53E-04	8.29E-04	1.10E-03	1.38E-03
^{143}Nd	2.36E-04	4.55E-04	6.56E-04	8.35E-04	9.88E-04
^{145}Nd	1.68E-04	3.29E-04	4.85E-04	6.34E-04	7.77E-04
^{147}Sm	7.67E-05	1.39E-04	1.89E-04	2.28E-04	2.59E-04
^{149}Sm	5.94E-06	5.41E-06	4.89E-06	4.41E-06	3.99E-06
^{150}Sm	6.79E-05	1.45E-04	2.25E-04	3.04E-04	3.82E-04
^{151}Sm	2.12E-05	2.53E-05	2.59E-05	2.56E-05	2.51E-05
^{152}Sm	4.90E-05	1.01E-04	1.43E-04	1.75E-04	2.01E-04
^{153}Eu	2.83E-05	6.91E-05	1.17E-04	1.67E-04	2.14E-04
^{155}Gd	4.12E-06	5.93E-06	9.18E-06	1.35E-05	1.82E-05
^{156}Gd	1.53E-05	3.64E-05	6.61E-05	1.10E-04	1.73E-04
^{16}O	1.19E-01	1.20E-01	1.21E-01	1.21E-01	1.22E-01

E.2. BWR 9x9 Spent Fuel Assembly

Table E.3. Average isotopic composition of BWR 9x9 spent LEU fuel with 0% void fraction (3% ^{235}U, 5-yrs cooled).

Isotope	BWR Spent LEU Fuel: Average Weight Fraction [wt%]				
	10 GWd	*20 GWd*	*30 GWd*	*40 GWd*	*50 GWd*
^{234}U	6.19E-07	1.82E-06	4.11E-06	7.50E-06	1.14E-05
^{235}U	1.75E-02	1.08E-02	6.07E-03	2.98E-03	1.29E-03
^{236}U	1.54E-03	2.62E-03	3.33E-03	3.71E-03	3.83E-03
^{238}U	8.56E-01	8.56E-01	8.55E-01	8.53E-01	8.51E-01
^{237}Np	4.91E-05	1.36E-04	2.38E-04	3.37E-04	4.18E-04
^{238}Pu	4.13E-06	2.55E-05	7.31E-05	1.43E-04	2.18E-04
^{239}Pu	2.50E-03	3.28E-03	3.41E-03	3.34E-03	3.25E-03
^{240}Pu	4.65E-04	1.16E-03	1.76E-03	2.19E-03	2.43E-03
^{241}Pu	1.17E-04	3.93E-04	6.22E-04	7.55E-04	8.17E-04
^{242}Pu	1.40E-05	1.18E-04	3.50E-04	6.92E-04	1.10E-03
^{241}Am	3.30E-05	1.16E-04	1.90E-04	2.33E-04	2.51E-04
^{243}Am	5.67E-07	1.08E-05	5.05E-05	1.33E-04	2.56E-04
^{242}Cm	1.26E-10	1.41E-09	4.19E-09	7.32E-09	9.52E-09
^{244}Cm	2.51E-08	1.11E-06	9.04E-06	3.67E-05	9.99E-05
^{95}Mo	2.32E-04	4.43E-04	6.35E-04	8.06E-04	9.58E-04
^{99}Tc	2.34E-04	4.55E-04	6.61E-04	8.47E-04	1.01E-03
^{101}Ru	2.12E-04	4.26E-04	6.40E-04	8.53E-04	1.06E-03
^{103}Rh	1.40E-04	2.76E-04	3.95E-04	4.88E-04	5.53E-04
^{105}Pd	6.96E-05	1.74E-04	3.03E-04	4.52E-04	6.13E-04
^{109}Ag	9.82E-06	3.05E-05	5.81E-05	8.98E-05	1.22E-04
^{131}Xe	1.49E-04	2.77E-04	3.78E-04	4.49E-04	4.94E-04
^{133}Cs	3.44E-04	6.66E-04	9.61E-04	1.22E-03	1.45E-03
^{135}Cs	1.03E-04	1.97E-04	2.82E-04	3.61E-04	4.41E-04
^{137}Cs	2.98E-04	5.91E-04	8.81E-04	1.16E-03	1.44E-03
^{141}Pr	3.18E-04	6.25E-04	9.20E-04	1.20E-03	1.47E-03
^{143}Nd	2.92E-04	5.04E-04	6.32E-04	6.82E-04	6.73E-04
^{145}Nd	2.12E-04	4.02E-04	5.69E-04	7.12E-04	8.33E-04
^{147}Sm	8.52E-05	1.50E-04	1.96E-04	2.23E-04	2.36E-04
^{149}Sm	1.82E-06	1.76E-06	1.68E-06	1.62E-06	1.58E-06
^{150}Sm	6.83E-05	1.45E-04	2.23E-04	2.96E-04	3.59E-04
^{151}Sm	5.64E-06	6.56E-06	7.18E-06	7.71E-06	8.25E-06
^{152}Sm	3.83E-05	7.83E-05	1.14E-04	1.44E-04	1.70E-04
^{153}Eu	1.71E-05	4.74E-05	8.62E-05	1.28E-04	1.67E-04
^{155}Gd	1.34E-06	3.32E-06	6.36E-06	9.93E-06	1.34E-05
^{156}Gd	5.42E-06	2.01E-05	5.23E-05	1.12E-04	2.05E-04
^{16}O	1.19E-01	1.20E-01	1.21E-01	1.22E-01	1.23E-01

Table E.4. Average isotopic composition of BWR 9x9 spent LEU fuel with 40% void fraction (3% ^{235}U, 5-yrs cooled).

Isotope	BWR Spent LEU Fuel: Average Weight Fraction [wt%]				
	10 GWd	*20 GWd*	*30 GWd*	*40 GWd*	*50 GWd*
^{234}U	8.48E-07	2.59E-06	5.81E-06	1.06E-05	1.65E-05
^{235}U	1.79E-02	1.20E-02	7.73E-03	4.80E-03	2.88E-03
^{236}U	1.57E-03	2.61E-03	3.28E-03	3.67E-03	3.84E-03
^{238}U	8.54E-01	8.53E-01	8.51E-01	8.49E-01	8.46E-01
^{237}Np	6.60E-05	1.77E-04	3.02E-04	4.21E-04	5.23E-04
^{238}Pu	6.45E-06	3.80E-05	1.04E-04	2.00E-04	3.12E-04
^{239}Pu	3.22E-03	4.46E-03	4.95E-03	5.12E-03	5.17E-03
^{240}Pu	5.25E-04	1.25E-03	1.89E-03	2.38E-03	2.72E-03
^{241}Pu	1.72E-04	5.42E-04	8.69E-04	1.10E-03	1.25E-03
^{242}Pu	1.88E-05	1.34E-04	3.55E-04	6.49E-04	9.80E-04
^{241}Am	4.82E-05	1.61E-04	2.68E-04	3.46E-04	3.97E-04
^{243}Am	1.10E-06	1.71E-05	6.78E-05	1.57E-04	2.75E-04
^{242}Cm	2.04E-10	2.03E-09	5.70E-09	9.93E-09	1.36E-08
^{244}Cm	6.70E-08	2.40E-06	1.59E-05	5.40E-05	1.27E-04
^{95}Mo	2.27E-04	4.31E-04	6.17E-04	7.87E-04	9.43E-04
^{99}Tc	2.31E-04	4.47E-04	6.47E-04	8.31E-04	1.00E-03
^{101}Ru	2.11E-04	4.24E-04	6.35E-04	8.44E-04	1.05E-03
^{103}Rh	1.44E-04	2.83E-04	4.05E-04	5.06E-04	5.87E-04
^{105}Pd	7.67E-05	1.91E-04	3.28E-04	4.81E-04	6.43E-04
^{109}Ag	1.15E-05	3.42E-05	6.24E-05	9.31E-05	1.24E-04
^{131}Xe	1.46E-04	2.67E-04	3.61E-04	4.30E-04	4.78E-04
^{133}Cs	3.40E-04	6.54E-04	9.42E-04	1.20E-03	1.44E-03
^{135}Cs	1.16E-04	2.33E-04	3.46E-04	4.57E-04	5.66E-04
^{137}Cs	2.97E-04	5.89E-04	8.77E-04	1.16E-03	1.44E-03
^{141}Pr	3.15E-04	6.17E-04	9.10E-04	1.20E-03	1.47E-03
^{143}Nd	2.90E-04	5.10E-04	6.73E-04	7.85E-04	8.57E-04
^{145}Nd	2.08E-04	3.92E-04	5.54E-04	6.99E-04	8.27E-04
^{147}Sm	8.18E-05	1.41E-04	1.82E-04	2.09E-04	2.27E-04
^{149}Sm	2.15E-06	2.21E-06	2.19E-06	2.15E-06	2.12E-06
^{150}Sm	6.92E-05	1.47E-04	2.27E-04	3.03E-04	3.72E-04
^{151}Sm	6.95E-06	8.98E-06	1.06E-05	1.20E-05	1.33E-05
^{152}Sm	3.72E-05	7.44E-05	1.06E-04	1.33E-04	1.55E-04
^{153}Eu	1.87E-05	5.13E-05	9.07E-05	1.31E-04	1.69E-04
^{155}Gd	1.37E-06	3.51E-06	6.66E-06	1.03E-05	1.39E-05
^{156}Gd	6.17E-06	2.25E-05	5.57E-05	1.11E-04	1.92E-04
^{16}O	1.19E-01	1.20E-01	1.21E-01	1.22E-01	1.23E-01

Table E.5. Average isotopic composition of BWR 9x9 spent LEU fuel with 70% void fraction (3% ^{235}U, 5-yrs cooled).

Isotope	BWR Spent LEU Fuel: Average Weight Fraction [wt%]				
	10 GWd	*20 GWd*	*30 GWd*	*40 GWd*	*50 GWd*
^{234}U	1.26E-06	4.02E-06	8.93E-06	1.61E-05	2.52E-05
^{235}U	1.86E-02	1.35E-02	9.90E-03	7.34E-03	5.49E-03
^{236}U	1.64E-03	2.69E-03	3.35E-03	3.76E-03	3.98E-03
^{238}U	8.52E-01	8.48E-01	8.44E-01	8.40E-01	8.35E-01
^{237}Np	9.39E-05	2.42E-04	3.99E-04	5.45E-04	6.72E-04
^{238}Pu	1.13E-05	6.23E-05	1.61E-04	3.02E-04	4.74E-04
^{239}Pu	4.73E-03	7.29E-03	9.04E-03	1.04E-02	1.15E-02
^{240}Pu	6.03E-04	1.40E-03	2.13E-03	2.78E-03	3.34E-03
^{241}Pu	2.56E-04	7.70E-04	1.27E-03	1.71E-03	2.08E-03
^{242}Pu	2.33E-05	1.33E-04	3.09E-04	5.18E-04	7.40E-04
^{241}Am	7.20E-05	2.29E-04	3.96E-04	5.51E-04	6.89E-04
^{243}Am	2.09E-06	2.47E-05	8.09E-05	1.64E-04	2.62E-04
^{242}Cm	3.46E-10	3.06E-09	8.36E-09	1.50E-08	2.19E-08
^{244}Cm	1.89E-07	5.01E-06	2.63E-05	7.42E-05	1.51E-04
^{95}Mo	2.19E-04	4.13E-04	5.89E-04	7.52E-04	9.05E-04
^{99}Tc	2.27E-04	4.34E-04	6.25E-04	8.03E-04	9.68E-04
^{101}Ru	2.10E-04	4.19E-04	6.23E-04	8.22E-04	1.02E-03
^{103}Rh	1.49E-04	2.90E-04	4.14E-04	5.23E-04	6.19E-04
^{105}Pd	8.68E-05	2.12E-04	3.57E-04	5.13E-04	6.75E-04
^{109}Ag	1.37E-05	3.82E-05	6.66E-05	9.65E-05	1.27E-04
^{131}Xe	1.41E-04	2.49E-04	3.30E-04	3.91E-04	4.38E-04
^{133}Cs	3.32E-04	6.33E-04	9.07E-04	1.16E-03	1.39E-03
^{135}Cs	1.48E-04	3.15E-04	4.94E-04	6.82E-04	8.78E-04
^{137}Cs	2.94E-04	5.83E-04	8.69E-04	1.15E-03	1.43E-03
^{141}Pr	3.09E-04	6.05E-04	8.93E-04	1.18E-03	1.46E-03
^{143}Nd	2.85E-04	5.15E-04	7.12E-04	8.83E-04	1.04E-03
^{145}Nd	2.02E-04	3.76E-04	5.30E-04	6.69E-04	7.96E-04
^{147}Sm	7.67E-05	1.27E-04	1.61E-04	1.85E-04	2.02E-04
^{149}Sm	3.10E-06	3.57E-06	3.97E-06	4.32E-06	4.64E-06
^{150}Sm	6.92E-05	1.46E-04	2.23E-04	2.95E-04	3.61E-04
^{151}Sm	9.78E-06	1.49E-05	2.00E-05	2.51E-05	3.00E-05
^{152}Sm	3.48E-05	6.75E-05	9.41E-05	1.16E-04	1.35E-04
^{153}Eu	2.05E-05	5.42E-05	9.11E-05	1.26E-04	1.57E-04
^{155}Gd	1.46E-06	3.84E-06	7.26E-06	1.12E-05	1.53E-05
^{156}Gd	7.21E-06	2.54E-05	5.91E-05	1.10E-04	1.77E-04
^{16}O	1.19E-01	1.20E-01	1.21E-01	1.22E-01	1.22E-01

Table E.6. Average isotopic composition of BWR 9x9 spent MOX fuel with 0% void fraction (6% Pu, 5-yrs cooled).

Isotope	BWR Spent MOX Fuel: Average Weight Fraction [wt%]				
	10 GWd	*20 GWd*	*30 GWd*	*40 GWd*	*50 GWd*
^{234}U	5.62E-05	6.24E-05	6.88E-05	7.50E-05	8.01E-05
^{235}U	1.42E-03	1.18E-03	9.57E-04	7.46E-04	5.53E-04
^{236}U	5.33E-05	1.02E-04	1.45E-04	1.81E-04	2.11E-04
^{238}U	8.28E-01	8.28E-01	8.29E-01	8.29E-01	8.29E-01
^{237}Np	2.90E-05	5.77E-05	8.52E-05	1.11E-04	1.33E-04
^{238}Pu	1.17E-03	1.12E-03	1.12E-03	1.13E-03	1.15E-03
^{239}Pu	2.27E-02	1.74E-02	1.31E-02	9.79E-03	7.47E-03
^{240}Pu	1.43E-02	1.43E-02	1.37E-02	1.26E-02	1.12E-02
^{241}Pu	4.50E-03	4.74E-03	4.72E-03	4.45E-03	3.98E-03
^{242}Pu	4.00E-03	4.33E-03	4.77E-03	5.31E-03	5.90E-03
^{241}Am	1.42E-03	1.66E-03	1.76E-03	1.72E-03	1.56E-03
^{243}Am	3.37E-04	6.39E-04	9.19E-04	1.19E-03	1.44E-03
^{242}Cm	1.35E-08	3.49E-08	5.37E-08	6.70E-08	7.35E-08
^{244}Cm	3.27E-05	1.23E-04	2.65E-04	4.55E-04	6.94E-04
^{95}Mo	1.69E-04	3.35E-04	4.96E-04	6.52E-04	8.04E-04
^{99}Tc	2.27E-04	4.44E-04	6.52E-04	8.49E-04	1.03E-03
^{101}Ru	2.30E-04	4.58E-04	6.84E-04	9.07E-04	1.13E-03
^{103}Rh	2.54E-04	4.78E-04	6.71E-04	8.29E-04	9.51E-04
^{105}Pd	2.14E-04	4.26E-04	6.34E-04	8.38E-04	1.04E-03
^{109}Ag	6.07E-05	1.16E-04	1.66E-04	2.11E-04	2.51E-04
^{131}Xe	1.77E-04	3.26E-04	4.49E-04	5.47E-04	6.21E-04
^{133}Cs	3.41E-04	6.66E-04	9.73E-04	1.26E-03	1.53E-03
^{135}Cs	2.22E-04	4.25E-04	6.08E-04	7.70E-04	9.14E-04
^{137}Cs	3.01E-04	5.97E-04	8.88E-04	1.17E-03	1.45E-03
^{141}Pr	2.78E-04	5.55E-04	8.32E-04	1.11E-03	1.38E-03
^{143}Nd	2.36E-04	4.54E-04	6.48E-04	8.13E-04	9.40E-04
^{145}Nd	1.68E-04	3.31E-04	4.89E-04	6.40E-04	7.83E-04
^{147}Sm	7.90E-05	1.46E-04	2.03E-04	2.49E-04	2.85E-04
^{149}Sm	4.87E-06	4.26E-06	3.68E-06	3.18E-06	2.77E-06
^{150}Sm	6.87E-05	1.45E-04	2.23E-04	3.00E-04	3.75E-04
^{151}Sm	1.96E-05	2.16E-05	2.07E-05	1.94E-05	1.81E-05
^{152}Sm	5.17E-05	1.07E-04	1.53E-04	1.88E-04	2.14E-04
^{153}Eu	2.79E-05	6.82E-05	1.17E-04	1.67E-04	2.16E-04
^{155}Gd	4.32E-06	5.96E-06	9.04E-06	1.32E-05	1.78E-05
^{156}Gd	1.52E-05	3.62E-05	6.58E-05	1.11E-04	1.77E-04
^{16}O	1.19E-01	1.20E-01	1.21E-01	1.21E-01	1.22E-01

Table E.7. Average isotopic composition of BWR 9x9 spent MOX fuel with 40% void fraction (6% Pu, 5-yrs cooled).

Isotope	BWR Spent MOX Fuel: Average Weight Fraction [wt%]				
	10 GWd	*20 GWd*	*30 GWd*	*40 GWd*	*50 GWd*
^{234}U	5.65E-05	6.33E-05	7.09E-05	7.91E-05	8.76E-05
^{235}U	1.41E-03	1.19E-03	9.89E-04	8.11E-04	6.56E-04
^{236}U	6.19E-05	1.14E-04	1.57E-04	1.91E-04	2.17E-04
^{238}U	8.26E-01	8.25E-01	8.24E-01	8.23E-01	8.22E-01
^{237}Np	3.80E-05	7.45E-05	1.09E-04	1.40E-04	1.67E-04
^{238}Pu	1.18E-03	1.15E-03	1.18E-03	1.24E-03	1.32E-03
^{239}Pu	2.44E-02	2.07E-02	1.77E-02	1.52E-02	1.33E-02
^{240}Pu	1.39E-02	1.36E-02	1.31E-02	1.24E-02	1.15E-02
^{241}Pu	4.79E-03	5.24E-03	5.42E-03	5.38E-03	5.19E-03
^{242}Pu	3.86E-03	4.04E-03	4.29E-03	4.60E-03	4.93E-03
^{241}Am	1.50E-03	1.81E-03	2.00E-03	2.07E-03	2.04E-03
^{243}Am	4.25E-04	7.63E-04	1.04E-03	1.28E-03	1.49E-03
^{242}Cm	1.55E-08	4.03E-08	6.23E-08	7.84E-08	8.83E-08
^{244}Cm	5.58E-05	1.96E-04	3.93E-04	6.32E-04	9.03E-04
^{95}Mo	1.68E-04	3.31E-04	4.90E-04	6.44E-04	7.95E-04
^{99}Tc	2.23E-04	4.35E-04	6.35E-04	8.25E-04	1.00E-03
^{101}Ru	2.28E-04	4.52E-04	6.72E-04	8.88E-04	1.10E-03
^{103}Rh	2.50E-04	4.67E-04	6.53E-04	8.12E-04	9.43E-04
^{105}Pd	2.11E-04	4.17E-04	6.20E-04	8.19E-04	1.01E-03
^{109}Ag	5.80E-05	1.09E-04	1.55E-04	1.96E-04	2.33E-04
^{131}Xe	1.70E-04	3.08E-04	4.18E-04	5.04E-04	5.71E-04
^{133}Cs	3.36E-04	6.51E-04	9.45E-04	1.22E-03	1.48E-03
^{135}Cs	2.47E-04	4.83E-04	7.08E-04	9.20E-04	1.12E-03
^{137}Cs	2.99E-04	5.92E-04	8.80E-04	1.16E-03	1.44E-03
^{141}Pr	2.76E-04	5.52E-04	8.27E-04	1.10E-03	1.38E-03
^{143}Nd	2.35E-04	4.55E-04	6.59E-04	8.45E-04	1.01E-03
^{145}Nd	1.67E-04	3.28E-04	4.81E-04	6.27E-04	7.66E-04
^{147}Sm	7.60E-05	1.36E-04	1.85E-04	2.24E-04	2.54E-04
^{149}Sm	6.52E-06	6.03E-06	5.54E-06	5.09E-06	4.67E-06
^{150}Sm	6.70E-05	1.42E-04	2.18E-04	2.91E-04	3.63E-04
^{151}Sm	2.21E-05	2.78E-05	2.98E-05	3.07E-05	3.11E-05
^{152}Sm	4.71E-05	9.54E-05	1.34E-04	1.64E-04	1.87E-04
^{153}Eu	2.87E-05	6.94E-05	1.16E-04	1.63E-04	2.06E-04
^{155}Gd	4.02E-06	6.03E-06	9.45E-06	1.39E-05	1.86E-05
^{156}Gd	1.54E-05	3.66E-05	6.67E-05	1.10E-04	1.71E-04
^{16}O	1.19E-01	1.20E-01	1.21E-01	1.21E-01	1.22E-01

Table E.8. Average isotopic composition of BWR 9x9 spent MOX fuel with 70% void fraction (6% Pu, 5-yrs cooled).

Isotope	BWR Spent MOX Fuel: Average Weight Fraction [wt%]				
	10 GWd	*20 GWd*	*30 GWd*	*40 GWd*	*50 GWd*
^{234}U	5.63E-05	6.31E-05	7.09E-05	7.96E-05	8.92E-05
^{235}U	1.39E-03	1.16E-03	9.71E-04	8.13E-04	6.81E-04
^{236}U	7.76E-05	1.37E-04	1.82E-04	2.16E-04	2.39E-04
^{238}U	8.23E-01	8.20E-01	8.17E-01	8.13E-01	8.10E-01
^{237}Np	5.04E-05	9.73E-05	1.40E-04	1.77E-04	2.10E-04
^{238}Pu	1.18E-03	1.16E-03	1.20E-03	1.28E-03	1.39E-03
^{239}Pu	2.73E-02	2.61E-02	2.53E-02	2.46E-02	2.42E-02
^{240}Pu	1.35E-02	1.32E-02	1.29E-02	1.26E-02	1.23E-02
^{241}Pu	4.91E-03	5.46E-03	5.77E-03	5.94E-03	6.01E-03
^{242}Pu	3.70E-03	3.69E-03	3.73E-03	3.80E-03	3.88E-03
^{241}Am	1.53E-03	1.88E-03	2.12E-03	2.29E-03	2.40E-03
^{243}Am	5.08E-04	8.54E-04	1.10E-03	1.29E-03	1.44E-03
^{242}Cm	1.73E-08	4.53E-08	7.10E-08	9.18E-08	1.08E-07
^{244}Cm	8.75E-05	2.82E-04	5.24E-04	7.89E-04	1.06E-03
^{95}Mo	1.66E-04	3.27E-04	4.82E-04	6.32E-04	7.78E-04
^{99}Tc	2.19E-04	4.24E-04	6.16E-04	7.98E-04	9.71E-04
^{101}Ru	2.25E-04	4.43E-04	6.55E-04	8.60E-04	1.06E-03
^{103}Rh	2.44E-04	4.55E-04	6.39E-04	8.00E-04	9.42E-04
^{105}Pd	2.05E-04	4.04E-04	5.98E-04	7.87E-04	9.72E-04
^{109}Ag	5.45E-05	1.02E-04	1.44E-04	1.82E-04	2.18E-04
^{131}Xe	1.62E-04	2.84E-04	3.80E-04	4.55E-04	5.15E-04
^{133}Cs	3.28E-04	6.30E-04	9.10E-04	1.17E-03	1.41E-03
^{135}Cs	2.86E-04	5.69E-04	8.50E-04	1.13E-03	1.40E-03
^{137}Cs	2.95E-04	5.85E-04	8.70E-04	1.15E-03	1.43E-03
^{141}Pr	2.74E-04	5.46E-04	8.19E-04	1.09E-03	1.36E-03
^{143}Nd	2.34E-04	4.55E-04	6.65E-04	8.64E-04	1.05E-03
^{145}Nd	1.66E-04	3.22E-04	4.70E-04	6.09E-04	7.42E-04
^{147}Sm	7.23E-05	1.25E-04	1.65E-04	1.97E-04	2.21E-04
^{149}Sm	1.10E-05	1.11E-05	1.12E-05	1.12E-05	1.12E-05
^{150}Sm	6.21E-05	1.33E-04	2.03E-04	2.68E-04	3.29E-04
^{151}Sm	2.53E-05	3.66E-05	4.39E-05	4.98E-05	5.50E-05
^{152}Sm	4.17E-05	8.20E-05	1.14E-04	1.40E-04	1.62E-04
^{153}Eu	2.89E-05	6.75E-05	1.09E-04	1.47E-04	1.82E-04
^{155}Gd	4.19E-06	6.95E-06	1.13E-05	1.66E-05	2.25E-05
^{156}Gd	1.51E-05	3.63E-05	6.61E-05	1.08E-04	1.62E-04
^{16}O	1.19E-01	1.20E-01	1.21E-01	1.21E-01	1.22E-01

VITA

Name:	Adrienne Marie LaFleur
Address:	Texas A&M University Department of Nuclear Engineering Nuclear Security Science and Policy Institute 3133 TAMU College Station, TX 77843-3133
Email Address:	alafleur@lanl.gov adrienne.lafleur@gmail.com
Education:	B.S., Nuclear Engineering, Texas A&M University, 2007 Ph.D., Nuclear Engineering, Texas A&M University, 2011